Universität Stuttgart

Institut für Wasser- und Umweltsystemmodellierung

Mitteilungen

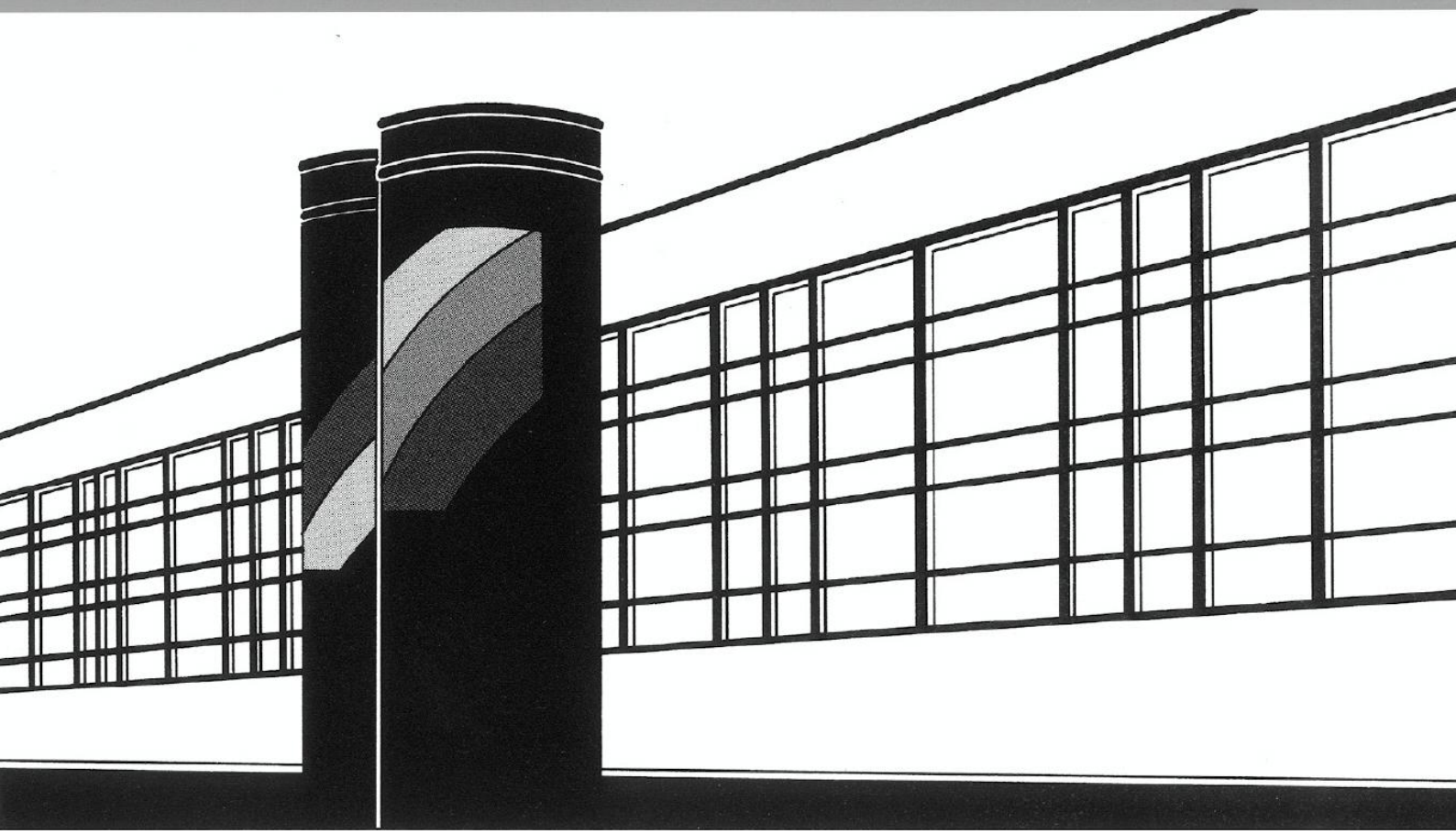

Heft 221 Lena Sophie Walter

Uncertainty Studies and Risk Assessment for CO_2 Storage in Geological Formations

Uncertainty Studies and Risk Assessment for CO_2 Storage in Geological Formations

Von der Fakultät Bau- und Umweltingenieurwissenschaften der Universität Stuttgart und dem Stuttgart Research Centre for Simulation Technology zur Erlangung der Würde eines Doktor-Ingenieurs (Dr.-Ing.) genehmigte Abhandlung

Vorgelegt von

Lena Sophie Walter

aus Tübingen

Hauptberichter:	apl. Prof. Dr.-Ing. Holger Class
Mitberichter:	Prof. Philip John Binning, Ph.D.
Mitberichter:	Prof. Dr. Dr. h.c. Ortwin Renn
Mitberichter:	Prof. Dr.-Ing. Rainer Helmig

Tag der mündlichen Prüfung: 04. Juli 2013

Institut für Wasser- und Umweltsystemmodellierung
der Universität Stuttgart
2013

Heft 221

Uncertainty Studies and Risk Assessment for CO_2 Storage in Geological Formations

von
Dr.-Ing.
Lena Sophie Walter

Eigenverlag des Instituts für Wasser- und Umweltsystemmodellierung
der Universität Stuttgart

D93 Uncertainty Studies and Risk Assessment for CO_2 Storage in Geological Formations

Bibliografische Information der Deutschen Nationalbibliothek
Die Deutsche Nationalbibliothek verzeichnet diese Publikation in der Deutschen Nationalbibliografie; detaillierte bibliografische Daten sind im Internet über http://www.d-nb.de abrufbar

Walter, Lena Sophie:
Uncertainty Studies and Risk Assessment for CO_2 Storage in Geological Formations von Lena Sophie Walter. Institut für Wasser- und Umweltsystemmodellierung, Universität Stuttgart. - Stuttgart: Institut für Wasser- und Umweltsystemmodellierung, 2013

(Mitteilungen Institut für Wasser- und Umweltsystemmodellierung, Universität Stuttgart: H. 221)
Zugl.: Stuttgart, Univ., Diss., 2013
ISBN 978-3-942036-25-2

NE: Institut für Wasser- und Umweltsystemmodellierung <Stuttgart>: Mitteilungen

Herausgegeben 2013 vom Eigenverlag des Instituts für Wasser- und Umwelt-systemmodellierung

Druck: Document Center S. Kästl, Ostfildern

Danksagung

An dieser Stelle möchte ich mich bei all denen bedanken, die zum Gelingen meiner Arbeit beigetragen haben. In diesem Zusammenhang möchte ich der Baden-Württemberg Stiftung, dem Bundesministerium für Bildung und Forschung (BMBF) und dem Stuttgart Research Centre for Simulation Technology (SimTech) für die finanzielle Unterstützung und Förderung danken.
Ganz herzlich möchte ich mich bei meinem Hauptberichter Holger Class bedanken. Durch seine nette und unkomplizierte Art hat das Arbeiten mit ihm immer sehr viel Spaß gemacht. In der Zeit am Institut konnte ich sehr viel von ihm lernen. Er hat es verstanden mich durch seine Tipps und Ideen immer wieder zu motivieren. Rainer Helmig danke ich für die Übernahme des Mitberichts und die tolle Atmosphäre, die er am Lehrstuhl durch seine freundliche und nette Art geschaffen hat. Meinem Mitberichter Philip Binning danke ich für die vielen hilfreichen Diskussionen und die Möglichkeit eines Aufenthalts an seinem Institut in Kopenhagen. Herrn Prof. Ortwin Renn möchte ich danken, dass er mir durch die Übernahme seines Mitberichts die Möglichkeit gegeben hat einen Einblick in die Sozialwissenschaft zu bekommen.
Für die große Hilfe beim parallelen Rechnen möchte ich Bernd Flemisch danken. Dirk Scheer danke ich für die Hilfe bei allen sozialwissenschaftlichen Fragen und Sergey Oladyshkin für seine Unterstützung bei statistischen Fragestellungen. Thomas Kempka und seinen Kollegen aus Potsdam möchte ich für die gute Zusammenarbeit und die Bereitstellung der geologischen Daten für die Ketzinsimulationen danken. Für die tolle Zusammenarbeit bei meinem ersten Projekt möchte ich Frauke Schäfer sehr danken. Andreas Kopp danke ich, dass er mir die Einarbeitungszeit durch seine Hilfe sehr leicht gemacht hat. Prudence Lawday und Maria Costa möchte ich für ihre Hilfe bei allen organisatorischen Dingen danken und Michelle Hartnick und David Werner für die Hilfe bei Software- und Hardwareproblemen. Bryan Flood danke ich für die sprachliche Korrektur meiner Arbeit.
Allen Kolleginnen und Kollegen am Lehrstuhl für Hydromechanik und Hydrosystemmodellierung möchte ich für die schöne Zeit am Institut danken. Die große Hilfsbereitschaft und das nette Miteinander habe ich immer sehr geschätzt. Besonders möchte ich Melanie Darcis, Karin Erbertseder und Maria Costa danken, die mir echte Freundinnen geworden sind. Alexander Kissinger und Johannes Hommel möchte ich für die tolle Zeit in unserem Büro und die guten Diskussionen danken. Andreas Geiges möchte ich danken, dass er mich das ein oder andere Mal beim Mittagessen aus einem Tief geholt hat.
Besonders bedanken möchte ich mich bei meinen Eltern, meinem Bruder und seiner Frau für die tolle Unterstützung während der ganzen Zeit und dass sie immer an mich geglaubt haben. Ganz herzlich möchte ich auch meinem Lebensgefährten Tobias für seine Unterstützung, sein Verständnis und den Rückhalt, den er mir immer gegeben hat, danken.

Contents

List of Figures

List of Tables

Notation

The following table shows the significant symbols used in this work. Local notations are explained in the text.

Symbol	Definition	Dimension
Greek Letters:		
α_l	longitudinal dispersivity	[-]
α_t	transverse dispersivity	[-]
Γ	overall measure of independence	[-]
λ	*Brooks-Corey*-parameter (grain size distribution)	[-]
λ_{pm}	heat conductivity of porous medium	[W/(m K)]
λ_α	mobility of phase α	[(m s)/kg]
μ	dynamic fluid viscosity	[kg/(m s)]
μ_α	dynamic fluid viscosity of phase α	[kg/(m s)]
ν	kinematic viscosity	[m^2/s)]
ϱ	mass density [kg/m^3]	
ϱ_α	mass density of phase α	[kg/m^3]
$\varrho_{mol,\alpha}$	molar density of phase α	[mol/m^3]
ϱ_s	density of the solid matrix [kg/m^3]	
σ	standard deviation	
σ_p	marginal standard deviation	
$\sigma_p^{'}$	conditional standard deviation	
σ^2	variance	
σ_p^2	variance of estimated parameters	
ϕ	porosity	[-]
ϕ_{init}	initial porosity	[-]
τ	tortuosity	[-]
τ_s	shear stress	[Pa]

Latin Letters:

C	rock compressibility	[1/Pa]
$\mathbf{C}_{pp}$	covariance matrix of the estimated parameters	
$\mathbf{C}_{zz}$	covariance matrix of the measurements	
c_s	specific heat capacity of the soil grains	[J/(kg K)]
$\mathbf{D}$	dispersion tensor	[m^2/s]
$\mathbf{D}_{pm}$	effective diffusion coefficient in the porous medium	[m^2/s]
$\mathbf{D}_{\alpha}^{\kappa},_m$	binary diffusion coefficient component κ in phase α	[m^2/s]
$\mathbf{D}_{\alpha}^{\kappa},_{pm}$	effective diffusion coefficient of component κ in phase α in the porous medium	[m^2/s]
d	distance	[m]
d_p	polynomial degree	[-]
$\mathbf{g}$	vector of gravitational acceleration $(0, 0, -\mathrm{g})^T$	[m/s^2]
g	skewness	
h	specific enthalpy	[J/kg]
h_α	specific enthalpy of phase α	[J/kg]
$\mathbf{J}$	Jacobien matrix	
K_x	horizontal permeability	[m^2]
K_z	vertical permeability	[m^2]
k_x	horizontal permeability	[m/s]
$\mathbf{j}_d$	diffusive flux	[mol/(m^2 s)]
$\mathbf{K}$	tensor of (intrinsic) permeability	[m^2]
$k_{r\alpha}$	relative permeability for phase α	[-]
M	molecular weight	[kg/mol]
m	mass	[kg]
m_α^κ	mass of component κ in phase α	[kg]
n_α^κ	number of moles of component κ in phase α	[kg]
N	number of uncertain or design parameters	[-]
P	number of terms in the polynomial chaos expansion	[-]
p	pressure	[Pa]
p_α	pressure of phase α	[Pa]
p_c	capillary pressure	[Pa]
p_d	entry pressure ($p_c(S_w)$-relationship after *Brooks-Corey*)	[Pa]
$\mathbf{q}_c$	flux due to heat conductivity	[J/(m^2 s)]
q	source/sink term	[kg/(s m^3)]
q_α	source/sink term for phase α	[kg/(s m^3)]
q_α^κ	source/sink term for component κ in phase α	[kg/(s m^3)]
q_h	source/sink term for energy	[J/(s m^3)]
$\mathbf{r}$	residual vector	
S	salinity	[-]
S_f	objective function	[-]
S_α	saturation of phase α	[-]
$S_{\alpha\,r}$	residual saturation of phase α	[-]

S_e	effective saturation	[-]
s_0^2	empirical variance	[-]
T	temperature	[K]
t	time	[s]
u	specific internal energy	[J/kg]
u_α	specific internal energy of phase α	[J/kg]
V	volume	[m^3]
v	specific volume	[m^3/kg]
$\mathbf{v}$	*Darcy* velocity	[m/s]
$\mathbf{v}_\alpha$	phase velocity of phase α	[m/s]
v	absolute value of Darcy velocity	[m/s]
w	kurtosis	
X_α^κ	mass fraction of component κ in phase α	[-]
X_S	mass fraction of the salt component	[-]
x_α^κ	mole fraction of component κ in phase α	[-]
$\bar{x}$	arithmetic mean	
$\bar{z}_i$	calculated system status	
$\bar{z}_i^*$	measured system status	

Subscripts:

α	phase
CO_2	CO_2 rich phase
brine	brine phase
n	non-wetting phase (CO_2)
w	wetting phase (brine)
s	salt
f	freshwater
$init$	initial value
max	maximum value

Superscripts:

κ	component

Summary

Carbon capture and storage (CCS) in deep geological formations is one possible option to mitigate the greenhouse gas effect by reducing CO_2 emissions into the atmosphere. The CO_2 is captured from the emissions of large stationary power plants, transported to suitable storage sites such as depleted oil and gas reservoirs, or saline aquifers, and is stored in these formations at a depth of at least 800 m. The assessment of the risks related to CO_2 storage is an important task. This work focuses on risk assessment and uncertainty studies for CO_2 storage in saline aquifers. Events such as CO_2 leakage and brine displacement could result in hazards for human health and the environment and therefore have to be investigated in detail. CO_2 that leaks out of the reservoir can reach and affect shallower groundwater resources caused by mobilization of (toxic) heavy metals. If CO_2 leaks back to the atmosphere the effectiveness of storage is decreased and under unlikely conditions, large CO_2 concentrations can arise in sinks, caves, or buildings if the heavier CO_2 is not mixed with the surrounded air, which could result in a suffocation hazard. The injected CO_2 will displace the brine that is initially present in the saline aquifer. The brine can be displaced over large areas and can reach shallower groundwater resources. High salt concentrations could lead to a degradation of groundwater quality.

Numerical models are an effective tool for assessing the risk related to processes in the subsurface, where experimental investigations are difficult. Two different models are applied to simulate the processes related to CO_2 storage: a model considering the two phases CO_2 and water only and a model that additionally considers compositional effects. To model the salt distribution in particular, a one-phase model considering the two components water and salt is used.

Depending on the risk and the processes which should be assessed, very complex models, large heterogeneous model domains, and possibly large time scales are required for adequate estimations. Additionally, the determination of probabilities requires many simulation runs (Monte Carlo simulations). Thus the investigation of the risks results in very high computational costs. To reduce computational costs a model reduction technique called arbitrary polynomial chaos expansion is applied with the idea to project the complex model onto an orthogonal polynomial basis. Monte Carlo simulations are then run with the polynomials instead of the complex model, which reduces the computational costs enormously. In addition, a model coupling concept to couple models of different complexity in space is used to further reduce the computational costs.

Concept for Risk Assessment The main purpose of this thesis is to develop a risk assessment concept and to investigate various uncertainties. The presented risk assessment

concept considers uncertainties on different levels: statistical uncertainty in parameter distributions, scenario uncertainty, e.g. different geological features, and recognized ignorance due to assumptions in the conceptual model set-up. Recognized ignorance and scenario uncertainty are investigated by simulating well defined model set-ups and scenarios. The damage which is relevant for the investigated event is defined as a model output. According to these damage values the set-ups and scenarios can be compared and ranked. For statistical uncertainty probabilities can be determined by running Monte Carlo simulations with the reduced model using the arbitrary polynomial chaos expansion. The results are presented in various ways: e.g., mean damage, probability density function, cumulative distribution function, or an overall risk value by multiplying the damage with the probability can be provided. If the model output (damage) cannot be compared to provided criteria (e.g. water quality criteria), analytical approximations are presented to translate the damage into comparable values.

Risk Assessment for Brine Displacement The overall concept is applied for the risks related to brine displacement and infiltration into drinking water aquifers. Salt concentrations in freshwater aquifers or in water production wells are the estimates of interest. The uncertainties and risks are investigated in three approaches: The first approach aims to test the risk assessment concept; to identify geological scenarios causing high risk; and to derive first risk and damage values for the considered scenarios. Scenario uncertainty resulting from different geological features and statistical uncertainty of different parameters are investigated. One important message is that whether brine is displaced into shallower aquifers strongly depends on the geology. The likelihood of salt infiltration is increased if a gap in the caprock or a fault zone exist. A sound understanding about the effects of different geological features is derived. The first approach results in conservative risk estimates because compositional effects are neglected. Thus, the CO_2 plume is larger and will displace more brine. In addition, the assumption of a constant salinity overestimates the salt concentration in the aquifer because the salinity in shallower aquifers is typically smaller. These assumptions are classified to the level of recognized ignorance.
In the second approach recognized ignorance is reduced by accounting for a variable salt content in the domain. To reduce computational costs a model coupling approach is applied to couple the CO_2-brine model in the storage reservoir with a water-salt model (accounting for variable salt content) in the overlying aquifers. Various geological scenarios are investigated and compared to the previous approach. The salt discharge into the water aquifer is decreased and many important pieces of information about the system behavior are derived such as that the salt is mainly displaced along a fault zone only.
For water suppliers the most important information is whether and how much salt is produced at a water production well. In third approach the salt concentrations at water production wells depending on different parameters are determined for the assumption of a 2D model domain accounting for groundwater flow. Recognized ignorance resulting from grid resolution is qualitatively studied and statistical uncertainty is investigated for three parameters: the well distance, the water production rate, and the permeability of the aquifer. Damage and risk for salt concentrations at the water production well can be provided. Mixing in the aquifer has a key influence on the salt concentration at the well. Dispersion and dif-

fusion are the relevant processes for mixing. Depending on the applied grid the numerical dispersion strongly influence the results as well. The distance of the well is a key parameter that influences the salt concentration at the well, thus the time that the salt has for mixing until reaching the well is relevant.

Uncertainty Studies for Realistic Storage Sites Before risks for a particular storage site can be estimated it is important to know the related uncertainties and to reduce them as much as possible. Uncertainty studies for realistic storage formations are thus performed in the second part of the thesis. For the pilot site Ketzin (Germany), many measurement data sets are available. However, many assumptions have to be made for modeling. Investigations of different uncertainties related to modeling assumptions (domain size, conceptual model, and grid type), which all belong the the category of recognized ignorance, are presented. History matching of the measurement data, in particular the pressure at the injection well and the arrival times at two observation wells is an important task for dynamic modeling and essential for future risk assessment. The arrival time at the first observation well was well predicted by the models but the pressure and the arrival time at the second observation well was underestimated. Different investigations for history matching are presented. Finally, a systematic approach to fit the data set is developed in this work. Inverse modeling is adapted to match the pressure for the first 50 days of injection and the first arrival time by modification of the overall permeability and porosity field and the relative permeability relationship. The extrapolation of the calibrated model to larger time scales is possible but limited. By including an additional degree of freedom: the distinction between near-well and far-field for the permeability and porosity field modification, the model can be fitted for the simulation time of about 1650 days. The calibrated model is able to predict the pressure for a limited extrapolation time, but the prediction of the plume evolution in space seems to not be reliable with the given data for permeability and porosity. Additionally, various uncertainties are studied for a realistic storage formation in the North German Basin. The aim is to investigate the influence caused by injection induced pressure increase from one storage formation to a second possible storage formation. The boundary conditions, accounting for rock compressibility, and the permeability of the reservoir are found to strongly influence the pressure evolution in the domain. For future risk assessment for realistic sites, e.g. for the Ketzin site, the uncertainty studies and the history matching approach provide important information.

Major Achievements of the Work Finally, CCS is discussed in the context of risk perception and the possible input of the risk assessment concept presented in this work is discussed. Overall, the risk assessment concept provides a systematic and comprehensive method to investigate various levels of uncertainties. The concept can be applied to other hazards such as those related to CO_2 leakage or related to other technologies in the subsurface such as methane storage or atomic waste disposal. The application of the overall risk assessment concept to a realistic (site specific) storage site is also an important future step. The presented risk assessment concept is ranked into the overall risk governance model and belongs to the phase of risk appraisal. This work is a first attempt to connect the technical risk assessment for CO_2 storage to the social science approach for risk assessment. It is

bridging the gap between engineering and social sciences by integrating the technical quantification of risk into the wider context of a comprehensive risk governance model.

Zusammenfassung

Carbon Capture and Storage (CCS) ist eine Möglichkeit um die Klimaerwärmung, hervorgerufen durch einen anthropogen verstärken Treibhauseffekt zu verringern. CCS bezeichnet einen dreistufigen Prozess: Das Abtrennen des CO_2 aus den Abgasen von stationären Kraftwerken, den Transport zu einer geeigneten Lagerstätte und das Speichern des CO_2 in tiefen, geologischen Formationen. Geeignete Lagerstätten sind unter anderem stillgelegte Öl- oder Gasreservoire und salinare Aquifere. Eine wichtige Aufgabe ist es die Risiken, die während der Lagerung des CO_2 auftreten könnten, zu untersuchen. Da gerade für Vorgänge im Untergrund experimentelle Untersuchungen oft limitiert sind, sind Simulationen ein geeignetes Werkzeug zur Risikoabschätzung. Diese Arbeit konzentriert sich auf die Untersuchung von unterschiedlichen Unsicherheiten und auf die Entwicklung eines Konzepts zur Risikoabschätzung für CO_2 Speicherung in salinaren Aquiferen. Ereignisse, die zu mögliche Gefährdungen führen können, sind der Austritt von CO_2 aus dem Reservoir, die Verdrängung des im Reservoir vorhandenen Salzwassers, oder die Druckerhöhung am Injektionsbrunnen. CO_2, das aus dem Reservoir austritt, könnte, da es leichter ist als das umgebene Salzwasser, in höher gelegenen Aquifere oder zurück an die Erdoberfläche gelangen. An der Erdoberfläche kann es unter sehr ungünstigen Bedingungen, z.B. in Senken, Höhlen oder Kellern zu hohen CO_2 Konzentrationen führen und ein Erstickungsrisiko hervorrufen. Löst sich das CO_2 im Grundwasser können durch den sinkenden pH Wert zum Teil giftige Schwermetalle mobilisiert werden. Salzwasser kann über weite Strecken verdrängt werden; erreicht es durchlässige Verwerfungszonen kann es ebenfalls in höher gelegene Grundwasserleiter gelangen, die zur Trinkwassergewinnung verwendet werden. Bei zu hohen Salzkonzentrationen kann dies dazu führen, dass das Grundwasser nicht mehr als Trinkwasser verwendet werden kann oder hohe Aufbereitungskosten zustande kommen. Zusätzlich könnten Habitate oder Oberflächengewässer von hohen Salzkonzentrationen gefährdet werden.

Das Ziel dieser Arbeit ist es ein geeignetes Konzept zu entwickeln, wie diese Risiken unter Berücksichtigung von vielen Unsicherheiten (z.B. in den geologischen Daten) abgeschätzt werden können. Hierfür werden unterschiedliche numerische Modelle und Methoden verwendet. Um die Prozesse während der CO_2 Speicherung zu simulieren werden zwei unterschiedliche Modelle verwendet: Ein Zweiphasen-Modell, das die Phasen CO_2 und Salzwasser berücksichtigt und ein detaillierteres Modell, das auch die Lösung und Diffusion der beiden Komponenten in den Phasen betrachtet. Für die Simulation der Salzwasserverdrängung wird ein Einphasen-Modell, das die Komponenten Wasser und Salz berücksichtigt verwendet. Um die enormen Rechenzeiten, die durch die komplexen Modelle und den Bedarf von unzähligen Rechnungen aufgrund der vorhandenen Unsicherheiten zu reduzieren, werden

Methoden der Modellkopplung und Modellreduktion verwendet. Für die Modellreduktion wird die "Arbitrary Polynomial Chaos Expansion" verwendet. Eine Modellkopplung im Raum erlaubt die Berücksichtigung der unterschiedlichen relevanten Prozesse in den jeweiligen Teilgebieten.

Konzept für die Risikoabschätzung Die Untersuchung von Unsicherheiten und die Entwicklung eines geeigneten Konzepts um Risiken zu bestimmen ist ein Hauptziel dieser Arbeit. Das Risikokonzept unterteilt die Unsicherheiten in unterschiedlicher Level: Statistische Unsicherheiten in Parameterverteilungen, Szenariounsicherheit, zum Beispiel unterschiedliche geologische Strukturen und "recognized ignorance" (bewusstes Ausschließen von Prozessen), das durch Modellannahmen entsteht. Recognized ignorance und Szenariounsicherheit werden durch Simulationen von unterschiedlichen, eindeutig definierten Modellkonzepten und Szenarien untersucht. Der Schaden, der relevant für die untersuchten Prozesse und Ereignisse ist, wird als eine Modellausgabe der Simulationen definiert. Die underschiedlichen Modellsetups und Szenarien können dann anhand des Schadens bewertet, verglichen und klassifiziert werden. Für statistische Unsicherheiten können neben dem Schaden auch Wahrscheinlichkeiten bestimmt werden. Hierfür werden zahlreiche Monte Carlo Simulationen mit dem reduzierten Modell (unter Verwendung der "Arbitrary Polynomial Chaos Expansion") durchgeführt. Die Ergebnisse können auf verschiedene Arten dargestellt werden: Z.B. als Mittelwerte des Schadens, als Wahrscheinlichkeitsdichtefunktion, als kumulative Verteilungsfunktion, oder als übergreifender Risikowert durch Multiplikation des Schadens mit der Wahrscheinlichkeit. Analytische Abschätzungen können zusätzlich verwendet werden um den Schaden, der als Modellausgabe definiert ist, in Werte zu übertragen, die mit Richtwerten (z.B. Trinkwasserkriterien) verglichen werden können.

Risikoabschätzung für Salzwasserverdrängung Die Anwendung des Konzepts zur Risikoabschätzung auf die Untersuchung von Risiken, die mit der Salzwasserverdrängung verbunden sind ist ein Hauptteil dieser Arbeit. Eine wichtige Größe, die im Zusammenhang mit Salzwasserverdrängung bestimmt werden sollte, ist die Salzkonzentration die in Aquiferen, welche zur Trinkwassergewinnung genutzt werden auftreten kann. Die Unsicherheiten und Risiken werden in drei Ansätzen untersucht: Der erste Ansatz hat das Ziel das Konzept zur Risikoabschätzung zu testen, geologische Szenarien, die hohe Risiken bergen zu identifizieren und erste Risiko- und Schadenswerte für die betrachteten Szenarien zu bestimmen. Szenariounsicherheit, aufgrund von unterschiedlichen geologischen Strukturen und statistische Unsicherheiten aufgrund variierender Parameter werden untersucht. Eine wichtige Erkenntnis ist, dass es stark von der Geologie abhängt, ob Salzwasser aufgrund der CO_2 Speicherung in Grundwasseraquifere gelangt. Ein gutes Verständnis der Auswirkung unterschiedlicher geologischer Strukturen konnte abgeleitet werden. Die Risiko- und Schadenswerte dieses ersten Ansatzes sind sehr konservativ, da Lösungsprozesse von CO_2 vernachlässigt werden. Hierdurch entsteht eine größere CO_2 Fahne und mehr Salzwasser wird verdrängt. Zusätzlich wurde die Salinität über die Höhe des untersuchten Gebietes als konstant angenommen woraus wiederum höhere Salzkonzentrationen im Wasseraquifer entstehen, da normallerweise der Salzgehalt mit der Höhe abnimmt. Diese Annahmen werden als "recognized ignorance" klassifiziert.

Im zweiten Ansatz wird durch die Einführung eines variablen Salzgehalts im Gebiet die durch "recognized ignorance" hervorgerufene Unsicherheit reduziert. Um den hohen Rechenaufwand zu reduzieren wird ein Modellkopplungsansatz verwendet um das CO_2-Salzwasser Modell, das im Speicherreservoir für die Simulation benötigt wird mit einem Wasser-Salz Modell, das den variablen Salzgehalt modellieren kann in den darüber liegenden Aquiferen zu koppeln. Verschiedene Szenarien werden untersucht und mit dem ersten Ansatz verglichen. Wichtige Erkenntnisse über das Systemverhalten wurden dadurch gewonnen; zum Beispiel wird das Salz hauptsächlich entlang der Störungszone verdrängt und der gesamte Salzfluss in den Wasseraquifer ist kleiner im Vergleich zum ersten Ansatz.

Eine wichtige Information für Wasserversorger ist die Menge an Salz die während der Wasserproduktion am Brunnen auftreten kann. Aus diesem Grund wird im dritten Ansatz die Salzkonzentration am Produktionsbrunnen, die in Folge einer CO_2 Speicherung auftreten könnte in Abhängigkeit verschiedener Parameter bestimmt. Hierfür wird ein 2D Modellgebiet verwendet mit dem der Grundwasserfluss abgebildet werden kann. Erneut wird die "recognized ignorance" in diesem Fall aufgrund unterschiedlicher Gittertypen und deren Auflösung qualitativ untersucht. Zusätzlich wird der Einfluss von statistischer Unsicherheit aufgrund des Brunnenabstands, der Produktionsrate am Brunnen und der Durchlässigkeit im Aquifer ermittelt. Werte für Schaden und Risiko für die Salzkonzentration am Brunnen können bestimmt werden. Die Vermischung durch Dispersion und Diffusion im Aquifer hat einen erheblichen Einfluss auf die Salzkonzentration am Brunnen. Jedoch beeinflusst auch numerische Dispersion abhängig vom verwendeten Gitter die Ergebnisse am Brunnen. Der Abstand des Brunnens ist der dominanteste Parameter für die Salzkonzentration, da hierdurch die Zeit, die zum Vermischen zur Verfügung steht, stark beeinflusst wird.

Unsicherheitsstudien für realistische Speicherformationen Bevor Risiken für eine spezifische Speicherstätte untersucht werden können, sollte möglichst viel Wissen über die relevanten Unsicherheiten gesammelt werden, um diese für die Risikountersuchungen möglichst zu reduzieren. Im zweiten Teil der Arbeit werden darum unterschiedliche Unsicherheitsuntersuchungen für realistische Speicherformationen durchgeführt. Für das Pilotprojekt Ketzin in Deutschland stehen viele Messungen zur Verfügung. Trotzdem müssen für die Modellierung einige Annahmen getroffen werden. Der Einfluss unterschiedlicher Unsicherheiten aufgrund von Modellannahmen (Modellgröße, konzeptionelles Modell, Gittertypen), die alle zu der Kategorie "recognized ignorance" gehören, wird systematisch untersucht. Eine wichtige Aufgabe für die dynamische Modellierung im Zusammenhang mit der Speicherstätte Ketzin ist das "History matching" von Messdaten (Modellvalidierung anhand von Messdaten) insbesondere des Drucks am Injektionsbrunnen und der Ankunftszeiten des CO_2s an zwei Beobachtungsbrunnen. Die Ergebnisse des "History matching" sind sehr wichtig für zukünftige Risikoabschätzungen. Bei vorherigen Simulationen wurde die erste Ankunftszeit sehr gut vorausgesagt, der Druck und die zweite Ankunftszeit aber unterschätzt. In dieser Arbeit werden verschiedene Ansätze für "History matching" diskutiert und schließlich ein systematischer Ansatz um das Modell für die vorhandenen Datensätze zu kalibrieren entwickelt. Hierfür wird der Ansatz der inversen Modellierung verwendet um das Modell an den Druck über die ersten 50 Tage der Injektion und die erste Ankunftszeit anzupassen. Für die Kalibrierung werden das Permeabilitäts-, das Porosi-

tätsfeld und die relative Permeabilitätsbeziehung verändert. Eine Extrapolation für längere Zeitskalen ist möglich, jedoch limitiert. Um das Modell für den Simulationszeitraum von 1650 Tagen zu kalibrieren wurde ein zusätzlicher Freiheitsgrad eingeführt: die Unterteilung eines Nahfelds um den Injektionsbrunnen und eines Fernfelds. Das kalibrierte Modell kann den Druck für einen gewissen Extrapolationszeitraum voraussagen, jedoch ist die Voraussage der CO_2 Verteilung mit den gegebenen Permeabilitäts- und Porositätsdaten nur bedingt möglich. Zusätzlich werden unterschiedliche Unsicherheiten für eine realistische (aber virtuelle) Speicherformation im Norddeutschen Becken untersucht und bezüglich der Unsicherheitslevel klassifiziert. Das Ziel ist hier den Einfluss des durch die Injektion ausgelösten Druckanstiegs in einer Speicherformation auf eine zweite mögliche Speicherformation zu bestimmten. Folgende Faktoren beeinflussen die Druckausbreitung und den Effekt auf eine zweite Speicherformation besonders: Die gewählten Randbedingungen des Modellgebiets, die Kompressibilität des Gesteins und die Permeabilität des Reservoirs. Die Ergebnisse der Unsicherheitsstudien und des "History matching" stellen wichtige Informationen für zukünftige Risikoabschätzungen dar.

Abschließende Einordnung des Konzepts Im Schlussteil der Arbeit wird CCS im Kontext von Risikowahrnehmung diskutiert und der mögliche Beitrag des präsentierten Konzepts der Risikoabschätzung eingeordnet. Insgesamt stellt das Konzept eine systematische und verständliche Methode dar, um Unsicherheiten auf verschiedenen Leveln zu untersuchen und Risiken abzuschätzen. Das Konzept kann auf andere Gefährdungen angewendet werden, wie zum Beispiel CO_2 Lekagen oder Gefährdungen bei anderen Technologien im Untergrund wie z.B. Methanspeicherung oder Atommüllendlagerung. Die Anwendung des kompletten Konzepts auf eine realistische standortbezogene Speicherstätte ist ein wichtiger zukünftiger Schritt. Das entwickelte Konzept zur Risikoabschätzung wurde in das gesamtheitliche Risiko-Governance Modell (Risikoregulierungskette) eingeordnet und gehört zu der Phase der Risikoermittlung (risk appraisal). Diese Arbeit ist ein erster Schritt um die technische Risikoabschätzung für CO_2 Speicherung mit sozialwissenschaftlichen Ansätzen zu verknüpfen, indem es die quantitative Risikoabschätzung in den erweiterten Kontext des Risiko-Governance Modells stellt.

1 Introduction

When new technologies are introduced and tested, one important task is to assess the risks, which are related to these technologies. These risks should be preferably evaluated before the real operation starts. Both experiments and numerical simulations can be valuable tools to test a technology in advance. However, experimental assessments are often limited, especially for technologies related to the subsurface. Technologies which operate on large scales in the subsurface are especially difficult to test in small scale experiments. For these fields, methodologies based on simulations are required to systematically assess the risk associated with the technology. Examples for such technologies are atomic waste disposal and storage of methane or CO_2 in geological formations, which is the focus of this thesis.

Climate change is an important and highly debated topic worldwide. Between 1906 and 2005 the air temperature near the surface has risen by $0.74°C \pm 0.18°C$ (Trenberth et al. (2007)). An increase in temperature may have various negative impacts on freshwater resources, the ecosystem and human health, for example: the desertification of whole landscapes, which could reinforce hunger crises, the increase of the sea level, which could result in flooding of landscapes and salinization of groundwater resources (see Parry et al. (2007)). To avoid or reduce these impacts, the temperature increase should be stopped. The main gases which contribute to the greenhouse effect are water vapor, CO_2, methane, and nitrous oxide (Metz et al., 2005). The main contributor from human activities within the greenhouse gases is CO_2. The CO_2 emissions have risen substantially since the beginning of the industrialization from a pre-industrial value of ca. 280 ppm to 379 ppm in 2005 (Le Treut et al. (2007)). For the year 2012 Dlugokencky and Tans presented an annual mean CO_2 concentration of 392.55 ppm (with an uncertainty of 0.1 ppm). In the special report on Carbon Dioxide Capture and Storage published by the IPCC in 2005 (Metz et al. (2005)), different options are summarized to mitigate climate change: reducing energy consumption by increasing efficiency of energy conversion, using less carbon intensive fuels such as natural gas instead of coal, using more renewable energy sources, increasing biological absorption capacity in forests, or capture and store the CO_2 . To reduce the CO_2 emissions, it is important to further develop all these options. This work focuses on the last option i.e. carbon capture and storage (CCS). CCS can be seen as a transitional technology, that can help to bridge the time until, e.g., renewable energies are established on a sufficient scale to replace fossil-fuel power plants.

CCS includes different steps: first, the CO_2 is captured from power plants or industrial point sources. Therefore different technologies are possible such as post-combustion capture, pre-combustion capture, or oxyfuel combustion. For details about the combustion methods one is referred to Metz et al. (2005). In the second step, the CO_2 is transported to suitable storage sites via pipelines or ships. In a last step, the CO_2 is stored in deep geological formations, which is the focus of this thesis.

Suitable storage sites are depleted oil and gas reservoirs, saline aquifers or coal seams. The IPCC report (Metz et al. (2005)) defines three criteria for suitable storage sites: "a sufficient capacity and injectivity, a good sealing caprock, a stable geological environment". The largest storage potential worldwide is predicted for saline aquifers. For Germany, the Federal Institute for Geosciences and Natural Resources (BGR) predicted in 2010 a storage potential between 6.3 und 12.8 billion tonnes CO_2 (Knopf et al. (2010)). This work focuses on CO_2 storage in saline aquifers.

The CO_2 is stored in the pore space of the porous rock. Various trapping mechanisms are responsible for storing the CO_2 safely: *structural trapping* by a closed caprock, *residual trapping* in the porous rock, *solubility trapping* in the water phase, and *geochemical trapping* by reactions with the rock matrix (Metz et al. (2005)). Structural trapping by a caprock of low permeability is necessary because the CO_2 is lighter than the brine in the aquifer and will tend to rise. This trapping mechanism is most relevant in the first phase of the storage period. With proceeding time residual trapping and solubility trapping become relevant. Residual trapping means that the CO_2 is trapped in the pore space as an immobile phase. Solubility trapping means that the CO_2 dissolves in the surrounding brine, which results in an increase of the brine density and a downwards migration of the CO_2-rich brine. After long time scales, the CO_2 will also be trapped by forming minerals. Depending on the relevant trapping mechanisms, different processes are relevant at different time scales (see Figure 1.1).

In Germany, CCS is a highly debated topic and the majority of the informed public is very skeptical about the technology. The recent situation of CCS in Germany is very sensitive and the development in the last years will be discussed here for providing an understanding of the situation. A lot of research on CCS was established in Germany in the last decade. In 2008, injection of CO_2 started at the first small scale pilot site in Ketzin near Berlin in Brandenburg (Würdemann et al. (2010)). For further research, two industrial scale test sites in Schleswig Holstein and Brandenburg were planned and should have started in 2009. However, the projects were delayed and finally canceled due to protests of the population and due to a missing regulation. The protest in Brandenburg and Schleswig-Holstein is based on different reasons and the situation as it is described in Schulz et al. (2010) is shortly summarized. The pilot project at the Ketzin site was seen positively by the local population because of the economic benefit that could be gained from the test site. CCS was seen as a chance to support the important energy supply by the local brown coal power plants in Brandenburg. However, the plan of Vattenfall to explore possible storage sites for an industrial scale demonstration site invoked large resistance by the local population. They did not want to have a "disposal zone" for CO_2 in their backyard. In Schleswig-Holstein the situation was different. The CO_2 from another demonstration power plant in Nordrhein-Westfalen and not "their own CO_2" was planned to be stored in a storage site in Schleswig-Holstein. In addition, the support of CCS is at odds with the wind energy that is an important source of income for many farmers in Schleswig-Holstein. RWE tried to force the admission procedure for the industrial scale storage site, which additionally resulted in mobilization of the public against the project. Thus, local and also national protests forced the federal state government of Schleswig-Holstein to finally change their positive attitude towards CCS and they stopped supporting CCS.

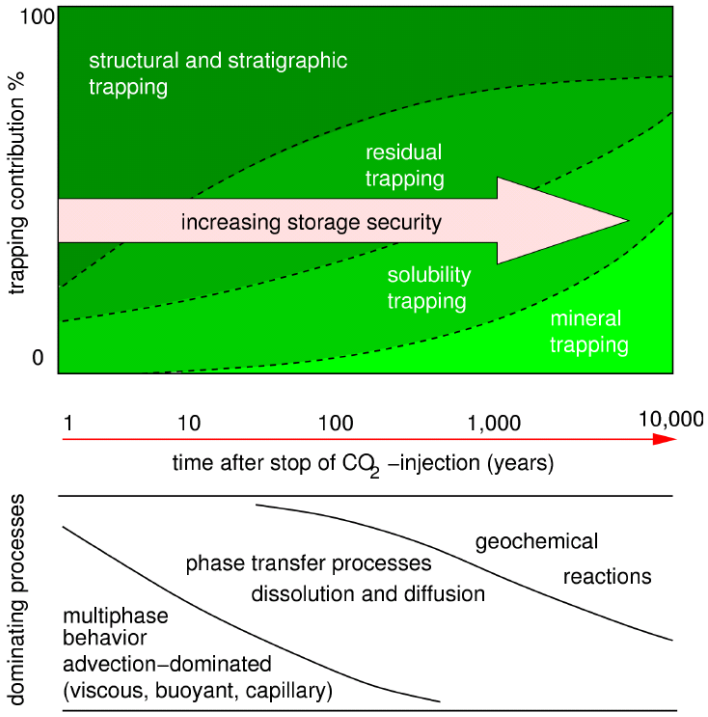

Figure 1.1: Trapping mechanisms and relevant processes at different time scales (modified according to IPCC report (Metz et al. (2005)).

The CO_2 storage technology is touched by many different fields of law such as mining law, water rights, and immission control. However, the new technology cannot be described completely by these laws. To this end, a new CCS law is needed for further research and test applications. The small scale pilot site in Ketzin is regulated by the mining law. However, the industrial size test sites have to be regulated by a new and problem-oriented law. For example, the liabilities have to be clarified; that means how long the operator is responsible for the storage site.

In 2009, the European Union passed a guideline about CCS, which regulates the selection, licensing procedure and the operation. This guideline is not directly valid for all EU-countries but all countries were forced to translate it into a national law within two years. In Germany, the first effort to establish a law started in 2009. However, the protest, especially in the affected parts of Germany (as described before) prevented the government from passing the law. After the elections in 2010, the new government had a controversial view and the new draft law was first finished in April 2011. The new law comprises a so called "Länderklausel", which gives each German Federal State the right to forbid CCS in its own state. However, it was not accepted by the Bundesrat (for more details see Schulz et al. (2010)). In the end of 2011, Vattenfall decided to stop their plans for the demonstration site in Brandenburg due to insufficient political support. In July 2012, the law ("Kohlenstoffdioxid-

Speichergesetz" KSpG) was finally passed, it includes the restriction that only 1.3 million tonnes of CO_2 per year and storage site are allowed to be stored and in total only 4 million tonnes per year are allowed to be stored all over Germany. The "Länderklausel" was also included and the law shall be evaluated in 2018 (BGBl Teil 1 Nr. 38)[1]. However, the research was already reduced, since for new insights into the technology, larger tests sites would be required.

As mentioned above, the main reason for the stop of the CCS research is the protest of the general public against the technology. An interesting point is that non-experts are predominantly against the technology whereas many experts in this field see the technology as a good way to reduce the CO_2 emissions. Why is the judgment of the non-experts and experts completely contradictory? The general public distrusts the feasibility of the technology and they see a high level of remaining risks and uncertainties. Thus, good and comprehensive risk assessment methods are required.

1.1 Risks Associated with CO_2 Injection and Risk Assessment Methods

Before discussing risks related to CO_2 storage a short definition of the wording is given. Hazards are defined in this context as "the potential of a technology, an event or an activity to cause harm to what people value" (Renn (2008a) p.50). In the context of risk assessment, "a hazard becomes a risk if a likelihood exists that this potential is released in a way that it produces harm" (Renn (2008a) p.50). The definition of risk is discussed in more detail in Section 3.1.1. In habitual language use, risk is often used in a wider sense and sometimes equivalent to hazard. In this work it is only distinguished between these words where it is important.

As stated before, risk assessment for new technologies is very important. Three main effects, which can cause local health, safety and environmental hazards are described in the IPCC report (Metz et al. (2005)): (i) effects of CO_2 gas phase at the subsurface or near the surface, which results from leaking CO_2 out of the reservoir, (ii) effects of the dissolved CO_2 on the groundwater chemistry and (iii) the effects of fluids which are displaced by the CO_2.

Thus, the events that are important to investigate for CO_2 storage in saline aquifers are CO_2 leakage, brine displacement and infiltration into freshwater aquifers, as well as structural failure due to large pressure peaks. In addition, the far-field pressure build-up is important to investigate because it is an indicator for brine displacement and brine infiltration.

If CO_2 leaks from a reservoir, it could rise to shallower aquifers or leak back to the atmosphere. CO_2 that leaks back to the atmosphere decreases the effectiveness of the storage, and under unfavorable conditions locally concentrated CO_2 can affect health, safety, and the environment. CO_2 is not a toxic substance but high CO_2 concentrations may lead to suffocation as a hazard to human health. A risk of suffocation can only arise if the CO_2

[1] Gesetz zur Demonstration und Anwendung von Technologien zur Abscheidung, zum Transport und zur dauerhaften Speicherung von Kohlendioxid, BGBl Teil 1 Nr. 38, 23.08.2012

is not mixed with the surrounding air as in confined outdoor environments, in caves or in buildings (Metz et al. (2005)). CO_2, that infiltrates into drinking water aquifers dissolves in the freshwater and decreases the pH-value. This could cause a decline in the drinking water quality. The change in pH could cause a change in the geochemical milieu, which can result in the mobilization of heavy metals which have the potential to cause environmental hazards. Very high concentrations of toxic metals could make the groundwater unsuitable for drinking.

The injected CO_2 will displace the initially present reservoir fluid. If CO_2 is injected into saline aquifers it will partly dissolve in the brine. The non-dissolved part of the CO_2 requires pore space, which is gained by compression of the fluids and the rock but mainly by displacement of the brine. The brine can be displaced horizontally over very large distances. The displaced brine could move into shallower aquifers through fractures, faults,

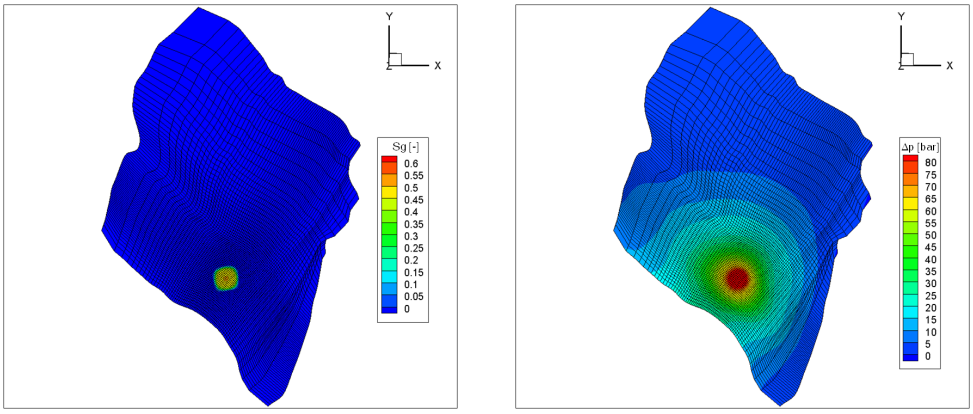

(a) CO_2 plume expansion. (b) Pressure evolution.

Figure 1.2: Comparison of the CO_2 plume and pressure evolution after 10 years of a CO_2 injection of 2.5 Mt/a in a domain of about 40 km x 40 km (Schäfer et al. (2011)).

or abandoned wells and subsequently infiltrate and pollute freshwater aquifers with salt and other contaminants. The increase of the salt content in the freshwater can exclude the groundwater for drinking or highly increase the costs for water production. In worst cases, wildlife habitats could be affected or surface water could be polluted. Figure 1.2 compares the extension of the CO_2 plume and the pressure evolution. The extension of the pressure evolution, which triggers the brine displacement is much larger than the extension of the CO_2 plume. Thus, CO_2 leakage has to be assessed locally around the injection zone, but brine displacement has to be evaluated in much larger domains. Large pressure peaks at the injection well can affect the rock matrix. Structural failures can occur and new leakage pathways can be formed. This can be avoided by an adequate injection strategy without exceeding certain threshold pressures. Figure 1.3 shows a schematic view of a CO_2 storage site and the possible events that could cause risks.

In the following a short literature review on risk assessment related to CO_2 storage is presented. One possible way to address the problem is to compare CO_2 storage with other natural or industrial analogues and to identify lessons, which can be learned, for risk assessment of CO_2 storage (e.g., Benson et al. (2002), Lewicki et al. (2007)). Benson et al.

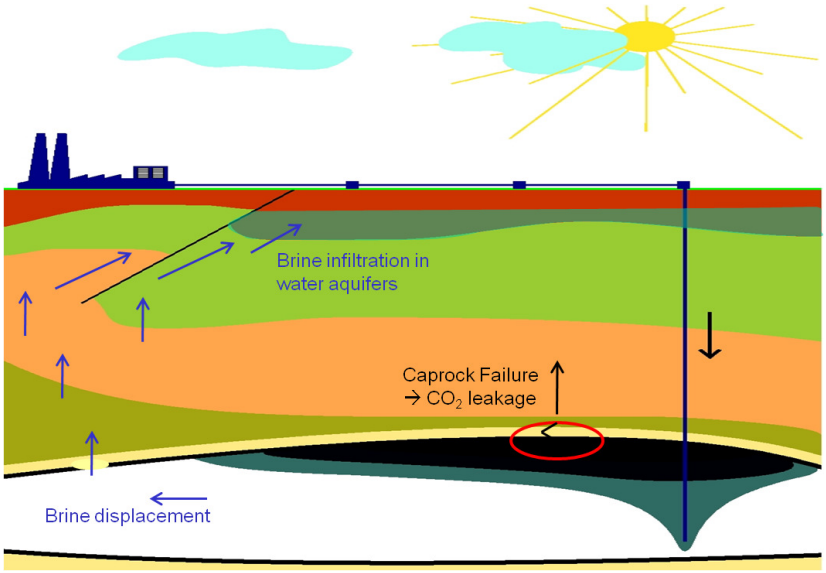

Figure 1.3: Schematic view of a CO_2 storage site and possible events, that may cause hazards/risks.

(2002) summarized the following five main lessons learned: (i) a lot of experience exists that suggests that CO_2 storage can be safe if geological storage sites are carefully selected and monitored; (ii) lots of information on human health effects due to CO_2 exposure are available; (iii) the nature of the release is more relevant than the size of the release; (iv) the experience from natural gas storage and deep injection of hazardous waste helps to understand the main risks of CO_2 storage; and (v) new regularities are needed for CO_2 storage since those of industrial analogues differ and do not address all important issues for CO_2 storage. Lewicki et al. (2007) identified features, events, and processes (FEPs) for CO_2 release based on these analogues and derived key lessons from these FEPs which should be adapted to risk assessment for CO_2 storage. Maul et al. (2007) discussed similarities and differences between radioactive waste disposal and CO_2 storage for performance and risk assessment. They summarized that there is a wealth of experience from radioactive waste disposal which is useful for CO_2 storage, e.g., the need to apply systematic and transparent methods and the need to get maximum information from natural systems.

Different applications for risk assessment for CO_2 storage can be found in the literature. The first approaches aim to select and rank storage sites among various possible sites and the second approaches investigate the hazards for one selected storage site. An example for selecting and ranking appropriate storage sites is presented in Bowden and Rigg (2004). They used quantitative techniques to determine risk estimates for key performance indicators of four different storage sites. Oldenburg (2008) developed a screening and ranking method for selecting suitable storage sites on the basis of health, safety and environmental risk occurring from CO_2 leakage. In Oldenburg et al. (2009), they presented a certification framework to certify storage sites based on safety and effectiveness. They describe an application of this risk assessment approach to evaluate CO_2 and brine leakage for the In Salah CO_2 storage project in Oldenburg et al. (2011).

Several projects investigate the risk of a particular site, e.g., the Weyburn site. These projects are summarized in Metz et al. (2005) (p.251). In Germany, risk assessment activities are ongoing at the pilot site Ketzin (Würdemann et al. (2010)). One approach to assess the risks for a particular storage site, is the FEPs (feature, events, processes) scenario approach. A list of FEPs is provided and their relevance is ranked by the user. Wildenborg et al. (2005) for example, presented a scenario approach as a methodology for long-term safety assessment for CO_2 storage. Their approach consists of three main steps: the scenario analysis based on identified FEPs, the model development and a consequence analysis. The method is presented for two CO_2 leakage scenarios, one along a fault and one through a failed well. In this approach risk is identified through different factors and no quantitative values are determined. Another approach is the probabilistic risk assessment, where quantitative risk information is provided and the likelihood of events can be calculated. Oladyshkin et al. (2011a) presented an approach to quantify the CO_2 leakage rate depending on different uncertain or design parameters with reduced computational costs. This approach will be applied in this work and is described in more detail in Section 3.2.2.

In the following, the different events and risks, which have to be considered and investigated for CO_2 injection applications and some examples of the current literature will be discussed. The first event is CO_2 leakage back to the atmosphere which would negate the goal of sequestration and could lead to suffocation hazard under unlikely situations; normally the CO_2 will quickly be mixed with the surrounding air. This was addressed by Lewicki et al. (2007), who compared the situation with natural analogues. Additionally, this effect is often addressed in studies which determine the potential of CO_2 leakage out of the reservoir, e.g., Oldenburg et al. (2009), Wildenborg et al. (2005), Pruess (2008), Kopp et al. (2010), Oladyshkin et al. (2011a), Celia et al. (2011), or Lu et al. (2012). For example, Kopp et al. (2010) addressed the risk related to CO_2 leakage by developing a risk assessment method for a leakage scenario, where the most relevant parameters and dependencies of all other parameters were used to estimate the risk by considering their range of variability. Celia et al. (2011) applied a semi-analytical model to evaluate the risk of CO_2 and brine leakage along old wells during the injection period for a specific field site in Alberta, Canada. They used a Monte Carlo framework to investigate the influence of, e.g., residual brine saturation or depth of injection. They concluded that residual brine saturation strongly influences the size of the CO_2 plume.

The impact of leaked CO_2 or displaced brine on groundwater resources is a highly relevant topic. Lemieux (2011) summarized the present scientific work regarding the potential impact of CO_2 storage into saline aquifers on groundwater resources. Two categories of impact are discussed: the near-field impact and the far-field impact. The near-field impact was defined as all risks due to the upwards migration of the CO_2 phase and the far-field impact is related to the risk due to brine displacement and infiltration into groundwater resources. For the near-field impact, the mobilization of trace elements are pointed out but still within the limits for potable water. The impacts of brine displacement are summarized as low impacts, however special geological situation can increase the risk. In the following some of the modeling studies will be shortly summarized for both the far-field impact and the near-field impact.

Bergman and Winter (1995) already mentioned that CO_2 could displace the initially present brine, which could change the flow velocity and hence the discharge rates into lakes or rivers. They also stated that the brine could move through permeable pathways into shallower zones and could affect drinking water aquifers. Several studies investigated the pressure evolution because the far-field pressure build-up is an indicator for brine displacement and possible brine infiltration into water aquifers. Birkholzer et al. (2009) investigated the pressure build-up in a stratified system and concluded that the far-field pressure evolution is very important to consider, especially for brine displacement and that the seal permeability significantly impacts the pressure buildup in shallower units. The regional impact of pressure for a storage scenario in the North German basin is discussed by Schäfer et al. (2011). Both studies show that very large domains are needed to predict the pressure without being influenced by the boundaries of the domain. Nicot (2008) investigated the large-scale extent of the pressure impact during CO_2 injection in the Golf Coast basin with an additional focus on brine displacement and its impact on fresh water aquifers. They simplified the investigations to a single phase problem, where the amount of water equivalent to the CO_2 mass is injected. Pressure perturbations in the freshwater updip section of the formation were observed but the water level change that is induced by the CO_2 injection is in the same order of magnitude as seasonal variations and the salinity was not significantly changed. However, they recommend that the risk to groundwater resources should be considered carefully. Yamamoto et al. (2009) investigated the large-scale pressure build-up on the regional groundwater flow for CO_2 injection into Tokyo Bay. For different parameters such as seal permeability, porosity, or compressibility, sensitivity studies were presented and they showed that these parameters could highly influence the prediction. They summarized that the groundwater pressure in shallower confined aquifers can rise by a few bar and that the groundwater discharge can be slightly increased. Keating et al. (2013) investigated the potential of upward intrusion of brine that is displaced by CO_2 rising along a fault zone. They concluded that upwards movement of CO_2 without salt intrusion can occur if the fault zone is wide and the CO_2 is mobile at low saturation. However, a narrow fault zone and nonlinear relative permeability relationships favor displacement of saline water along the fault and into a shallower aquifer.

CO_2 that leaks through abandoned wells, fractures, or faults can reach shallower groundwater aquifers. The CO_2 dissolves in the freshwater and increases the concentration of dissolved carbonate, which increases the acidity and decreases the pH (Lemieux (2011)). The decrease of pH is not a real problem for the water aquifer because carbonic acid is a weak acid and one would expect that it will be buffered by the minerals in the aquifer before decreasing to critical values. However, the decrease of pH will change the geochemical milieu. The solubility of minerals will strongly rise in a lower pH environment. These minerals can contain significant concentrations of hazardous trace elements such as arsenic or lead which will dissolve in the water. Additional to the dissolution of minerals containing hazardous trace elements, the decreased pH can also result in a mobilization of hazardous trace elements, which are originally adsorbed on the surface of existing minerals. This mobilization due to desorption is seen to be more relevant than the dissolution of minerals (Zheng et al. (2009) and Apps et al. (2010)). It is expected that the increase of hazardous trace elements will be the main impact on drinking water quality. Laboratory and field observations were

performed, e.g., Kharaka et al. (2010) investigating the changes in the concentration of various compounds during CO_2 injection on the ZERT (Zero Emission Research and Technology Center) test field in Bozeman, Montana. Food-grade CO_2 was injected into the shallow subsurface to investigate, e.g., near surface CO_2 detection techniques or groundwater geochemistry. The field measurements of Kharaka et al. (2010) showed a rapid decrease of pH and increase of alkalinity and electrical conductance. In additional laboratory analyses an increase in the concentration of trace metals (e.g. Pb, Fe, As, Cd) was shown. Several numerical investigations can be found in the literature. Wang and Jaffe (2004) presented the first 2D reactive-transport model to investigate the effect of CO_2 intrusion on pH change and trace metal solubilization. They investigated the effect of decreasing pH on the dissolution of galena (PbS) and the resulting mobilization of lead (Pb). The lead concentration was lower for an aquifer well buffered by calcite. However, they do not include any adsorption/desorption processes. A more realistic generic study was carried out by the Lawrence Berkley National Laboratory (Birkholzer et al. (2008), Zheng et al. (2009), and Apps et al. (2010)). For example, Zheng et al. (2009) included adsorption and desorption beneath the dissolution processes and investigated the mobilization of lead and arsenic resulting from the pH change during CO_2 intrusion into a groundwater aquifer. They concluded that both the lead and arsenic concentrations clearly rise, however the critical value (maximum contamination level of the US EPA) was not exceeded. Additionally, they also stated that the adsorption/desorption processes are more relevant for mobilization of lead and arsenic than the dissolution processes. Siirila et al. (2012) presented a quantitative methodology to assess the risks to human health, that can occur if CO_2 leaks into groundwater. They summarized that flow and transport parameters are the basis for assessing the risks.

1.2 Scope and Structure of the Thesis

The primary aim of this thesis is to develop a concept to systematically investigate different levels of uncertainties and to assess the risks associated with CO_2 storage. The risk assessment concept will be presented for brine displacement and infiltration into freshwater aquifers. Complex models, large model domains, and long time scales are required for the simulations, which result in high computational costs. In addition, many Monte Carlo simulations are needed to determine probabilities. These challenges will be managed by applying techniques to reduce the computational costs: a model reduction technique via polynomial chaos expansion for running Monte Carlo simulations and a spatial model coupling approach for considering only the relevant processes in different domains are applied. For risk assessment, uncertainties in the model set-up or in the scenarios should be reduced as much as possible. Thus, uncertainty studies for the pilot site Ketzin and a theoretical storage formation in the North German Basin are presented. In addition, a history matching procedure is proposed for the pilot site Ketzin to reduce uncertainties for further risk assessment studies.

In Chapter 2, the basic quantities, relationships, functions, and processes, which are needed for the simulation of CO_2 storage and corresponding brine displacement modeling are described. Chapter 3 summarizes different concepts of risks, the risk governance model, and

basics for the technical risk assessment. In Chapter 4, the overall concept how to handle uncertainties and to assess risk is described. Applications for the risk assessment concept are presented in Chapter 5. In the first section, the concept is applied for investigation of statistical and scenario uncertainties for brine displacement and infiltration. Recognized ignorance is investigated and reduced by applying a model coupling approach in the second part. The chapter ends with investigations of recognized ignorance and statistical uncertainties for a drinking water production scenario. Chapter 6 focuses on uncertainty studies for two realistic storage scenarios: the pilot project Ketzin and a potential (but virtual) storage site in the North German Basin. For the Ketzin site, a systematic history matching is applied to calibrate the model to measurement data. The work is summarized and discussed in Chapter 7. In addition, CCS is discussed in the context of different risk perception classes and an attempt is given to interpret the situation of CCS in Germany. In the end, an outlook for future work, for example to apply the risk assessment concept to the pilot site Ketzin is given. Parts of this thesis are published in Walter et al. (2012). In this paper, mainly Section 5.1 and parts of Chapter 4 are included.

2 Numerical Simulation of Multiphase Flow in Porous Media

2.1 Definitions

The processes during CO_2 storage in geological formations are all related to processes in the porous underground. In this thesis, different multiphase, multicomponent models are applied to risk assessment and uncertainty studies for CO_2 storage processes. In the following chapter, some basic definitions about multiphase flow in porous media are summarized. Helmig (1997) can be referred for more detail. The CO_2-brine model concept is based on the original model implemented in MUFTE-UG described in Bielinski (2006) and Kopp (2009). The DuMu^x implementation of the CO_2-brine model which is applied in this work is presented in Darcis (2012).

2.1.1 Scales

Physical processes and properties can be described on different scales, e.g, the molecular scale, the microscale, or the macroscale. On the molecular scale the properties of single molecules and the interactions between the molecules are described. The consideration of individual molecules would result in high computational costs because of the large number of molecules. To reduce the computational costs, one possibility is to describe groups of molecules and average the properties over all containing molecules. This averaging process over a sufficient amount of molecules is described by the continuum approach that assumes continuous matter. On the microscale an averaging is done over the molecular scale assuming the continuum approach. On this scale, the information of the geometry of the porous medium, the distribution of the fluid phases, and the pore space distribution are still available. The averaging over the microscale properties gives rise to the macroscale. On this scale the quantities are averaged over a representative elementary volume (REV), which has to be large enough to assure its properties are independent on its size. Thus, the porous medium is treated as a continuum and information of, e.g., pore space distribution is lost. New basic equations, e.g., Darcy's law and new parameters, e.g., porosity or saturation are created. The macroscale is also called Darcy or REV scale in this context.

2.1.2 Phases and Components

On the continuum scale phases are introduced. Each phase is described by distinct properties as e.g. density, viscosity. Two phases are separated by a sharp interface, where the

thermodynamic properties suddenly change. Solid, liquid and gaseous phases can exist. A phase can consist of one type of molecules or several different types of molecules (components).

In the current work, two fluid phases are relevant: the wetting phase (w) water/brine and the nonwetting phase (n) CO_2 and one solid phase: the porous matrix. In deep geological saline storage sites, the water contains a certain amount of salt. Therefore, the formation fluid is called brine. Brine consists of water and a high content of total dissolved solid (TDS). In this work, only the major component sodium chloride (NaCl) is considered. In the one-phase two-component model that will be described in Section 2.4.3, the amount of NaCl is variable and can become zero, which results in the existence of pure water. The relevant components are CO_2 , H_2O and sodium chloride (NaCl). If the pseudo component brine is used in a model it is defined as a mixture of H_2O and NaCl.

2.1.3 Mass Fraction, Mole Fraction and Salinity

The composition in a phase is described by mass or mole fractions. The mass fraction of component κ in phase α is defined as:

$$X_\alpha^\kappa = \frac{m_\alpha^\kappa}{\sum_i m_\alpha^i}\,, \tag{2.1}$$

where the mass of component κ in phase α is m_α^κ. The mole fraction is defined similarly:

$$x_\alpha^\kappa = \frac{n_\alpha^\kappa}{\sum_i n_\alpha^i}\,, \tag{2.2}$$

where n_α^κ is the number of moles of component κ in phase α. In each phase the sum of the mole or mass fractions has to be unity. Mass and mole fractions are related via the molecular weight $M = m_\alpha^\kappa / n_\alpha^\kappa$. In this work mass fractions are used in all models.

As described before, the formation water in saline aquifers contains a significant amount of salt. In this work only NaCl will be considered. To describe the amount of salt dissolved in the formation water the salinity S is used. The salinity is defined as the ratio of the mass fraction of salt (NaCl) to the total mass of the solution in $kg_{NaCl}/kg_{solution}$. In all models where a CO_2 phase can exist the salt content is not modeled as a variable component but is set to a constant salinity value. In the one-phase two-component model considered in this work salt is modeled as its own variable component.

2.1.4 Properties of the Porous Medium

On the macroscale, the porosity and the intrinsic permeability are the most important properties of the porous medium. If nonisothermal effects are taken into account the heat capacity and heat conductivity have to be considered as well.

Porosity The porosity ϕ is defined as the volume fraction of pore space in the REV divided by the volume of the total REV. For CO_2 storage the porosity is an important quantity because it describes the pore space where CO_2 can be stored.

Intrinsic Permeability The intrinsic permeability $\mathbf{K}$ is a measure for the resistance that a fluid encounters by the porous medium. The resistance is dependent upon the pore size and shape of the pores and how the pores are connected with each other.

Heat Capacity The heat energy that is necessary to increase the temperature of the porous medium, is described by the heat capacity c_s of the solid matrix.

Heat Conductivity The heat conductivity describes a proportionally constant for the flow of thermal energy caused by a temperature gradient. To describe the heat conduction in a porous media containing fluids, local thermal equilibrium is assumed and the heat conductivity is averaged. The approach proposed by Somerton et al. (1974) applied:

$$\lambda_{pm} = \lambda_{pm}^{S_w=0} + \sqrt{S_w}(\lambda_{pm}^{S_w=1} - \lambda_{pm}^{S_w=0}) + \sqrt{S_n}(\lambda_{pm}^{S_n=1} - \lambda_{pm}^{S_n=0})\,. \tag{2.3}$$

2.1.5 Properties for Fluid-Porous Media Interactions

Fluids that flow through the porous medium interact with the rock matrix. If more than one fluid is present the following properties describe the fluid-matrix interactions.

Saturation The saturation of phase α (S_α) is a quantity which is defined on the REV scale and represents as the ratio between the volume that is filled by the fluid phase α and the total pore volume. In addition, the sum of the saturations of all fluid phases has to be one.

Residual Saturation The residual saturation $S_{\alpha r}$ defines the amount of fluid phase α that is held back in the pore matrix when the fluid phase is displaced by another fluid phase.

Relative Permeability The relative permeability $k_{r\alpha}$ accounts for the resistance due to the interactions between the fluid phases if more than one fluid phase is present. The flow behavior of one phase is disturbed by the other phase because the pore space where the fluid phase can flow through is reduced by the other fluid phase. On the macroscale, these effects are represented by a relative permeability saturation relationship $k_{r\alpha}(S_\alpha)$ of phase α, which is bounded between 0 and 1 and is multiplied with the intrinsic permeability in the Darcy equation (see Section 2.3.1). For all examples shown in this work except for the Ketzin example presented in Section 6.1, the relation of Brooks and Corey (1964) is adopted for relative permeability of the wetting phase k_{rw}

$$k_{rw} = S_e^{\frac{2+3\lambda}{\lambda}} \tag{2.4}$$

and of the nonwetting phase k_{rn}

$$k_{rn} = (1 - S_e)^2(1 - S_e^{\frac{2+\lambda}{\lambda}}) \tag{2.5}$$

with the effective permeability $S_e = \frac{S_w - S_{wr}}{1 - S_{wr}}$ and the fitting parameter λ.

Capillary Pressure At the interface between two phases, forces caused by surface tension (molecular cohesion effects within the phases and adhesion effects between the phases) cause a pressure difference at the interface between the phases, the capillary pressure p_c (Helmig (1997)). On the microscale the capillary pressure is defined by the Laplace equation (see Helmig (1997)). On the macroscale a semi-empirical formulation with the capillary pressure as a function of the saturation is applied: $p_c = p_c(S_w)$. In this work the formulation of Brooks and Corey (1964) is used:

$$p_c = p_d \, S_e^{-\frac{1}{\lambda}} \, , \tag{2.6}$$

where p_d is the entry pressure which has to be overcome by the nonwetting phase to displace the wetting phase from the largest pore. The wetting phase pressure p_w and the nonwetting phase pressure p_n are related via the capillary pressure in a two-phase system:

$$p_w = p_n - p_c \, . \tag{2.7}$$

2.2 Fluid Properties

As described in Section 2.1.2, the following fluid phases are considered: CO_2 and water/brine. Figure 2.1 shows the different possible phase states of CO_2: gaseous, liquid, and supercritical. To assure the highest storage safety, CO_2 is preferably stored in supercritical state, which is reached for a pressure of 73.8 bar and a temperature of 30.95°C (critical point). This conditions are present in a minimum depth of about 800 m, which should be chosen for a storage site. The supercritical state is preferable because the CO_2 has a gas-like viscosity and a liquid-like density. The viscosity leads to a low flow resistance and the higher density leads to a reduction of the buoyancy forces and the best utilization of the storage volume. For the considered ranges of pressure and temperature brine is always present in liquid state.

The relevant properties for describing the fluid flow are the density and the viscosity. If nonisothermal effects are considered the fluid enthalpy and the internal energy need to be defined as well. These properties are shortly introduced in the following for each phase that is considered in this work. For a detailed description and visualization of the functions one is referred to Bielinski (2006) and Darcis (2012).

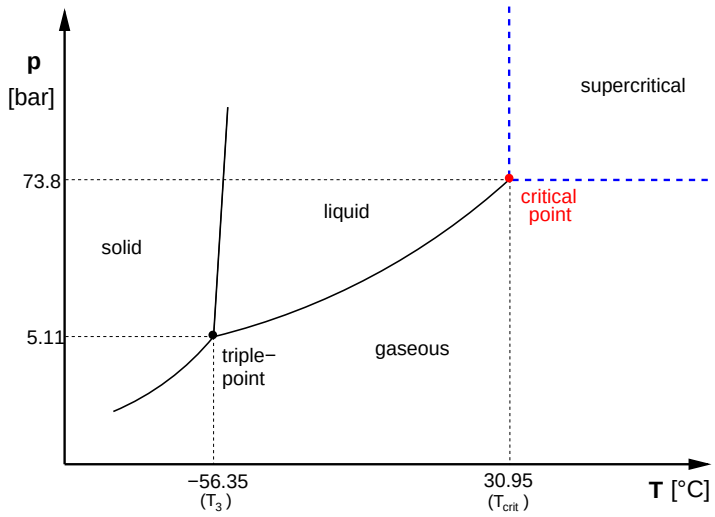

Figure 2.1: Phase diagram of CO_2 (Bielinski (2006)).

2.2.1 Density

The density ϱ defines either the mass m or the mole n per unit volume V. In this work the mass density is used:

$$\varrho = \frac{m}{V} \,. \tag{2.8}$$

The density of the CO_2 phase depends on pressure and temperature, according to the formulation presented in Span and Wagner (1996). Overall, the CO_2 density is decreased with increasing temperature and decreasing pressure. For a detailed description see Darcis (2012). The brine density depends on temperature, pressure, salinity, and the amount of dissolved CO_2. The formulations for density of pure water, and for the influence of salinity and CO_2 dissolution can be found in IAPWS (1997), Batzle and Wang (1992), and Garcia (2001). The brine density slightly decreases with increasing temperature. A salinity increase and the dissolution of the dissolution of CO_2 in brine increases the density as well.

2.2.2 Viscosity

The viscosity is a measure of the resistance of a fluid that is raised against shear or tensile stress. The dynamic viscosity μ is defined as the shear stress τ_s divided by the velocity gradient:

$$\mu = \frac{\tau_s}{dv_x/dy} \,. \tag{2.9}$$

The kinematic viscosity ν is linked to the dynamic viscosity by the density:

$$\nu = \frac{\mu}{\varrho} \,. \tag{2.10}$$

The viscosity of the CO_2 phase is a function of pressure and temperature and is defined according to Fenghour et al. (1998). Increasing the pressure results in an increase of the CO_2 viscosity and increasing the temperature decreases its viscosity. The brine viscosity is a function of temperature and salinity and is described according to Batzle and Wang (1992). The influence of pressure on the brine viscosity is negligible. With increasing temperature the brine viscosity decreases and with increasing salinity the brine viscosity increases.

2.2.3 Internal Energy and Enthalpy

The specific internal energy u is the total energy of a molecule pro mass unit. It contains of kinetic energy due to the motion of the molecules and of potential energy due to interactions between the molecules. Specific enthalpy is defined as the total energy of a system, which comprises the internal energy and the volume changing work. The specific enthalpy h is defined as:

$$h = u + pv\,. \tag{2.11}$$

with the specific volume v. The CO_2 phase enthalpy is defined following Span and Wagner (1996) and is a function of pressure and temperature. For the brine enthalpy which is a function of pressure, temperature, salinity, and the amount of dissolved CO_2 the relations given in IAPWS (1997), Michaelides (1981), and Duan and Sun (2003) are applied.

2.2.4 Solubility

Between the CO_2 and brine phases, mass is transferred. In the model implemented in MUFTE-UG, the solubility of CO_2 in brine was implemented according to the approach presented by Duan and Sun (2003). Kinetic effects are neglected, thus the equilibrium mass fraction of CO_2 in brine is dependent on the temperature, pressure and the salt content in the brine phase. The solubility of H_2O in the CO_2 phase was set to a constant equilibrium value. In DuMu^x a relation for both the solubility of CO_2 in brine and of H_2O in the CO_2 phase is implemented. The approach proposed by Spycher and Pruess (2005) is followed. The equilibrium compositions in both phases are described depending on temperature, pressure, and salt content (for details see Darcis (2012)).

2.3 Transport Processes

In this section the flow and transport processes, which are relevant for the different applications studied in this work, such as CO_2 storage and brine displacement are explained.

2.3.1 Advection

Advection is a mass transport process due to a velocity field. The driving forces are pressure gradients or density differences. The velocity can be described by Darcy's law:

$$\mathbf{v} = -\frac{\mathbf{K}}{\mu}(\text{grad}p - \varrho\mathbf{g}) \,, \tag{2.12}$$

where $\mathbf{v}$ is the Darcy velocity and $\mathbf{g}$ the gravity vector. If more than one phase is considered, the extended Darcy equation for each phase α including the relative permeability is used.

$$\mathbf{v}_\alpha = -\frac{k_{r\alpha}\mathbf{K}}{\mu_\alpha}(\text{grad}p_\alpha - \varrho_\alpha\mathbf{g}) \,. \tag{2.13}$$

In the context of CO_2 storage, advective flux due to pressure gradients results mainly from the injection of CO_2. If the driving forces are density differences then the term buoyancy is used. Buoyancy is an important process in this field of applications because the CO_2 is much lighter than the surrounding brine and tends to rise.

2.3.2 Molecular Diffusion

Molecular diffusion is a process that is caused by concentration gradients. The diffusive flux can be described by Fick's first law:

$$\mathbf{j_d} = -\varrho_{mol,\alpha}\mathbf{D}^\kappa_{\alpha,pm}\ \text{grad}x^\kappa_\alpha \,. \tag{2.14}$$

The effective diffusion coefficient $\mathbf{D}^\kappa_{\alpha,pm}$ is smaller compared to the molecular diffusion coefficient $\mathbf{D}^\kappa_{\alpha,m}$ because of the tortuous and longer path lines in the porous medium. To this end, the tortuosity τ is taken into account and for the effective diffusion coefficient $\mathbf{D}^{\kappa,pm}_\alpha$ yields:

$$\mathbf{D}^\kappa_{\alpha,pm} = \phi\tau S_\alpha \mathbf{D}^\kappa_{\alpha,m} \ . \tag{2.15}$$

According to Bielinski (2006) the molecular diffusion coefficient of CO_2 in brine is $D^{CO_2}_w = 2 \cdot 10^{-9} m^2/s$. The molecular diffusion coefficient of water in CO_2 is a function of the temperature and gas-phase viscosity (for details see Darcis (2012)). For the molecular diffusion coefficient of salt (NaCl) in water (considered in the 1p2c model) a constant value of $D^{NaCl}_w = 1.587 \cdot 10^{-9} m^2/s$ (Riquelme et al. (2007)) is taken.

2.3.3 Dispersion

Dispersion is a process resulting from fluctuations in the velocity field. The velocity field is normally heterogeneous in nature, which results in spreading and mixing of the dissolved substances. Since the variability of the velocity field can not be resolved on all scales its effect is described as an upscaled process called dispersion. On the microscale dispersion results from the parabolic velocity profile of the fluids in the pore channels. Dispersion

on the macroscale occurs due to the heterogeneity of the properties of the porous medium. Thus, dispersion is scale dependent. On the Darcy scale, the dispersive flux is described similar to the diffusion process by adding the dispersion coefficient to the effective diffusion coefficient:

$$\mathbf{D} = \frac{\mathbf{v}\mathbf{v}^T}{||\mathbf{v}||}(\alpha_l - \alpha_t) + \mathbf{I}(D_{pm} - \alpha_t)||\mathbf{v}||\,, \tag{2.16}$$

where α_l and α_t are the longitudinal and transverse dispersivities, and D_{pm} is the diffusion coefficient of Equation 2.14. In a multiphase system, the data known about dispersivities is rare, therefore, dispersion is only considered for the one phase water-salt model and neglected for the two phase CO_2-brine model.

2.3.4 Heat Convection and Heat Conduction

The transport of heat with the fluid flow is referred to as heat convection. In the energy balance, heat convection is considered similar to advection. The other process that is taken into account for heat transport is heat conduction, which is caused by temperature differences. The direction of the heat flow is always in opposite direction to the temperature gradient. Heat conduction is described by the Fourier's law:

$$\mathbf{q}_c = -\lambda_{pm}\text{grad}T\,, \tag{2.17}$$

where λ_{pm} is the heat conductivity. The CO_2 storage process is dominated by convective heat flux during the injection phase. After the injection stops, the temperature change due to the CO_2 injection is reduced by heat conduction until the initial temperature field is rebuilt.

2.4 Model Concepts

In this thesis, three model concepts are used. For modeling CO_2 storage processes two different model concepts are applied: either a two-phase model with the phases CO_2 and brine, or a (nonisothermal) two-phase, two-component model with the phases and components CO_2 and brine. The first approach, the two-phase model consists of two separate immiscible fluids in the porous matrix. The advective transport of brine and CO_2 is modeled and dissolution and diffusion are neglected. The negligence of dissolution results in a larger free CO_2 plume and a higher pressure increase, which is a conservative approximation for simulation of CO_2 storage. This approach is appropriate for risk assessment applications since often worst case situation are investigated. A more exact concept is to apply a (nonisothermal) two-phase, two-component model. This approach includes dissolution and diffusion processes of the components and accounts for nonisothermal effects. Nonisothermal processes are neglected for several applications in this work to reduce computational costs. The third concept is a one-phase, two-component model, with the fluid phase water/brine and the components water and salt to model the salt distribution in freshwater aquifers. In the following, the balance equations for the different models are presented.

2.4.1 Two-phase (2p) Model

The two-phase (2p) model considers two immiscible fluids. For each phase α, a mass balance equation is solved:

$$\frac{\partial(\phi \varrho_\alpha S_\alpha)}{\partial t} - \operatorname{div}\left\{\varrho_\alpha \frac{k_{r\alpha}}{\mu_\alpha}\mathbf{K}\left(\operatorname{grad} p_\alpha - \varrho_\alpha \mathbf{g}\right)\right\} - q_\alpha \quad = \quad 0, \qquad \alpha \in \{w, n\}. \tag{2.18}$$

with the porosity ϕ, the phase density ϱ_α [kg/m^3], the phase saturation S_α, the relative phase permeability $k_{r\alpha}$, the dynamic viscosity μ_α [kg/(m s)], the intrinsic permeability tensor $\mathbf{K}$, the phase pressure p_α, the gravity vector $\mathbf{g}$ and the source and sink term q_α [kg/(s m^3)]. As primary variables for the CO_2-brine problem, the pressure of the wetting brine phase p_w and the CO_2 (nonwetting) saturation S_n are chosen. The following auxiliary conditions have to be fulfilled:

$$\sum_\alpha S_\alpha = 1 \quad \text{and} \quad p_w = p_n - p_c(S_w)\,. \tag{2.19}$$

Rock compressibility is accounted for by the following equation:

$$\phi(p_n) = \phi_{init}(1 + C(p_n - p_n^{ref}))\,, \tag{2.20}$$

where Φ [-] is the effective porosity, ϕ_{init} [-] the initial porosity, C the rock compressibility of $4.5 \cdot 10^{-10}$1/Pa (see Birkholzer et al. (2009)), p_n [Pa] the gas pressure, and p_n^{ref} [Pa] the initial reference pressure.

2.4.2 (Nonisothermal) Two-phase, Two-component (2p2c(ni)) Model

For the 2p2c and the 2p2cni models, two compositional mass balance equations have to be solved:

$$\begin{aligned}&\frac{\partial(\phi \sum_\alpha \varrho_\alpha X_\alpha^\kappa S_\alpha)}{\partial t} - \sum_\alpha \operatorname{div}\left\{\varrho_\alpha X_\alpha^\kappa \frac{k_{r\alpha}}{\mu_\alpha}\mathbf{K}\left(\operatorname{grad} p_\alpha - \varrho_\alpha \mathbf{g}\right)\right\} \\ &- \sum_\alpha \operatorname{div}\left\{\mathbf{D}_{\alpha,pm}^\kappa\ \varrho_\alpha \operatorname{grad} X_\alpha^\kappa\right\} - \sum_\alpha q_\alpha^\kappa \quad = \quad 0 \qquad \kappa \in \{w, n\}.\end{aligned} \tag{2.21}$$

In addition to the equations given in (2.19), a further auxiliary condition has to be fulfilled for each phase in the 2p2c/2p2cni model:

$$\sum_\kappa X_\alpha^\kappa = 1\,. \tag{2.22}$$

As in the 2p model it is accounted for compressibility by Equation 2.20. If nonisothermal effects are taken into account (2p2cni model), an additional energy equation has to be solved

for this model. Only one energy equation is required for all phases because local thermodynamic equilibrium is assumed, which means that the temperature of all fluid phases and the solid phase is equal locally:

$$\frac{\partial \left(\phi \sum_\alpha \varrho_\alpha u_\alpha S_\alpha\right)}{\partial t} + (1-\phi)\frac{\partial(\varrho_s c_s T)}{\partial t} - \sum_\alpha \operatorname{div}\left\{\varrho_\alpha h_\alpha \frac{k_{r\alpha}}{\mu_\alpha}\mathbf{K}\left(\operatorname{grad} p_\alpha - \rho_\alpha \mathbf{g}\right)\right\}$$
$$-\operatorname{div}\left(\lambda_{pm}\operatorname{grad} T\right) - q_h \quad = \quad 0\,, \tag{2.23}$$

where ϱ_s is the density of the solid matrix.

2.4.3 Single-phase Two-component (1p2c) Model

This model describes the transport of a salt component in a single fluid phase brine/water. The following mass balance is solved for the fluid phase:

$$\frac{\partial(\phi\,\varrho)}{\partial t} - \operatorname{div}\left\{\varrho\,\frac{\mathbf{K}}{\mu}\left(\operatorname{grad} p - \varrho\,\mathbf{g}\right)\right\} - q \quad = \quad 0\,. \tag{2.24}$$

For the dissolved salt component, a transport equation can be derived:

$$\frac{\partial(\phi\,\varrho\,X)}{\partial t} - \operatorname{div}\left(\varrho\,\frac{\mathbf{K}\,X}{\mu}\left(\operatorname{grad} p - \varrho\,\mathbf{g}\right) + \varrho\,\tau\,\phi\,\mathbf{D}\operatorname{grad} X\right) \quad - q \quad = 0\,, \tag{2.25}$$

where X is the mass fraction of the dissolved salt component, τ is the tortuosity and $\mathbf{D}$ is either the diffusion coefficient or the dispersion coefficient [m^2/s] (see Section 2.3.2 and 2.3.3) depending on which processes are considered. The primary variables are the water/brine pressure p and the mass fraction of the dissolved salt component X_s. Rock compressibility is also applied in the 1p2c model (see Eq. 2.20).

2.4.4 1p2c - 2p Model Coupling

Various approaches for model coupling exist in the literature. In Darcis (2012), an overview of the various coupling approaches is given. Two main reasons for model coupling are discussed: increasing the capability of a model by coupling models with different features or reducing computational time by coupling models in space or time. In this work model coupling is adapted to reduce the enormous computational costs due to the complex processes that have to be considered for the described applications. One possibility to reduce computational time is to couple models of different complexity in space. In many applications different processes are relevant in different regions of the model domain. In this thesis, the spatial coupling concept presented by Mosthaf et al. (2011) is adapted to the brine displacement problem. For brine displacement and infiltration into freshwater aquifers resulting from CO_2 injection, different processes are relevant in separate regions. The CO_2 injection process into the storage reservoir is dominated by the CO_2 flow. In this region, it is necessary to describe the advective processes of CO_2 and brine or even dissolution and diffusion processes. Above the storage reservoir the salt migration is the relevant process, e.g. to assess

the salt infiltration into freshwater resources. In this region, it is not necessary to describe the CO_2 phase if it is assumed that CO_2 will not leak out of the reservoir. To describe the salt migration process, one fluid phase and two components have to be considered. Thus, a 2p model could be applied in the region where CO_2 migrates, if dissolution and diffusion is neglected. A 1p2c model can describe the processes in the region above instead of modeling the complete region with a 2p3c model. A 2p3c model would need to solve 3 equations in the whole domain. The coupling approach reduces the number of equations to 2 in both regions. At the interface between the two domains coupling conditions have to be applied, which will be described in Section 5.2 where the application is introduced.

2.5 Discretization Methods

For most of the numerical simulations the simulator DuMu^x (DUNE for Multi-Phase, Component, Scale, Physics, ...) is used (Flemisch et al. (2011)). DuMu^x is a tool for simulating multiphase flow and transport processes in porous media. DuMu^x is based on DUNE, the Distributed and Unified Numercis Environment, a framework for solving partial differential equations. All described model concepts are implemented in DuMu^x. For some of the examples in Chapter 6, the CO_2 model implemented in the precursor simulator MUFTE-UG was used (see Bielinski (2006)). All equations required by the models are discretized using either a fully-coupled-vertex-centered finite volume (box) scheme or a cell-centered finite volume method for spatial discretization and the implicit Euler method for time discretization.

Time Discretization In the implicit Euler scheme, all unknowns are evaluated for the new time step. For the time derivatives a backward difference approximation is used.

Spatial Discretization Most of the applications are discretized using the fully-coupled vertex-centered finite volume scheme (box method). The box method is locally mass conservative and can handle unstructured meshes such as tetrahedron meshes. For the box method a secondary finite volume mesh is constructed based on a finite element mesh by connecting the barycenter of the element with the midpoints of the element edges. The fluxes are balanced over the subcontrol volumes of each element and the discrete values are calculated at the nodes of the elements. For the Ketzin example (see Section 6.1), the cell-centered finite volume method is used because the hexahedron mesh resulted in better convergence than using the box method. The cell-centered finite volume method is robust and mass conservative, but it is restricted to structured meshes. For the cell centered finite volume method only one finite volume mesh is required. The fluxes are balance over these control volumes and all discrete values are determined at the center of the grid cell.

3 Introduction to Risk and Risk Assessment

In this chapter, the main basics of the risk assessment theory, which are relevant for the risk assessment concept developed in this thesis, are summarized. In the first part some general definitions of risk and risk assessment are described. An attempt to link the theory to CCS and how the risk assessment concept developed can be classified into the theory is given in Section 7.1. In the second part, the focus is on the technical risk assessment and the statistical fundamentals and tools, which are needed for the risk assessment concept that will be described in Chapter 4.

3.1 Understanding of Risks in Science and Society

In this section, the terms risk and risk assessment, are defined and discussed and the overall risk governance model presented by Renn (2008b) is summarized. The theory that is presented, is based on Renn et al. (2007), Renn (2008a) and Renn (2008b).

3.1.1 Defining Risks

The term risk is defined in different ways among the various disciplines and the word is used in many different meanings. In our life, many different kinds of risk exist, e.g., social risk, business risk, economic risk, and safety risk (Kaplan and Garrick (1981)). The challenge is to find a consistent and general definition of the word. In the literature, the term risk is widely discussed. In the scope of this work only a few definitions are summarized.

A definition of risk is given by Soanes and Stevenson (2010): risk is a "situation involving exposure to danger". Another possible definition of risk is that "it implies the likelihood that an undesirable effect may occur resulting from a natural event or human activity" (Renn (2008a) p.50). This definition means that risk contains three different elements: "outcomes that have an impact upon what humans value; the likelihood of occurrence; and a specific context in which the risk may materialize" (Renn (2008a),p.50).

In general, risk can be defined as a "possibility of unknown consequences of an event" without defining whether the consequences are negative or positive (see Renn et al. (2007), p.21). However, the term risk often considers only negative consequences. Renn et al. (2007) (p.21) defines risk as "uncertain consequences of events or activities, that directly or indirectly result in impairment of live, health or environment".

One difficulty for defining risk is that every person has a different perception of risk. The risk concept assumes that risks are mental products, which means that human actors define

and select in their mental imagination what a risk is. This assumes that the human actor believes that the future can be influenced by his own actions. Whether an event is seen as a risk also strongly depends on the values that humans have. This means that only an event that endangers things that humans value will be seen as a risk. For details one is referred to Renn et al. (2007), (p.20).

From the technical point of view risk is often defined as the probability that a hazardous event occurs multiplied by the damage (extent) of the event. This is used in technical risk approaches (will be discussed below) and comes from the insurance business (see Bechmann (1997), Metz et al. (2005)). For the definition of risk, it is important to distinguish between different risk related words: risk, uncertainty, hazard, and safeguards. Kaplan and Garrick (1981) define that risk involves uncertainty and damage, this means that if you are uncertain you do not necessarily face a risk if no loss is connected with the uncertainty. Thus, they define risk as: risk = uncertainty + damage. They argue that the multiplication of probability and damage could be misleading because the resulting value does not show if the damage or the probability is high, which would result in two totally different situations. Hazard is defined as "source of danger" and risk includes again the likelihood that this source of danger results in a loss (damage). A similar definition is also presented in Renn (2008a), where hazard is defined to describe the potential to cause harm to values that people have and it becomes a risk if a likelihood exists that this potential could harm what people value. Safeguards can help to decrease the risk that could occur by a certain hazard, which Kaplan and Garrick (1981) define as: risk=hazard/safeguards.

3.1.2 Risk Concepts from Various Perspectives

A uniform definition of risk is difficult and how to assess the risk is seen differently by various sciences. It is often distinguished between different perspectives or concepts for risk (see e.g. Bradbury (1989), Renn et al. (2007), Renn (2008a), Bechmann (1997)). Bradbury (1989) looks at two types of risk concepts, risk as a physical attribute, which means that "objective facts, which can be explained, predicted, and controlled by science are separated from subjective values" (p.381) and risk as a social attribute (the results derived by risk estimation always include values). In Bechmann (1997) three objectives of risk are discussed: the formal-normative approach where the aim is to find a universally valid risk measure, thus risk is commonly defined as probability times damage. The psychological-cognitive approach looks at the real decision behavior in situations of risk, and the cultural-sociological approach is interested in which factors influence the opinion on technical risk. The concepts of risk presented by Renn (2008a) classify similar risk objectives but a fourth perspective is presented. The concepts are: risk from the perspective of the natural and technical science, the economic perspective, the psychology of risk perception, and the social and cultural concept of risk (Renn (2008a), Renn et al. (2007)). These four concepts are shortly summarized in the following paragraph.

Technical Perspective of Risk

The first risk concept presented in Renn et al. (2007) and Renn (2008a) is the risk concept from the perspective of the natural and technical sciences. In this kind of technical risk approach, the aim is to determine an objective expectation value (Renn et al. (2007), Renn (2008a)). This is done by averaging possible undesired events over time and space and using relative frequencies or estimated probabilities as mean values for the likelihood.

Renn (2008a) distinguishes between three different technical risk concepts. The actuarial analysis, where the expected value is the "relative frequency of an event averaged over time" and "multiplied by the sum of insurance of the event" (p.51). The undesired event is defined as physical harm to humans or the ecosystem, which can be directly observed or measured. Requirements for this kind of risk estimates are the existence of enough statistical data to make reasonable predictions and the agents that cause the negative effect must be constant over the time period. In the end, the risk estimate has one single dimension.

The second concept is called causal models for risks. Here, the risk assessment becomes more difficult because the effect is not directly linked to the result caused by an agent (Renn (2008a), Bedford and Cooke (2001)). Models are used to find the link between the exposure and the effect. This approach can be used as an early warning system to inform about substances that could cause harm to humans or the environment.

The probabilistic risk assessment (PRA) is the third concept presented in Renn (2008a). It is a well known technical risk analysis and is a systematic approach to estimate risk. It is a tool to model failures and consequences, when people get in touch with technological risk.

The technical risk assessment concept is often criticized by social scientists. Some critical points are shortly summarized in the following, for more detail one is referred to Renn (2008a). One critical comment is that values and preferences of people should be taken into account if undesirable effects are defined. Another point of criticism is that human activities and the resulting consequences are connected with higher complexity than simply averaging probabilities, or that the multiplication of damage times probability implies a similar weight of the two components, which would result in the same ranking of a high-damage/low-probability and a low-damage/high-probability event, even though people most likely have a preference for one of the options (see, e.g., Renn (2008a), Slovic (1987), Kaplan and Garrick (1981)). However, the technical risk assessment is an important part of the overall risk governance circle to gain new knowledge about the given risk. The technical risk assessment is adressed in more detail in Section 3.2.

Economic Perspective of Risk

The economic perspective as described in Renn (2008a) differs from the technical approach by transforming the undesired effects into "utilities". Utility is defined as the degree of satisfaction or dissatisfaction related to an action. According to Renn (2008a) (p.53) the classical measure of utility is "the amount of money that somebody is willing to pay for a change that provides a higher (lower) degree of benefit (loss)" compared to the current situation. This

dissatisfaction or satisfaction can be measured for all consequences and the translation into utilities can provide a measure to compare different options depending on the satisfaction. Two main selection rules are offered: a risk can be accepted if the benefit of an action gives more utility than the risk of this action takes from the utility; or if different options are available, the option with the lowest risk providing the same benefit can be chosen. The utilities are determined by either reviewing how people behaved in the past, by the use of surveys, or by directly asking people. In the economic perspective, the risk has also to be weighted by probabilities. In addition, it is important to consider the time in the assessment because a benefit has different impact, depending on when it occurs. For further detail one is referred to Renn (2008a).

Psychological Perspective of Risk

The psychological perspective described in detail in Renn et al. (2007) and Renn (2008a), defines the unit for risk as the subjective expected utility. Studies in the field of the psychological risk perspectives have found that most individuals do not rate risks on expected values, and the research field has the attempt to identify reasons for this different perception. Several interesting behavior patterns have been identified: e.g. many individuals underestimate risk that they remember well, or underestimate the relevance of probabilities (Renn et al. (2007) p.42). In addition, particular criteria have been determined which are used to evaluate a risk by individuals: e.g., the voluntariness to take a risk, or the possibility to control the risk. Semantic images are identified in the literature where risk can be classified depending on the perception they provoke. The semantic images will be briefly presented in Section 3.1.3. The research in the field of psychological risk perspective shows that risks are not only judged based on a potential damage but on particular criteria related to the current situation (see Renn et al. (2007) p.43).

Social and Cultural Concepts of Risk

The sociological or cultural concept of risk as described in Renn (2008a) and Renn et al. (2007) looks not only at undesirable events as physical harm to humans or the environment but also at such events that are socially specified or constructed. The consequences of an event are influenced by the values and interests of a group and their social interpretation. What can happen in the future depends not only on the calculation of probabilities but on knowledge or visions of a considered group. It is claimed that to neglect the relation between social organizations and technological performance can under- or overestimate the likelihood of an event (see Renn (2008a) p.57). There exit several sociological concepts of risk which all have in mind that risk seen from humans is influenced by social and cultural meanings and depends, e.g., on the social, or business environment. The different concepts are classified in Renn (2008a) regarding to two dimensions: individualist versus structuralist and realist versus constructivist. The first dimension defines the unit of the analysis. On the one hand, the individual is in the center of investigation, on the other hand a social aggregate such as institutions or subcultures are considered as the center. The second dimension

distinguishes between risk as a real physical and observable consequence and risk as a as a social artifact fabricated by social groups and institutions (see Renn (2008b) p.24). Six different social concepts of risk are discussed and classified by these two dimensions (see Renn (2008a) and Renn et al. (2007) for detail).

3.1.3 The Risk Governance Approach as a Heuristic Tool

In this section the "Risk Governance Model" which is presented in Renn et al. (2007) and Renn (2008b) in detail, is shortly summarized. In addition, it is tried to link CCS to the risk governance approach by providing some short examples. A more detailed discussion about CCS and the different classifications is given in Section 7.1.

The "Risk Governance Model" provides structures and procedures for how to handle risks and decision-making concerning risk questions. It consists of five parts: pre-assessment, risk appraisal, risk characterization and evaluation, risk management, and risk communication. The first four steps are followed one by one including iterative exchange between the steps. Risk communication belongs to all phases (see Figure 3.1). Overall, it is an "open, cyclical, iterative and interlinked process" (Renn (2008b)p.48). In addition, risk participation is an important topic during the risk assessment procedure. In this thesis, the focus is mainly on a concept for technical risk assessment for the process of CO_2 storage. To this end the phase of technical risk assessment will be described in more detail in Section 3.2.

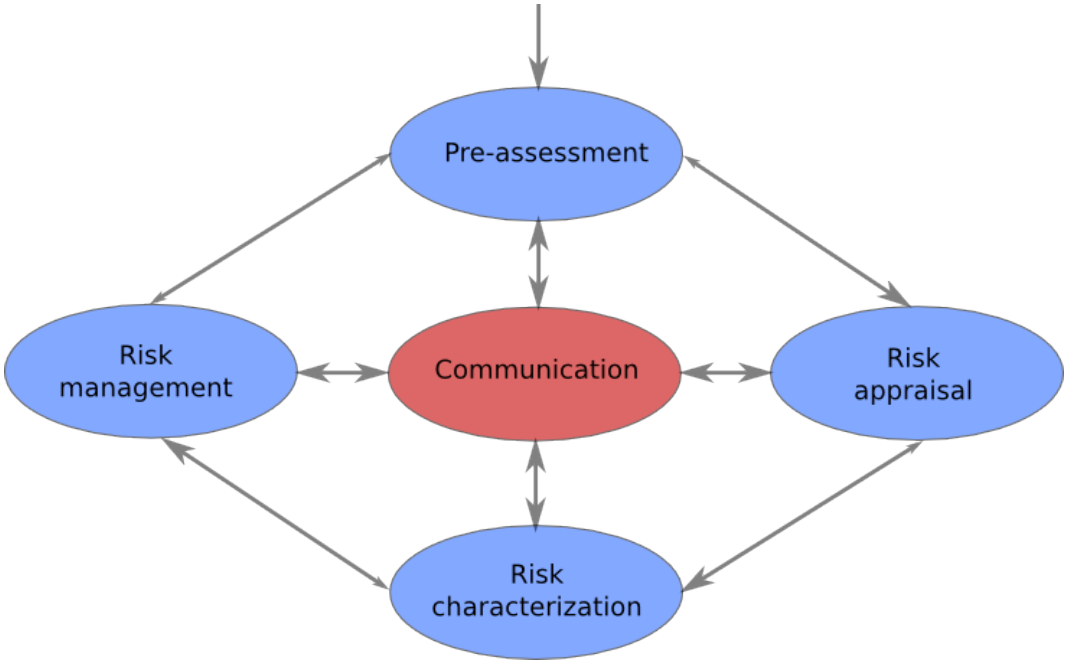

Figure 3.1: Elements of risk governance (after Renn (2008b)).

Pre-assessment During the process of pre-assessment the general framework for risk assessment and evaluation and the overall problem is defined. An intensive analysis what is

seen as a hazard by actors, stakeholders, and the general public is included. All information about the hazard is collected and the functional chain, which should be considered is identified. This framing procedure should be already embedded into the transparent governing structure because all affected or interested groups can have different ideas regarding what should be included into the risk assessment process. For details about this phase of the governance framework one is to Renn (2008b) p.47ff.

In the context of CCS, stakeholders and the public should be interviewed to find out which hazards are seen to be most relevant for a specific storage site. For example, in the current context water suppliers have seen the risks that are related to brine displacement to be most relevant. The relevant processes (CO_2 and brine migration) that have to be considered, the time scale (the injection period and several decades of the post injection period) for investigation and the area of investigation (larger domains are required for investigation of the pressure induced brine displacement) have to be defined.

Risk Appraisal The second phase, risk appraisal, consists of the scientific assessment of physical harm that a risk includes (estimation of damage and probability) and the assessment of risk perception (see Renn (2008b), p. 67ff). Related to CCS the physical harm that a risk includes could be, e.g. the potential of suffocation due to very high CO_2 concentrations, the impact of salt infiltration on groundwater resources (exclusion of the groundwater for drinking or impact on wildlife habitats), or toxicity of mobilized heavy metals in drinking water.

The first part is the technical risk assessment, which has the purpose to collect knowledge about the event and the resulting risk and determine values for damage and probability. Renn (2008b) presents three core components which are followed in the process of risk assessment, even if the exact structure depends on the risk source itself: first the hazard is identified and preferably estimated. Then the exposure or vulnerability is assessed and lastly the risk is determined by bringing together likelihood and severity. The technical risk assessment is the main focus of this work and will be described in more detail in Section 3.2.

In the second step; the concern assessment, the results of the risk assessment part are expanded by information about concerns. The concern assessment investigation is based on "risk perception studies, economic impact assessment, and the scientific characterization of social response to the risk source" (Renn (2008b) p.173). Various approaches are suggested to evaluate public concerns. The UK Treasurey Department suggests to handle the risk considering six hazard related factors as: e.g., "the perception of familiarity and experience with the hazard", "understanding the nature of the hazard and its potential impacts", or "the degree of trust in risk management" (see Renn (2008b) p.73). The German Advisory Council on Global Change (WBGU) chooses nine criteria to characterize risk. The criteria beneath damage and probability investigated in the technical risk assessment part are incertitude (a measure of the remaining uncertainty), ubiquity (a measure how far the damage is distributed), persistency (temporal extension of the damage), reversibility (possibility to restore the situation before the damage occurs), delay effect (period between the event and the actual damage), violation of equity (distribution of benefit and risk), and mobilization (potential to generate social conflicts or psychological reactions) (see Renn (2008b) p.73/74

or p.161). All these criteria essentially exceed the understanding of technical risk assessment which "only" refer to likelihood and extent of damage.

The research field of risk perception involves the appraisal of several of these criteria. In the following some basics of this research field as it is presented in Renn et al. (2007) and Renn (2008b) are summarized. A general definition of risk perception is given in Renn (2008b) p.98: "Risk perception denotes the processing of physical signals and/or information about potentially harmful events or activities, and the formation of a judgment about seriousness, likelihood and acceptability of the respective event or activity". Every human classifies risk dependent on subjective perception. The perception of risk is not aligned with the methodical criteria of the risk assessment, but it is based on subjective experience and personal sensation. Personal interests and interpretations of the reality or the trust in experts and politicians are some of the facts that influence the perception of the risk (Renn et al. (2007)). According to Rohrmann and Renn (2000) four elements mainly influence risk perception: "intuitive judgment processes associated with probabilities and damages", "conceptual factors relating to the perceived characteristics of the risk and to the risk situation", "semantic associations linked to the risk source, the people associated with the risk, and the circumstances of the risk-taking situation", "and trust and credibility of the actors involved in the risk debate" (see Renn (2008b) p. 20).

However, people follow a consistent pattern to evaluate risks. When people face risk, four basic strategies exist: escape, fight, play dead, and trial and error experiments (Renn (2008b) p.93). These basic patterns are completed by several cultural patterns which are subdivided into risk-related patterns and situation-related patterns. Risk-related patterns are based on the properties of the source of risk as the potential to have catastrophic consequences or the impression of the reversibility of a consequence (see Renn et al. (2007) p. 78). Situation-related patterns are based on the characteristic of the risky situation, for example, the impression if the benefit and the risk is fairly distributed or the trust in the public control of the risk (see Renn et al. (2007) p.79). These qualitative criteria can be classified into five risk perception classes, which are called semantic risk images in the literature (see Renn et al. (2007) p.80ff or Renn (2008b) p.111ff for details):

- Risk as a pending danger: mostly technical risk source with large catastrophic potential (e.g. nuclear power)
- Risk of a stroke of fate: e.g. natural risk sources
- Risk as a personal thrill: presents a challenge, e.g. sport activities
- Risk as a gamble: e.g. lotteries
- Risk as an indicator of insidious danger: e.g negative effects on health or environment due to e.g. food additives or pesticide residue

The classification of a risk into these semantic risk images helps to predict how people may react. The intuitive reactions related to a risk are often not plausible and are sometimes out of all proportion to the real risk for health and the environment (Renn et al. (2007) p.86).

According to Renn et al. (2007) natural risk, risk that can be controlled by oneself, or risks with low catastrophic potential are often underestimated and risks that are caused by humans, forced risks, or risks that mostly cause deaths are often overestimated. Ranking of CCS within these semantic risk images is not definitively possible but it could be judged as a pending danger (see Section 7.1 for more detailed discussion).

The following additional patterns regarding how people interpret probabilities and risks are presented in psychological research (see Renn (2008b) p.95): The availability bias describes the effect that the probability is often overestimated if a risk is easier and faster recognized. The second pattern, the anchoring effect, is the overestimation of risks that are associated to known (catastrophic) events. If losses from a risk source are constant over time and occur later in time the probability will be underestimated. The last pattern describes the effect that the loss expectations of a low risk are overestimated and the loss expectations of high risks are underestimated, if the uncertainty of loss expectation is high.

All these aspects should be taken into account in a complete risk governance circle. Renn (2008b) suggests to include all this risk perception information into the risk governance by equally including all different factors that concern the various groups such as scientists, stakeholders, or the public (see Renn (2008b) p.96).

There exist three maior challenges in the phase of risk appraisal, which denotes the "state and quality of knowledge available" about the considered hazard and the corresponding risk: complexity, uncertainty and ambiguity (see Renn (2008b) p.74). Complexity denotes the level of knowledge how the processes are linked. Low complexity marks simple and straightforward risks, highly complex risks have extensive relationships that are difficult to describe. The high complexity risks need to be described by sophisticated models. The second component is uncertainty, which can be found in the complete assessment procedure and is linked to a lack of knowledge or variability of the nature. The various levels of uncertainty are discussed in detail later in the section on technical risk assessment and uncertainty quantification. The last component is the ambiguity, which describes the differences in the interpretation of input and output by actors and stakeholders. The differentiation between the three elements help to define risk management and risk communication strategies and to get an adequate procedure for risk participation.

Risk Characterization and Evaluation If all necessary data of the effects of a risk are collected or determined, they have to be interpreted and characterized in the third phase. The risks are evaluated depending on their tolerability or acceptability. In the current procedure of risk governance the traffic light model is used as a simplified way to judge the risk. In this model, the probability is the y-axis and extent of an event (damage) on the x-axis. In this diagram, acceptable risks are located near the origin, followed by tolerable risks and intolerable risks with either high damage or probability, or both (see Renn (2008b) p.150 Fig.5.1). Following this model, only three alternatives are possible: Either to accept the risk as it is and do not take any management actions, to do risk mitigation actions for tolerable risks, or to forbid the action that causes intolerable risk.

The question is how to find out in which region of the traffic light model the considered risk is located. The German Advisory Council on Global Change (WBGU) defined risk classes

inspired by Greek mythology. These classes are based on 9 criteria. As described in the previous section, technical risk assessment and risk perception should be considered for a comprehensive risk evaluation. In the technical risk assessment the two main categories to assess risk are the damage of an event and the probability that the event occurs. Choosing criteria to represent social concerns is much more difficult because people perceive risk differently due to many criteria. The criteria to judge tolerability chosen by the WBGU were already described in the section of "Risk appraisal" and are damage, probability, incertitude, ubiquity, persistency, reversibility, delay effect, violation of equity, and mobilization (see Renn (2008b) p.161). The six classes that are deduced from these criteria are discussed in detail in Renn et al. (2007) and Renn (2008b) and only briefly summarized as follows: The risk class "sword of Damocles" is related to events that result in catastrophic damage if the event occurs. However, the probability is very low (e.g., nuclear energy). In the class "Cyclops" the extent of damage is high as well but the probability that it occurs is uncertain (e.g., earthquakes). Whereas the probability and the extent of the damage (could be very high) are largely uncertain in the class of "Pythia" (e.g., greenhouse gas effect). This also holds for the risk class "Pandora's box", but the additional criterion of high persistence characterizes this class as well. The risk class "Cassandra" is located in the intolerable area of the traffic light model because of a high potential of damage and high probabilities. Additionally, a very long delay between the event and the actual damage characterizes this class. The last class is called "Medusa" and is characterized by low extent of damage and low probability. However, the potential for mobilization is very high. This is often the case for new phenomena. These six risk classes are integrated into the traffic light model and they help to arrange the regarded risk more easily into the model. Then, an adequate risk management strategy which is proposed for each category, can be applied. CCS related risks could be rank to the class of "Medusa", which is discussed in more detail in Section 7.1.

Risk Management In the last step of risk management, measures are identified to avoid or reduce risks which are characterized to be not tolerable. As described in the section of risk evaluation, the risk management is confronted with one of three possible outcomes from the previous assessment and evaluation steps: the intolerable situation, which implies that the risk source has to be either banned or replaced; the tolerable situation, where risk reduction actions are needed; or the acceptable situation, where no risk reduction is needed but risk-sharing can be organized. (see Renn (2008b) p. 173).

Additionally, the actors can agree or disagree with the classification of the considered risk. All these factors influence which adequate instruments should be chosen in the risk management phase. The most challenging class of risk for the risk management are tolerable risks because actions to make the risk acceptable have to be found. An example for a risk reduction technique for tolerable situations in the context of CCS is the placement of biofilms into the reservoir to avoid CO_2 leakage (see Ebigbo et al. (2010)).

Renn (2008b) describes risk management strategies based on four different risk characteristics depending on the challenges of complexity, uncertainty, and ambiguity described before. The types of risk are: linear risk problems, complex risk problems, risk problems due to high unresolved uncertainty and risk problems due to interpretative and normative am-

biguity. Risks related to CCS touch three of the types, since they are complex, uncertain and ambiguous (see Section 7.1). The risk management step is not the focus of this work and one is referred to Renn (2008b) (p. 173ff) for details.

Risk Communication In all phases an intensive communication between scientists, politicians, and stakeholders is intended. In the beginning, risk communication was developed as a tool to communicate the results derived by experts to the public (educating the public). Today, risk communication is seen as a two-way process, where the public and the risk managers are expected to learn from each other. Four major risk communication functions are presented in Renn (2008b) p. 203. Risk communication has the functions of educating and enlightening; risk training and initiating changes in behavior; providing assurance that the risk management does handle the risk effectively, fairly and efficiently; and involving stakeholders and the public in decisions concerning the risk. Renn (2008b) gives some guidelines for effective risk communications. The main challenges in the field of risk communications are: e.g., to explain how the probabilities are determined by the statistical methods, to explain how risk and hazard differ, to deal with long timescales, or to communicate with different stakeholders (Renn (2008b) p. 242). In the recommendations, it is distinguished between three communication levels which refer to: "factual evidence and probabilities; institutional performance, expertise and experience; and conflicts about world views and value systems" (Renn (2008b), p.244). The first level is an information transfer, where the technical expertise should be presented in an open way showing the knowledge of the risk and how remaining uncertainties are treated. It is important that the audience understands the message and that all their concerns are addressed. The second level is a two-way dialogue with the stakeholders and the public to distribute the risks and benefits and to show that they can trust the risk management institution. Thus, institutional openness and competence is required instead of only technical expertise. In the third level, the conflict is based on social values and world views and additional forms of stakeholder involvement are needed such as open forums or mediation. In such debates solutions which are tolerated by all parties can be searched. According to Renn (2008b), these different communication levels can be related to the risk types presented before. Linear risks, which are well known by the scientists and the remaining uncertainties are low belong to the first level. An adequate information transfer of the technical expertise is needed to, e.g., show how the people can avoid to face the risk related to an action. For highly complex risks, which are characterized by complex relationships between causes and effects of a risk, either level 1 or 2 are related depending on the exact issue. Risks with high uncertainty require communication on level 2 (sometimes even on level 3). The remaining uncertainties and the corresponding fears by the public have to be addressed by the risk managers. The last risk type of high potential for ambiguity clearly needs to be addressed by the third risk communication level. These risk types do not have to be highly uncertain; they can be ones to which people react controversial and emotional. Thus, the communication must include dialogues and mediation. Since risk related to CCS are complex, uncertain, and ambiguous the third communication level should be applied.

This short summary of risk communication is not complete, but the further details are not the focus this work and one is referred to Renn (2008b) p.251ff, who provides a list of recommendations for effective communication.

Risk Participation In the following, the theory of risk participation as explained in Renn (2008b) is shortly presented. Risk participation means that stakeholders and the affected (or interested) public are involved in the overall risk governance process. Four different groups are mentioned that should be involved in risk decisions depending on the kind of risk: stakeholders, which are social groups that will be affected or have interest in the results from an event, directly affected public (individuals that will be affected by the event), observing public (e.g. media), and the general public (all individuals that are not directly affected). Depending on the type of risk (linear, complex, uncertain, ambiguous) the degree of participation varies (see Renn (2008b) pp.276ff). For linear risk problems, the involvement of the affected group is not necessary because the results are clear and often simple. The agency staff is often the only group that is involved in the assessment and decision process. The participation should be expanded for complex risk problems by involving external experts from academia, government, industry, or civil society. The aim is to gain new or additional knowledge to solve the complex problem via, e.g., Delphi methods or scientific consensus conferences. If the uncertainty of the risk estimates is very high, the main stakeholders are suggested to be included into the overall risk management circle. The following question has to be answered: "how much uncertainty and ignorance are the main actors willing to accept in exchange for some given benefit?" (Renn (2008b) p.277). Methods for this kind of participation are for example, open forums or roundtables. For the last type of risk due to high ambiguity, the risk regulators should open the overall risk governance circle to the general public. A method for this participatory discourse is, e.g, a platform for discussing conflicts openly. For investigation of CCS risk (complex, uncertain, and ambiguous) all groups should be included in the process (see Section 7.1).
Following features should be part of any participatory procedure: transparency (in selection of stakeholders, in accounting for stakeholders interests, methods of reaching agreement), competence (considering state of the art knowledge), fairness (equal speaking and debating opportunities), efficiency (cost-effective use of techniques and methods), clear mandate (of the expectation from the participatory exercise), diversity (considering various perspectives and disciplines), and professionalism (of the structure and summary of the process) (see Renn (2008b) p.282/283).

This short summary of the risk governance model helps to rank the risk concept developed in this thesis into the overall risk theory (see Chapter 4 and Section 7.1). In addition, a short discussion of CCS in the context of risk perception is presented in Section 7.1. Since the focus of this work is on technical risk assessment, the following section describes this part in more detail.

3.2 Technical Risk Assessment

In the technical risk assessment as much knowledge as possible about the event and its consequences is collected. As described before, the risk is often defined as damage times probability (see e.g. Bechmann (1997), Metz et al. (2005)) or a probability distribution for damage values is presented. The quantitative definition of risk discussed in Kaplan and Garrick (1981) fits into the technical perspective of risk. Kaplan and Garrick (1981) defines

three questions, which have to be answered to quantify risk: "What can fail? How likely is it that it can fail? What are the consequences if a system fails? ". They also discuss how the common definition that risk is probability times damage could be misleading because a low probability, high damage scenario would have the same value as a high probability, low damage scenario, which is not the same. They prefer looking at risk as the curve/function of probability and damage instead of taking one value of risk as the mean of the curve, and they define risk as uncertainty + damage (see Section 3.1.1).

3.2.1 Risk Assessment and Uncertainty Quantification Methods

Scenario techniques are often used in the field of CO_2 storage (e.g. Wildenborg et al. (2005)). Here, possible future states are described that result in certain risks or a reference case is set up that represents the most probable situation (Metz et al. (2005)). As discussed in Chapter 1, the features, events and processes (FEP) methodology is used in many risk investigations. A catalog is set up where features (parameters related to CO_2 storage such as reservoir or caprock permeability), events (processes that could result in a risk such as seismic events, well blow-outs, etc.), and processes (physical and chemical processes related to CO_2 storage) are listed. In the scenario approach the chosen scenarios are often related to selected FEPs; see Wildenborg et al. (2005). A common risk assessment framework including the assessment of probabilities for certain risks is called "Probabilistic Risk Assessment (PRA)", which started its systematic development in the aerospace sector and was further developed in the nuclear sector (Bedford and Cooke (2001)). Here, the consequences (magnitude of an hazardous event) are numerically assessed and the likelihood of occurrence is given by probabilities. The results are often presented by a risk curve that presents damage via probability. To provide an overall risk estimate the definition that risk equals probability times damage can be used. In PRA, event tree or fault tree analyses are often used, which help to get more knowledge about the cause-effect relationship (see Renn (2008a), Bedford and Cooke (2001)).

The challenge in risk assessment is to determine the probabilities in the presence of many different uncertainties. Faragher (2004) presents an overview of various methods for uncertainty analysis. It can be distinguished between non-probabilistic and probabilistic methods for uncertainty quantification. If not enough data or knowledge is available to define a probability density function, non-probabilistic methods such as the interval analysis or Fuzzy theory are adaptable. In the interval analysis the greatest possible uncertainty is predicted by using the minimum and maximum value of a parameter (Faragher (2004)). The Fuzzy logic estimates output uncertainties from input parameters, which are described by membership functions. It allows to approximate the behavior if only sparse data is available (see Faragher (2004)).

In the field of uncertainty quantification various methods exist to determine probabilities. For the application of probabilistic methods, sufficient knowledge about the variability of the uncertain input parameters is required. Examples for probabilistic methods are, e.g., the Monte Carlo method, the perturbation method, the moment method, or the polynomial chaos expansion. A well established method is the Monte Carlo analysis, where many dif-

ferent variations of uncertain parameter sets are randomly chosen for running thousand of simulations. In the end, probability distributions for certain risks can be derived. The prior distribution of the input parameters is given by available data or expert judgments (Metz et al. (2005)). Monte Carlo simulations for complex models as they are needed for CO_2 storage result in high computational costs. Thus, the models have to be simplified or reduced. The perturbation method is useful for relatively small variability in the input parameter. A small variation in the parameter results in an exact solution. In this work, an approach following the polynomial chaos expansion is used. The idea of the polynomial chaos expansion is to project the original complex model onto orthogonal polynomial basis, i.e. to replace the complex model by a response surface that represent the model output dependent on uncertain model input. The theory of the polynomial chaos expansion will be explained in Section 3.2.2.

For risk assessment and uncertainty quantification it is important to know what kind of uncertainty it is handled with. In the literature various kinds of uncertainty are distinguished. The main differentiations are shortly presented below.

Uncertainties In a broader sense, uncertainty can be defined as the absence of information or knowledge (Rowe (1994)). In the field of uncertainty quantification, there are often distinctions between two categories: epistemic and aleatory uncertainty (e.g., Helton (1994), Hoffman and Hammonds (1994), Wojtkiewicz et al. (2001)). Epistemic uncertainty is also denoted as reducible, subjective, or type B uncertainty and results from a lack of information about the system. Such an uncertainty can be reduced by further research or measurements. Aleatory uncertainty is also known as variability, irreducible, stochastic, or type A uncertainty and results from the fact that a system can react in many different unpredictable ways. Some authors additionally distinguish between dimensions of uncertainties (e.g., Rowe (1994) and Walker et al. (2003)). Walker et al. (2003) divides uncertainties not only into different natures (epistemic and aleatory) but also into the location and the level of uncertainty. The location identifies the source of uncertainty, i.e. where the uncertainty is situated within the model complex, whereas the levels categorize the uncertainty into ranges of knowledge. Levels of knowledge range from determinism to total ignorance. Determinism means that everything is known exactly, which would be an ideal situation. Total ignorance is the other extreme, where nothing is known. Walker et al. (2003) describe it as a state, where "we do not even know what we do not know". The levels inbetween are statistical uncertainty, scenario uncertainty and recognized ignorance. Statistical uncertainties can still be described by statistical terms (e.g., probability density function, or histogram). The next level is scenario uncertainty (or conceptual uncertainty). Such uncertainties, e.g. different geological models cannot be described sufficiently by statistical terms. According to Walker et al. (2003) is a scenario a possibility how the system may develop in the future. Recognized ignorance is defined by Walker et al. (2003) as fundamental uncertainty about the mechanisms and functionalities. These uncertainties can be divided into reducible ignorance and irreducible ignorance. Reducible ignorance can be reduced by further research or development whereas irreducible ignorance cannot be resolved because no sufficient knowledge about the relationships can be provided by the research.

3.2.2 Statistical Tools

Statistics are essential for the quantification of risk. In the first part of this section the most relevant tools and fundamentals needed in this work are presented. All definitions are based on Bedford and Cooke (2001) and Rychlik and Ryden (2006). In the second part, the model reduction technique (Oladyshkin and Nowak (2012), Oladyshkin et al. (2012)), which is applied in this work is presented.

Moments

For the description of a distribution, the arithmetic mean, variance, skewness and kurtosis are highly relevant. These parameters are called moments of a distribution. All of these parameters are dependent on each other. The general analytical definition of moments of a random variable η can be written as:

$$M_k = \int_{\xi} \eta^k d\Gamma(\xi) \tag{3.1}$$

In practice, theoretical probability density functions (PDF) are often not available and just raw data is present. However, the probability of measure of this data can be described by statistical moments. The first four statistical moments are the most relevant ones to describe a distribution. In the following, these moments will be defined. The first moment is the arithmetic mean $\bar{x}$, defined as:

$$\bar{x} = \frac{1}{n} \sum_{i=1}^{n} x_i \,. \tag{3.2}$$

x_i is an arbitrary sample space $x_1, ..., x_n$ of n values. The second moment is the variance σ^2 of the sample and is defined as:

$$\sigma^2 = \frac{1}{n-1} \sum_{i=1}^{n} (x_i - \bar{x})^2 \,. \tag{3.3}$$

The standard deviation is the square root of the variance: $\sigma = \sqrt{\sigma}^2$. For interpretation of results the standard deviation is very helpful because it has the same unit as the uncertain quantity. The third moment is the skewness g, which represents the symmetry of a distribution:

$$g = \frac{1}{n} \sum_{i=1}^{n} (\frac{x_i - \bar{x}}{\sigma})^3 \,. \tag{3.4}$$

The last moment of relevance is the kurtosis, which is a measure of the peakedness of a distribution:

$$w = \frac{1}{n} \sum_{i=1}^{n} (\frac{x_i - \bar{x}}{\sigma})^4 \,. \tag{3.5}$$

These moments can be treated directly by the arbitrary chaos expansion that will be described below.

Cumulative Distribution and Probability Density Function

In this section the probability density function and the cumulative distribution function are defined. The cumulative distribution function is defined as (Rychlik and Ryden (2006)):

$$F(x) = P(X \leq x),\ x \epsilon R \tag{3.6}$$

where $P(X \leq x)$ is the probability that the numerical output of an experiment or observation X is smaller than a real value x. Thus, the cumulative distribution functions can tell the probability that a certain value is not exceeded. If $F(x)$ is differentiable, the probability density is defined as:

$$f(x) = \frac{dF(x)}{dx}\,. \tag{3.7}$$

In Rychlik and Ryden (2006), it is defined that a function F(x) that is increasing in x, $F(-\infty) = 0$, and $F(+\infty) = 1$ is a distribution of random variables and a random variable is the number associated with the outcome of an experiment. For the construction of random variables it is referred to Rychlik and Ryden (2006).

Important Distributions

Data is often given as a distribution, and an outcome of an experiment or an observation is described by various distributions. In the following, the most important distributions used in this work are presented. All definitions are based on Bedford and Cooke (2001).

Uniform Distribution The probability density function of a uniform distribution on the interval [a,b] is defined as:

$$f(x) = \begin{cases} \frac{1}{b-a} & \text{for } a \leq x \leq b, \\ 0 & \text{for } x < a \text{ or } x > b \end{cases} \tag{3.8}$$

The uniform distribution describes a situation where every outcome has the same probability.

Normal Distribution The normal distribution is a continuous distribution with a bell shape form. The probability density functions is defined as:

$$f(x) = \frac{1}{\sigma\sqrt{2\pi}} \exp\left(-\frac{(x-\bar{x})^2}{2\sigma^2}\right)\,. \tag{3.9}$$

The normal distribution is the standard to describe the variability of measurements in science and technology (Rychlik and Ryden (2006)).

Lognormal Distribution An outcome of an experiment or observation X is lognormal distributed $LN(\bar{x}, \sigma)$ if $Y = logX$ (log=natural logarithm) is normally distributed $N(\bar{x}, \sigma)$. The probability density function is defined as:

$$f(x) = \frac{1}{\sigma\sqrt{2\pi}x} \exp\left(-\frac{1}{2}\left(\frac{logx - \bar{x}}{\sigma}\right)^2\right) . \tag{3.10}$$

The expected value and the standard deviation of the lognormal distribution are:

$$E(x) = \exp(\bar{x} + \frac{\sigma^2}{2}) \tag{3.11}$$

and

$$E(x) = \sqrt{(\exp(2\bar{x} + 2\sigma^2) - \exp(2\bar{x} + \sigma^2)} . \tag{3.12}$$

Beta Distribution The beta distribution is a continuous distribution for the interval [0,1] and the density function with the shape parameters α and β is defined as:

$$f(x) = \frac{1}{B(\alpha, \beta)} x^{\alpha-1}(1-x)^{\beta-1} \tag{3.13}$$

with the beta integral $B(\alpha, \beta)$:

$$B(\alpha, \beta) = \int_0^1 x^{\alpha-1}(1-x)^{\beta-1} dx . \tag{3.14}$$

Beta distribution is important if unknown discrete failure probability is described (Rychlik and Ryden (2006)).

Uncertainty Estimation via Model Reduction Techniques

A possible way of estimating statistical uncertainties (see Section 3.2.1) and providing probabilities is performing numerical Monte Carlo (MC) simulations. Numerous set-ups of the uncertain parameters are randomly chosen for running thousand of simulations. This approach is a often used and well established for uncertainty estimation. However, the MC approach is computationally very demanding because many simulation runs are needed to get an appropriate statistical accuracy. For the considered problem of CO_2 storage in deep porous rocks complex models and large space and time scales are required. Thus, it is often hardly possible to run thousands of MC simulations with the complex model.

Handling the complexity and uncertainties with acceptable computational costs is possible by running MC simulation with a reduced model, for example using the polynomial chaos expansion technique (PCE). The principal idea of the classical chaos expansion, originally introduced by Wiener (1938), is to replace the full model by a response surface that is able

to represent the model output (e.g. leakage, pressure) dependent on the chosen uncertain parameters. Therefore, the output of a simulation model is projected onto a higher order orthogonal basis of polynomials. The PCE-techniques can be divided in intrusive and non-intrusive methods. Intrusive approaches require the change of the governing equations that means that the model code itself has to be adapted. Non-intrusive approaches (i.e. "black-box") do not require any modification in the governing equations, thus the simulation code does not have to be adapted, e.g. the probabilistic collocation method (Oladyshkin et al. (2011a)). The non-intrusive approach for the definition of the PCE form has lately been receiving increasing attention. The original PCE technique (Wiener (1938)) is only optimal for Gaussian distributed input variables because it is based on Hermite polynomials. However, there is often a lack of information about the distribution of data in environmental engineering field and the data often does not follow a normal distribution because the natural phenomena are very complex. For applications, the different distributions of the parameters are transformed into normal distributions. Oladyshkin et al. (2011a) applied this original PCE technique, combined with the nonintrusive probabilistic collocation method (PCM) for CO_2 storage. An additional application is presented in Walter et al. (2011). However, the transformation into normal variables is not optimal because it results in slow convergence (e.g. Xiu and Karniadakis (2003) and Oladyshkin et al. (2011b)). The classical PCE was further extended to the generalized polynomial chaos (gPC) to account for following distributions: beta, uniform or gamma distribution and increase efficiency (e.g. Xiu and Karniadakis (2003) or Wan and Karniadakis (2006)). The problem of the described techniques is that the probability density functions of the input distributions are required and the mentioned distributions from the Askey scheme (Askey and Wilson (1985)) does not fully cover the needs for applications. For example to describe permeability log normal distributions are most feasible. Additionally, for data as permeability or porosity in a reservoir a probability density functions is often not known because only limited data is available. To this end, the most recent generalization of the chaos expansion technique (Oladyshkin and Nowak (2012), Soize and Ghanem (2004)), which accounts for arbitrary distributions of modeling parameters is used in this thesis. In the so-called arbitrary polynomial chaos expansion (aPC), an arbitrary probability density function of the input parameters or data with unknown distribution functions, when only some statistical moments are known, can be used. The aPC approach provides improved convergence in comparison to classical PCE techniques, when it is applied to input distributions that fall outside of the range of classical PCE (Oladyshkin and Nowak (2012)). Moreover, it can align the complexity and the order of analysis with the reliability and detail level of statistical information on the input parameters. The fidelity of the reduced model has been tested via a full model using classical PCE techniques in Oladyshkin et al. (2011a) and using recent generalization aPC in Oladyshkin et al. (2011b) for the CO_2 benchmark presented by Class et al. (2009).

Arbitrary Polynomial Chaos Expansion combined with Probabilistic Collocation Method In the following, the main steps of the aPC combined with the PCM, which is applied for investigation of statistical uncertainty are summarized based on Oladyshkin and Nowak (2012) and Oladyshkin et al. (2012). The simulation output Ω can be projected onto an orthogonal basis of polynomials, i.e. the model output can be represented by the polyno-

mial chaos expansion (Wiener (1938), Oladyshkin et al. (2011b)). Thus, any model output Ω depending on the input parameters $\boldsymbol{\omega} = (\omega_1, ...\omega_N)$ can be represented by the expansion as:

$$\boldsymbol{\Omega}(\boldsymbol{\omega}, x, y, z, t) = \sum_{j=1}^{P} c_j(x, y, z, t)\boldsymbol{\Psi}_j(\boldsymbol{\omega})\,. \tag{3.15}$$

The coefficients c_j quantify the dependence of the model output Ω on the input parameters ω. Here, Ψ_j is a simplified notation for the multi-variate orthogonal polynomial basis (polynomials of more than one variable) for the input parameters $\omega = \{\omega_1, \omega_2, ...\}$. The CO_2 storage problem is solved at each grid point in space and time. Therefore, the polynomial form depends on the three spatial dimensions (x, y, z) and the time (t). The number of terms P, depends on the number of uncertain input parameters N and the desired order of the expansion d_p:

$$P = \frac{(N + d_p)!}{N!d_p!}\,. \tag{3.16}$$

For the construction of the data-driven orthogonal polynomial basis, the only information required is the moments of the input distribution. For each individual input variable ω_j a data-driven orthogonal basis as a set of polynomials $P_j^0, ..P_j^d$ of degree d_p is constructed. The polynomial P_j^k of degree k in the input variable ω_j can be defined as:

$$P_j^k(\omega_j) = \sum_{i=1}^{k} p_{i,j}^k \omega_j^i,\ k = 0, ..., d_p,\ j = 0, ..., N, \tag{3.17}$$

where $p_{i,j}^k$ are the coefficients for the polynomial $P_j^k(\omega_j)$. To construct the data-driven orthogonal polynomial basis of order d_p for each input parameter ω_j, finite moments up to order $2d_p - 1$ are required. Then the unknown polynomial coefficient $p_{i,j}^k$ for each orthogonal basis can be defined from the moment matrix equation (see Oladyshkin and Nowak (2012)):

$$\begin{bmatrix} M_0 & M_1 & ... & M_k \\ M_1 & M_2 & ... & M_{k+1} \\ ... & ... & ... & ... \\ M_{k-1} & M_{k-2} & ... & M_{2k-1} \\ 0 & 0 & ... & 1 \end{bmatrix} \begin{bmatrix} p_0^{(k)} \\ p_1^{(k)} \\ ... \\ p_{k-1}^{(k)} \\ p_k^{(k)} \end{bmatrix} = \begin{bmatrix} 0 \\ 0 \\ ... \\ 0 \\ 1 \end{bmatrix}\,. \tag{3.18}$$

For simply getting e.g. the mean or variance it is useful to normalize the derived orthogonal basis (for details how to normalize the basis see Oladyshkin and Nowak (2012)).

The multi-dimensional basis for the independent input parameters within $\boldsymbol{\omega}$ is the product of the univariate polynomials:

$$\boldsymbol{\Psi}_k(\boldsymbol{\omega}) = \Pi_{j=1}^{N} P_j^{a_j^k}(\omega_j), \tag{3.19}$$

with a_j^k the multivariate index, containing the information how to specify the possible products of individual univariate basis functions.

If the basis is constructed, the remaining step is to determine the unknown coefficients c_j in the chaos expansion to represent the model output with the polynomials. In this work, the coefficients are obtained by the non-intrusive probabilistic collocation technique (PCM). As described before non-intrusive methods do not require any knowledge or modification of the governing equations of the model. The (full complexity) model has to be run P times with different sets of collocation points to directly fit the polynomial representation of Ω. This leads to a system of linear equations, that can be directly solved:

$$\boldsymbol{P}_{\Psi}(\boldsymbol{\omega})\boldsymbol{V}_c(x,y,z,t) = \boldsymbol{V}_{\Omega}(\boldsymbol{\omega},x,y,z,t)\,, \tag{3.20}$$

where $\boldsymbol{P}_{\Psi}$ (P x P matrix) contains the polynomials, $\boldsymbol{V}_c$ is a vector of length P with the unknown coefficients c_j. The optimal choice of collocation points is the roots of the polynomial that is one degree higher than the order d used in the chaos expansion (see Villadsen and Michelsen (1978)).

After the determination of the unknown coefficients, a set of polynomials forming a response surface is available for estimating the model output dependent on the uncertain model input. If the basis is normalized the mean and the variance can be simply derived by the coefficients: $\mu(\Omega) = c_1$ and $\sigma^2 = \sum_{j=2}^{N} c_j^2$. Additional arbitrary output statistics can be derived by Monte Carlo analysis of the polynomials. This Monte Carlo analysis is much faster than running a Monte Carlo simulation with the complex model.

4 Concept for Risk Assessment

This chapter describes the overall workflow for the risk assessment concept developed in this work, which is applied for brine displacement and infiltration in Chapter 5. A workflow is developed regarding how to handle uncertainties and to assess the risk of CO_2 storage in saline aquifers. The overall workflow can also be applied to assess the risk of other applications that can be investigated based on numerical simulations.

The risk assessment concept presented belongs to the first part of the phase of risk appraisal in the overall risk governance model described in Section 3.1.3: the scientific assessment of physical harm that a risk includes. For the overall risk governance process important information about the risk can be derived and values for damage and risk can be provided which can be taken as a basis for the concern assessment, risk evaluation, and risk management. Risk is defined in this context as damage multiplied by probability. The numerical models introduced in Chapter 2 are used to determine the damage, which is defined as a model output. For calculation of probabilities Monte Carlo simulations combined with the model reduction technique introduced in Section 3.2 are applied. For the procedure of the overall risk assessment concept the division of the uncertainties into different levels of knowledge is followed (see Section 3.2.1, Walker et al. (2003)).

First, all relevant uncertainties are identified and selected. These uncertainties are categorized to the corresponding level of uncertainty. Three kinds of uncertainty are addressed in this work: statistical uncertainty, scenario uncertainty and recognized ignorance. If all three levels are investigated in one risk assessment, the best order is to start with the investigation of recognized ignorance to define an adequate model set-up. In the next step, different scenarios with the defined model set-up can be investigated and at least the most important scenarios can be chosen for investigation of statistical uncertainty. However, it is difficult to address all levels in each risk assessment. Thus, in many investigations the most relevant levels are chosen. The assessment of the uncertainties is performed by numerical simulations and statistical methods. In the risk assessment step, the result is either damage or risk. The estimated risk or damage can be optionally translated to another risk or damage value, which is more comparable to regulation criteria. For the translation analytical approximations can be applied. In Figure 4.1 the workflow of the risk assessment procedure is presented. In the following the methodology is described in more detail.

4.1 Identification and Classification of the Uncertainties

Various kinds of uncertainties can be found when risks associated with any kind of material storage (e.g. CO_2 or methane) in the underground are estimated (e.g. uncertainties in

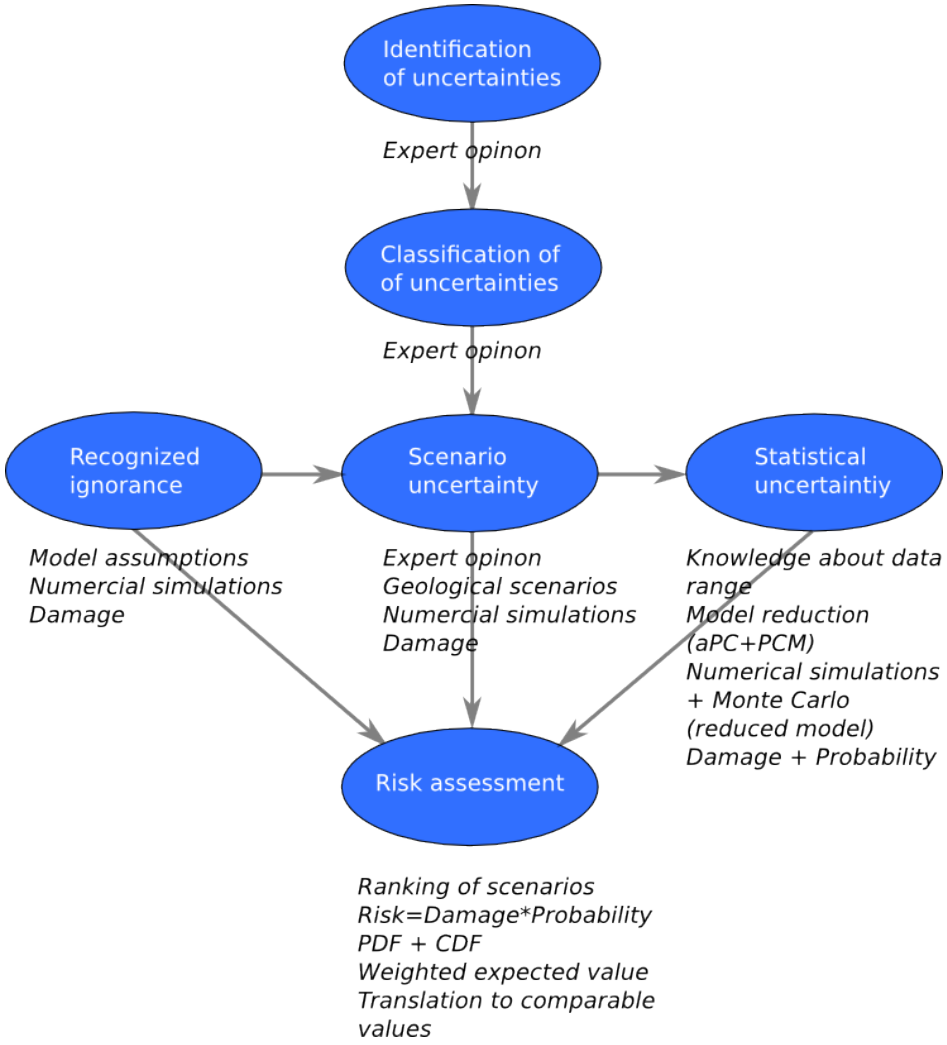

Figure 4.1: Overview of the risk assessment concept.

the data and their spatial distribution, the detailed geological set-up, the geochemistry and the geomechanics in the affected subsurface regions, the operational strategy etc.). In this thesis, the approach of Walker et al. (2003) (described in Section 3.2.1) is followed and the uncertainties are categorized into levels of knowledge. Figure 4.2 shows the different levels from determinism to total ignorance. The different levels are interpreted in the scope of this work as follows:

- Statistical uncertainty can be described statistically, thus the probabilities of the input parameters are known.
- Scenario uncertainty can not be described statistically, thus the probabilities are unknown. Scenarios are physically motivated, e.g. different geological features. Adequate scenarios have to be chosen properly by considering the opinion of experts in the field of interest, e.g., geologists.

- Recognized ignorance are uncertainties due to limitations in the conceptual and numerical model. In this work only the reducible ignorance is considered. Thus, assumptions in the model (e.g. neglecting compositional effects or geochemistry, limited extent of the model domain) belong to this level. Recognized ignorance is not based on different possible description how a system may react as scenario uncertainty (see Walker et al. (2003)) but rather on the fact that models can only describe the nature with limitations.

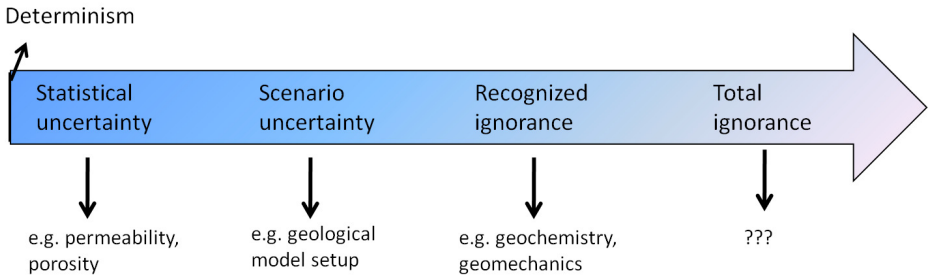

Figure 4.2: Levels of uncertainty after Walker et al. (2003).

At first, the relevant uncertainties corresponding to a certain risk (e.g. the risk of brine displacement and infiltration into freshwater aquifers) which should be assessed, have to be identified. This important task should be carried out carefully, since all relevant uncertainties need to be collected. Thus, experts in the field of interest should already be consulted for this step. In a second step, the uncertainties are classified according to the different levels shown in Figure 4.2.

In the case of CO_2 storage, such uncertainties that can be described statistically can be found, for example, in the permeability or porosity distribution, or in different anisotropy values. Uncertainties such as the geological layering considered in the model, a gap in the caprock, a fault zone along the layers, or the dip or topography of the domain cannot be described sufficiently by statistical terms and are classified as scenario uncertainties. The choice of the considered processes (e.g. advection, diffusion, dispersion, dissolution, geomechanics, geochemistry) in the model concept belong to the level of recognized ignorance, which are defined as fundamental uncertainties about the mechanisms and functionalities and assumptions made in the model set-up. For example, the geochemical effects during CO_2 storage are very often neglected since not all the interacting complex processes can be described properly yet, and accounting for it, even if equations and corresponding data were available, would increase computational costs enormously. The grid type or its resolution or the domain size are other examples for the level of recognized ignorance.

Measurements and site exploration typically reduce uncertainty. For example, drilling an exploration well together with a seismic campaign might substantially improve the knowledge of number and orientation of distinct geological features, while still leaving much uncertainty as to their specific properties. When considering uncertainty due to geological features, there can be a continuous transition between the two categories of statistical or scenario uncertainty. The modeler must consider both the unknown natural conditions and

interpretations of available expert opinions. The uncertainties are sorted in the most suitable level.

For a given system, all these levels of uncertainties can be found. All levels of uncertainty discussed in this work, except for total ignorance, can be also classified into the commonly used concept of epistemic and aleatory uncertainty, (the nature dimension in Walker et al. (2003)). The described examples for uncertainties such as permeability, the geological model set-up, or geochemistry are epistemic uncertainties since more measurements or more sophisticated models reduce uncertainty. However, in engineering practice there will always remain an aleatory uncertainty in parameters like permeability or porosity due to insufficient measurements.

The most relevant uncertainties have to be chosen for investigation. For the step of identification, classification, and selection of the uncertainties, experts in the field of interest should be involved. At this stage it is already important to incorporate stakeholders who could be affected by the risk. These stakeholders have a different perception of the techniques and the associated risks, and additional uncertainties could be identified or other uncertainties could be considered to be more relevant. The procedure to rank the uncertainties helps to provide a good and comprehensive overview of the related uncertainties. In this workflow, recognized ignorance, scenario and statistical uncertainties are addressed. The methods how they are investigated are presented in the following.

4.2 Investigation of Recognized Ignorance and Scenario Uncertainty

Both recognized ignorance and scenario uncertainty are investigated by numerical simulations of different model set-ups or scenarios. The quantity to compare the model set-ups or scenarios is called the damage and is defined as a model output or is derived from the model output. However, the mathematical definition of damage has to be carefully chosen for each risk assessment individually.

For the investigation of recognized ignorance different model set-ups are compared. The uncertainties that are investigated are basic fundamentals in the model concepts or assumptions made for the selected domain. Numerical simulations with, e.g., different conceptual models, domain sizes, or grid resolutions are performed. For example, the influences of dissolution and diffusion processes can be investigated by comparing simulations with a 2p and 2p2c model. Investigations of recognized ignorance can help to reduce the uncertainties for further investigations of scenario and statistical uncertainties by choosing an adequate model concept, domain size, or grid resolution.

Scenario uncertainty is addressed by numerical simulations of various well defined scenarios. A systematic investigation of scenario uncertainty is presented, e.g., in Aisopou et al. (2012). For the selection of the scenarios, expert opinions are important. In most instances, it is not possible to address all uncertainties, identified in the first step. However, the most

relevant uncertainties should be covered by the scenarios. For each scenario, a full complex numerical simulation is performed and the damage is calculated. The complexity of the model for the numerical simulations has to be adapted to the processes that are relevant for the risk investigated (recognized ignorance). The different scenarios can be compared depending on the damage in the next step of risk assessment.

4.3 Investigation of Statistical Uncertainty

For statistical uncertainties, both damage and probabilities are determined. The damage is calculated in the same way as for the scenario uncertainty and recognized ignorance and is defined as a model output. To determine the probabilities, the (statistical) uncertainties are considered. Statistical uncertainties occur in the spatial distribution of parameters, but also in their averaged values. A possible way of dealing with the statistical uncertainties is by performing Monte Carlo simulations with the complex model, which would be computationally very costly. An alternative approach for handling these uncertainties with acceptable computational costs is to reduce the model via the polynomial chaos expansion technique (Oladyshkin et al. (2011b)) and its recent generalization for arbitrary parameter input (Oladyshkin et al. (2011a)). This technique which is described in Section 3.2.2 is applied in this work.

4.4 Risk Quantification

For the categories of recognized ignorance and scenario uncertainty, there is no statistically representative information on the features of a selected model set-up or scenario available. The determination of probabilities would require an adequate statistical description of how the parameter varies. However, the complexity of the different model set-ups or scenarios cannot be described statistically. Thus, it is not possible to determine probabilities on the basis of the aPC/PCM approach. To this end, only damage values are calculated for the different model set-ups and scenarios. For these levels a real quantification of risk is not possible, but the model set-ups and scenarios can be ranked depending on their damage.

When uncertainty is statistical, both damage and probability can be calculated, since the distribution of parameters like permeability or anisotropy can be quantified. The approach to quantify risk followed in this work is often found in the literature, and defines risk as

$$\text{Risk} = \text{Probability} \times \text{Damage}\,. \tag{4.1}$$

This means that the risk is the expected loss incurred by an accident, which is defined as damage multiplied by the probability of an accident occurring. As already mentioned, the mathematical definition of damage has to be chosen carefully for each risk assessment individually depending on the hazard which is evaluated. It is necessary that damage can be derived from the model output of the numerical simulations. As discussed in Section 3.1, the

definition of risk as one value is often criticized because of the same weighting of low probability/high damage and high probability/low damage events. Thus, several possibilities (e.g. mean values, PDF, CDF) to present the risk or damage are discussed here.

To determine the probability of a certain damage, a stochastic approach is required. As explained in Section 3.2.2 and 4.3, the complex model is reduced via the arbitrary polynomial chaos expansion (aPC) combined with the probabilistic collocation method (PCM). Mean values and variances of the model output can be easily computed with the polynomials. To calculate the probabilities, Monte Carlo calculations on the polynomials can be performed, which is much faster than using the complex model for hundreds or thousands of runs. This can provide a probability density function (PDF), where the probability distribution for the whole range of the damage can be read, or a cumulative distribution functions (CDF) for the damage, where the evidence probability can be determined for a certain value (e.g. high pressures or brine discharge events). In addition an overall risk value can be estimated by summing each damage and probability value of the sample and dividing by the sample size N:

$$\mathrm{E[Risk]}_i = \frac{\sum_i^N \mathrm{Damage}_i \mathrm{Probability}_i}{N} \tag{4.2}$$

The result can be interpreted as the probability-weighted expectation of damage. The output that is presented (mean damage, PDF, CDF, or expected risk) should be chosen depending on the hazard that is evaluated and the people (politicians, stakeholders, public), who are addressed. The aim is to present the results in a way that non experts can interpret them as well.

4.5 Translation into Comparable Results

The model output of the numerical simulations defined as the damage (e.g. brine discharge in kg/s) is sometimes not adequate for comparison with, e.g., maximum permissible values (e.g. concentrations in mg/l). To this end, analytical approximations can help to close the chain of reasoning. The aim of these simple analytical approximations is to emphasize that a comprehensive risk assessment requires a set of consistent methods which allow various levels of uncertainties as well as operational strategies to be considered. For brine displacement, analytical approximations such as the fully mixed or the salt water upconing approach can be applied (see Chapter 5). For the CO_2 leakage problem, the heuristic model to predict the intrusion rate of contaminant vapors into buildings presented by Johnson and Ettinger (1991) could be applied to estimate the effects of a CO_2 intrusion into building on the overall CO_2 concentration inside (not in the scope of this thesis). The various methods are linked to achieve an integral risk assessment methodology, which ultimately needs to be comprehensive for decision makers as well.

5 Application of the Risk Assessment Concept for Brine Displacement

In this section, the risk assessment concept described in Section 4 is applied for brine displacement and infiltration into a freshwater aquifer during CO_2 injection into a saline aquifer. It has to be underlined that this is a principle study with the main purpose to present the overall method. To this end, it is tested for the risk of brine displacement for simplified geological models and not based on a realistic storage site. However, all simulation paramters that are applied are taken from realistic data related to CO_2 storage sites and freshwater aquifers.

As described in Section 1, the injected CO_2 will displace brine which is initially present. Injected CO_2 (partly) dissolves in the brine and the non-dissolved gaseous CO_2 requires pore space. The pore space is gained by compression of the fluids and the rock and mainly by displacement of the resident brine. The displaced brine could move into shallower aquifers through caprock failure, fractures, faults, or abandoned wells and subsequently infiltrate and pollute freshwater aquifers with salt and other contaminants. An important question is, where the brine will migrate to during the CO_2 injection and in the post-injection period. Obtaining estimates for damage events and their likelihood is of major interest to water suppliers, thus the focus will be on the salt transport and potential damage to freshwater resources. High salt concentration in water aquifers can exclude the use of groundwater for drinking or affect wildlife habitats, or pollute surface waters.

To assess comparable damage values and probabilities for the event of brine displacement into freshwater aquifers three steps are presented: In the first step, the main purpose is to test and present the overall risk concept; to identify the most relevant scenarios; and to derive damage and probabilities for a conservative model assumption. In the second part, recognized ignorance is reduced by increasing the model complexity to account for more processes and to calculate more exact damage values for different scenarios. The last part concentrates on the processes in a freshwater aquifer and includes water production to derive damage and risk as salt concentrations in water production wells.

5.1 Brine displacement and infiltration during CO_2 injection - 2p model [1]

The risk assessment concept described in Section 4 is followed in this section: Scenario and statistical uncertainty are investigated and risk is calculated. Finally, the risk is translated into values which are comparable to water quality criteria. Recognized ignorance is not investigated in this part and will be addressed in Section 5.2 in particular. The main part of this section is published in Walter et al. (2012).

Scenario uncertainty is investigated by simulating 6 scenarios with different geological setups and subsequent ranking according to the resulting damage. Accounting for statistical uncertainties requires the further testing of parameter spaces. Thus Monte Carlo simulations with the reduced model using polynomial chaos expansion combined with the probabilistic collocation method (see Section 3.2.2) are performed. In order to quantify the impact of brine migration on a resource like potable groundwater, it is necessary to consider both brine migration from the reservoir and its mixing with freshwater resources. Therefore, additional approximations for assessing the salt concentrations in the water aquifer and for investigating salt water upconing at water-production wells are discussed.

Section 5.1.1 shortly discusses which uncertainties are identified and considered and Section 5.1.2 provides a description of the simulation model. In Section 5.1.3 the results for 6 different scenarios are shown. Section 5.1.4 discusses the influence of the parameter variation. Section 5.1.5 characterizes the risk of brine breakthrough. In Section 5.1.6, analytical approaches to translate the derived damage into values that can be compared to water quality criteria are presented. It is concluded with discussions and conclusions in Section 5.1.7.

5.1.1 Identification of Uncertainties

Before the simulation and risk assessment is started, the related uncertainties have to be defined and classified. It is impossible to consider all uncertainties in one study, thus it is very important to select the most important ones. In this study uncertainties are selected by CO_2 modeling experts. In a real case study, more experts like geologist and local stakeholders should be involved into the selection. For this study, the geological layering and the existence of geological features is seen to be the most important scenario uncertainty by the experts. Thus, a gap in the caprock, a fault zone, different permeable zones in the fault, and low permeable barriers are considered. Such a list of scenarios is, of course, never complete; other scenarios such as with inclined caprock or with the existence of an abandoned well are only two examples. However, the considered list of scenario uncertainties contains a representative selection of possible features. There exist a lot of statistical uncertainties when modeling CO_2 storage, as already discussed in Section 4.1. Once again, the most relevant ones have to be chosen by experts for risk evaluation. Here, the considered uncertain

[1] Parts of this section are published in Walter, L., Binning, P. J., Oladyshkin, S., Flemisch, B., and Class, H. Brine migration resulting from CO_2 injection into saline aquifers an approach to risk estimation including various levels of uncertainty. International Journal of Greenhouse Gas Control, 9:495-506, 2012.

parameters are the permeability of the reservoir, fault permeability, and anisotropy of all layers.

It is important to have in mind the uncertainties which exist in the model and are classified as recognized ignorance, which is not investigated in this section. In this study, geochemistry and geomechanics are neglected. Accounting for both would highly increase computational costs and is not the purpose of this study. In addition, the variability of the salt content is neglected which results in conservative risk estimates, since typically, salinity is increased with depth. This is considered justified if, like here, a primary goal is just to identify geological setups having high potentials for brine displacement. Dissolution of CO_2 is neglected as well, which is a conservative approximation for simulation of CO_2 storage, since the amount of CO_2, which will dissolve in water stays in the gas phase. This results in a larger CO_2 plume and an increased brine displacement. This approach is feasible to use in risk assessment applications since often a worst case situation should be investigated.

The simplification of the model domain to a radial symmetric domain also belongs to this category, which means that it can not be accounted for groundwater flow. All these assumptions and simplifications are reasonable for the main purpose of presenting the overall method and identifying geological situations which have a high potential of brine leakage.

5.1.2 Model Set-up

The model set-up is based on the assumption that drinking water is pumped from a depth of 500 m. Such a deep pumping depth is considered because it is assumed that municipal authorities wish to protect all drinking water resources above a CO_2 reservoir and the deepest system would be those first polluted if leakage occurred. It is further assumed that the freshwater aquifer is located above the CO_2 storage reservoir, separated by 7 geological layers in between. The storage reservoir is located in a depth of 817.5 m. At this depth, pressure and temperature are high enough to assure supercritical conditions. For CO_2 storage it is important that the CO_2 is in the supercritical state because it has a higher density than in gaseous or liquid state, which increases the storage capacity and safety.

The model domain is confined at the bottom by the storage reservoir, into which the CO_2 is injected, and at the top by the freshwater aquifer, with a caprock and low permeable layers (aquitards) in between. All layers, except for the freshwater aquifer, initially contain brine of equal constant salinity (0.1 kg salt/kg solution). Compared to the most probable situation of salinity increasing with depth, this is a conservative assumption. Figure 5.1 shows a schematic view of the domain for the reference scenario.

A radially symmetric 3D model domain is set up with an inner radius of 1 m representing the injection well. The domain has a height of 350 m and an outer radius of 10 km (see Figure 5.2). The simulated domain represents 1/12 (30°) of a circle, which means that extensive values like brine discharge or injection rate need to be multiplied by 12 to account for the entire domain. The upper and lower boundaries as well as the segments' symmetric boundaries are modeled with closed no-flow boundary conditions. Closed boundaries on the top and the bottom of the reservoir lead to higher pressures than would be obtained with open

boundaries. This assumption corresponds to the existence of aquitards of very low permeabilities at top and bottom. The outer boundary at 10 km distance is a hydraulically open constant-head boundary. This also has an influence on the pressure in the domain since the prescribed injection rate causes primarily a pressure gradient. Thus, dependent on the size and the traveling speed of the pressure signal, a fixed head at the boundary can lead to an underestimation of pressure in the domain during injection. Therefore, to minimize errors induced by this boundary condition, the distance to the investigated locations should be large. The CO_2 injection period is 25 years at a rate of 1 Mt CO_2/a. The actual injection rate into the radially symmetric section corresponds to 1/12 Mt/a.

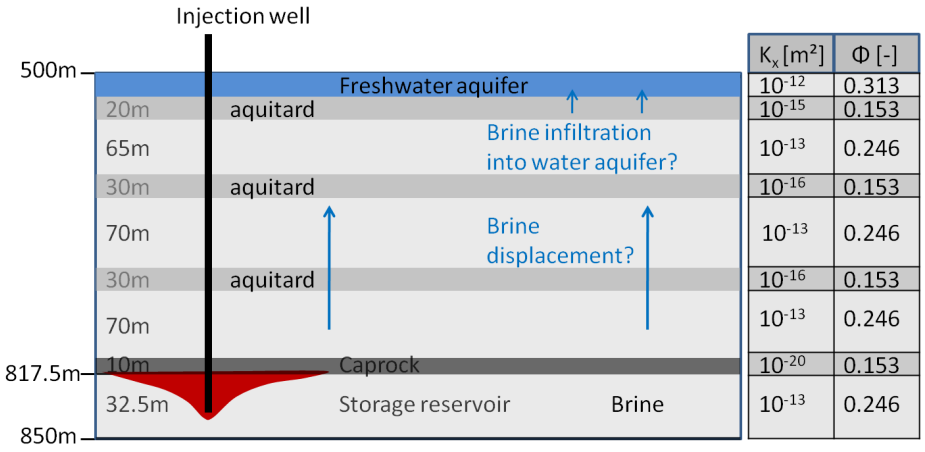

Figure 5.1: Schematic cross-sectional view of the reference scenario to estimate the risk of brine infiltration into a freshwater aquifer including permeability and porosity values for all layers ($K_z = 0.1 \cdot K_x$).

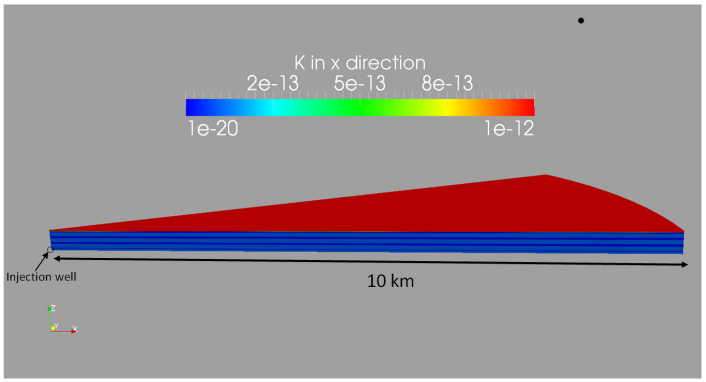

Figure 5.2: Model domain (1/12 segment of a circle).

A two-phase (2p) model (see Section 2.4.1) implemented in the simulator DuMu^x including only the phases CO_2 and brine is applied, which means that the model does not distinguish between salt water (brine) and freshwater. The output of interest is the brine discharge into the water aquifer. For the 2p model (no compositional effects considered), only advective

discharge is calculated, which is defined for each phase as:

$$\text{Discharge} = -\mathbf{K} \cdot ((\text{grad} p_\alpha) - \rho_\alpha \, \mathbf{g}) \, \rho_\alpha \, \lambda_\alpha \, A \cdot \mathbf{n} \, , \tag{5.1}$$

with the discharge in [kg/s], the mobility λ_α in [1/Pa s], the surface area A in [m^2], and the unit normal vector $\mathbf{n}$. For rock compressibility it is accounted for by Equation 2.20.

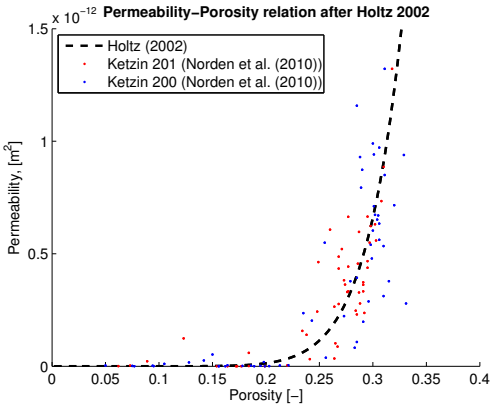

Figure 5.3: Relations between permeability and porosity.

The horizontal permeabilities K_x and porosities for the reference scenarios are shown in Figure 5.1. The anisotropy for all layers is set to 0.1 (for vertical permeability yields: $K_z = 0.1 \cdot K_x$). The porosity is related to the different permeabilities of the layers using (Holtz (2002) and Kumar et al. (2005)):

$$\Phi_{init} = \sqrt[9.61]{\frac{K_x^*}{7e^7[mD]}} \, , \tag{5.2}$$

where K_x^* is the horizontal permeability in [mD]. Figure 5.3 shows the relationship and a comparison with real data determined from core samples from the Ketzin site located near Berlin in Germany (Norden et al. (2010)). The values of porosity and permeability for two core samples are shown. The used relation fits well with the sampled data. For permeabilities lower than 1 mD ($10^{-15}$$m^2$), the relationship is not verified by data. However, this relationship is also used to determine the porosity in layers of low permeability and the caprock since the values obtained are reasonable. Birkholzer et al. (2009) use similar values for the aquitards in their simulations. Based on this reference scenario, different variations are chosen to estimate which geological structure is associated with the highest risk of brine infiltration into the freshwater aquifer, see Section 5.1.3.

5.1.3 Impact of Scenario Uncertainty

Scenario uncertainty is addressed by numerical simulations of various well-defined scenarios (see Section 4.2). Brine infiltration into the shallower freshwater aquifer is obtained by simulating the CO_2 injection process into a deep geological reservoir; in this case, a 25 years injection period and 25 years of the post-injection period are simulated. Various geological

features such as fractures, faults, or seal weaknesses can influence the success of storage and are considered to explore uncertainties attributed to different scenarios. They influence the amount of brine infiltrating into a shallow freshwater aquifer.

Figure 5.4 shows the scenarios with the characteristics which are considered relevant by experts for the risk assessment. Scenario 1 is the base case with a closed caprock as described in Section 5.1.2. In Scenario 2, the caprock ceases to cover the CO_2 reservoir at 5 km distance from the injection. In Scenario 3, a vertically oriented fault zone of higher permeability (K_{fault}=10^{-12} m^2) exists at the same horizontal distance. The aquitard zones along the fault zone are less permeable (K= $5.5 \cdot 10^{-15}$ m^2) in Scenario 4 compared to Scenario 3. Scenarios 5 and 6 consider worst-case (in terms of brine migration) modifications of Scenario 3, where low permeable barriers are introduced: in Scenario 5 only in the reservoir, in Scenario 6 over the whole depth.

Due to the grid resolution, only very simplified fault zones extending some hundred meters (in this study: 370 m) are investigated. Such broad fault zones are nevertheless reasonable since larger zones of different rocks are often found in geological formations, as a result of subrosion for example.

Results Figure 5.5 shows the total brine mass discharge over time into the water aquifer for each scenario. Figure 5.6 presents the brine mass discharge only from the region, where the fault zone is (S3-S6), or would be (S1, S2). Figure 5.7 illustrates the pressure profile directly above the caprock in a horizontal direction for selected cases.

In Scenario 1, i.e. the reference case, no brine discharge into the aquifer is observed (see Figure 5.5 and 5.6) because the caprock has no leaking fault and has a permeability of $K_{Caprock} = 10^{-20}$ m^2. The brine is displaced in a horizontal direction and leaves the model domain laterally through the open (constant-head) boundary at the end of the domain. The pressure profile above the caprock in Figure 5.7 shows no increase. This implies that brine is not displaced through the caprock. A simple calculation shows how much brine would actually be displaced if incompressibility was assumed for the fluids and the rock. The given CO_2 injection of 2.64 kg/s then corresponds to a displaced brine discharge of 4.53 kg/s.

In Scenario 2 (see Figure 5.4b), the caprock ceases at about 5 km distance and the overlying sediment has a high permeability. The gap in the caprock leads to a maximum discharge into the aquifer of 0.31 kg/s and the pressure above the caprock increases strongly (see Figure 5.5 and 5.7). However, the brine discharge through the gap, along the region, where the fault zone would be, is almost zero (see Figure 5.6), and the highly concentrated salt water from the reservoir does not reach the freshwater aquifer directly. Rather, the increase in pressure leads to a flow of brine from the layer directly below into the aquifer. The difference in salt concentration is not modeled because the salinity is constant in the model. A clear pressure peak directly at the gap zone of the caprock can be identified. The aquitards in between the reservoir and the aquifer apparently do not act as completely impermeable layers like the caprock above the reservoir. However, the intermediate aquitards cause a partial retention of the brine and the highly concentrated salt water is held back in lower layers.

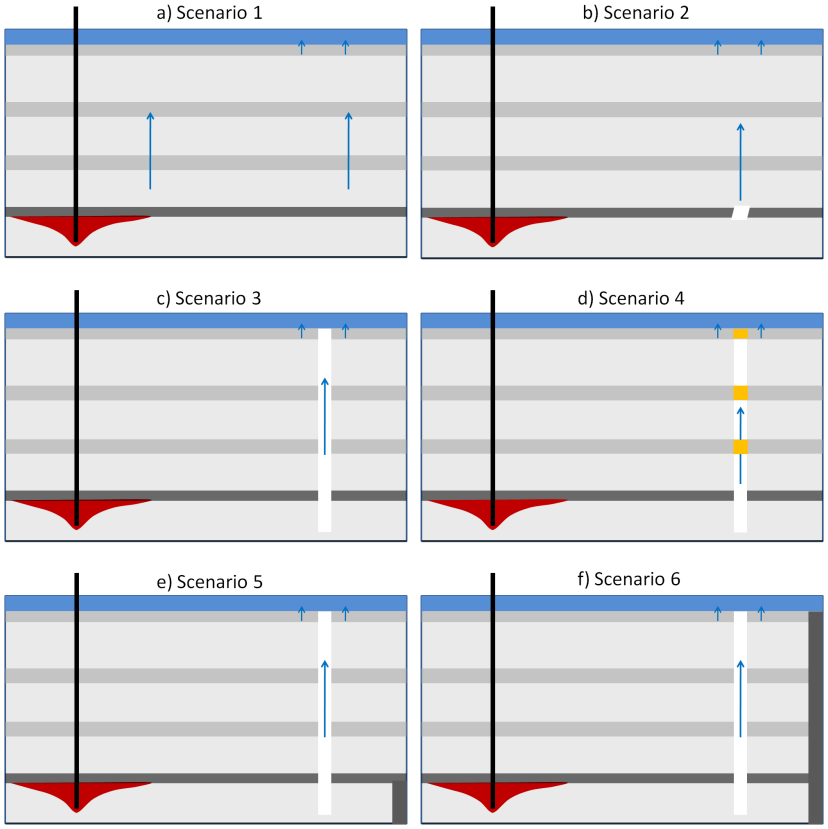

Figure 5.4: Schematic view of the different geological scenarios. Scenario 1: reference scenario with closed caprock, see Figure 5.1; Scenario 2: gap in the caprock at about 5 km distance; Scenario 3: fault zone at about 5 km distance ; Scenario 4: lower permeability of the fault zone in the aquitard layers; Scenario 5: barrier of low permeability within the reservoir (at 9500 m); Scenario 6: barrier of low permeability over the whole domain (at 9500 m);

The importance of the low permeability aquitards above the caprock becomes clear when comparing Scenario 2 with Scenario 3, which has a fault zone at about 5 km distance throughout the vertical extent of the domain (see Figure 5.4c). Here, all aquitards are crossed by a highly permeable zone. A much higher discharge into the aquifer with a maximum of 1.86 kg/s occurs since the brine can be displaced more easily through the highly permeable fault zone. Comparing the brine discharge over the whole layer with the discharge along the fault zone alone shows that almost all the brine is displaced along the fault zone (97%). The pressure above the caprock is much lower than in Scenario 2, since the pressure can propagate more easily through the highly permeable fault zone.

Scenario 4 is a variation of Scenario 3: the fault zone is less permeable (K=$5.5 \cdot 10^{-15}$ m^2) where it passes through the aquitards (see Figure 5.4d). These barriers reduce the brine discharge and the ratio of discharge through the fault is slightly changed (91% discharge through the fault zone). The pressure peak above the caprock is higher than in Scenario 3 but still much lower than in Scenario 2, since the pressure can still propagate through the

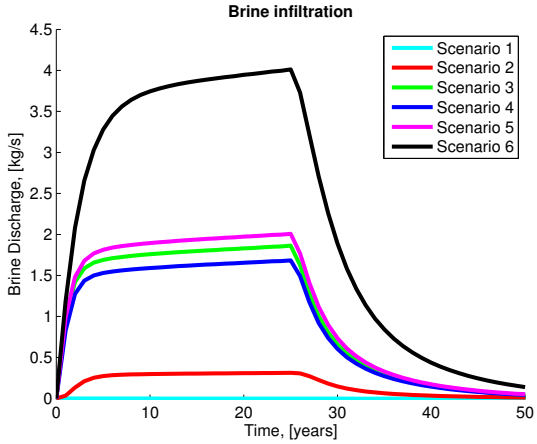

Figure 5.5: Total brine discharge into the freshwater aquifer (over the whole domain) for the different scenarios.

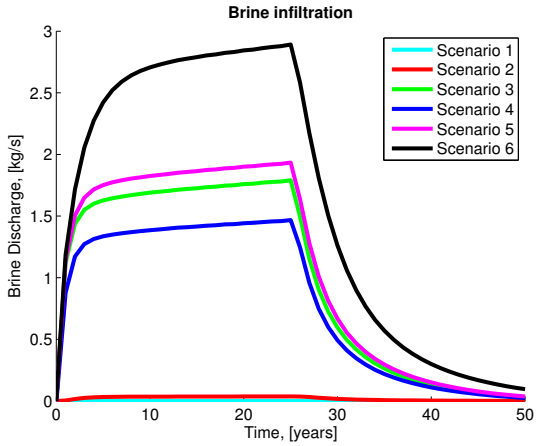

Figure 5.6: Brine discharge into the freshwater aquifer (along the fault zone) for the different scenarios.

fault zone.

Scenario 5 and 6 are very unfavorable scenarios, where there is a fault zone as in Scenario 3 and there are barriers of low permeability at about 9500 m distance from the injection. In Scenario 5, the barrier of low permeability is only in the reservoir (see Figure 5.4e), whereas in Scenario 6, the barrier reaches from the reservoir through the whole vertical profile up to the aquifer (see Figure 5.4f). The discharge into the aquifer is increased in both scenarios in comparison to Scenario 3 since, in the latter case, more brine can be displaced horizontally from the reservoir (see pink and black lines in Figure 5.5). Particularly in Scenario 6, the observed discharge is more than double and reaches a value of 4.01 kg/s. Nearly all the displaced brine infiltrates the aquifer. An interesting point is that 97% of the brine still discharges through the fault zone in Scenario 5 but only 72% is displaced through the fault zone in Scenario 6. In Scenario 6, the pressure in the layer directly below the aquifer is higher

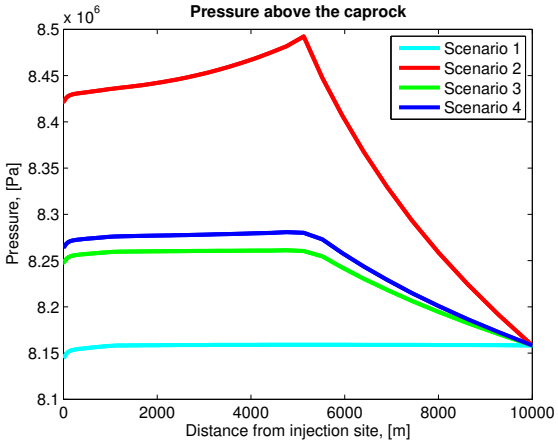

Figure 5.7: Pressure above the caprock along the model domain ($p_{initial}$= $8.1582 \cdot 10^6$Pa).

due to the barrier; therefore, the displaced brine is distributed over a larger area and cannot be displaced in the horizontal direction. It infiltrates the aquifer due to the higher pressure near the barrier. For Scenario 5, the pressure above the caprock is the same as in Scenario 3, and for Scenario 6, the pressure increases only slightly.

In most of the scenarios, the brine discharge has ceased after 50 years (25 years after CO_2 injection stops). A small amount of brine is still infiltrating the upper aquifer only in the worst of the selected cases (Scenario 6). An important issue is the different brine discharge areas of the scenarios. In Scenario 2, a discharge can be measured over the whole layer underneath the aquifer, but nearly no brine is displaced directly along the region, where the fault would be as in Scenario 3. This means that the discharged brine is water which originates from directly below the freshwater aquifer and is expected to have a significantly lower salt content than water from greater depth. This is not modeled in these simulations since a salt component of variable concentration is not explicitly considered and the salinity is constant (0.1 kg salt/kg solution). For the highly likely situation that salinity decreases at shallower depth, the obtained result is a conservative estimate. For the scenarios with a fault zone (scenarios 3-6), it is more probable than in Scenario 2 that highly concentrated brine reaches the aquifer, since it is displaced directly along the fault zone. The values for brine discharge along the fault zone in Scenarios 3-6 are more realistic since here, water with high salt content can migrate directly from the reservoir to the aquifer. However, these values are still overestimated since the rising, highly concentrated brine would mix with the surrounding, less concentrated water. These effects of dilution and mixing are investigated in Section 5.2.

5.1.4 Impact of Statistical Uncertainty

Many parameters like reservoir permeability, porosity, and anisotropy are uncertain. Often these uncertainties can be described statistically, but to do so requires adequate distributions. In the best case, measurement data are available for the uncertain parameters to provide an appropriate distribution. In the following, Scenario 4, which has a fault zone with

lower permeability in the aquitard zones, is chosen as an example to investigate statistical uncertainties. Thus, the aPC combined with PCM is applied in the investigation (see 3.2.2 and 4.3). The uncertain upscaled/averaged parameters are the permeability in the storage reservoir, the anisotropy for all layers except the fault zone, and the aquitard permeability in the fault zone. For the distribution of the reservoir permeability, the Ketzin data (see Norden et al. (2010)) are used. The other distributions for anisotropy and fault permeability are selected based on a reasonable range of values. Anisotropy is chosen between 0 and almost 1 with a higher probability for smaller values. The data for aquitard permeability in the fault zone are varied between 10^{-17}m^2 and 10^{-12}m^2. For both parameters, a beta distribution is taken as the basis. Figure 5.8 shows the resulting distributions of the three parameters.

Third-order polynomials are used to project the complex model onto a response surface. Third-order is a sound trade-off between accuracy and computational effort (Oladyshkin et al. (2011a)). Three uncertain parameters and third-order polynomials result in $P = 20$ unknown coefficients in the expansion, see Eq. (3.16), and as a consequence require 20 simulation runs (snapshots). The four collocation points chosen for each parameter are listed in Table 5.1.

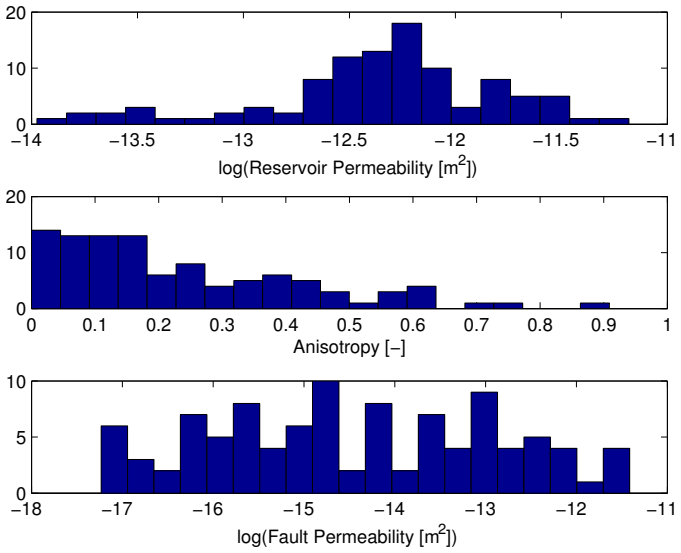

Figure 5.8: Distributions for the uncertain parameters: Permeability of the reservoir, anisotropy, and fault permeability in the aquitard layers.

Reservoir permeability [m^2]	Anisotropy [-]	Fault permeability [m^2]
$1.7826 \cdot 10^{-14}$	0.0435	$1.2278 \cdot 10^{-17}$
$1.3915 \cdot 10^{-13}$	0.2291	$4.4076 \cdot 10^{-16}$
$6.9912 \cdot 10^{-13}$	0.5294	$4.1062 \cdot 10^{-14}$
$3.4914 \cdot 10^{-12}$	0.8573	$1.3027 \cdot 10^{-12}$

Table 5.1: Collocation points for snapshot simulations.

Results With set-ups of 20 different combinations of the collocation points, the original model is projected onto the polynomials. For a detailed interpretation of the dependencies, Figure 5.9 shows the change in brine discharge for each uncertain parameter while the other parameters are held constant. The points shown represent a selection of snapshot runs with the same values for the remaining parameters, and the polynomials are constructed to fit through these points. In the following, the dependence of the brine discharge on each parameter and the accuracy of the polynomials are discussed.

For anisotropy, the polynomial reflects the continuously increasing behavior very well (see Figure 5.9a). Higher anisotropy increases the brine discharge into the aquifer. Increasing the anisotropy means a lower flow resistance in the vertical direction. The anisotropy in all layers except for the fault zone is increased. Thus, more brine is displaced vertically and the brine discharge into the aquifer becomes greater.

An increase of the fault permeability has a similar effect as increasing anisotropy (see Figure 5.9b). More brine infiltrates the aquifer with higher fault permeability, since the resistance of the flow path along the fault is decreased. This continuous increase diminishes for high-value fault permeabilities and the brine discharge remains almost constant (see the two snapshot runs with higher permeability in Figure 5.9b) because the resistance is already low enough to let the displaced brine flow. The behavior of the brine discharge depending on the fault permeability is reflected well by the polynomial in regions of lower permeability. In the region of higher permeabilities, the highly nonlinear behavior cannot be reflected adequately by the polynomials. The extrapolation for higher permeabilities outside the range of snapshot simulations yields the wrong characteristics, and one has to be careful while using the polynomials for risk assessment. The limitations of the collocation method will be discussed in more detail in Section 5.1.7.

While both anisotropy and fault permeability lead to a more or less monotonic response of the brine discharge, this is not the case for reservoir permeability. At the beginning of injection, the brine discharge first increases and then decreases again with increasing permeabilities (see Figure 5.9c permeability after 2 years of injection). If the permeability is very low, the pressure during CO_2 injection will be higher, due to higher flow resistance. The higher pressure increases the effect of compressibility of the fluids and the rock. Thus, less brine needs to be displaced. Higher permeability of the reservoir results in smaller pressure peaks. Thus, at lower pressures, the compressibility effect is reduced. Consequently, more brine has to be displaced to free the required pore space, and more brine infiltrates the aquifer. At a certain value of the reservoir permeability, the brine discharge decreases again. Here, the permeability of the reservoir is similar to the permeability of the fault zone. In this situation, more brine can be displaced in the horizontal direction from the reservoir instead of vertically against gravity. At this early stage of injection, the polynomials resemble the behavior well.

As the injection proceeds, the situation changes and the effect of very small permeabilities in the reservoir on the reduction of brine discharge diminishes (see Figure 5.9d: permeability after 25 years of injection). The two snapshot runs for smallest permeabilities result in almost the same brine discharge. At later stages, the compressibility is less important since the pressure at the injection well does not rise further and the displacement becomes

more relevant. Thus, the effect that the brine discharge is lower for smaller permeabilities cannot be observed. Comparing the snapshot runs at the collocation points with the fitted polynomial at later times shows that the behavior is described well by the polynomial for higher permeabilities but a discrepancy can be identified for smaller values. Between the two snapshot runs on the left, the polynomial overestimates the brine discharge because of overshooting in the third-order polynomial. This overestimation is acceptable for the risk calculations since it gives a conservative estimate. However, the steep decrease for further decreasing permeabilities is not seen in further simulations and should not be considered in the risk estimation.

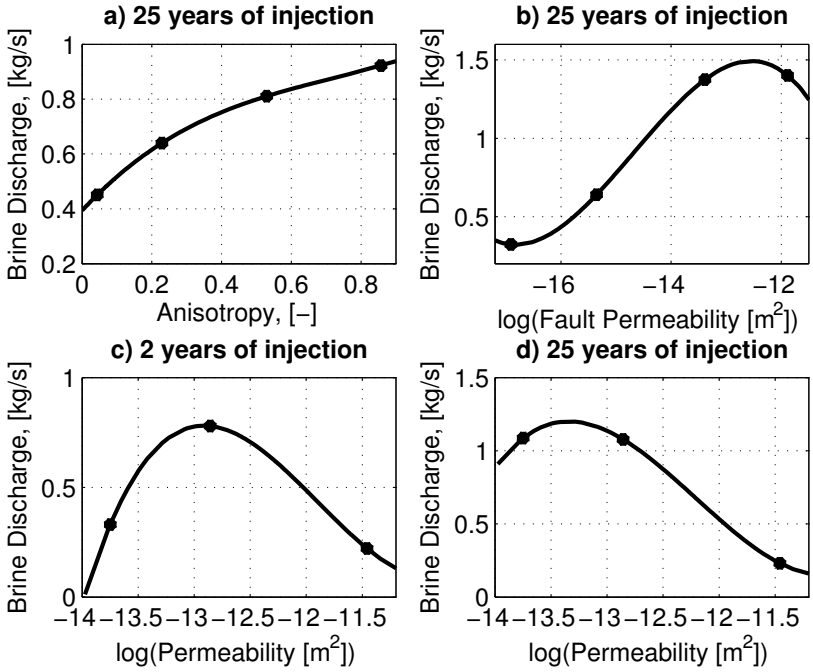

Figure 5.9: Brine discharge versus the uncertain parameters: Snapshot runs (bullets) and fitted polynomials a) for anisotropy after 25 years of injection, b) for fault permeability after 25 years of injection, c) for reservoir permeability after 2 years of injection, and d) for reservoir permeability after 25 years of injection

5.1.5 Risk Assessment

In Kopp et al. (2010), risk is used as a statistical leakage probability that could occur at a well and is calculated by multiplying the likelihood of failure times the consequence of failure. In their work, only the cases were considered when CO_2 leaks. In this study, no explicit failure event occurs for the considered Scenario 4, because in any case brine is displaced and some damage always occurs. Risk, as it is defined here, is the probability-weighted expectation of damage.

As discussed in Section 4.4, the mathematical definition of damage has to be chosen carefully

for each risk assessment individually depending on the hazard which is evaluated. In this study, the damage is defined as the amount of infiltrated brine per time (brine discharge) into the shallower freshwater aquifer:

$$\text{Damage} = \frac{\text{Mass of brine[kg]}}{\text{Time[s]}} . \tag{5.3}$$

5.1.5.1 Scenario Uncertainty

As described in Section 4.4, there is no statistically representative information on the features of a selected scenario available for the category of scenario uncertainty. To this end, only damage values for the scenarios are calculated and these values are compared.

The brine discharge calculated and discussed in Section 5.1.3 corresponds to the damage as defined in this work. With the results from the previous section, the damage in the scenarios can be ranked (S6>S5>S3>S4>S2>S1). Scenario 6 with a fault zone and a barrier of low permeability results in the biggest damage, and is thus the most unfavorable geological structure within the selected scenarios. It is followed by Scenario 5, which results in a smaller damage due to the fact that the brine can also flow in horizontal direction as soon as it leaves the reservoir. Scenario 3 with the laterally open reservoir reduces the damage further, which is also the case when there is a lower permeability in the aquitard zones of the fault (Scenario 4). A substantial reduction of damage is predicted for Scenario 2, and Scenario 1 is the safest one with practically no damage at all. It can be concluded that the caprock integrity and faultless overlying aquitards are the key geological features to keep brine migration to shallower aquifers at a minimum. Other geological features also have significant impact on brine migration, but not to the same extent as faults in the caprock.

5.1.5.2 Statistical Uncertainty

When uncertainty is statistical, both damage and probability can be calculated (Section 4.4), since the distribution of parameters like permeability or anisotropy can be quantified. Here, a cumulative distribution function (CDF) and a probability density function (PDF) are used, and risk is estimated for Scenario 4. Figure 5.10a shows a CDF for the damage (brine discharge) after 25 years of injection for the given uncertain parameters, in this case permeability in the reservoir, fault permeability, and anisotropy. If a certain threshold value for a maximum brine discharge is given, the probability that this value is not exceeded can be determined by the CDF. Example: For a given threshold of 1.84 kg/s, the probability that this value is not exceeded is 95%. Figure 5.10b shows the PDF of the damage (brine discharge). Overall it says that damage values smaller than 1 kg/s are, for example, more probable than damages above this value. However, the risk calculation would shift the significance to larger values of damage since damage and probability are multiplied. An overall risk value for the given Scenario 4 can be estimated with the mean value for risk, i.e. the expected value of risk:

$$\text{E[Risk]}_i = \frac{\sum_i^N \text{Damage}_i \text{Probability}_i}{N} \tag{5.4}$$

where N is the number the sample size of the model parameters. For Scenario 4, the overall risk is then 0.4722 kg/s. This value is interpreted as the probability-weighted expectation of damage for this particular scenario.

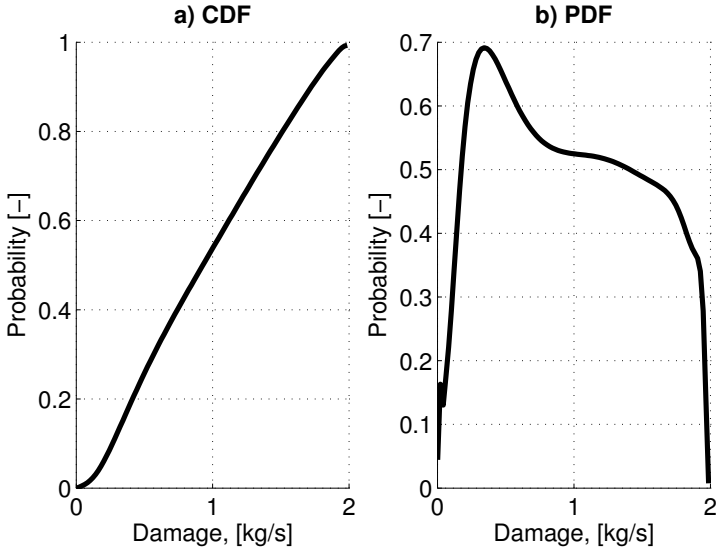

Figure 5.10: Cumulative distribution function and probability density function for brine discharge into the water aquifer after 25 years of injection.

5.1.6 Estimates for Salt Concentration and the Impact on the Freshwater Aquifers

Using estimates of damage and the risk of brine discharge into the freshwater aquifer from the methods, the question of the impact on the freshwater aquifer, i.e. the drinking-water resources can be addressed. For potable water, salt concentrations, or total dissolved solids (TDS) must not exceed a certain value. The World Health Organization (WHO) does not regulate the amount of TDS; however several countries define a critical value for TDS, e.g. Denmark defines a critical value of 1500 mg/l, and Australia does not allow TDS higher than 500 mg/l (Rygaard et al. (2011)). Germany allows a maximum concentration of 250 mg/l for chloride ions and 200 mg/l for sodium but no cumulative value for TDS. The gap between the calculated risk of brine discharge, obtained from numerical methods, on the one hand and salt concentration in drinking water wells on the other hand is bridged with some simple analytical considerations (see Section 4.5).

5.1.6.1 Fully Mixed Approach

Let us assume that the freshwater aquifer can be considered a fully mixed reactor. A steady-state salt-mass balance can then be formulated as:

$$q_{out} A_{out} c_{out} = q_{in} A_{in} c_{in} + S D_{brine} \,, \tag{5.5}$$

where q [m/s] and c [kg/m^3] are the groundwater flow and concentration into and out of the control volume respectively, A [m] is the area of the cross section, S [-] the salinity used in the numerical simulations, and D_{brine} [kg/s] the mass discharge of brine as given by Equation (5.3). It is assumed that the incoming groundwater flow contains no salt ($c_{in} = 0$), yielding the following equation for the salt concentration in the aquifer:

$$c_{out} = \frac{12\,\mathrm{S}\,D_{brine}}{q_{out}\,w_f\,b_{aq}}\,. \tag{5.6}$$

$A_{out} = w_f\,b_{aq}$, where w_f is the width of the diluting volume and b_{aq} is the thickness of the aquifer (here 22.5 m). The brine discharge is multiplied by 12 since the results of the numerical model are only valid for a twelfth of the whole area and the entire circular domain is considered here. The salinity of the brine discharge into the freshwater aquifer is $\mathrm{S} = 0.1$ (as before). For the groundwater flow q_{out}, 1m/d=1/86400m/s is assumed. Figure 5.11 shows the top view of the model domain with the fault circle and the segment for the numerical simulation. The assumption of a circle-shaped fault is not very realistic, but it simplifies calculations, thus fulfilling its purpose in this principal study. Two different approximations are now discussed. In the first, the brine discharge over the whole layer (the whole circle) is used. Here, the width of the diluting volume is twice the width of the full model domain ($w_{f1} = 2 \times 10000m$). For the second approximation, only the brine discharge through the fault zone is considered and the width of the diluting volume is twice the distance from the injection site to the fault zone ($w_{f2} = 2 \times 5500\,m$).

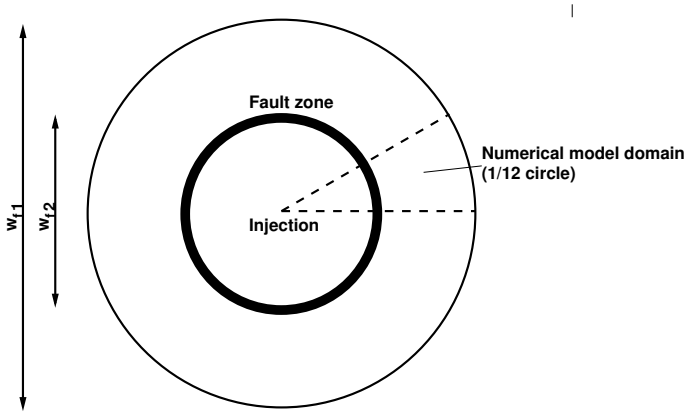

Figure 5.11: View of the model domain from above.

Table 5.2 lists the maximum brine discharge obtained from the numerical simulations and the corresponding concentrations calculated by Equation (5.6) for the two different approximations and for each scenario. The concentration from the approach that considers mixing over the whole domain is lower despite the larger brine discharge due to the larger diluting volume. For Scenarios 1 and 2, no salt concentrations from infiltration via the fault zone are calculated, since the fault zone is not connected to the freshwater aquifer. The concentrations c_{out} of each scenario are compared with the drinking water criteria, given in Rygaard et al. (2011). The guideline value of Denmark (1500mg/l) is not exceeded in any of the scenarios if the brine discharge is assumed to occur over the whole domain. The most critical one is Scenario 6, which exceeds the TDS criterion of Australia but not that of Denmark.

	Brine discharge whole domain		Brine discharge fault only	
Scenario	D_{brine} [kg/s]	c_{out} mg/l	D_{brine} [kg/s]	c_{out} mg/l
1	0	0	-	-
2	0.3135	72.0	-	-
3	1.8631	429.2	1.8063	756.7
4	1.6236	387.9	1.4803	620.1
5	2.0079	462.6	1.9466	815.5
6	4.012	924.4	2.892	1211.5

Table 5.2: Maximum brine discharge (from numerical simulations) and estimated salt concentration for the different scenarios and for the two different approximations: (i) brine discharge over the whole domain, and (ii) brine discharge through the fault zone

For the case where the infiltration occurs only through the fault zone, the drinking-water criterion in Australia is exceeded in all four scenarios, while the Danish criteria would still tolerate these concentrations. The validity of the approximation can be tested using the mixing length L_{mix} [m] (see Binning and Celia (2008)):

$$L_{mix} = \frac{b_{aq}^2}{2\,\alpha_t}. \tag{5.7}$$

Here, α_t = 0.018 m is a reasonable value for the transverse dispersivity (Binning and Celia (2008)). L_{mix} defines how far downstream the aquifer can be assumed to be fully mixed. For the water aquifer above, the mixing length is 14.06 km, which means that the calculated values (Table 5.2) are valid for a water production well at a distance of at least 14.06 km downstream of the discharge zone. Closer to the zone of discharge, concentrations can be higher.

These calculations prove that it is just as important to calculate the diluting volume (given by $w_f \times b_{aq}$) as it is to calculate the brine discharge D_{brine}. Depending on the diluting volume, the fully-mixed concentration in the drinking water aquifer changes significantly. As already indicated in Section 5.1.3, it appears more realistic to consider the infiltration associated with the fault zone since, in Scenarios 3-6, highly concentrated salt water can be displaced through the fault zone directly from the reservoir up to the water aquifer. The assumption of a fully-mixed system mitigates this unfavorable situation because of the large diluting volume, and it has to be stated again that this situation is only valid far downstream from the discharge zone.

Both approximations show high values for the salt concentrations compared with the drinking water criteria, which at least in part results from the fact that the salt content is not explicitly modeled in the numerical simulation. The initial salinity is set to 0.1 over the whole domain, which means that, even directly underneath the water aquifer, the model calculates with this high salinity. Furthermore, mixing effects cannot be addressed with the current numerical model. Therefore, the concentrations shown are rather conservative estimates. Explicitly accounting for the salt concentration and a variable salinity over depth in investigated in Section 5.2.

5.1.6.2 Analytical Approximation of Salt-water Upconing

Near the zone of brine infiltration, i.e. for distances less than L_{mix}, the fully-mixed assumption cannot be made. A conservative approach is then to assume that concentrated brine is at the bottom of the aquifer and has impacts on the water produced by upconing at the drinking water wells. It is interesting to determine the operating conditions under which the concentrated salt water will be pumped in the well. As soon as upconing salt water reaches the well screen, it will affect the quality of the water produced. Simplified estimates with an analytical approximation allow us to develop an operational strategy for water suppliers.

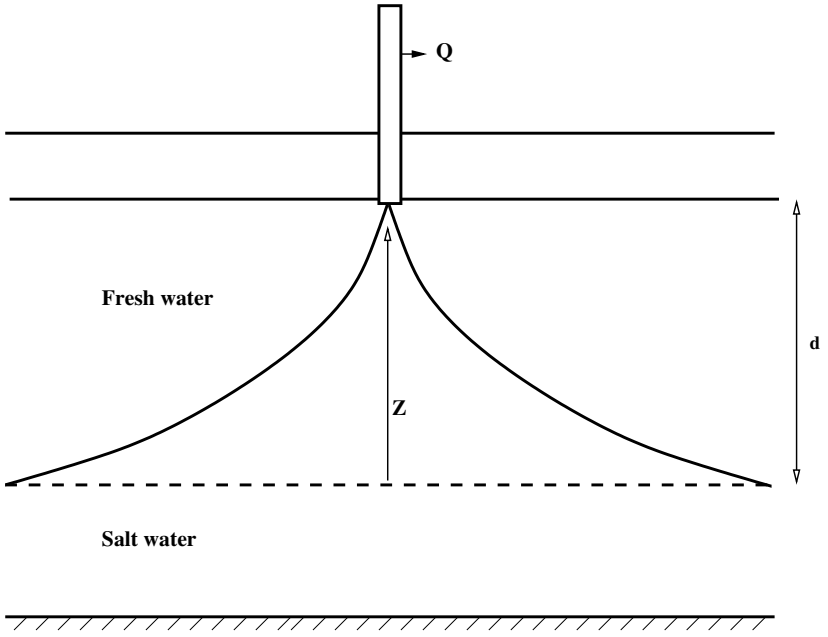

Figure 5.12: Upconing of salt water to a pumping well after Schmorak and Mercado (1969).

Schmorak and Mercado (1969) and Todd (1980) presented an analytical approach to investigate the upconing of sea water caused by a drinking-water well. This approach can be adapted to the brine infiltration problem here. A few assumptions are necessary. First a sharp interface between the salt and the freshwater is assumed. Furthermore, only the region directly beneath the drinking water well ($r = 0$) is considered and it is assumed that the system is at steady state ($t \to \infty$). This assumption leads to a conservative estimation of upconing and thus is appropriate for risk assessment. The situation under consideration is shown in Figure 5.12. According to Schmorak and Mercado (1969) and with these assumptions, the upconing of the salt water can be defined as:

$$Z(r = 0, t \to \infty) = \frac{Q_v}{2\Pi d \frac{\Delta\rho}{\rho_f} k_x}\,, \tag{5.8}$$

where $Z[m]$ is the rise of the interface above the initial state, Q_v [m^3/s] the pumping rate in the well, d [m] the distance between the salt-water layer and the drinking water well, $\frac{\Delta\rho}{\rho_f}$ the dimensionless difference between salt and freshwater density ρ_f and k_x $[m/s]$ the horizontal

permeability. Schmorak and Mercado (1969) stated that this relation is limited to a critical rise Z_{crit}. When Z_{crit} is reached, a spontaneous breakthrough of the salt water occurs. In their experiments, they found that sudden breakthrough occurs for upconing higher than $Z_{crit} = d/3$.

For the water aquifer already investigated in the numerical simulations, Table 5.3 shows the values of model parameters at the depth of 500 m. Let us assume that the brine forms a thin layer at the bottom of the aquifer. Then the distance d between the salt layer and the well screen in Equation 5.8 is the aquifer thickness (22.5 m).

$Q[m^3/s]$	0.004
$d[m]$	22.5
$T[K]$	298
$p[bar]$	50.16
$\rho_{brine}[kg/m^3]$	1068.5
$\rho_f[kg/m^3]$	998.2
$K_x[m^2]$	10^{-12}
$k_x[m/s]$	$1.0978 \cdot 10^{-05}$

Table 5.3: Physical values for the given problem.

Figure 5.13 shows the approximation of the salt-water rise for different vertical distances between the salt-water layer and the drinking-water well. A constant pumping rate of 0.004 m^3/s in the well is assumed. It is obvious that a smaller vertical distance between the well and the salt-water layer results in higher upconing. Without considering the effect of a sudden rise, the salt water would affect the well for distances smaller than ca. 29 m. For larger distances d, the well is not reached by saline water. However, to ensure that no salt is pumped into the drinking water well, the upconing needs to fall below the critical rise of $Z_{crit} = d/3$. This linear relation is also shown in Figure 5.13. For the situation to the left of the intersection of the two curves ($d < 50$ m), the upconing has exceeded Z_{crit}, and the well is affected by saline water. For larger distances, Z_{crit} is not exceeded and freshwater can be pumped at the given rate.

Equation (5.8) further allows an estimation of how strongly the drinking-water well is affected by the saline water. For example, the green point in Figure 5.13 represents the situation where the salt-water layer is 22.5 m below the well. In this case, salt-water upconing is greater than 37 m. This corresponds to a height of about 14.5 m salt-water infiltration into the well.

The pumping rate of an operational strategy is obviously a design parameter. According to Equation (5.8), the upconing depends linearly on the pumping rate. Without considering the critical rise and the abrupt jump of the brine layer, the well would be reached by salt water with a pumping rate of 0.0025 m^3/s. However, considering the critical rise, the maximum permissible pumping rate is only $8.194 \cdot 10^{-4}$ m^3/s.

An interesting point is that the upconing is inversely proportional to the density difference between salt and freshwater. A higher salt content will result in a low estimate for upconing.

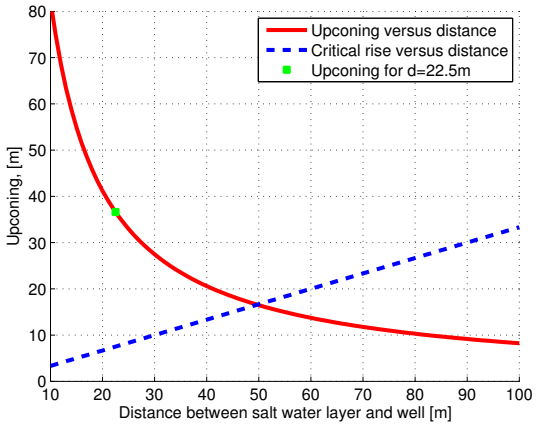

Figure 5.13: The rise of the brine interface versus distance from brine layer to the pumping well (using $Z_{crit} = d/3$).

However, the greatest impact has upconing occurring at the highest concentration. Figure 5.14 shows how the upconing decreases with increasing density difference.

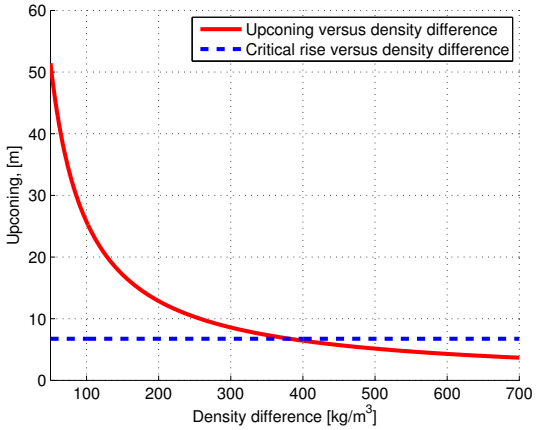

Figure 5.14: The rise of the brine interface versus the density difference.

The section concludes by examining how the analytical model can be linked to the brine discharge obtained from the numerical simulation. A first approach is to check at which salt concentrations upconing of brine would actually occur. As discussed above, upconing is inversely proportional to the density difference between salt water and freshwater. The maximum concentration at which upconing occurs can be calculated. If the concentrations in the water aquifer are above this critical concentration, then upconing is not an issue. For this example, the values in Table 5.3 are used with the reservoir thickness of $d = 22.5$ m and a pumping rate of 0.004 m^2/s. The maximum density difference is 343.03 kg/m^3 and the corresponding salinity equals 0.4233. The concentration is calculated by multiplying the salinity with the brine density of 1341.3 kg/m^3 resulting in c_{crit} = 567.78 kg/m^3. Such a high salinity has, of course, no physical meaning since the water will be fully saturated with

salt for a salinity of about 0.35. It must thus be concluded that in the presented example with the small aquifer thickness of $d = 22.5$ m, upconing will always occur. This means that within a radius of 14.06 km from the brine discharge zone, the drinking water could be affected by the salt concentration.

5.1.7 Conclusions

The study has shown that it is important to address uncertainties on different levels for a comprehensive assessment of risk related to CO_2 storage. In this approach, a distinction is made between scenario uncertainty and statistical uncertainty. Scenario uncertainty requires expert opinion to identify relevant geological scenarios; statistical uncertainty requires information on parameter distributions as well as a concept for testing the parameter space, for example with Monte Carlo methods. The concept applied here uses Monte Carlo testing on computationally very cheap polynomials which represent the response surface of the full-complexity models on the basis of the arbitrary polynomial chaos expansion combined with the probabilistic collocation method. The ultimate aim is to determine a reliable order of magnitude for occurring damages and corresponding probabilities; in this study, damage represents brine discharge and, eventually, the concentration of salt in a drinking water well.

The suggested practical work flow of risk assessment has been presented for brine displacement and infiltration and includes the following steps:
(i) It is necessary to identify those scenarios which are both realistic and lead to high damage. Expert opinion and geological knowledge is inevitable. This was shown in Section 5.1.3. The total volume of displaced brine depends on the volume of injected CO_2, although compressibility effects can lead to a time-shift of brine displacement. The displaced brine has several possible escape routes: (a) towards the outer regions of the injection horizon if the formation is large enough and not sealed at its edges, (b) through the caprock, or (c) through faults. The study gives clear evidence that fault structures are the most important features in these scenarios and brine discharge to freshwater aquifers crucially depends on the connectivity between the storage reservoir and the freshwater aquifer. The likelihood of large brine discharge into freshwater aquifers is far smaller if faults do not connect the two layers, even if the caprock is not faultless.
(ii) For a selected scenario with given geological features (gap in the caprock, fault zone, aquifers, aquitards, etc.), the statistical uncertainties can be included, i.e. the variability of parameters such as permeability, porosity, or anisotropy. Section 5.1.4 addressed this issue for Scenario 4. Knowing the expected range of the tested parameter space and the corresponding distribution functions, it is possible to quantify probabilities of certain damage events. The aPC method allows, for example, the calculation of response surfaces and cumulative distribution functions. For the particular geological set-up of Scenario 4, a value could be assigned to the risk of brine discharge into the freshwater aquifer (here: 0.4722 kg/s).
(iii) The risk of brine discharge needs to be transformed into the risk of exceeding drinking-water criteria in water-production wells. Using simple analytical approaches, it could be shown that this can be done on the basis of a few assumptions. For example, a fully mixed

state of the aquifer appears realistic if the production well is far enough from the discharge zone. If the salt intrusion into the freshwater aquifer occurs rather close to a production well, fully-mixed conditions are not achieved and salt water can be assumed to form a layer at the bottom of the reservoir due to gravity. In such a case, upconing of salt water is the relevant mechanism that could lead to salt concentrations in the water production well (see Section 5.1.6). This topic will be investigated in Section 5.3.

A conservative assumption in the presented study is that of a constant salinity of all water below the freshwater horizon: this overestimates the concentration arriving in the aquifer. This is considered in Section 5.2 by using spatially coupled models with a multiphase model in the region where the CO_2 phase spreads and a single-phase compositional model in the major part of the model domain.
This study suggests that salt-water intrusion into freshwater aquifers due to CO_2 storage is probably a locally confined problem, at least in terms of salt concentration. It does not occur over large areas if storage sites with multiple barriers are chosen. To which extent geochemistry is changed by intruding brine remains an issue to be investigated.

This study showed that the probabilistic collocation method combined with the arbitrary polynomial chaos expansion could not reproduce all the non-linearities occurring in the model. Over- and undershooting between the collocation points can occur with even more problems beyond the collocation points. However, according to PCM the modeler can extract a lot of information in the main range of the parameter distribution, which is sufficient to understand the principal behavior. In that way, the aPC via PCM framework helps to keep the compromise between the computational effort and degree of expansion. Higher-order polynomials could probably improve this, however only at higher computational costs for determining the polynomials.

In the simulations of this work, the calculated overall brine discharge varied from almost zero to about 4 kg/s for the different scenarios, while the statistical variability considered in Scenario 4 lead to a brine flux variation between zero and almost 2 kg/s. Therefore, it appears as if scenario uncertainty is a little higher here, but still of the same order of magnitude as statistical uncertainty. More knowledge decreases both scenario and statistical uncertainty.

Finally, the presented set of methods is a reasonable trade-off between computational effort and desired accuracy for combining quantitative and qualitative uncertainty assessment in modeling CO_2 storage.

5.2 Salt Infiltration During CO_2 Injection - Reduction of Recognized Ignorance [1]

As discussed in the previous section, the 2p-approach used is a conservative estimation of the salt concentration in a water aquifer because the salt was not explicitly simulated. Instead, the brine is assumed to have a constant salinity value of 0.1. Typically, salinity increases with depth (Bonnesen et al. (2009)). Therefore, the necessary assumption of a constant salinity in an immiscible two-phase model leads to an overestimation of the salt content in shallower layers. While the aim of the previous section was to identify the geological setups with the greatest potential for brine infiltration, this study aims at explaining the processes in the overlying aquifers including mixing, migration, and intrusion of salt into a freshwater aquifer. The salt component is explicitly modeled in this study and the results are discussed within the risk-assessment framework outlined in Chapter 4.

The problem of saltwater and freshwater mixing is a typical example for density-driven effects. Various problems occur in the field of porous-media flow where density-driven flow is a relevant phenomenon, e.g. salt intrusion in coastal aquifers, saltwater upconing from deeper aquifers, or saltwater flow around salt domes used as storage sites (Johannsen et al. (2002)). The characteristic effects resulting from density differences have been investigated intensively. Various benchmark studies compare numerical results from different simulators with one another or with analytical solutions. For example, the Henry problem of steady-state seawater intrusion is a commonly used example for comparing numerical results with semi-analytical solutions (e.g. Henry (1964), Huyakorn et al. (1987) Segol (1994)). The Elder problem considers the fingering in an unstable situation (e.g. Elder (1967), Voss and Souza (1987), Kolditz et al. (1998)) and the Hydrocoin problem describes a simplified salt-dome problem (e.g. Kolditz et al. (1998), Oldenburg and Pruess (1995)). The latter two benchmark studies are inter-comparison exercises for different simulators, where no analytical solutions are available. Johannsen et al. (2002) and Oswald and Kinzelbach (2004) present a physical benchmark experiment that considers a less-dense fluid overlying a denser fluid in a porous medium in a 3D laboratory tank. Their aim is to test variable-density flow models in 3D. A good summary of the state of the art for variable-density flow in porous media is given in Diersch and Kolditz (2002). Voss et al. (2010) also summarize the existing 2D and 3D benchmark examples and present an additional 3D benchmark for matching semi-analytic stability modes for steady unstable convection. This brief literature review shows that the problem of salt water mixing with fresh water and the corresponding density effects have been investigated intensively and are well understood. The focus of this work is not on benchmarking salt- and freshwater mixing; instead, salt- and freshwater mixing is needed to be modeled to estimate the salt discharge into freshwater aquifers resulting from CO_2 injection.

The conservative assumption of non-miscible brine migration in Section 5.1 falls into the latter category of recognized ignorance. Here, our attempt is to reduce the uncertainty in-

[1] Parts of this section are submitted to Advances in Water Resources with the title: Walter, L., Binning, P. J., and Class, H. Predicting salt intrusion into freshwater aquifers resulting from CO_2 injection - a study on the influence of conservative assumptions., 2012

troduced by recognized ignorance and to investigate scenario uncertainty with the more accurate model. The flow and transport model, as explained in the next section, introduces two major changes compared with the two-phase (2p) approach applied previously. (i) Salt is considered explicitly, i.e. varying salt concentration, advective transport, and diffusive transport. (ii) A model coupling concept is applied, where the complexity of the flow and transport model is adapted to the required physics in different subregions. One purpose of this approach is to optimize the computational efficiency when using a more sophisticated model.

Section 5.2.1 describes the coupling concept and the model set-up used for the simulations. In Section 5.2.2, the various scenarios are described and the simulation results for the different scenarios are presented and compared with the 2p approach of Section 5.1. Furthermore, the contribution to the risk framework is discussed in Section 5.2.3. In Section 5.2.4 the work is concluded.

5.2.1 Model Concept

A number of processes can have an influence on salt infiltration into a freshwater aquifer during or after CO_2 injection; however, not all of them are equally important and considered in the model concept. For example, a two-phase three-component model (2p3c) with the phases CO_2 and water and the components CO_2, water and salt, could account for advective multiphase flow, dissolution, and mixing due to diffusion/dispersion. A 2p3c model requires the solution of three balance equations, and - depending on how the appearance/disappearance of fluid phases is treated (Lauser et al. (2011); Class et al. (2002)) - a phase switch (as in this model) or a flash calculation or complementarity conditions need to be calculated, all of which would cause a further increase in computational effort. Thus, a 2p3c model would result in a more expensive simulation than the simulations with the 2p model in the previous study. One possibility to reduce computational costs is to use a one-phase, two-component model (1p2c) for modeling the water-salt system only and neglecting the CO_2 storage process. The CO_2 injection could be modeled via a pressure input into the model domain. However, the pressure build-up due to the CO_2 injection must be determined by a reference simulation. Another possible way of reducing computational costs is to couple models spatially (Helmig et al. (2013)) and to adapt the complexity of the equations as required for each subregion as introduced in Section 2.4.4.

To model brine displacement and salt infiltration into freshwater aquifers resulting from CO_2 injection, the conceptual model can take advantage of different processes occurring in distinct subregions. The process of CO_2 injection into the storage reservoir is predominantly a (partly miscible) two-phase flow system of CO_2 and brine. Neglecting solubility effects would be a conservative approach with respect to pressure increase and brine displacement. Therefore, the application of a two-phase (2p) model without compositional effects (see Section 2.4.1) in the storage reservoir (including the caprock) can be justified.

Above the storage reservoir, the advective brine flow and mixing processes dominate the salt migration. It is assumed that all CO_2 is structurally and residually trapped in the storage reservoir. CO_2 does not reach any fault or fracture zone where it could rise to a shallower

aquifer. Here, brine is considered to be the only fluid leaking out of the storage reservoir. Thus, in the region of a fault and above the caprock, it is not necessary to model the CO_2, either as a phase or as a component. The salt-migration process can be described by a single-phase two-component (1p2c) concept, with the prevalent water component and salt as a dissolved component (see Section 2.4.3). In the current study dispersion is neglected in the 1p2c model because the velocities outside the reservoir are rather small (no groundwater flow is considered).

As discussed in Section 2.4.4 the two models - 2p in the storage reservoir and 1p2c in the other regions - are spatially coupled (see Fig. 5.15). The coupling concept uses a Dirichlet-Neumann technique (Baber et al. (2012)), which is applied to the CO_2 storage/brine displacement problem for the first time. Both models, the 2p and the 1p2c model, require two balance equations to be solved. Thus, the coupling approach reduces the number of equations to two instead of three in both regions, resulting in a speedup of the computation. For investigations of the speedup due to the reduction of the number of governing equations, one is referred to Darcis et al. (2011), where models of different complexity were coupled in time.

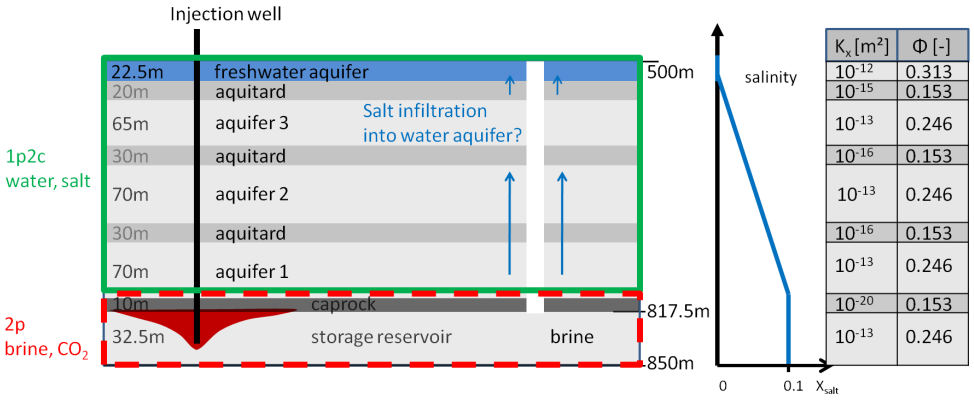

Figure 5.15: The model domain with the two subdomains and the parameters for the different layers.

5.2.1.1 Coupling Concept

The coupling of two subdomains requires coupling conditions to be formulated at the interface. Here, a Dirichlet-Neumann approach as introduced by Baber et al. (2012) is used. The conditions at the interface can be considered as internal boundary conditions; thus the information from the 2p model is transferred to the 1p2c model and back, while the overall system is solved monolithically. Generally, the primary variables (p_w, S_n in the 2p model and p, X_s in the 1p2c model) need to be exchanged between the two submodels and they have to be defined at the interface. Additionally, the continuity of the fluxes has to be fulfilled.

The coupling of the models currently applied requires assumptions for the conditions at the interface because the two models include different species. On the one hand, the 1p2c model

does not account for the CO_2 component; on the other hand, the variable salt component is not modelled in the 2p model. To this end, it is assumed that (i) no CO_2 reaches the layers above the storage reservoir, either by leaking through the caprock or by a fault. This is reasonable since CO_2 leakage is not the issue of investigation here. It is further assumed that (ii) the salt content of the brine in the 2p domain (the storage reservoir) is constant and equals 0.1 (see Fig. 5.15). These assumptions in combination with the assumption of local thermodynamic equilibrium result in the following coupling conditions at the interface. Assumption (i) implies that the CO_2 saturation S_n at the interface to the 1p2c model is zero. This is implemented as a constant Dirichlet boundary condition S_n=0. Assumption (ii) results in the continuity of the mass fraction X_s:

$$\mathrm{S} = [X_s]^{1p2c} = 0.1 \tag{5.9}$$

which implies that the mass fraction $[X_s]^{1p2c}$ for the 1p2c model at the interface to the 2p model is equal to the constant salinity S in the 2p model. The mass fraction is simply set as a fixed Dirichlet boundary condition of $X_s = 0.1$. Thus, no particular coupling conditions are applied for the primary variables CO_2 saturation and salt mass fraction.

The coupling conditions for the two pressures p_w in the 2p model and p in the 1p2c model are given by the mechanical equilibrium that is represented by the continuity of brine pressure:

$$[p_w]^{2p} = [p]^{1p2c}\,, \tag{5.10}$$

and the continuity of normal mass fluxes:

$$[\rho_w \mathrm{v}_w \mathbf{n}]^{2p} = [\rho\, \mathrm{v}\, \mathbf{n}]^{1p2c}\,. \tag{5.11}$$

Thus, the coupling conditions at the internal interface can be interpreted as a Dirichlet-like condition for p_w in the 2p model and as a Neumann-like inflow condition for the general mass balance equation in the 1p2c model. Equation 5.11 is valid because the condition in Equation 5.9 ensures that the density, which is a function of the pressure, temperature and salt mass fraction at the interface, is equal in both domains. These two conditions are implemented as real coupling conditions which are passed on simultaneously from one domain to the other in each iteration. The Neumann-type condition at the interface in the 1p2c model contains the pressure gradient at the interface. As explained in detail in Baber et al. (2012), this requires a special consideration for the box discretisation method used (see Helmig (1997) for details). In the box method, the gradients are normally evaluated at the subcontrol volume faces for the boxes. At the coupling interface, the approximation at the element edges is needed. However, at the element edges, discontinuities in the gradient approximation occur. To avoid this problem, the normal fluxes across the interface are calculated via the sum of incoming and outgoing fluxes and the change inside the control volume (see Eq. 13 in Baber et al. (2012)).

5.2.1.2 Model Set-up

To achieve comparable results, the same radially symmetric model domain of 10 km length as described in Section 5.1 is used (see Fig. 5.17). Figure 5.15 shows the schematic view of

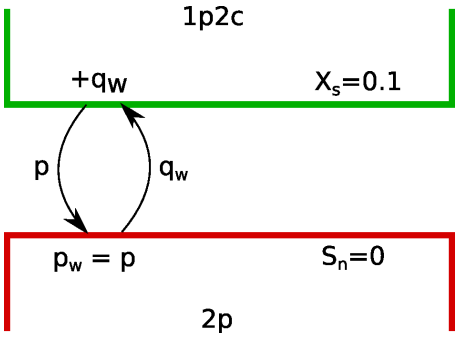

Figure 5.16: The coupling conditions at the interface between the two subdomains.

the model domain with the two subdomains, the 2p subdomain and the 1p2c subdomain. The parameters such as permeability and porosity are similar to those used previously in the 2p approach of Section 5.1. The other parameters including those needed additionally for the 1p2c model are listed in Tab. 5.4. The recent reference model setup (Scenario A and B) is similar to Scenario 3 in Section 5.1, where there is a fault zone of 370 m thickness at about 5 km distance. All boundaries except for the boundary at 10 km distance are set to Neumann no-flow conditions as in Section 5.1. As an initial and boundary condition at the 10 km boundary, a constant head condition for the pressure is set. In the 2p domain, the CO_2 saturation is initially zero, and the salt mass fraction in the 1p2c domain is assumed to increase linearly with depth from a value of zero directly underneath the freshwater aquifer to 0.1 in the storage reservoir, where the salinity is set constant to 0.1. A linear change with depth is assumed acceptable, as this is in accordance with the measurement results for salinity changes with depth recorded in Bonnesen et al. (2009). The simulation time is 25 years where CO_2 is injected at a rate of 1 Mt CO_2/a which results in an actual injection rate of 1/12 Mt/a for the radial symmetric section and 25 years of the post-injection period. Brine leakage from the reservoir can occur via the fault zone only.

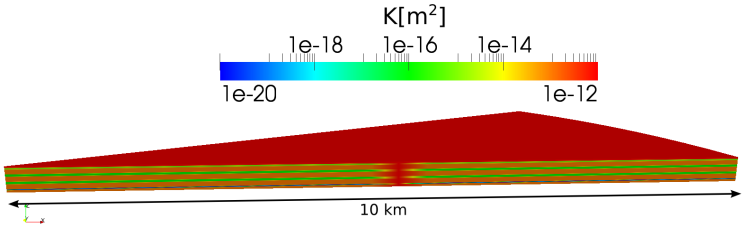

Figure 5.17: Radially symmetric model domain (1/12 segment of a circle) including permeability (K) distribution (see Section 5.1).

The output of interest in this approach is the salt discharge (instead of the brine discharge as in Section 5.1), which infiltrates for example the freshwater aquifer. The salt discharge is determined by the sum of the advective and diffusive flux:

$$\text{Salt discharge} = -\varrho \frac{\mathbf{K}X}{\mu} (\text{grad}p - \varrho \mathbf{g}) - \varrho \tau \phi D \text{grad}X \tag{5.12}$$

Anisotropy	0.1 [-]
Tortuosity	0.5 [-]
Diffusion coefficient D_{salt}	$1.587e^{-9}m^2/s$
Fault permeability K_{fault}	$10^{-12}m^2$
Fault porosity ϕ_{fault}	0.313

Table 5.4: Simulation parameters

where X is the mass fraction of salt.

5.2.2 Investigation of Recognized Ignorance and Scenario Uncertainty

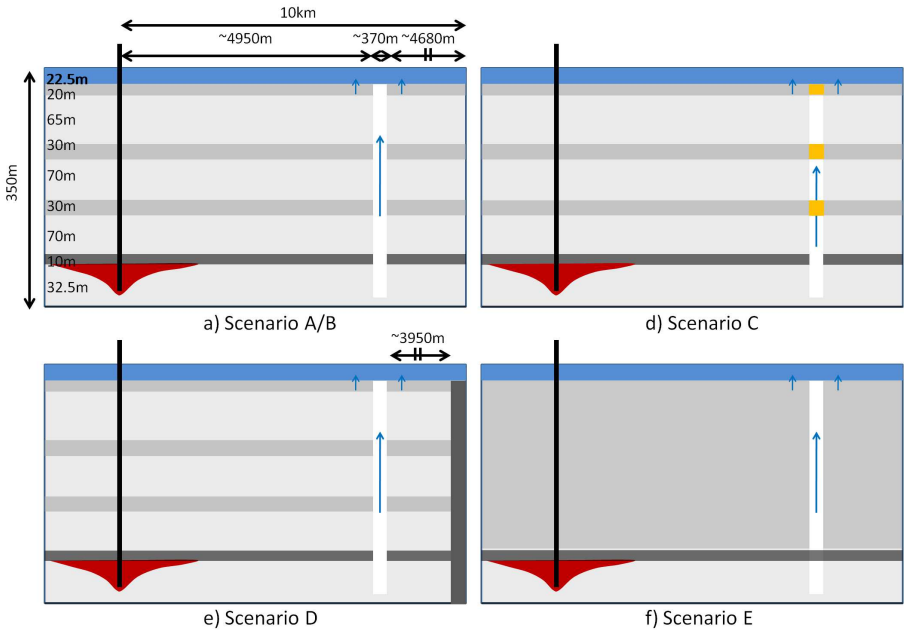

Figure 5.18: Selection of geological scenarios used for the study.

In the following, Scenarios B, C, and D of the current study are denoted as Scenarios 3, 4, and 6 in Section 5.1 (see Table 5.5). Scenario E is an additional setup to investigate the mixing effects (see Fig. 5.18). Scenario A serves as a reference.

5.2.2.1 Reference Scenario A with Constant Salinity

This section uses the coupling concept as outlined above with salinity as a variable parameter, while an immiscible two-phase model with constant salinity is used in Section 5.1. The aim of this referencing exercise is the comparison of the two different modeling approaches for the same boundary, initial, and geological conditions. Thus, Scenario A is the geological setup of the reference scenario combined with the conceptual assumption of a constant

Scenario (variable salinity approach)	Scenario (constant salinity approach)	Geology
A/B	3	fault zone (reference geology)
C	4	fault zone interrupted by blocks
D	6	barrier at 9 km distance
E	-	low permeable aquitards

Table 5.5: Scenario denotation in the variable salinity approach and the constant salinity approach of Section 5.1 and the corresponding geology description.

salinity of 0.1 in the whole domain. The choice of the constant salinity prevents mixing effects, thus the results of the coupling approach are expected to be the same as for the 2p approach.

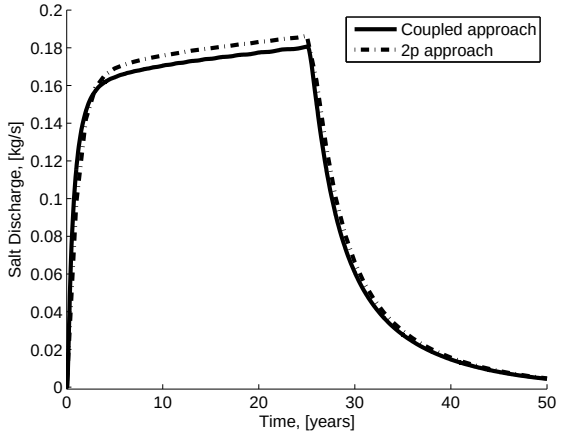

Figure 5.19: Comparison of the salt discharge into the freshwater aquifer (over the whole layer) for the coupled 2p/1p2c approach and the 2p approach

Fig. 5.19 shows the salt-infiltration rates into the freshwater aquifer for Scenario A. For the 2p approach, the results of the brine discharge are simply multiplied by 0.1 to obtain the corresponding salt discharge. The two curves are in satisfactory agreement. Small deviations are of numerical origin resulting from the different approaches. Since the difference is small, this issue is not further investigated.

5.2.2.2 Comparison of Scenarios: Salt discharge into the Freshwater Aquifer

In contrast to the previous approach with constant salinity, there are now two new phenomena taken into account: (i) a linear salinity profile (see Fig. 5.15), and (ii) the mixing of highly saline water with less salty water. A comparison of the geological Scenarios B, C, D, and E provides a better understanding of how these processes affect the salt discharge into the freshwater aquifer.

Scenario B is the reference scenario (see Fig. 5.15) and has the same geological setup as Scenario A. The only difference is the linear salinity profile as it is assumed for all following

scenarios. In Scenario C, the fault zone is interrupted by blocks of lower permeability in the aquitard zones. Scenario D has a barrier of very low permeability at about 9 km distance from the injector, extending over the whole depth. These three scenarios are chosen as those of greatest interest for a comparison and for an investigation of the influence of the intermediate layers between the storage reservoir and freshwater aquifer. Scenario E has no equivalent in the previous study: it represents a storage reservoir with a very thick caprock or overburden, where no mixing of salt can occur in intermediate aquifer layers. Such a caprock is, for example, found at the In Salah injection site, where the storage reservoir is sealed by a caprock of 900 m thickness (Rutqvist et al. (2008)). Thus, the permeability of the intermediate layers is set to 10^{-16} m^2 for Scenario E. Figure 5.18 gives a schematic view of all the scenarios considered.

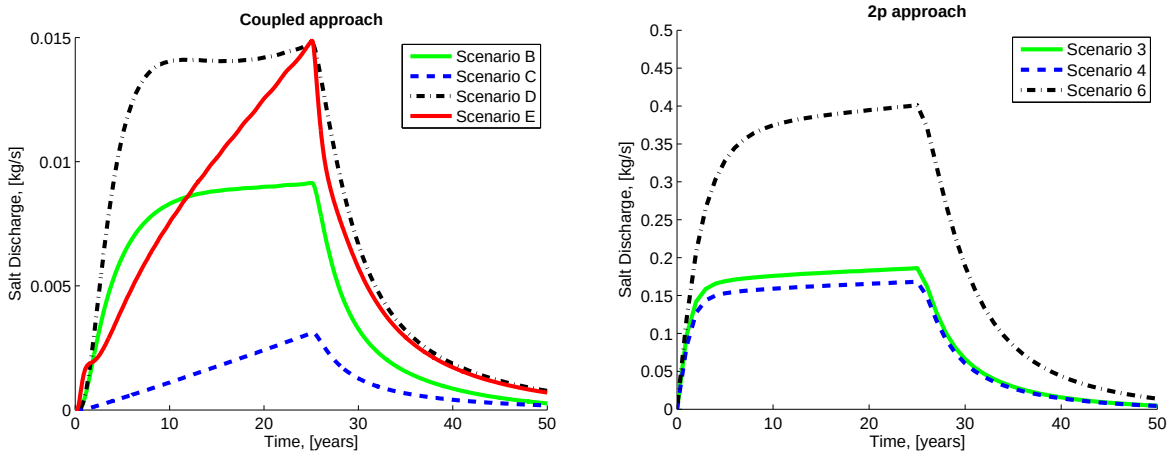

(a) Coupled approach

(b) 2p approach with constant salinity

Figure 5.20: Total salt discharge into the freshwater aquifer a) for the coupled approach with varying salinity and b) for the 2p approach with constant salinity of 0.1.

Figure 5.20a shows the total salt discharge into the freshwater aquifer over time (measured across the whole bottom boundary) for Scenarios B, C, D, and E, all obtained with the coupled 2p/1p2c model. Fig. 5.20b repeats the results of the corresponding scenarios presented in Section 5.1, calculated with the immiscible two-phase model and constant brine salinity. For a comparison of salt discharge values, the brine discharge obtained by the 2p approach is multiplied by the salinity (0.1). The 2p approach reveals a large difference between the salt discharge that occurs in total across the whole bottom boundary of the freshwater aquifer and the salt discharge that occurs only through the fault zone into the fresh water. On the basis of the data in Tab. 5.6, it is observed in the coupled model that the discharge through the fault is almost the same as the total discharge for all scenarios. Thus, nearly all the salt infiltration only occurs through the fault zone.

The scale applied to the vertical axis in Fig. 5.20 shows that the salt discharge is smaller by more than one order of magnitude when miscibility and a salinity profile are considered. The ranking of the three scenarios B,C, and D is still the same as in the 2p approach: the discharge in Scenario D is the largest, followed by Scenario B and Scenario C. However, the relative difference between Scenarios B and C is larger in the coupled approach than

Scenario	Coupled approach: D_{salt} [kg/s]		2p approach: D_{salt} [kg/s]	
	total	only fault	total	only fault
B	0.0091	0.0091	0.1863	0.1806
C	0.0031	0.0031	0.1624	0.1480
D	0.0148	0.0145	0.4012	0.2892
E	0.0149	0.0148	-	-

Table 5.6: Maximum salt-discharge rates into the freshwater aquifer; (i) in total summed up over the whole domain and (ii) only through the fault zone, both compared for the coupled (miscible) and the 2p (immiscible) approach (Section 5.1).

in the 2p approach, because the blocks of lower permeability in Scenario C reduce the salt transport through the fault, thus the mixing of more saline water with the surrounding water volumes of lower salinity is increased. In the 2p approach, this severe reduction of vertical salt transport due to lateral mixing could not be observed, since this process was neglected in the conceptual model (recognized ignorance). This explanation is further confirmed by the slope of the salt-discharge curves over time. They increase gradually during the injection period but, in Scenario C, this clearly occurs more slowly than in Scenario B, and the 2p version of Scenario C does not show this retarded increase.

Scenario D and Scenario E can be seen as the two worst-case scenarios among those selected, although for different reasons. In Scenario D, the brine cannot be displaced horizontally and all the displaced brine has to move to shallower layers. However, with the improved compositional model, even this worst-case scenario results in a much smaller salt discharge into the freshwater aquifers than all the others before with conservative assumptions. For the corresponding scenario of the 2p approach, there is a significant difference between the total brine discharge and the discharge through the fault zone (Tab. 5.6). This is not observed for the coupled 2p/1p2c model, because - as already seen above - the vertical transport of salt is more or less exclusively along the fault. It is concluded that the conceptual assumptions in the previous model were highly conservative and summing up all discharge across the whole bottom of the freshwater aquifer leads to a strong overestimation of the salt discharge into this aquifer. The second worst-case situation is Scenario E. The salt-discharge curve here is clearly above the curve of Scenario B. The intrusion of salt into the intermediate aquifers is prevented. Thus, the salt displaced from the reservoir is mixed only with the initially less salty water in the fault. It must be noted that the fault zone is very broad (370 m) in all scenarios. Thus, the mixing volume remains very large and the maximum discharge is almost the same as in the closed-reservoir Scenario D (see Tab. 5.6).

In summary, the brine arriving in the freshwater horizon has a comparatively low salinity for all scenarios in the coupled approach, in particular in Scenario C, where the blocks in the fault zone prevent the movement of high saline water to the upper aquifers. The prevention of horizontal flow and mixing in the intermediate layers yields the highest salt discharges into the water aquifer.

5.2.2.3 Analysis of the Mixing and Displacement Processes

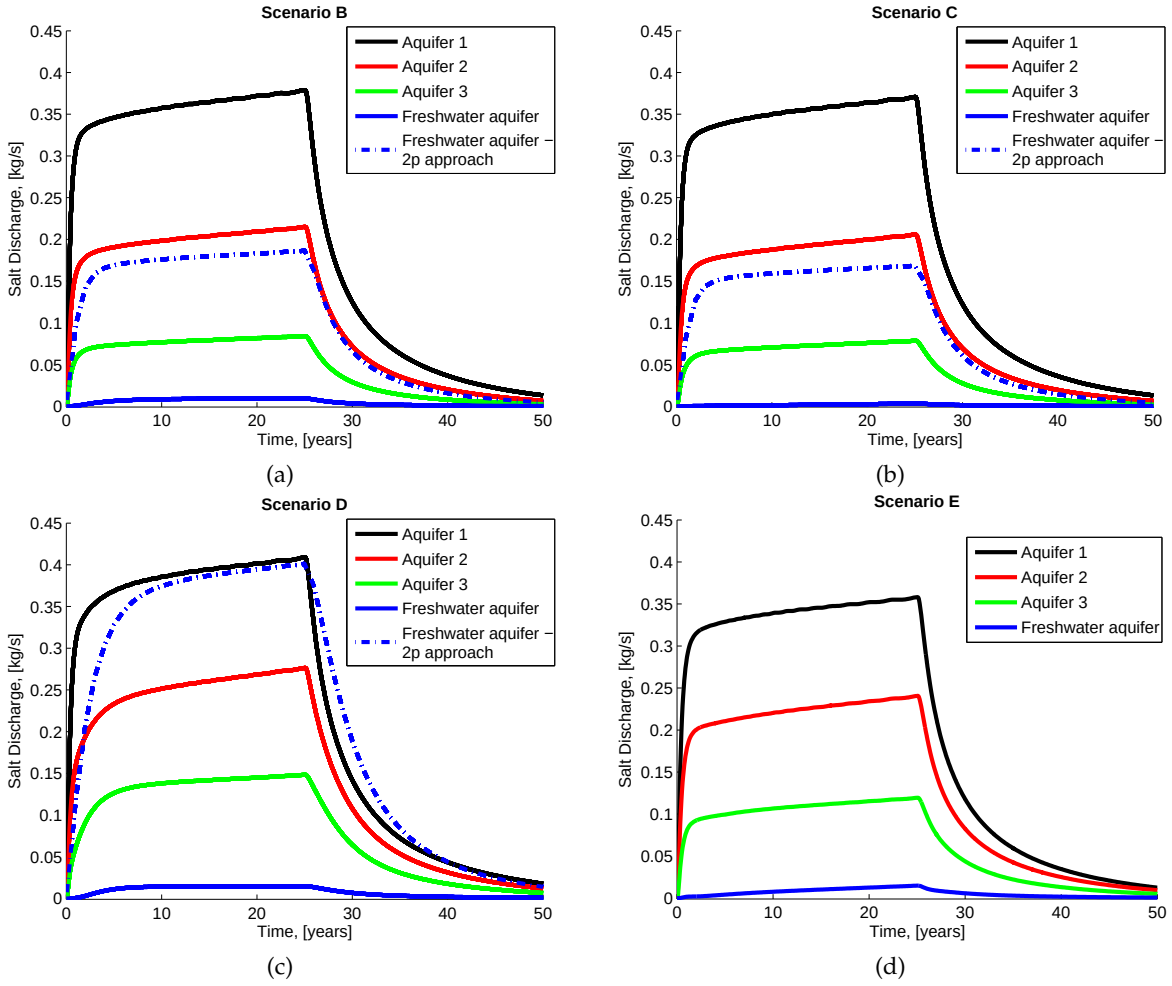

Figure 5.21: Salt discharge into each aquifer for a) Scenario B b) Scenario C c) Scenario D, and d) Scenario E. For comparison, the total salt discharge into the freshwater aquifer as obtained by the 2p (constant salinity) model is also plotted.

Where is the salt load leaking from the reservoir transported to? Figure 5.21 gives an answer; it shows the lumped salt discharges into the various aquifers (each of them with a different initial salinity due to the imposed salinity profile) for Scenarios B, C, and D, compared with the total salt discharge into the freshwater aquifer obtained from the constant salinity approach. Obviously, the salt discharge into shallower layers is less than into deeper ones. Both the mixing of salt due to different permeabilities in the aquifers and the linear decrease of initial salinity contribute to these reduced discharges into shallower aquifers. This means that parts of the transported salt must be stored in the fault zone and the intermediate aquifers. In Scenario B, 2.4% of the leaking salt load into the fault (into aquifer 1) infiltrates the freshwater aquifer, whereas this portion is much smaller in Scenario C (0.8%). Scenario D allows a larger portion of the leaking salt (3.6%) load to reach the freshwater aquifer. Less mixing of highly saline water with the water in the intermediate

aquifers occurs because the advective flux along the fault dominates the migration more distinctly than in Scenarios B and C. Thus, mixing can still occur within the fault, but much less in the laterally attached regions. In Scenario E, there is almost no mixing other than within the fault zone. Thus, the infiltration of salt into the intermediate aquifers is much less than in the other scenarios and 4.2% of the leaking salt from the reservoir reaches the freshwater aquifer.

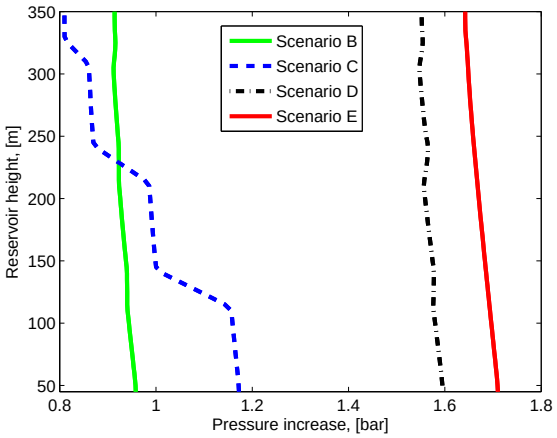

Figure 5.22: Pressure increase in the middle of the fault zone over depth (after 25 years of injection).

Figure 5.22 shows the pressure increase in the fault zone over depth. A higher pressure increase in the fault zone results in a higher salt load entering the freshwater aquifer, thus the ranking of the scenarios resembles the pressure profiles in the fault zone. Additionally, the pressure profile shows the decrease of the pressure in the intermediate layers in Scenario C due to the blocks of low permeability.

Figure 5.23 compares the brine (water and salt) discharges into the various aquifers. In Scenarios B and C, the brine discharge decreases almost linearly with depth. The brine discharges in Scenario C are only slightly smaller than in Scenario B due to the lower permeability in the fault zone. However, as discussed above, the salt discharge is influenced strongly by these blocks of low permeability as a result of increased mixing in the intermediate aquifers.

For Scenario D, we observe another picture (see Fig. 5.23c). The storage reservoir and the three aquifers are almost impermeable at about 9 km distance. This leads to a distinctly higher pressure which propagates into the fault and generates pressure gradients of the same order of magnitude in all aquifers. The brine discharge into the different aquifers looks almost similar for Scenario E. Brine is only transported along the fault since the flow into the aquifers is prevented by their low permeabilities.

In Figure 5.24, we look at Scenario D in further detail; here the total salt and brine discharges into the freshwater aquifer are compared with those through the fault zone. As already mentioned, the total salt discharge into the freshwater aquifer is similar to the salt

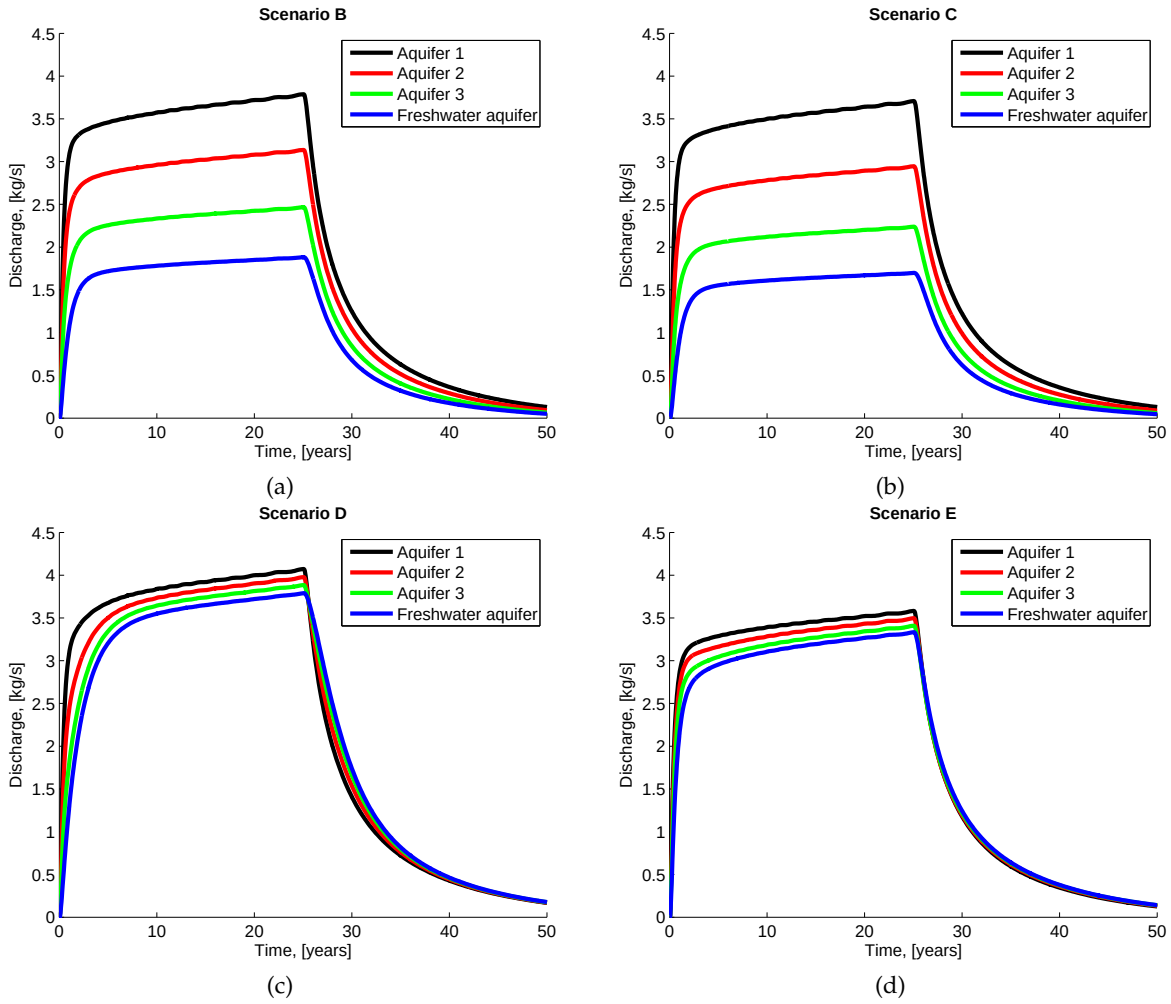

Figure 5.23: Total brine (water+salt) discharge into each aquifer for a) Scenario B b) Scenario C c) Scenario D and d) Scenario E.

discharge through the fault, because salt infiltrates almost exclusively via the fault zone in all scenarios. The salt discharges into the intermediate aquifers are also similar for both measures in Scenarios B, C, D, and E (see Fig. 5.24a for Scenario D). The same holds for the brine discharges in Scenarios B, C, and E, while the distribution of the brine discharges changes in Scenario D, in particular the brine discharge into the freshwater aquifer (see Fig. 5.24b). The maximum total brine discharge into the freshwater aquifer is 3.79 kg/s, and the discharge via the fault zone is only 2.76 kg/s, whereas the salt discharge alone is almost the same for both measurements (see Tab.5.6). This explains the large differences between the total discharge value and the discharge through only the fault zone in the constant salinity approach. Water is displaced over the whole domain due to a large pressure gradient, but the highly concentrated salt from lower regions is mainly displaced along the fault zone, since in the intermediate aquifers high saline brine is found mainly in the lower parts. This clearly proves that the major contribution to the total salt discharge into the freshwater has its origin in the deeper subsurface and should not be modeled (as in the constant salinity

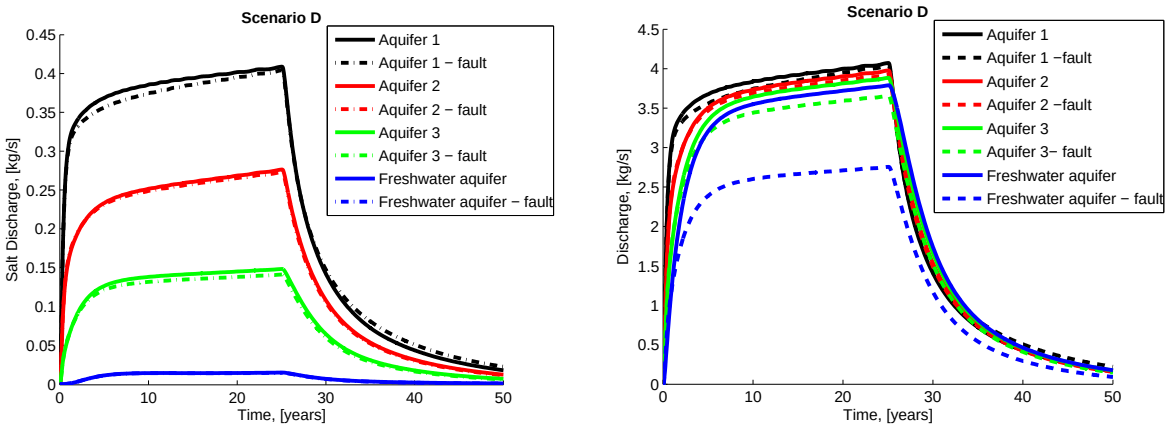

(a) Salt discharge

(b) Brine discharge

Figure 5.24: Scenario D: Comparison of the total salt and brine discharges and those through the fault zone only.

approach) by simply multiplying water fluxes with a salinity value. The migration of salt is dominated by density-driven mixing within the intermediate aquifers.

5.2.2.4 Salt Distribution in the Freshwater Aquifer

To evaluate the impacts of freshwater salinazation, it is important to know how the salt spreads in the freshwater aquifer. The presented approach can theoretically provide salt concentration in the water aquifer. However, the major effects on the spreading are due to density differences and groundwater flow. The radially symmetric model domain of this study cannot account reasonably for groundwater flow. Therefore, a 2D domain is applied, which is sufficient to show the principle effects qualitatively. Of course, the 2D assumption is conservative for estimates of salt concentration because the spreading in the third spatial direction is neglected. The same 1p2c model as in the coupled approach is used to simulate the processes in the freshwater aquifer. Additionally, diffusion and dispersion is now considered. Thus, the coefficient D in Equation 2.25 now contains diffusion and dispersion (see Equation 2.16). For the longitudinal and transverse dispersivities the values presented in (Garabedian et al. (1991)) are applied ($\alpha_l = 0.96$ and $\alpha_t = 0.018$). The new model domain consists of a freshwater aquifer of 22.5 m thickness and 15 km length; it is confined at the top and bottom by layers of low permeability (Neumann no-flow boundaries). The conditions at the left and the right boundary are hydraulically open constant head boundaries (Dirichlet). Between the two boundaries, a gradient of $4.4 \cdot 10^{-4}$ m depth per m length is applied (Lange et al. (2013)).

The injection rate of water and salt at the bottom left of the domain is based on the maximum discharge for Scenario B. The infiltration area is smaller in this model (370 m^2) but the same amount per m^2 as displaced through the fault and infiltrated into the freshwater is injected over 25 years. Figure 5.25 shows the salt distribution after 25 years of injection for 4 different situations. The saltwater injection q_{in} corresponds to the values derived by the coupled

approach for the situation shown in Fig. 5.25a and b and to the values given by the 2p approach for the situation in Fig. 5.25c and d. The permeability is varied between 10^{-12} m^2 and 10^{-9} m^2 to represent the influence of different groundwater velocities.

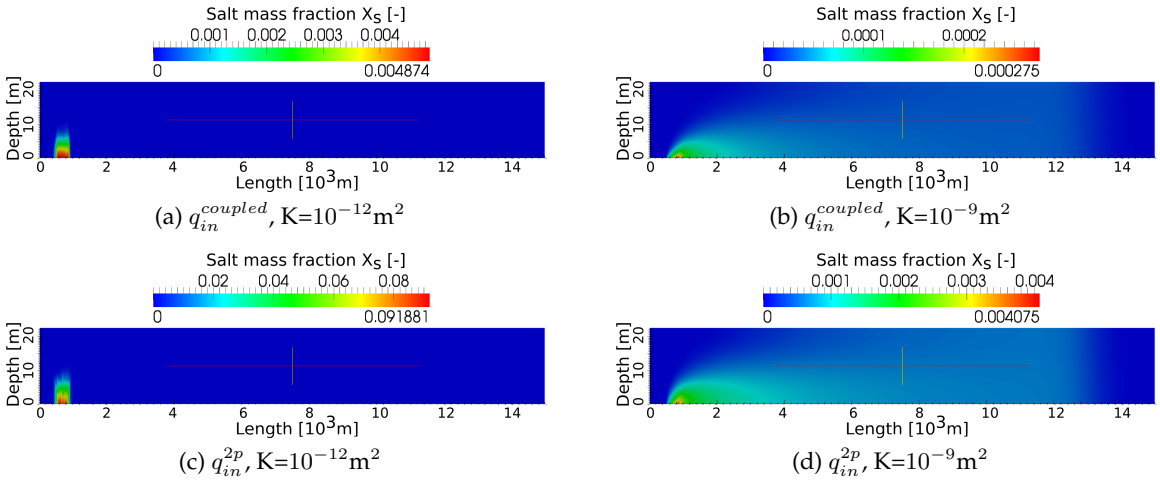

(a) $q_{in}^{coupled}$, K=10^{-12}m^2 (b) $q_{in}^{coupled}$, K=10^{-9}m^2

(c) q_{in}^{2p}, K=10^{-12}m^2 (d) q_{in}^{2p}, K=10^{-9}m^2

Figure 5.25: Salt distribution in the freshwater aquifer for salt infiltration rates based on Scenario B (after 25 years of infiltration).Vertical exaggeration=100.

The low permeability results in a very small background velocity (about $5 \cdot 10^{-9}$m/s for the given conditions) for the given hydraulic gradient (Fig. 5.25a and c). The infiltrated salt is virtually not moving in the direction of the groundwater flow and its spreading is mainly influenced by the pressure gradient due to the infiltration of brine and diffusion. The mixing of salt occurs only very locally. The density difference dominates the distribution and the salt remains mainly at the bottom of the aquifer next to the infiltration area.

In freshwater aquifers with higher permeability (Fig. 5.25b and d), the salt distribution is dominated by the hydraulic gradient resulting in a velocity about $5 \cdot 10^{-6}$ m/s. The salt is transported in a horizontal direction along the aquifer. Diffusion and dispersion contribute to the spreading in a vertical direction. Thus, the salt is mixed and diluted, and only small concentrations are observed. The density difference is not dominant for these small concentrations and the salt is nearly completely mixed over the aquifer thickness at about 12 km distance.

Depending on the permeability of the freshwater aquifer, two situations are observed: either highly concentrated salt remains near the injection zone or salt with a low concentration distributes over a large area. The comparison between the discharge originally derived by the coupled or the 2p approach shows that this assumption strongly influences the salt concentration in the aquifer.

5.2.3 Consequences for Risk Assessment

For the selected scenarios, the comparison between the two different modeling approaches

(i) the constant salinity two-phase (2p) approach as in Section 5.1, and

(ii) the coupled 2p/1p2c model with salinity as an independent variable and a linear vertical profile of initial salinity

shows a severe difference in the predicted salinization of the freshwater aquifer. In the context of a framework for risk assessment, this must be taken into account when choosing the model to be applied as well as when evaluating the results. Conservative approaches are desirable to be on the safe side with estimates of hazards and risks. On the other hand, overly conservative results may prevent the implementation of projects, when risk assessment yields numbers that are too high. Depending on the (hydro-)geological conditions in the freshwater aquifer, two kinds of situations are observed:

- locally defined and rather severe damage (highly concentrated salt) or
- widespread and locally rather small damage (salt of low concentration).

For risk assessment, it would be important to investigate the influence of a water production well. The salt concentration of the water produced should be determined depending on groundwater flow, permeability, pumping rate, or distance between the salt intrusion and the well. This is not the part of this investigation and is addressed in Section 5.3.

While Section 5.1 addressed scenario uncertainty and statistical uncertainty in particular, this study has investigated the influence of recognized ignorance for different scenarios. Neglecting variable salt concentrations, mixing effects, and the density-driven flow of brine of varying salinity means introducing a conservative assumption in the conceptual model, which falls exactly into the category of recognized ignorance. The consideration of the spatially and temporally changing salinity and the mixing effects reduces recognized ignorance. The results predicted for damage due to salinization are now reduced by more than one order of magnitude (20-50 times smaller), which proves the significance of this category for the evaluation of risk predictions.

5.2.4 Conclusions

This study aims at investigating salt-infiltration scenarios with a model using less conservative assumptions than in a previous 2p approach with constant salinity presented in Section 5.1. The new concept reduces uncertainty introduced by recognized ignorance. The coupling concept presented in Baber et al. (2012) is applied to the CO_2 storage/brine displacement problem for the first time and works well for the considered problem. The coupling of a 2p model only in the storage reservoir with a 1p2c model in the overlying aquifers is an efficient and more exact approximation for investigating the salt-intrusion problem during CO_2 injection. The important mixing effects of highly saline brine in less salty shallower layers and a more realistic profile of salinity over depth are considered.

For the three scenarios B, C, and D selected here for comparison, the predicted salt discharge into the water aquifer is much smaller than in the 2p approach. The values are about 20 to

50 times smaller. The simulation with the conservative 2p approach highly overestimates the salt discharge. Furthermore, the coupled approach shows that salt is mainly transported along the fault zone and almost no salt infiltrates into the water aquifer in regions with an intact aquitard layer.

Although the discharge (damage) values are drastically reduced in the improved model, the ranking of the scenarios is still the same as in the 2p constant-salinity approach. For the additional worst-case Scenario E, where mixing in the intermediate layer is prevented, larger discharge values than in Scenario B are observed, but the values are still low compared with all the 2p scenarios.

In Section 5.1, it was concluded that statistical and scenario uncertainty are of the same order of magnitude (between a brine discharge of 0-2 kg/s and 0-4 kg/s). As discussed before, the use of the coupled compositional model results in discharge values 20 to 50 times smaller than in the 2p approach. Thus, the reduction of recognized ignorance is much higher here than statistical uncertainty or scenario uncertainty. The different scenarios considered in this work lead to a variation of salt discharge by a factor of less than 5. Statistical uncertainty was not explicitly investigated here, but, for example, the variation of the permeability in the reservoir as was done in the 2p approach is expected to result in a relative variation of the same order of magnitude here as well. A very important parameter that deserves further investigation in future work is the salinity profile. In this study, a linearly increasing profile is assumed, but other profiles might be relevant as well.

The introduction of the more sophisticated model also introduces new uncertainties, for example, due to a coarse grid resolution. In the 2p model with constant salinity, the grid resolution was not important because no mixing effects in the intermediate layers were modeled. The recent approach now accounts for the salt component and the mixing effects, thus the grid resolution next to the fault zone becomes important. In the large grid cells next to the fault, more salt can be mixed than in smaller grid cells. However, as it could be seen from simple grid convergence investigations (not shown in this work), the uncertainty introduced by the coarse grid is clearly smaller than the reduction of uncertainty by using this improved conceptual approach.

It is noticeable for this study that the fault zone has a huge lateral extension of 370 m. Smaller faults would clearly allow less water discharge, but most likely with higher salt concentrations because a smaller fault contains less freshwater to mix with the salt. Presumably, this would change the situation completely. While the overall problem far downstream of a small fault probably becomes even less severe, there might be a rather local problem of high salt concentration. In a comprehensive risk assessment, this has to be considered, including its economic aspects; this is beyond the scope of this study.

The large difference in predicted salt discharges and concentrations requires a comment on the value of the approach applied in Section 5.1. The comparison of both approaches suggests that the conceptual assumptions of the approach presented in Section 5.1 may be far too conservative to yield realistic estimates of salt infiltration. However, it is claimed that the immiscible 2p approach is still reasonable for estimating the transport of other dissolved substances which do not mix as a result of density-driven effects within the water phase.

5.3 Salt Concentrations during Water Production

In Section 5.1, the risk concept has been tested for the brine displacement process during CO_2 injection for investigation of scenario and statistical uncertainty. Additional analytical approximations are required to translate the risk or damage derived by the model into values (e.g., concentrations) that are comparable with water quality criteria. In the second part, recognized ignorance is reduced and the focus is on the processes in the overlying aquifers including mixing and migration of salt in the water phase (see Section 5.2). More exact values for the salt discharge into the water aquifer are obtained. The main interest of water suppliers related to salt problems is the salt concentration that is produced by a drinking water well. This part thus focuses on the processes occurring in the freshwater aquifer due to salt infiltration caused by CO_2 injection during water production. The influence of various parameters on the salt concentration in the production well is investigated.

5.3.1 Identification of Uncertainties

Various kinds of uncertainties are found for the considered case of salt infiltration into a freshwater aquifer. Recognized ignorance is further reduced compared to the previous investigations because groundwater flow and dispersion effects are considered. However, recognized ignorance is still found in, e.g., the grid resolution or the dimension of the model domain. For scenario uncertainty various features could be addressed: heterogeneities in the aquifer, the depth of the aquifer, different aquifer thicknesses, dipped or horizontal aquifers, or barriers of low permeability in the aquifer. However, the focus of this part is on statistical uncertainty. Most of the uncertainties found can be described statistically. The recharge rate and the corresponding hydraulic gradient, the permeability and the porosity of the aquifer, the dispersion coefficients, or the amount of infiltrated salt all are examples of uncertain parameters. Additionally, the distance of the water production well or its water production rate are design parameters which are also variable. The distance of the well can also be interpreted as scenario uncertainty as well because the location of the salt infiltration areas is often not known. Thus, the variation of the distance addresses also the uncertainty of the location of the fault zone.

The uncertain and design parameters chosen for investigation are the permeability of the aquifer, the distance of the water production well from the salt infiltration area and its production rate. In addition, the type of the grid and its resolution (recognized ignorance) highly influence the mixing of the salt and will be investigated as well.

5.3.2 Model Set-up

The model domain consists of a freshwater aquifer which is based on the aquifer considered in the previous investigations (see Figure 5.26). However, a 2D (x-z) model domain of 1 m depth instead of the 3D radialsymmentric domain is used to account for groundwater flow. The 2D assumption will overestimate the salt concentration in the production well because

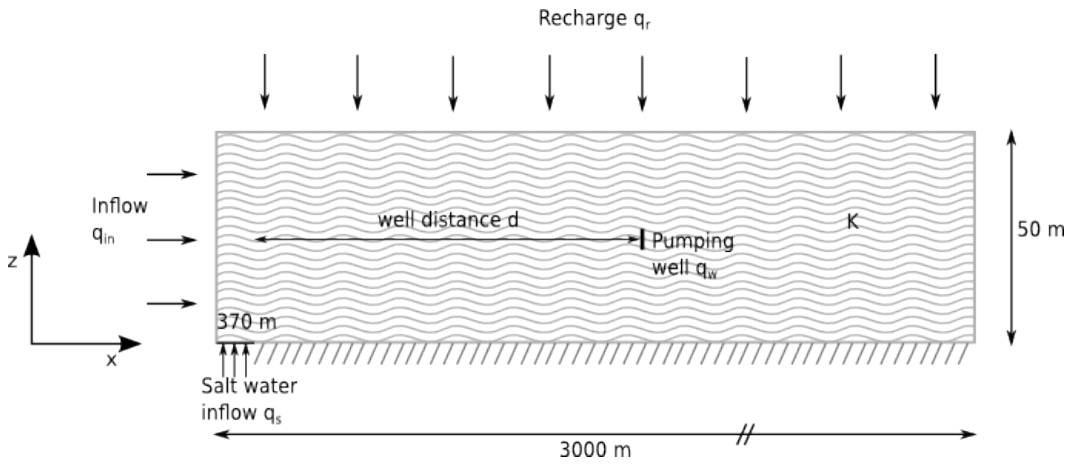

Figure 5.26: The conceptual model domain.

the spreading in the third spatial direction is neglected. Nevertheless the influence of the different uncertain parameters can be presented while the risk estimates are conservative.

The top of the aquifer is situated at 50 m depth and has a thickness of 50 m and a length of 3 km. The model domain is based on the domain presented in Aisopou et al. (2012). From the top layer a water recharge of 200 mm/a is given as a constant influx. The boundary on the left is a water inflow boundary as well, assuming that the water aquifer continues for 5 km on the left side, where it is confined by a low permeable layer. Thus, the water inflow on the left corresponds to the recharge over the 5 km. On right end of the domain, where the water flows out, a hydraulically open constant head boundary is applied.

The salt infiltrates from the bottom on the left side of the reservoir over 25 years. Assuming that the fault zone from the previous investigations reaches the water aquifer, the salt infiltration zone is 370 m wide. The infiltration rates are determined depending on the output obtained from Scenario B of the radial symmetric simulations in Section 5.2. The specific water (q_w) and salt (q_s) infiltration rate are calculated by dividing the discharge into the freshwater aquifer of Scenario B (D_{water}=1.811 kg/s, D_{salt}=0.0091 kg/s) by the area of the fault zone in the radial symmetric domain (about $1.0036 \cdot 10^6$ m^2). The values for q_w and q_s are given in Table 5.7. The remaining part of the bottom boundary is set to a Neumann no flow boundary condition assuming a low permeability layer.

For the base case, one of the set-ups required for the aPC+PCM calculations (see Section 5.3.4) is applied. Thus, a water production well that produces freshwater at a constant rate is situated at a distance of 241 m from the salt infiltration zone (in total 241+370=611 m from the left boundary). The aquifer has a homogeneous permeability and porosity field and it is assumed that no salt is contained initially. The maximum sustainable pumping rate is the sum of the recharge from the left boundary (recharge rate q_r x 5000 m^2) and the recharge from the top upstream of the well (q_r x 611 m). The actual pumping rate is defined as: $Q = Q_{max} * f$, where f is the production rate factor that is varied in Section 5.3.4.

A one-phase two component (1p2c) model including the water with the component salt as described in Section 2.4.3 is applied. Besides advective transport, molecular diffusion and

dispersion with the coefficients α_l and α_t presented in Garabedian et al. (1991) are taken into account. All applied parameters are listed in Table 5.7.

Parameter	Value
Permeability K [m^2] (K_z =K_x=K)	$1.2681 \cdot 10^{-9}$
Porosity $\phi[-]$	0.25
Initial salt mass fraction $X_{S,\text{init}}[-]$	0
Well distance d [m]	241
Maximum water production rate Q_{max} [kg/s]	0.03558
Production rate factor f [-]	0.1972
Diffusion coefficient D [m^2/s]	$1.587 \cdot 10^{-9}$
Longitudinal dispersion coefficient $\alpha_l[-]$	0.96
Transversal dispersion coefficient $\alpha_t[-]$	0.018
Recharge rate q_r [kg/sm^2]	$6.34 \cdot 10^{-6}$kg/sm^2 (200 mm/a)
Inflow (left) cause by recharge q_{in}[kg/sm^2]	$6.34 \cdot 10^{-4}$kg/sm^2 ($q_r \cdot 5000/50$)
Salt infiltration rate q_s [kg/sm^2]	$9.0674 \cdot 10^{-9}$
Water infiltration rate q_w [kg/sm^2]	$1.8049 \cdot 10^{-6}$

Table 5.7: Physical values for the base case.

5.3.3 Impact of Recognized Ignorance

During the investigations of the parameters, a significant influence of the type of the grid and its resolution was identified. Two different types of grids are compared: a triangular grid and a cubic grid. The triangular grid is unstructured and has the advantage that local grid refinement is easy and very efficient because the grid refinement is only where locally required. Whereas the cubic grid requires refinement in larger parts of the domain to avoid hanging nodes. In the triangular grid a finer resolution of maximum 1 m in the region where the salt distributes and a maximum resolution of 0.5 m in the near well region is chosen. Behind the well the grid is coarsened because the salt distribution in this region is not relevant for the results at the well. The cubic grid is resolved by 1 m x 1 m in the region from the left boundary up to 200 m behind the water production well. Behind the water production well the grid is logarithmically coarsened in x-direction, but the vertical discretization of 1 m has to be kept to avoid hanging nodes. The results for the two meshes are compared for the base case presented in 5.3.2.

Figure 5.27a-d shows the salt distribution for the triangular mesh compared to the cube mesh 6 years after the salt infiltration starts. The following processes influence the distribution of the salt: (i) advection acts mainly in the horizontal direction (x) due to the recharge from the left boundary; (ii) diffusion and dispersion result in mixing of the salt mainly in the vertical (y) direction; (iii) buoyancy forces due to density differences act against the vertical mixing because the denser saltwater tends to sink to the bottom of the reservoir. The buoyancy forces are very small because only a small density difference (about 0.5 kg/m^3) arises due to small salt mass fractions.

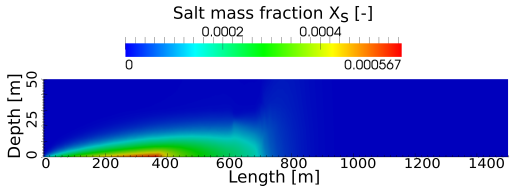

(a) Triangle grid $X_{s,max} = 0.000567$ (advection, diffusion, dispersion)

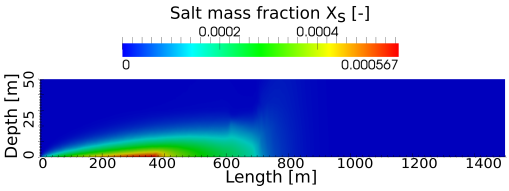

(b) Triangle grid $X_{s,max} = 0.000606$ (advection)

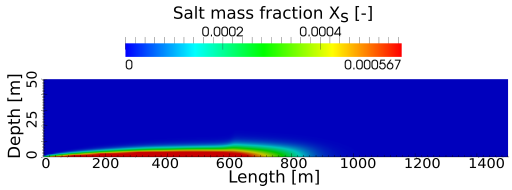

(c) Cubic grid $X_{s,max} = 0.001725$ (advection, diffusion, dispersion)

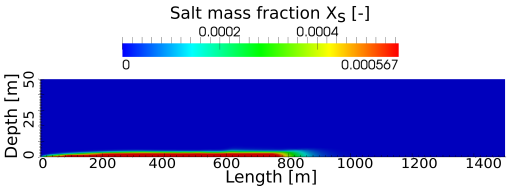

(d) Cubic grid $X_{s,max} = 0.002852$ (advection)

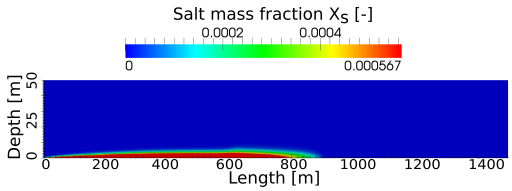

(e) Adaptive grid $X_{s,max} = 0.002545$ (advection, diffusion)

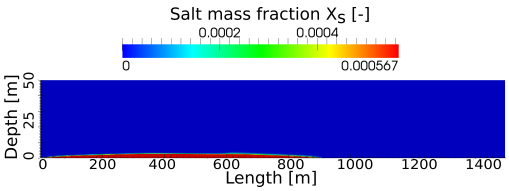

(f) Adaptive grid $X_{s,max} = 0.003081$ (advection)

Figure 5.27: Comparison of the salt distribution using a triangular, a cubic, and an adaptive cubic grid after 6 years of salt infiltration (5 times vertically exaggerated). $X_{s,max}$ represents the maximum salt mass fraction.

The vertical spreading of the salt is larger for the triangular grid (Figure 5.27a) than for the cubic grid (Figure 5.27c). The increased mixing in the triangular grid does not only result from physical dispersion processes but from numerical dispersion. In Figure 5.27 b and d, the salt distribution of the both grids are presented for simulations without diffusion or dispersion processes. While the difference compared to the simulation with diffusion and dispersion is very small for the triangular grid (Figure 5.27a,b), a larger difference is observed for the cubic grid (Figure 5.27c,d). A possible explanation for the increased mixing in the triangular mesh is that the main flow direction is parallel to the orientation of the domain. The only processes that should spread the salt in the vertical direction are diffusion and dispersion. The triangular mesh intensifies the distribution in the vertical direction because the normal vectors of the elements do not point in the flow direction due to the characteristic angles and non-orthogonal connections of a triangle. Thus, a small part of the advectively transported salt is always transported into the vertical direction as well, although the main flow direction is horizontal. For the current problem, where the main flow direction is clearly defined in the horizontal direction the triangular mesh overestimates the mixing in the aquifer.

In this case, adaptive grid refinement is an efficient way to resolve the salt distribution properly without refining the whole domain. In the simulator DuMu^x, adaptive grid refinement

is implemented for the decoupled models (the pressure and transport equation are solved sequentially for every time step, (see Fritz et al. (2012) for details). Thus, a decoupled model for one-phase and two-components is used including advection and diffusion. Dispersion is not yet implemented into the decoupled model. The implementation of dispersive fluxes would require an operator splitting where diffusion and dispersion processes are solved implicitly. Otherwise very small time steps are required to solve the system exactly. Thus, the simulation with the adaptive, cubic grid is run including advection and diffusion only. The grid is refined adaptively in regions where a certain gradient of the salt mass fraction occurs. Figure 5.27e shows that the mixing is still smaller compared to the cubic grid. On one hand the lower mixing is caused by the negligence of dispersion, on the other hand the finer grid further reduces numerical dispersion. The comparison with the implicit model using a triangular or a cubic grid accounting only for advection shows that both (cubic and triangular) grids without adaption are not fine enough to resolve the salt front correctly (Figure 5.27f). Thus, the results are clearly superimposed by uncertainties given by the mesh. Whether the salt actually reaches the well or not depends on the grid type and its resolution. In the simulation with the triangular mesh, the salt reaches the well, which can be seen in Figure 5.27, whereas the well is not affected by any salt for the simulation with the adaptive grid refinement neglecting dispersion.

Further refinement of the triangular mesh reduces the numerical disperison. Figure 5.28 shows the salt distribution for a refinement of a factor 2 in all regions for the triangular mesh. The vertical mixing is reduced but still larger than for the adaptive and the cubic mesh.

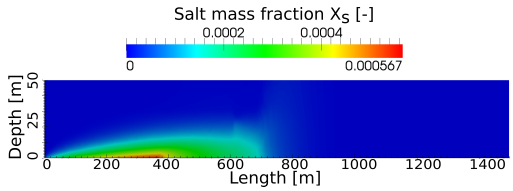

(a) Triangular grid (advection, diffusion, dispersion). Same figure as 5.27a

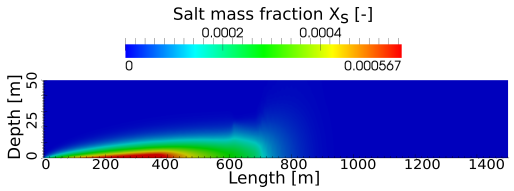

(b) Refined triangular grid (advection, diffusion, dispersion)

Figure 5.28: Comparison of the salt distribution after 6 years for the coarse and the refined triangular mesh (5 times vertically exaggerated).

The situations represented by the three grids could also be physically interpreted. The Peclet number defines the ratio of advective to diffusive flux:

$$Pe = \frac{advective flux}{diffusive flux} = \frac{\mathrm{v} L_z}{D}\,, \tag{5.13}$$

where L_z is the system length and v the flow velocity. Here, it is assumed that D accounts also for the dispersion process.

The three meshes could be interpreted as reflecting three different Peclet numbers, thus three different physical situations. The triangular mesh (small Peclet number) reflects a physical

situation with enlarged diffusive and dispersive flow, which could occur in strongly heterogeneous aquifers (high dispersion). Whereas a larger Peclet number represents a less dispersive situation.

The truth most likely lies between the simulation with the cubic grid including diffusion and dispersion and the simulation with the adaptive grid refinement, which resolves the salt distribution more exactly but does not account for dispersion.

5.3.4 Impact of Statistical Uncertainty

For the investigation of statistical uncertainty, the aPC combined with PCM as described in Section 3.2.2 is applied. The variation of the parameters is presented using the triangular grid. Thus, a situation with enlarged dispersive processes (strongly heterogeneous aquifer) is assumed and the trend for the salt concentration at a water production well given by the variation of the parameters is presented.

The uncertain and design parameters for this investigation are the permeability of the aquifer (K), the distance (d), and the water production rate of the well ($Q_p = Q_{max} * f$). The permeability is assumed to be lognormally distributed, ranging between 10^{-10} m^2 and 10^{-8} m^2. For the two design parameters uniform distributions are applied. The defined range for the well distance (d) is 0 to 2000 m starting from the end of the salt infiltration zone (x=370 m). The refinement zone of the grid is enlarged corresponding to the well distance applied. For the water production factor (f) a range of 0 to 0.4 is chosen. To avoid effects to neighboring aquifers (outside the considered domain), larger water production rates are not applied. Second order polynomials (d_p=2) are used, which results in combination with the three varied parameters (N=3) in ten required simulation runs (see Equation 3.16). The collocation points, which are used for the different combinations for the ten snapshot runs are shown in Table 5.8.

Permeability [m^2]	Pumping rate factor [-]	Well distance [m]
$K_1 = 1.1350 \cdot 10^{-10}$	$f_1 = 0.0461$	$d_1 = 241$
$K_2 = 1.2681 \cdot 10^{-9}$	$f_2 = 0.1972$	$d_2 = 1013$
$K_3 = 1.7857 \cdot 10^{-8}$	$f_3 = 0.3523$	$d_3 = 1760$

Table 5.8: Collocation points for aPC snapshot simulations.

Figure 5.29 shows the averaged salt concentration at the well (averaged concentration over the whole well screen) over time (a) and the salt concentration along the well screen (z=20-30m) (b) for snapshot runs with three different well distances. The production rate and the permeability are the same in all three runs (see Table 5.8: f_2, K_2). In the following description the abbreviations SR1, SR2 and SR3 correspond to the three snapshot runs with the well distances d_1, d_2, and d_3 respectively shown in Figure 5.29 .

The lowest concentration at the well arises for SR1 with the smallest well distance (d_1=241 m). With increasing distance of the well, the concentration increases (SR2, d_2=1013 m). However, the concentration does not rise further with increasing distance if a

certain well distance is reached. The averaged concentration at the well for SR3 (d_3=1760 m) is very similar to the concentration in SR2. With increasing distance from the salt infiltration zone the salt is spread more and more vertically due to diffusion and dispersion and the salt is distributed over the whole aquifer thickness.

This trend is confirmed by Figure 5.29b, where the salt concentration along the well screen is shown for the three snapshot runs. The difference between the salt concentration in the lower and upper part of the well is larger for closer wells (d_1). Thus, the majority of the salt is still in the lower part of the aquifer at a well at distance d_1. As discussed above, with increasing distance from the salt infiltration zone, the salt becomes more and more mixed across the aquifer (see SR2/SR3) and the concentration along the well screen assimilates more and more to a constant value with increasing well distance (see Figure 5.29b d_2, d_3). The largest local salt concentration is observed at the closest well (d_1).

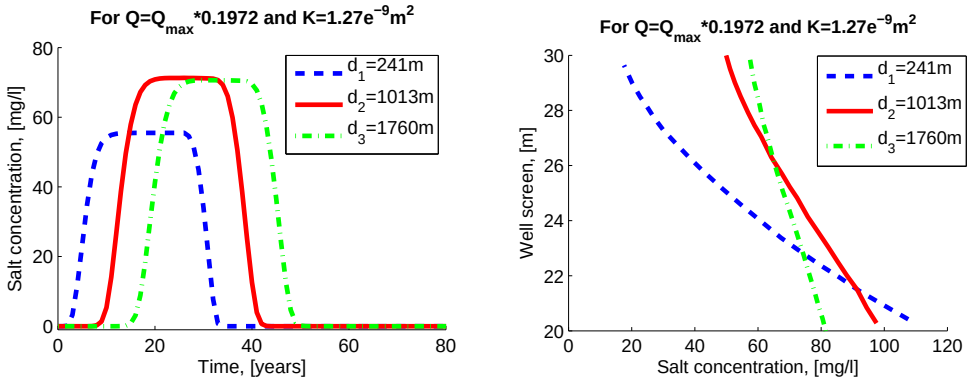

(a) Averaged salt concentration at the well over time.

(b) Salt concentration along the well screen, after 27 years of salt infiltration.

Figure 5.29: Averaged salt concentration at the well (a) and concentration distribution along the well (b) for different distances of the well.

Figure 5.30 shows the averaged salt concentration at the well over time (a) and the salt concentration along the well screen (b) for snapshot runs with varying production rates and for two different well distances (with constant d_1 or d_2, K_2, see Table 5.8). An increase of the pumping rate results in an increase of the averaged concentration at the well (Figure 5.30a). The difference in the salt concentration for varying production rates is smaller for wells that are further away from the salt infiltration zone. As already discussed, the salt is almost fully mixed over a larger vertical distance. Thus, an increase in the production rate increases the total amount of salt that is produced but the concentration remains more or less constant. Figure 5.30b shows that the salt concentration at the bottom of the well is increased and the concentration at the top of the well is decreased with increasing production rate. At the bottom of the well more salt is pumped from below, while more freshwater from above the well is produced at the top, if the water production rate is increased.

In Figure 5.31 the salt concentration at the well over time is shown for three different permeabilities (with constant d_2 and f_2, see Table 5.8). The influence of permeability is only significant for larger permeabilities (about 10^{-8}m^2). Then, the salt concentration at the well is decreased compared to cases with lower permeability. An increase in permeability results

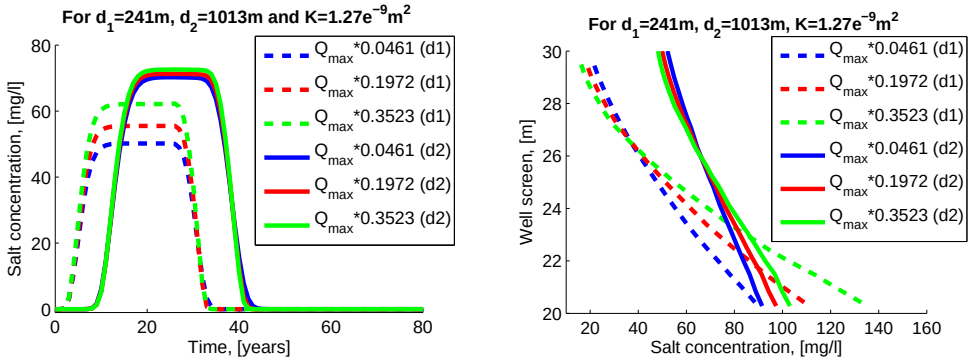

(a) Averaged salt concentration at the well over time.

(b) Salt concentration along the well screen, after 22 years of salt infiltration.

Figure 5.30: Averaged salt concentration at the well and concentration distribution along the well for different production rates and the two distances d_1 and d_2.

in a reduction of the overall pressure gradient, Thus the influence of buoyancy forces becomes more significant. The density differences are very low (about $0.5\,\mathrm{kg/m^2}$), however, for high permeabilities the pressure gradient becomes very small as well. This is in agreement with the gravitational number, which is defined as

$$Gr = \frac{gravitational\,forces}{viscous\,forces} = \frac{\Delta\rho \mathrm{g} K}{\mu \mathrm{v}}\,. \tag{5.14}$$

where $\Delta\rho$ is the density difference between salt- and freshwater and v is the characteristic velocity. An increase in permeability intensifies the influence of gravitational forces. At a critical value for the permeability the gravitational forces dominate and more salt sinks to the bottom of the aquifer. This will lead to a reduction of the mixing and a decrease of the concentration at the well. This fact is only discussed qualitatively here; the quantitative investigation of the interaction between the two forces and the correlation with the gravitational number is not in the scope of this work. For CO_2 plume expansion, Kopp (2009) investigated the influence of gravitational and viscous forces in detail.

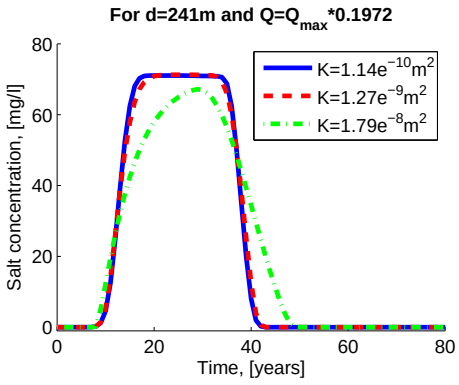

Figure 5.31: Averaged salt concentration over time at the water production well for different permeabilities.

Figure 5.32 shows the dependence of the salt concentration (averaged over the well screen)

on the pumping rate (a), the well distance (b), and the permeability (c) after 27 years of salt infiltration. At this time the salt has arrived at all wells with the distances given by the collocation points. The curves are derived by the aPC+PCM method whereas the two remaining parameters, whose dependency is not shown in the respective figure, are averaged over the whole parameter range (given by the input distributions) by running Monte Carlo on the polynomials. The mean and the standard deviation (std) caused by the two remaining parameters are presented. In addition, selected snapshot runs are plotted to test if the polynomials reproduce the trend correctly. The influence of the water production rate is well represented by the polynomial: the salt concentration is increased with an increasing pumping rate (see 5.32a). The same trend shown by the snapshot runs is met. The absolute values of the snapshot runs differs from the mean curve because fixed values for K and d were set in the snapshot runs. As the standard deviation that is caused by the two parameters K and d shows, the influence of K and d is larger for smaller production rates.

The increase of the salt concentration with increasing well distance is also reproduced by the polynomials. However, the influence of well distances larger than about 1200 m is falsified due the typical characteristic of the polynomial: The salt concentration at the well is decreased with increasing well distance. The snapshot runs seem to confirm this trend: the salt concentration for the largest distance (d_3) is smaller than for d_2. However, this is only valid at the presented time of 27 years: the maximum salt concentration has not yet reached the well in a distance of d_3=1760 m. As shown in Figure 5.29, the maximum concentration for the two wells in distance d_2 and d_3 are the same. For the current simulations a situation that the maximum concentration is reached at all three wells at the same time does not exist. Even if the polynomials do present the right trend in this situation, the extrapolation yields an artifact by the method. It is expected that the concentration will be at a constant value for well distances larger than d_3. The standard deviation caused by the permeability K and the water production rate Q shows that the influence of these parameters is larger for smaller well distances.

The behavior of the salt concentration depending on the permeability is well represented by the polynomial: as discussed before, the concentration is almost constant for variation in small permeability ranges and is reduced for large permeabilities. Overall, the well distance has the largest influence in the considered range of parameters. Thus, the mixing time is relevant. Here, the influence of different Peclet number is interested as well, which was qualitatively shown by the comparison of the three meshes in Section 5.3.3.

5.3.5 Implications for Risk Assessment

In this section, the risk assessment for the considered problem is discussed. It is however important to keep still in mind that the mixing of the salt is overestimated by the triangle grid. Different possibilities are presented as to how the results can be demonstrated. Damage may be defined as the concentration at the well averaged over the well screen.

Figure 5.33 shows the mean salt concentration at the well over time. It is derived by taking the mean from the polynomial response for the whole input parameter distribution for permeability, well distance, and pumping rate. The maximum mean value for the damage is

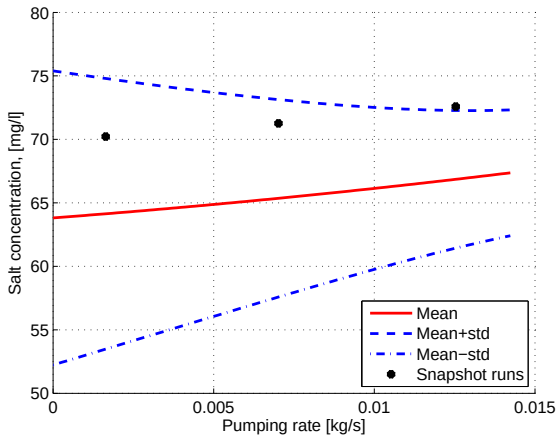

(a) For mean and std: averaged d and K. For snapshot runs: d_2 and K_2.

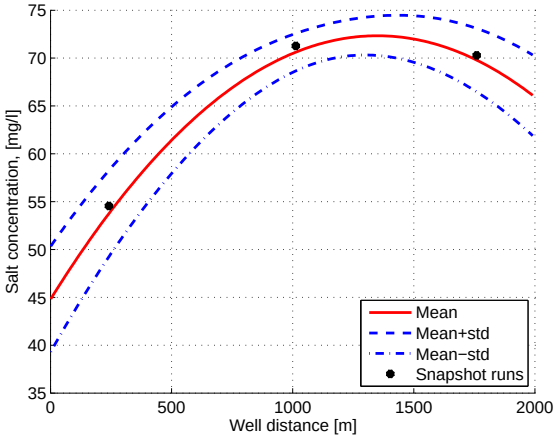

(b) For mean and std: averaged f and K. For snapshot runs: f_2 and K_2.

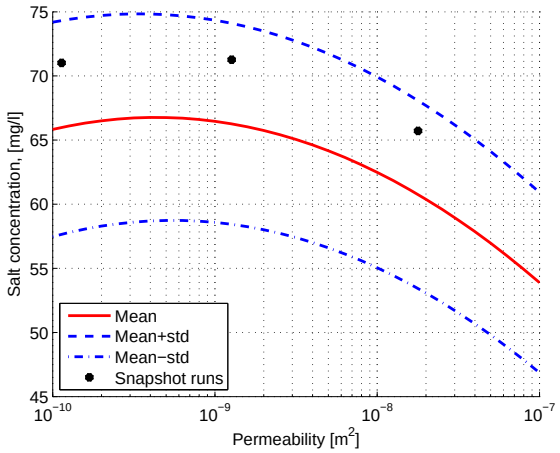

(c) For mean and std: averaged d and f. For snapshot runs: d_2 and f_2.

Figure 5.32: Mean salt concentration (red line) and corresponding standard deviation (blue, dashed lines) at the well depending on a) the water production rate, b) the well distance, and C) the permeability after 27 years of salt infiltration.

66 mg/l and arises about 26 years after the salt infiltration started. The mean value gives a rough estimate what kind of concentration can be expected for wells which are in the given range of permeabilities, well distances and production rates. An important piece of information out of this figure is that after 50 years no more salt is expected at the well in the case where salt infiltration is presumed to last for 25 years.

Another indicative information is to present a probability density function (PDF) for a certain time. Figure 5.34a shows the PDF after 27 years of salt infiltration. The function gives further details as to which concentration is expected to be most probable to occur at the well. In addition, a cumulative distribution function (CDF) can be presented (Figure 5.34b), which can provide the probability that a certain damage is not exceeded. Finally, an overall risk value for a given time can be calculated by using Equation 4.2. To get a risk value in the same units as damage, the values for probability are derived by normalization of the values from

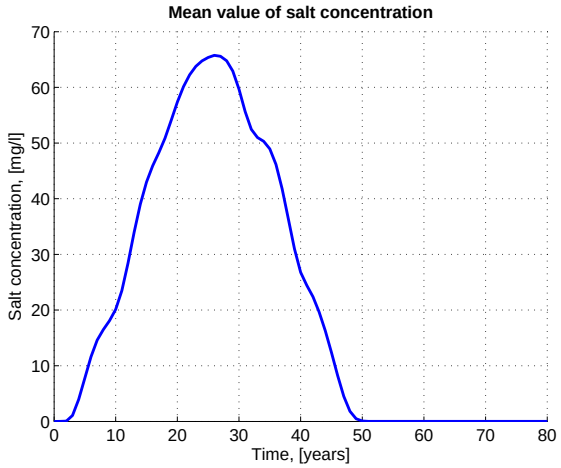

Figure 5.33: Mean salt concentration over time at the water production well.

the PDF by the maximum value of 76 in the PDF. Thus the normalized probability-weighted expectation for the concentration at the well is derived: 14.62 mg/l (after 27 years of salt infiltration). All these values can be compared to the water quality criteria given in Section 5.1.6 and can help to decide if water should be produced in a region where salt infiltration is expected. For the current model set-up the criteria are not exceeded.

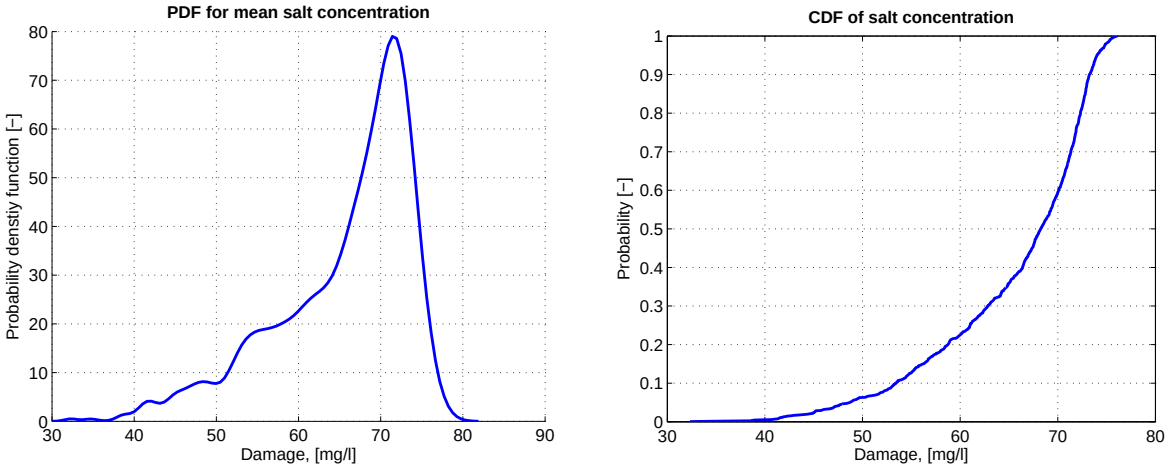

(a) (b)

Figure 5.34: Probability density function and cumulative distribution function for salt concentration at the well as damage (after 27 years of salt infiltration).

5.3.6 Conclusions

The key messages which can be gained from the presented investigations are shortly summarized and discussed.

(i) As presented by the grid comparison study, mixing of the salt with water is the key factor

for the salt concentration at the water production well. Whether salt is produced or how much salt is produced by the well depends on the mixing in the aquifer and of course on the mass discharge from the fault zone.

(ii) The mixing in the model strongly depends on the type of grid that is applied and its resolution. Thus, coarse grids overestimate the mixing and salt is pumped earlier by the well than in reality. An adequate grid type has to be chosen for the considered problem and its resolution needs to be fine enough to describe the mixing properly.

(iii) Even if the grid resolution can reproduce the mixing adequately, uncertainties still exist concerning the dispersion coefficients, which reproduce heterogeneities of the permeability field, which are not considered. Thus the influence of different heterogeneous permeability fields could be tested in future work to better understand their effects.

(iv) The influence for the three varied parameters (permeability, well distance, and water production rate) could be well represented by the triangle mesh as well. The well distance has the largest influence on the salt concentration at the well among the parameters. Thus, the mixing time is highly relevant.

(v) Various results could be provided for assessing the risk and making decisions: mean damage, PDF, CDF, or an expected value for risk. The values can be directly compared with water quality criteria. The mean values over time can provide an estimate which kind of concentrations can be expected. The PDF for a given time represents which concentrations are the most probable ones and which range of concentration can be expected. The CDF is a very helpful tool for risk assessment when comparing the results with a certain threshold value (quality criterion). One can provide a probability that a certain threshold is not exceeded. The probability weighted expectation of damage (risk) value shifts the mean damage by consideration of probabilities, which can give an estimate which concentration can be expected when probabilities are taken into account. All of the results presented here are of theoretical character because of the uncertainties introduced by the grid and other arbitrary assumptions.

Compared to the results given in the previous investigations (see Section 5.1 and 5.2), concentrations at the water production well can be directly provided and compared with criteria. For water suppliers and decision makers it is more practical to have concentration values directly at the well instead of brine discharge into the aquifer or fully mixed concentration. The comparison of the fully mixed concentrations with the water quality criteria is also possible but these values are only valid at a certain distance from the infiltration zone. For the considered aquifer of a thickness of b_{aq}=50 m the mixing length ($L_{mix} = b_{aq}^2/2\alpha_t$) is 69.4 km, thus the fully mixed concentrations are not valid for wells closer to the infiltration zone. In this region, the simulations presented in this section provide more reliable salt concentrations at the well, which are larger than fully mixed concentrations. However, for the determination of the salt concentrations at the well with the presented approach, the previous investigations in Section 5.2 are required for determining the amount of salt that infiltrates. The concentrations do not exceed the criteria for the presented scenario. On one hand, the 2D assumption results in conservative estimates, on the other hand the increased

mixing by the grid falsifies the salt concentrations. The density difference between salt- and freshwater is very small due to the small salt concentrations caused by mixing, thus the effect of abrupt upconing as discussed in Section 5.1 is not relevant in the particular case. However, under certain conditions (less mixing, larger salt infiltration), the concentration could be higher because of upconing of water with higher salt concentration.

In the current approach, only recognized ignorance and statistical uncertainty are investigated. However, the variation of the well distance can be also interpreted as scenario uncertainty. The existence of a fault zone is often not known and thus the variation of the distance also reflects the uncertainty of where the fault zone is exactly located.

The model reduction via aPC and PCM is adequate for estimating the dependencies. However, the results have to be interpreted precisely and overshooting or underestimations given by the polynomials have to be considered in the risk assessment.

Since the time until the salt reaches the well is relevant for mixing it is suggested to investigate the influence of the ratio between advection and diffusion/disperion (Peclet number) quantitatively in future work.

6 Uncertainty Studies for Realistic CO_2 Storage Sites

In this chapter uncertainty studies and history matching are performed for a realistic CO_2 storage pilot project, the Ketzin site project, and a hypothetical pressure study for a realistic reservoir in the North German Basin (Schäfer et al. (2011)). No risk assessment as introduced in the previous chapters is performed. It is crucial however, to reduce the uncertainties in the model as much as possible for future risk assessment. Thus the uncertainty studies and history matching help to collect valuable information for future risk assessment about uncertainties and sensitivities of the available data and applied model assumptions. The investigated uncertainties are discussed in the scope of the different levels of uncertainty presented in the risk assessment concept (see Chapter 4).

In Section 6.1, a history matching approach including detailed preliminary considerations to calibrate the dynamic model is developed. The uncertainties introduced by missing data, model assumptions or the predicted parameters are discussed in detail. A study on pressure propagation for a hypothetical realistic reservoir in the North German Basin (Schäfer et al. (2011)) including the investigation of the influence of parameters and scenarios is briefly presented in Section 6.2.

6.1 History Matching for a Real Life Project: CO_2 Storage Site in Ketzin

The Ketzin pilot site is the first on-shore CO_2 storage site in Europe and is located near the town Ketzin in Brandenburg, 40 km west of Berlin, Germany. The site is an abandoned gas storage site, where gas had been stored at 250 m to 400 m depth for about 30 years. The saline aquifer which is used as the CO_2 storage formation is located below the gas storage formation at about 630 m to 650 m depth (Martens et al. (2012)). The operation at the Ketzin site started within the CO_2SINK project, a European pilot project for CO_2 storage in saline aquifers (Würdemann et al. (2010)). In April 2004, the project started with the pre-injection work such as getting regulatory approvals, informing the public, drilling the wells, building facilities at the site, and installing monitoring tools. The actual injection of CO_2 started in the end of June 2008. The total amount of CO_2 that are allowed to be stored is limited by legal regulations to 100000 tones for this research project (Martens et al. (2012). CO_2 is injected at slightly supercritical pressure and temperature into the about 72 m thick Stuttgart formation (Upper Triassic sandstones) at 650 m depth. In the formation sand channel facies of high permeability exist beneath flood plain facies rocks with low permeability (Förster

et al. (2006)). Three wells were drilled before the injection started: the actual injection well Ktzi 201, and two observation wells Ktzi 200 and Ktzi 202. Ktzi 200 is located 50 m east of Ktzi 201 and Ktzi 202 is 112 m northeast of Ktzi 201. Various procedures were performed to collect as much data as possible about the geological structure of the Ketzin site, e.g., seismic surveys (Juhlin et al. (2007)), interpretations of the core material and well-log data (Norden et al. (2010)), and hydraulic pumping tests (Wiese et al. (2010)).

The CO_2SINK project ended in March 2010. Further research and development at the Ketzin site is performed CO_2MAN project which started in September 2010 (Martens et al. (2012)). In addition, several other projects are associated with the Ketzin pilot project (see Martens et al. (2012)). The main aims during the period of the CO_2MAN project are the monitoring of the injected CO_2 and development of concepts for monitoring, characterization and quantification of the interaction between CO_2, other fluids, the rock and the microbial species, validation of the modeling tools, and transfer of knowledge[1]. One milestone was the drilling of the observation well Ktzi 203, between the wells Ktzi 201 and Ktzi 202 to gain core material that has been exposed to the CO_2 for about three years for further investigations of e.g. the mineralogy. Until end of January 2013, 62.144 t of CO_2 has been injected into the saline aquifer.

The tasks for modeling changed during the work process. In the pre-drilling period, simulations were performed to investigate, e.g., temperature effects, near-well and large scale scenarios, or the effect of different model extensions. All these investigations aimed to help develop a first geological model (see Section 6.1.2.1). In addition, what-if scenarios were modeled for better planning of the laboratory and injection experiments. Before the injection started in June 2008, the modeler task was to predict the arrival time at the two observation wells Ktzi 200 and Ktzi 202 (see Kempka et al. (2010)). The prediction was performed for the geological model version 3.0 (see Section 6.1.2.1) which included the interpretations and information from the well logs and the core material. Two simulators MUFTE_UG (see Section 2.5) and Eclipse E300 were used for the prediction. The arrival time at Ktzi 200 could be reproduced almost exactly with the existing geological model and the knowledge of the exact injection rates by both simulators. However, the arrival time at Ktzi 202 and the pressure measured at the injection well Ktzi 201 was underestimated by both simulators.

6.1.1 Aim and Structure of this Study

The main task of current dynamic modeling activities is to achieve a history match of the measurements on the basis of the statistical geological model. The measurements that are available are the pressure at the injection well Ktzi 201 which is measured over the whole time period since June 2008. Additionally, the arrival time of the CO_2 in free phase at two observation wells Ktzi 200 and Ktzi 202 are measured. Measurement data of the pressure at the second observation well Ktzi 202 for a limited time period exists.

As discussed above, the arrival time at the first observation well was well predicted by the models, but the arrival time at the second observation well Ktzi 202 and the pressure at the

[1] CO_2MAN Project - CO_2-Reservoirmanagement (www.co2ketzin.de)

injection well were significantly underestimated by the models. Although the geological model was further updated based on new measurement data (see Section 6.1.2.1, Version 5) the pressure at the injection well and the second arrival time are still underestimated by the models. By including anisotropic permeability multipliers Kempka and Kühn (2013) could achieve a good match for the pressure and the arrival time (see also Section 6.1.3.2). Here a new approach will be presented using inverse modeling. For demonstration, Table 6.1 summarizes the observed and simulated arrival times for the different versions of the geological model (see Section 6.1.2.1) and the different simulators and meshes (see Section 6.1.2.2), which are applied in this study. For the pressure curves for the two simulations using version 5 one is referred to Figure 6.12.

Simulator	Geologial model	Grid type	Arrival at Ktzi 200	Arrival at Ktzi 202
Measurement	-	-	21.7 days	271 days
MUFTE-UG	Version 3	Hexahedron	21 days	79 days
DuMu^x	Version 5	Tetrahedron	24.8 days	129.3 days
DuMu^x	Version 5	Hexahedron	17.7 days	116.7 days

Table 6.1: Arrival times at Ktzi 200 and Ktzi 202 for the different versions of the geological model (see Section 6.1.2.1).

Before the history matching approach is performed the following questions should be discussed. The answers help to structure the history matching procedure and can strongly influence the results.

- What is known from various measurements and previous investigations? How reliable is the known data?
  The geological model and the data required for numerical modeling are presented and discussed in Section 6.1.2. In addition, the results of two former history matching approaches are presented in Section 6.1.3 to provide helpful information for the new approach.
- What are the uncertainties that are based on model assumptions?
  The influence of the domain size, the model concept, the grid type, or the discretization is investigated and discussed in Section 6.1.4.
- Which parameters are the most sensitive ones?
  Based on the former investigations and simple, obvious guesses, the sensitivities of various parameters (permeability, porosity, relative permeability, capillary pressure, skin factor, anisotropy) are discussed in Section 6.1.5.
- How many degrees of freedom should be allowed for history matching?
  More degrees of freedoms results in a more exact calibration. However, the correlation between the parameters can be very high and the uniqueness of the best fit parameters is questionable (see Section 6.1.5).

Based on the discussion of the presented questions, the decisions for the applied history matching procedure and the related model assumptions are made. The key factors that

should be defined are: (i) the conceptual model, the model domain, the grid type, and the discretization for the numerical simulations, (ii) the number of degrees of freedom that are allowed for calibration and the corresponding estimation parameters, and (iii) the overall history matching approach (trial and error or automatic parameter calibration).

Since the computational costs for the simulation of the highly heterogeneous and nonlinear problem are very high a systematic procedure is adapted for the history matching applied in this work (see Section 6.1.6). The following choices are made:

- A tool for automatic parameter estimation, iTOUGH2 (Finsterle (1999b)) is applied for matching the pressure for the first 50 days of injection and the arrival time at Ktzi 200. For the numerical forward simulations a 2p2c model is applied for a model domain of 5 km x 5 km. A hexahedron mesh with permeability and porosity data based on Version 5 of the geological model is applied using the cell-centered finite volume method. To keep the arbitrariness low, only 3 estimation parameters are chosen for the inverse modeling approach, thus 3 degrees of freedom are allowed.
- The calibrated model is then extrapolated to longer time scales for predicting the pressure for 1650 days, trying to match the pressure over the whole simulation period.
- The second arrival time is matched by including a geological feature (here a "barrier" of low permeability).

Finally, the results and conclusions that can be gained from the presented investigations and the history matching approach are discussed in detail in Section 6.1.7.

6.1.2 Data Basis

In this Section, the first question is addressed, and the available data for modeling is described. The geological model is continuously updated based on new measurement data or knowledge gained from dynamic modeling. Thus, the development of the geological model is briefly summarized in Section 6.1.2.1. The the adapted grids and the modeling data available are described in Section 6.1.2.2.

6.1.2.1 Geological Model

The Stuttgart formation is of Middle Keuper (Upper Triassic) age and is a lithologically heterogeneous formation, where sandy channel-facies with good reservoir properties alternate with flood-plain-facies with poor reservoir properties. The thickness of the sand channels can reach up to 30 m. A caprock of playa-type rocks is located above the reservoir. For details about the baseline characterization of the Ketzin storage reservoir one is referred to Förster et al. (2006). During the pre-drilling phase a first geological model (version 0.0) was set up using a geostatistical approach based on information from an existing well in the study area and from additional wells outside this area, which penetrate the Stuttgart

formation. The geological model includes the Stuttgart formation and covers a horizontal area of 10 x 10 km. The details on this version are published in Förster et al. (2006). After drilling the first well the geological model was locally updated in version 1.0. The base-case for the prediction of the arrival times was version 3.0, which was updated by including the information from well logs and core material of all three wells (Norden et al. (2010)) and information from the seismic 3D investigation (Juhlin et al. (2007)). The seismic 3D investigation helped to define the model volume and major faults were detected. The base model has a size of 5 x 5 km and does not include any fault. For the petrophysical modeling of the spatial distribution of porosity within each facies, the log data for porosity was used. For the permeability field, a porosity-permeability relationship was set up from the limited permeability data from core material and from well-log data. The petrophysical interpretation is described in detail in Norden et al. (2010). A geostatistical approach is used to describe the facies distribution. The geological concept to construct the reservoir model is presented in detail in Norden and Frykman (2013). The current geological model (version 5) is revised by including new information (Ben Norden, GFZ, personal communication). The fault zone, which is located north of the injection well, is included in the model for the first time. The facies modeling is renewed by including the information of the monitoring results from the 3D repeat seismic investigation (Martens et al. (2012)) in the model. A Gaussian simulation is applied to describe the distribution of the petrophysical properties within the facies. The permeability is related to the porosity distribution using determined porosity-permeability relationships (Norden and Frykman (2013)).

6.1.2.2 Modeling Data and Model Set-up

In this section the properties and conditions used for all simulations are presented. Where other relations are applied this will be highlighted in the beginning of each section. The heterogeneous permeability and porosity field is given from the geological model described in Section 6.1.2.1 and is interpolated on the constructed grids. For the interpolation of the data from the geological model Version 3 on the hexahedron grid used in the simulator MUFTE-UG, the kriging method which is implemented in the visualization software tecplot is used. Version 5 of the geological model is the basis for the interpolation on the tetrahedron and hexahedron mesh used in the simulator DuMu^x and an inverse distance approach is applied for the interpolation. Both meshes does not consider the fault zone. The domain size is 5 km x 5 km in the horizontal and about 70 m in the vertical direction. A 2p or a 2p2cni model is used in the simulator MUFTE-UG. In DuMu^x a 2p2c model neglecting nonisothermal effects is applied. For details about the applied models see Section 2.4.1 and 2.4.2. For the simulations with MUFTE-UG the box method is used. In DuMu^x, the box-method is applied for all simulations with the unstructured tetrahedron mesh, whereas the cell-centered finite volume method is used for the simulations with the hexahedron mesh due to better convergence. All different model set-ups are summarized in Table 6.2.

For the initial and boundary conditions of the pressure, hydrostatic conditions based on the pressure of 62 bar at 639.5 m below surface and the pressure gradient given in Table 6.3 are assumed. The temperature is 34°C at 639.5 m depth and a thermal gradient of 0.03°C/m is applied. In all simulations the top and bottom boundary conditions are no-flow (Neumann)

Model	Simulator	Model	Geologial model	Grid type	Discretisation method
1	MUFTE-UG	2p	Version 3	Hexahedron	box-method
2	MUFTE-UG	2p2cni	Version 3	Hexahedron	box-method
3	DuMu^x	2p2c	Version 5	Tetrahedron	box-method
4	DuMu^x	2p2c	Version 5	Hexahedron	cell-center finite volume

Table 6.2: Applied models for the different investigations.

Property	Value
Salinity	S=0.2 kg_{salt}/kg_{brine}
Pore compressibility	C=7.2 $\cdot 10^{-10}$ 1/Pa
Anisotropy	K_v/K_h=1/3
Initial pressure at 639.5 m	p_{init}=62 bar
Pressure gradient	1.14 Pa/m
Initial temperature at 639.5 m	T_{init} = 34°C
Temperature gradient	0.03°C/m
Capillary pressure parameter	λ = 1.011613
Entry pressure	p_d = 10952.87 Pa
Residual saturation of brine	S_{wr} = 0.15 (0.1-0.2)
Residual saturation of CO_2	S_{nr} = 0.05 (0.03-0.07)
Relative permeability parameter	$k_{rw,eq}$ = 1.0
Relative permeability parameter	$k_{rCO2,eq}$ =0.85 (0.8-0.9)
Relative permeability parameter	n_w = 5.5 (5.0-6.0)
Relative permeability parameter	n_{CO2} =1.25 (1.0-1.5)

Table 6.3: Properties for the simulation model (the possible range provided by measurements is shown in brackets).

conditions assuming layers of low permeability, and the lateral boundaries are hydraulically open, constant head boundaries (Dirichlet). The parameters for salinity, anisotropy and pore compressibility (using Equation 2.20) are shown in Table 6.3. For the capillary pressure, the Brook Corey relation presented in Section 2.1.5 with the parameters λ and p_d given in Table 6.3 is used. The parameters are based on measurements carried out during the CO_2SINK project (unpublished data). Additionally, the following relative permeability curves were recommended:

$$k_{rw} = k_{rw,eq}\left(\frac{S_w - S_{wr}}{1 - S_{wr}}\right)^{n_w} \tag{6.1}$$

and

$$k_{rn} = k_{rn,eq}\left(\frac{1 - S_w - S_{nr}}{1 - S_{nr} - S_{wr}}\right)^{n_{CO2}} . \tag{6.2}$$

In the current simulation the mean values of the recommended ranges for the parameters $k_{rw,eq}$, n_w, $k_{rCO2,eq}$, n_{CO2} are applied (see Table 6.3). The large range of the parameters for the relative permeability and the capillary pressure relationships illustrate the uncertainties of

the data. The actual injection regime, which varies every hour, is summarized into minimum 2 days periods.

6.1.3 Former Assessments for History Matching

Former history matching approaches help to identify sensitivities, which are important for the selection of the estimated parameters. Additionally, information is provided for defining the individual steps of the overall history matching procedure. Two investigations were already performed: A short study how the second arrival time can be matched and an overall history matching procedure which is focused on matching all measurements (pressure at Ktzi 201 and Ktzi 202 and arrival times at Ktzi 200 and Ktzi 202).

6.1.3.1 Influence of a Barrier of Low Permeability

One possibility that could explain the late arrival time of 271 days at Ktzi 202 is the existence of a distinct geological feature (e.g. a "barrier" of low permeability) between the two wells. A first step in the procedure of history matching was the investigation of how a barrier of low permeability could influence the second arrival time. For this investigation, Version 3 of the geological model using the mesh and model domain of 5 x 5 km presented in Section 6.1.4.1 is used and the simulations are performed with MUFTE-UG (Table 6.2 Model 2). The arrival time predicted by the current model was 79 days for the unmodified geological model. Thus, a "barrier", a low permeable zone is included into the geological model. The shape of such a barrier is unknown, thus it is simplified to a cuboid in this study. For a rough estimation for the dimension of the barrier a 2p model neglecting dissolution is used (Table 6.2 Model 1).

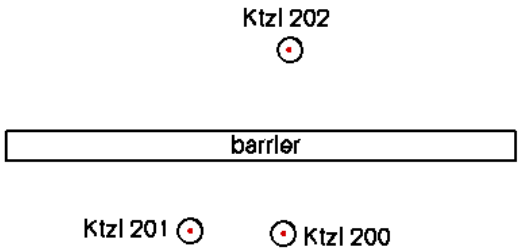

Figure 6.1: Top view on the barrier between Ktzi 201 and Ktzi 202.

Figure 6.1 shows a top view on the location of the barrier which results in an arrival time close to the measured arrival time for the 2p model (261 days). The barrier has the dimension of 280 m x 20 m x 35 m and the permeability is reduced by a factor of 1000. The simulation of the scenario with the current barrier with a 2p2cni model results in an overestimation of the arrival time (larger than 350 days). However, this barrier is used as a base case for the variation of the length, the depth, and the permeability of the barrier using a 2p2cni model. For each of the parameters several variations are simulated. All variations are presented

and discussed in a project report of the CO_2SINK project. In the following only the best estimate for each variation is presented. The dimension and properties of the barrier and the corresponding arrival time at Ktzi 202 are presented in Table 6.4 for four scenarios.

Scenario	Barrier	Arrival time [days]
1	no barrier	79
2	reduction of length 240m x 20m x 35m	238
3	reduction of depth 280m x 20m x 10m	268
4	variation of K 280m x 20m x 35m $K_{barrier}$=K/50	258

Table 6.4: Dimension and properties of the barrier and resulting arrival time for each variation.

Figure 6.2 shows the permeability field for a section between the injection well Ktzi 201 and the observation well Ktzi 202. The deep barrier in Scenario 2 and 4 cut the permeable sand channel between the two wells completely (see Figure 6.2b), whereas a permeable connection still existed for the flat barrier in Scenario 3 (Figure 6.2c).

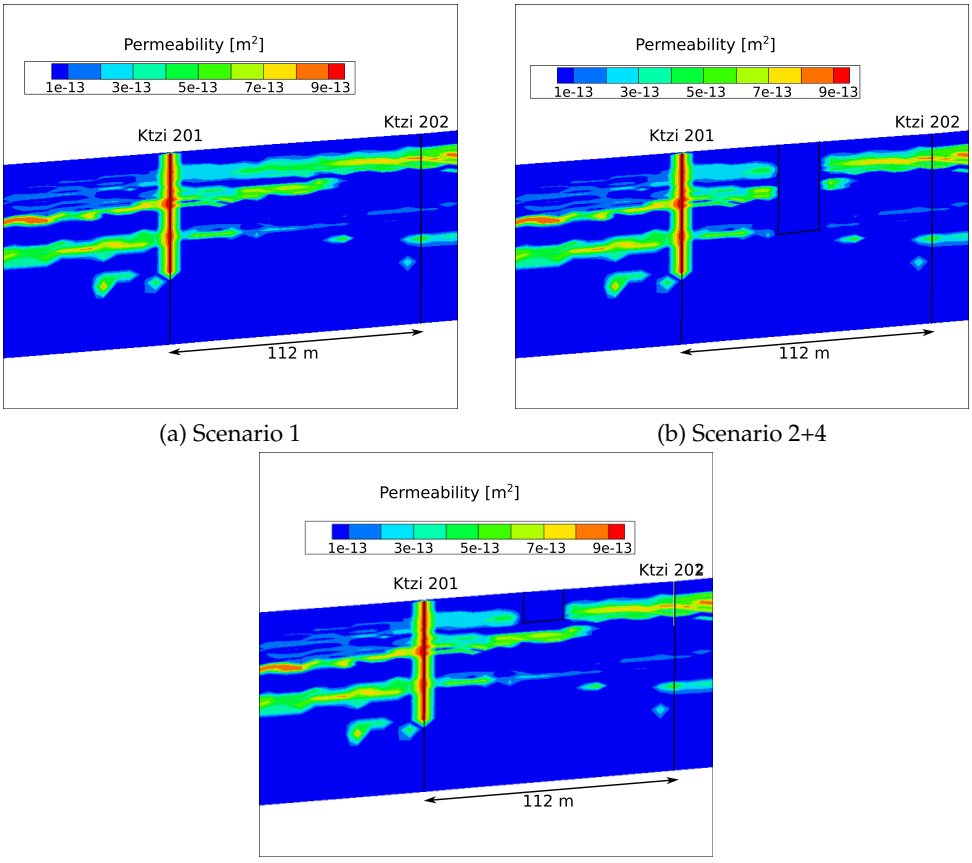

(a) Scenario 1

(b) Scenario 2+4

(c) Scenario 3

Figure 6.2: Section through Ktzi 201 and Ktzi 202: Permeability field.

In Figure 6.3, a top view on the CO_2 plume expansion at arrival is presented for each scenario. The plume has a circular shape for the reference scenario 1, where no barrier exists,

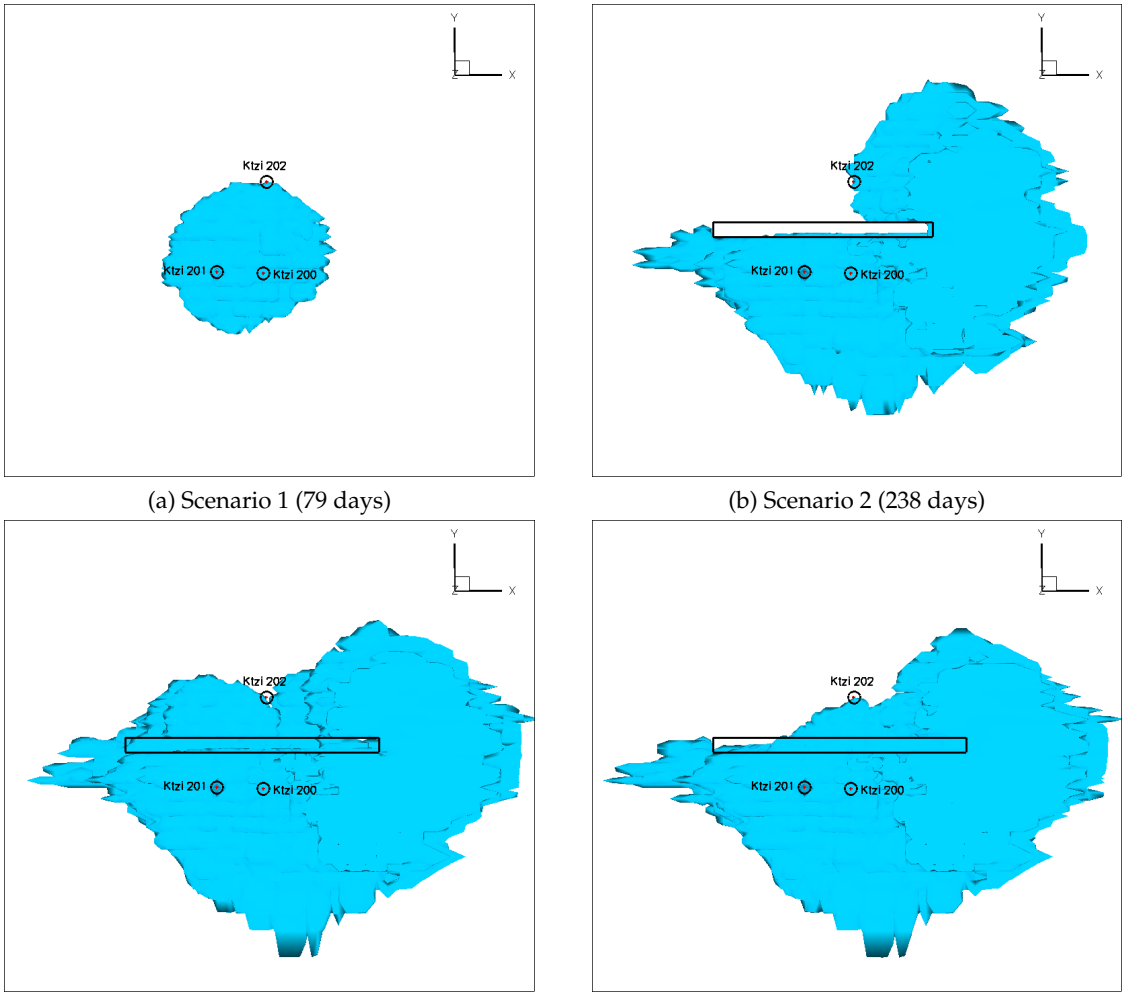

(a) Scenario 1 (79 days)

(b) Scenario 2 (238 days)

(c) Scenario 3 (268 days)

(d) Scenario 4 (258 days)

Figure 6.3: Top view on the CO_2 plume at the arrival time at Ktzi 202 for each Scenario.

and arrives at Ktzi 202 after 79 days. The variation of length, depth, and permeability all result in a scenario that almost matches the arrival time of 271 days (see Table 6.4). However, the flow paths of the CO_2 differs for each variation. The deep barrier of low permeability in Scenario 2 forces the CO_2 to move around the right side of the barrier (see Figure 6.3b). In Scenario 3 the depth of the barrier is reduced. Figure 6.4 shows the CO_2 plume at arrival for a section between Ktzi 201 and Ktzi 202 comparing Scenario 3 and the reference case. The CO_2 is the lighter one of the two fluid phases (water and CO_2), and is retained at this barrier and will start flowing beneath the barrier when a certain threshold amount of CO_2 is reached at the barrier. The increase of permeability of the barrier (Scenario 4) results in a retarded flow through the barrier.

The presented variations demonstrate that several possibilities to match the arrival time exist. Beneath the described possibilities, other variations are feasible such as a different width of the barrier. The study shows the sensitivity of the arrival time to distinct structures in the subsurface and provides information about the flow processes in the heterogeneous

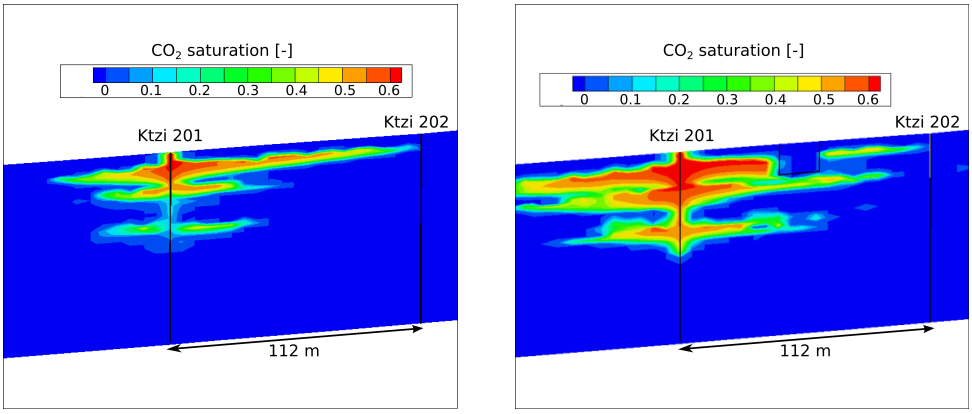

(a) Scenario 1 (79 days) (b) Scenario 3 (268 days)

Figure 6.4: Section through Ktzi 201 and Ktzi 202: saturation at arrival time at Ktzi 202 for Scenario 1 and 3.

structure. The results of the pumping tests (Wiese et al. (2010)) show that a hydraulic connection exists directly between the two wells Ktzi 201 and Ktzi 202. Thus, the "barrier" with a reduced depth presented in Scenario 3 seems to be the most realistic variation. In the one-phase pumping test such a small "barrier" does not influence the results. Whereas the "barrier" strongly influences the multi-phase system since the CO_2, which is lighter than the surrounding brine, is hindered when flowing by the "barrier".

6.1.3.2 History Matching with Anisotropic Permeability Multipliers

Another possibility is to match both the pressure curves and the arrival times by anisotropic permeability multipliers. Kempka and Kühn (2013) presented an approach to fit the pressure and the arrival time by including anisotropic multipliers for the permeability using TOUGH2 and Eclipse. In addition, a distinction for the multipliers between a near-well field and a far-field was applied. In total 6 different multipliers are used. An adequate matching for the pressure and the arrival time could be achieved. A similar procedure is applied for matching the pressure and the arrival times for the 5 x 5 km tetrahedron mesh (geological model Version 5) using DuMu^x (Model 3 in Table 6.2).

	Simulation 1		Simulation 2		Simulation 3	
Region	Near-well	Far-field	Near-well	Far-field	Near-well	Far-field
Multiplier x-direction	0.34	0.34	0.272	0.85	0.136	1.02
Multiplier y-direction	0.07	0.07	0.056	0.175	0.028	0.21
Multiplier z-direction	0.07	0.07	0.056	0.175	0.028	0.21
Arrival at Ktzi 200	25.5 days		26.92 days		27.7 days	
Arrival at Ktzi 202	502.46 days		562.24 days		765.82 days	

Table 6.5: Permeability multipliers applied in the near-well and the far-field region and corresponding arrival times.

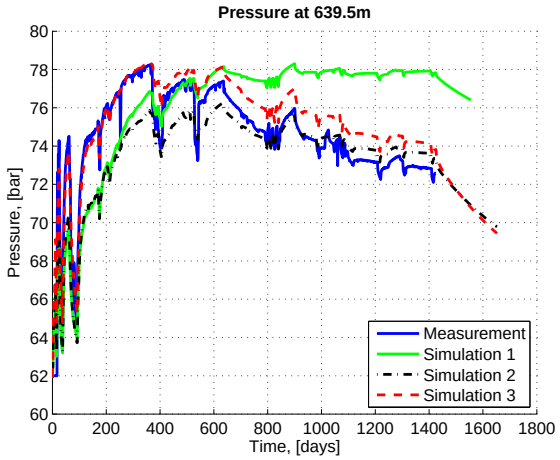

Figure 6.5: Pressure at the injection well Ktzi 201.

A high priority is given to the matching of the pressure measurements. The permeability field as given by the geological model is therefore modified with permeability modifiers, thereby introducing some additional degrees of freedom. A total of 6 multipliers are used, one for each spatial direction in the far-field (distance greater than 500 m from the injection well), and the same in the near-field around the well. This choice is arbitrary but against the background of a huge number of local degrees of freedom in the geological model, this appears as a justified method to identify one out of many possible geological scenarios to fit the pressure curves. For the first simulation the same multipliers as used for the near-well region in Kempka and Kühn (2013) are applied for the near-well and the far-field (see Table 6.5 Simulation 1). The resulting pressure curve at the injection well underestimates the pressure during the first 500 days and overestimates the pressure at longer time scales (see Figure 6.5). Thus, the near-well permeability is systematically reduced and the permeability in the far-field is increased by trial-and-error runs. The anisotropy ratio is kept constant. In Simulation 2 the near-well region is reduced by a factor of 0.8 and the far-field region is increased by a factor of 2.5 compared to Simulation 1. During the first 800 days the pressure is still underestimated but at longer time scales the pressure is close to the measurements. Thus, the permeability of the near-well region is further decreased and the permeability of the far-field increased in Simulation 3. This simulation fits the pressure for the first 400 days well, later the pressure is still overestimated. The second criteria for matching is the arrival time which is discussed for Simulation 3 only. For Simulation 3 both arrival times are overestimated by the model, 27.7 days instead of 21.7 days in the first observation well, and 765.8 days instead of 271 days in the second well. While the slight retardation in the first arrival time is most likely caused by the modification of the geological model in the near-field towards lower (apparently too low) permeabilities, the second arrival time is retarded also by the properties of the geological model and the additional anisotropy by the permeability multipliers. This can be seen in the evolution of the CO_2 plume (see Figure 6.6), where a distinct kink can be observed near the second observation well, apparently caused by a local low permeability guiding the CO_2 around this well.

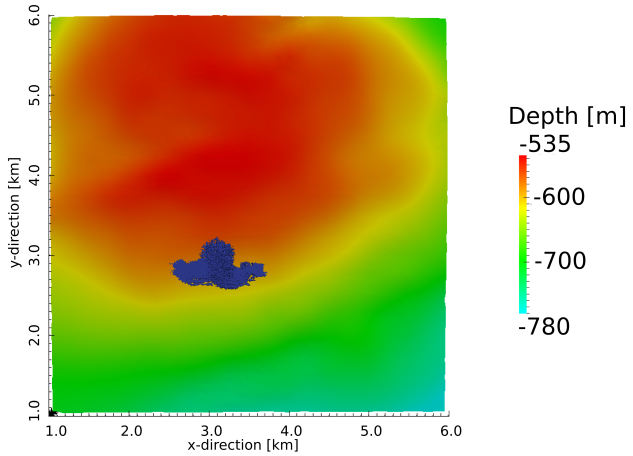

Figure 6.6: Top view on the plume expansion after 1652 days.

Discussion of the Results A more exact fit for the pressure curve would be obtained by more trial-and error runs with further adaption of the near-well and the far-field multipliers. However, this is not the scope of this work and no new insights would be obtained. The results show that a satisfactory match of the measured pressure curve is possible, while still afflicted with huge uncertainty in the details of the geological model. The evolution of the CO_2 plume (see Figure 6.6) shows a tendency towards a preferred migration into the northwestern direction from the injection well. This is in agreement with observations from the monitoring in Ketzin. Since the predicted arrival is a little too late even for the first observation well, the permeability multipliers used in the near field (<500 m from the injection) may result in permeabilities, which are too small. In other words, there are supposedly sources of error that lead to a systematic underestimation of the pressure signal at the injection well. One reason could be that a skin factor is not considered which accounts for the reduction of permeability directly around the well caused by the drilling mud. Eventually, the influence of the Dirichlet boundary (constant head at the lateral boundary) results in an underestimation of the pressure in the domain. This is stronger the closer the Dirichlet boundary is to the injection well, and the closer the pressure measurement is to the boundary (see Section 6.1.4.1). For this study, the area of 5 x 5 km is already rather big, and the measurement is directly in the injection well. Thus, the influence of the Dirichlet boundary is expected to be small, especially in the beginning of the injection. The permeability multipliers that lead to a match of the pressure curve are strikingly different for the DuMu^x simulations (see Table 6.5) compared to the simulations done by Kempka and Kühn (2013) with TOUGH2 and Eclipse. The major difference between the two approaches is the grid and the corresponding representation of the geological model. The tetrahedron mesh underestimates the pressure as it will be discussed in Section 6.1.4.3. Thus, it is recommended to apply a hexahedron mesh for further investigations.

6.1.4 Uncertainties Caused by Model Assumptions

In this section, the influence of various uncertainties caused by model assumptions is discussed. All the uncertainties are of the level of recognized ignorance. The influence of the domain size, the applied model concept, and the grid type are investigated. The choice of the distretization method also belongs to this level and needs to be investigated as well. Whether the box method or the cell-center finite volume method is chosen can influence the results. However, the benchmark study published by Class et al. (2009) showed no significant influence of the distretization method. The investigations can help to identify the right assumptions and to apply the most adequate model for the steps of history matching or risk assessment.

6.1.4.1 Influence of the Domain Size

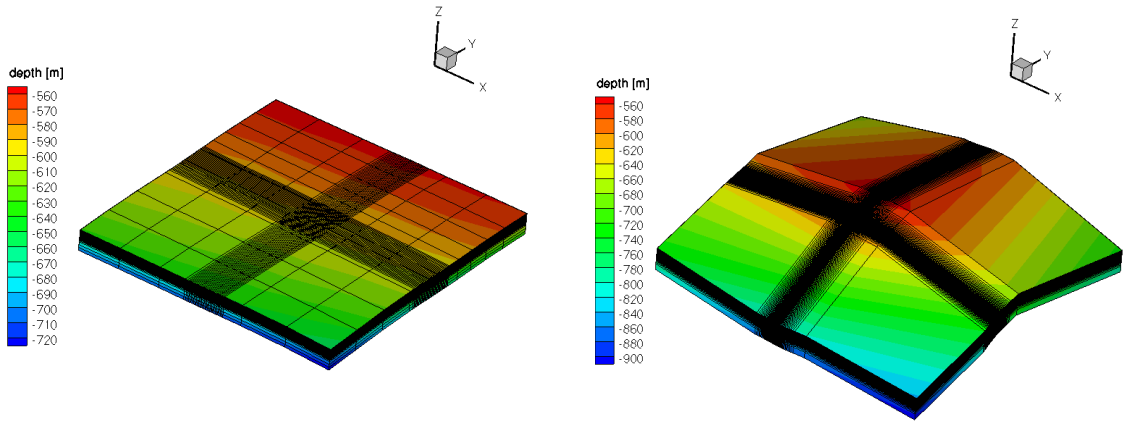

(a) 1 km x 1 km domain

(b) 5 km x 5 km domain (5 times vertically exaggerated)

Figure 6.7: Model domain of 1 x 1 km and 5 x 5 km and the applied grid.

The domain size has to be carefully chosen depending on the result of interest. The distance of the boundary conditions can have a large influence on the results. The pressure study that will be presented in Section 6.2 shows a strong influence of the boundary conditions on the pressure response in the domain. Thus, for investigation of the pressure propagation and brine displacement which is induced by the pressure increase, large domains are required to reduce the influence of the boundary conditions. If the CO_2 plume distribution is the focus of investigation, the boundary conditions have a lower influence.

In the following the pressure evolution for two different domain sizes for the Ketzin reservoir, a 1 x 1 km and a 5 x 5 km domain is compared. For the investigation, the 2p2cni model implemented in MUFTE-UG is applied (Model 2 in Table 6.2). The same interpolation technique for permeability and porosity field (Version 3) as for the 5 x 5 km grid (kriging) is used for the 1 x 1 km grid. The two model domains are shown in Figure 6.7. The boundary conditions are equal in both domains: Neumann no-flow conditions at the top and the

bottom of the domain and Dirichlet constant head conditions at the outer boundaries. In Figure 6.8 the pressure over time at the injection well and at 336 m from the injection well are presented. After 10 days of injection the pressure measured at the injection well starts to differ significantly between the two domain sizes. The fixed pressure value at the lateral boundary reduces the pressure at the injection point in the smaller 1 x 1 km domain. Closer to the boundary (335 m from injection), the influence is observed a bit earlier and is much more distinctive (see Figure 6.8b). In both domains, the CO_2 arrives at Ktzi 200 after about 21 days. Thus, the arrival time and the plume propagation is not affected by the boundaries.

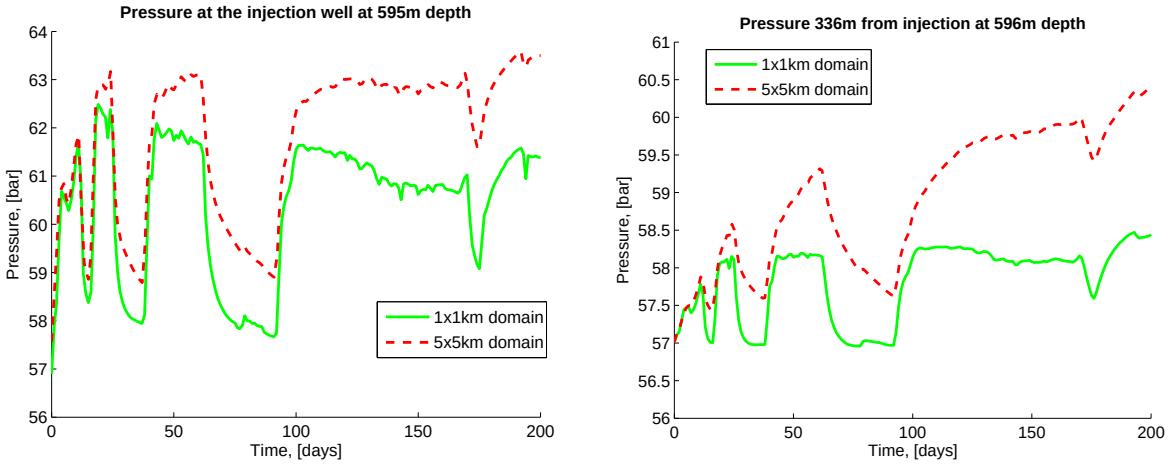

(a) Pressure at the injection well at 595 m depth

(b) Pressure 336 m from injection at 596 m depth

Figure 6.8: Pressure evolution over time for a 1 x 1 km and a 5 x 5 km domain

As mentioned before, the choice of the domain size is classified to the level of recognized ignorance. If the boundaries are close to the measurement location the results can be falsified and thus it is important to know and classify the effects of the boundary.

6.1.4.2 Influence of the Model Concept: 2p Compared to 2p2cni Model

The choice of the conceptual model is an important step before starting to simulate an application. The modeler has to weigh up which processes are relevant in the current application. The 2p model (see Section 2.4.1) neglects the compositional and nonisothermal effects compared to the 2p2cni model (see Section 2.4.2). In general, on one hand a 2p model will overestimate the plume expansion and the pressure evolution, but on the other hand the computational time will decrease. The differences in the plume expansion are analyzed for the sand channel structure of the Ketzin storage site using the simulator MUFTE-UG. In Figure 6.9, the CO_2 plume expansion in the horizontal direction after 50 days of injection simulated with a 2p model is compared to the simulation with a 2p2cni model (see Table 6.2 Model 1 and 2). The plume of the 2p model is much wider spread than in the 2p2cni model. The CO_2 is retained at a barrier between the wells Ktzi 201 and Ktzi 202 because the current investigation was conducted in the course of a barrier study for history matching, which was discussed in detail in 6.1.3.1. Figure 6.10 shows a section through the injection

well Ktzi 201 along the x-axis. In the 2p model the CO_2 plume extent is larger in the channels than in the 2p2cni model.

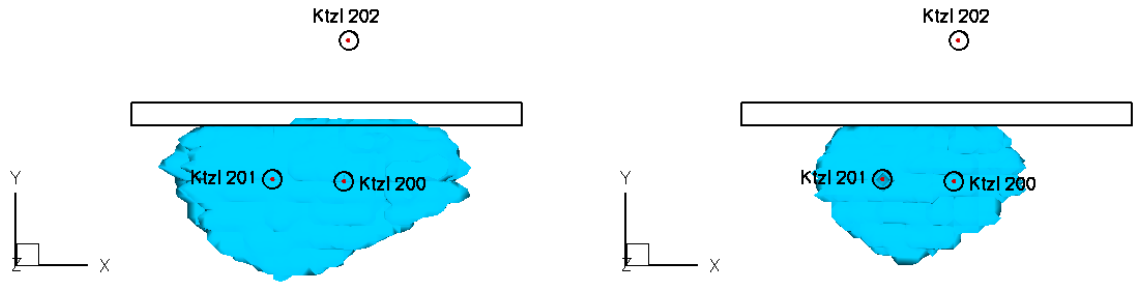

(a) 2p model (b) 2p2cni model

Figure 6.9: Top view of the CO_2 plume expansion in horizontal direction after 50 days of injection.

Usually, the assumption of neglecting the dissolution processes during the injection phase is reasonable since advective and buoyant forces strongly dominate the flow system (see discussion in Darcis et al. (2011)). However, in this case neglecting dissolution leads to a high overestimation of the CO_2 plume expansion because already 34% of the CO_2 is dissolved in the brine phase in the heterogeneous Ketzin reservoir after 50 days of injection.

Two reasons can be discussed: First the cyclic injection in the Ketzin case results in longer periods without injection. During this time the CO_2 is no longer pushed forward and it has more time to dissolve than during continuous injection. However, this is expected to have a minor influence. Second, the contact surface between CO_2 and water is significantly larger in the heterogeneous channel structure compared to the compact plume in a homogeneous reservoir. Therefore, a higher amount of CO_2 can dissolve in the heterogeneous channel system. Certainly, the discretization has to be taken into account if the higher contact surface is discussed. In our models, every grid node is surrounded by a control volume. If the CO_2 reaches a new node, it has to dissolve in the complete volume first before CO_2 as gas phase appears. If the contact surface between water and CO_2 is larger, this effect will be enhanced. Therefore, further investigation of the influence of the discretization length has to be performed. Adaptive mesh refinement would be excellent for testing the influence without high computational costs.

The choice of the model concept is on the level of recognized ignorance. For the considered storage site, the uncertainties that would be introduced by the use of a 2p model are very high. Thus, recognized ignorance would be probably more significant than scenario or statistical uncertainty in this considered case. However, the omission of compositional effects is a conservative assumption for risk estimation, because the pressure and the plume

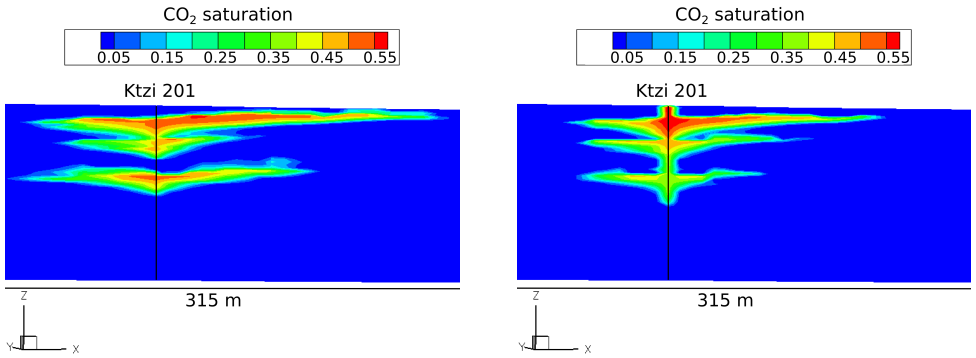

(a) 2p model (b) 2p2cni model

Figure 6.10: Section through Ktzi 201: CO_2 plume expansion in the channel system after 50 days of injection.

expansion will be overestimated.

6.1.4.3 Influence of the Grid Type and Resolution

Besides the domain size the grid resolution is an important factor for the accuracy of a simulation result. During the process of history matching two different meshes are used for the simulation with DuMu^x. First a tetrahedron mesh was constructed for the investigation which is shown in Section 6.1.3.2. The comparison of the results derived by the tetrahedron mesh with results presented by Kempka and Kühn (2013) show that the tetrahedron mesh seems to result in a larger underestimation of the pressure. Therefore, a hexahedron mesh is constructed and the influence of the two meshes is discussed in the following.

A tetrahedron mesh that has a circular refinement around the three injection wells and a coarse resolution in the far-field, and a hexahedron mesh which is also refined around the injection well are compared. The two different meshes are shown in Figure 6.11. For the hexahedron mesh the refinement has to be extended into the outer region of the domain to avoid hanging nodes (see cross shape grid in Figure 6.11b). The unstructured tetrahedron mesh can be refined only in the near-well region. For the tetrahedron mesh the box method is applied, (Model 3 in Table 6.2) whereas the cell centered finite volume method is used for the hexahedron mesh because of better convergence (Model 4 in Table 6.2). Version 5 of the geological model is the basis for the current simulation. In the following the results for pressure at the injection well and the arrival times are compared for the two meshes.

	Arrival at Ktzi 200 [days]	Arrival at Ktzi 202 [days]
Measurement	21.7	271
Tetrahedron mesh	24.8	129.3
Hexahedron mesh	17.7	116.7

Table 6.6: Arrival times at Ktzi 200 and Ktzi 202 for the tetrahedron and hexahedron mesh.

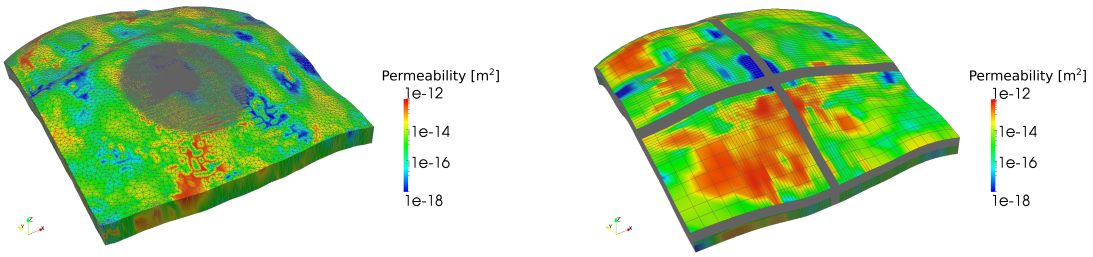

(a) (b)

Figure 6.11: Tetrahedron and hexahedron mesh with the interpolated permeability field (5 times vertically exaggerated).

Figure 6.12 shows the pressure at the injection well Ktzi 201 at 639.5 m depth for a simulation with the tetrahedron and the hexahedron mesh compared to the measurement data. The pressure is underestimated for both simulations. However, the pressure in the simulation with the tetrahedron mesh is even lower than the pressure in the hexahedron simulation. The comparison of the arrival times (Table 6.6) shows that the CO_2 arrives earlier at both observation wells in the simulation with the hexahedron mesh than with the tetrahedron mesh. A possible explanation is the grid resolution of the two meshes. The grid resolution of the hexahedron mesh is 5 m in the horizontal direction in the near well region. The vertical discretization is 0.5 m in the upper part of the reservoir, increasing to 2 m in the middle and up to 5 m in the lower part. Although the grid resolution of the tetrahedron mesh is less than two meters in the near-well region, the grid resolution in the vertical direction is larger than in the hexahedron mesh. A refinement in the vertical direction is directly connected to the same refinement in the horizontal direction because strongly spoiled tetrahedrons would result in very bad grid quality. Thus, the vertical grid resolution of the tetrahedron mesh (max. 2 m) cannot resolve the fine channel structure of the reservoir. Compared to the hexahedron mesh, the channels are slightly enlarged in the vertical direction (see Figure 6.13a,b). More high permeable pore space is thus available for the CO_2 to spread into, and the pressure build up is lower for storing the same amount of CO_2. In addition, the tetrahedron mesh does not resolve the channels in the vertical direction in the far-field, thus, the influence of the channel structure on the displacement of the water can not be represented. The later arrival times in the simulation with the tetrahedron mesh are consistent with the lower pressure because more high permeable pore space exists, where the CO_2 can spread until it reaches the observation wells. The CO_2 plume expansion around the injection well for both meshes is shown in Figure 6.13 c,d after 22 days. The CO_2 is wider spread in the hexahedron mesh.

The type of the grid and its resolution also belong to the category of recognized ignorance. In the present case, it is very important to adequately resolve the channel structure. The hexahedron mesh thus reduces recognized ignorance in the current investigation because the channel structure of the geological model is resolved more exact than in the tetrahedron mesh.

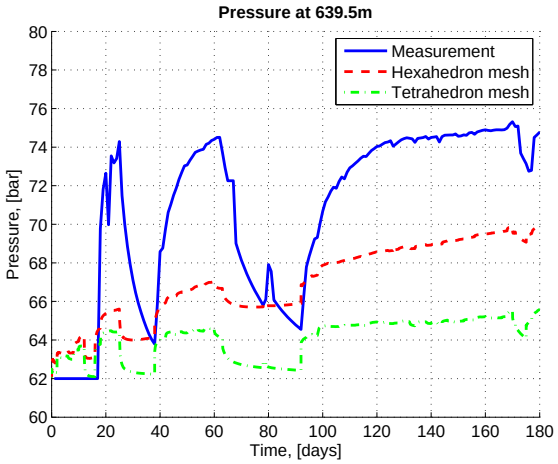

Figure 6.12: Comparison of the pressure at the injection well Ktzi 201 at 639.5 m depth for the tetrahedron and hexahedron mesh.

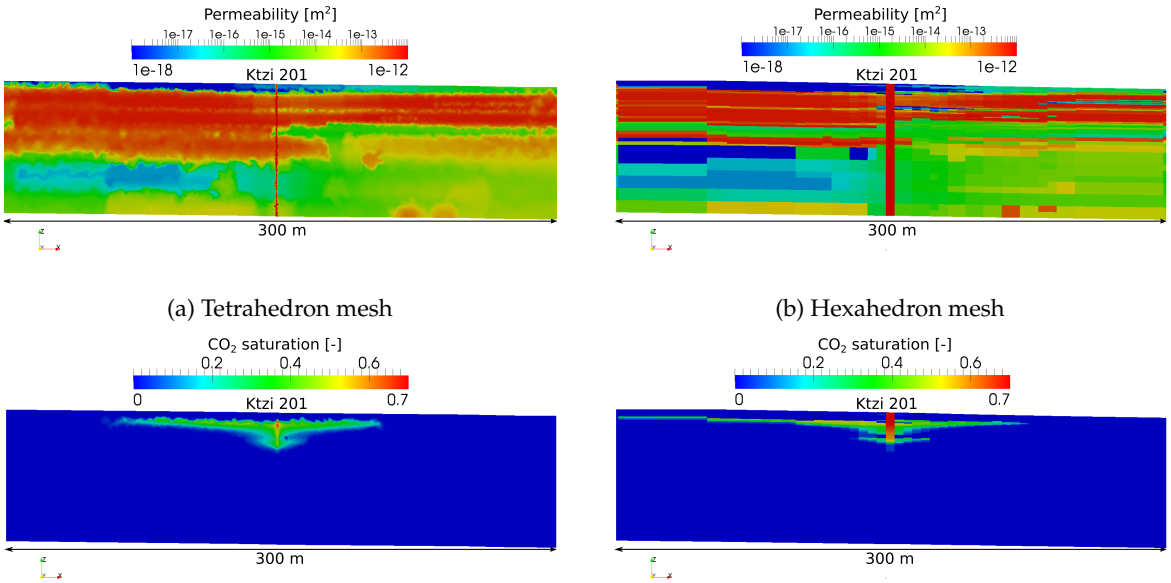

(a) Tetrahedron mesh

(b) Hexahedron mesh

(c) Tetrahedron mesh

(d) Hexahedron mesh

Figure 6.13: Permeability field of the tetrahedron (a) and hexahedron (b) mesh and CO_2 plume after 42 days of injection for the tetrahedron (c) and hexahedron (d).

6.1.5 Sensitivity of Parameters and Degrees of Freedom

When applying history matching methods the question of which parameters should be estimated arise, regardless if trial and error methods or automatic calibrations methods are chosen. For the current site, the pressure at the injection well and the arrival times at the two observation wells are the measurements of interest. The previously discussed investigations help to give first statements on the sensitivities of various parameters having more or less influence on these measurements:

- The permeability directly appears in the geological model. Former investigations (see Kempka and Kühn (2013), Section 6.1.3.2) showed that varying permeability strongly influences the system behavior; the pressure is especially sensitive to the variation of the permeability. The arrival times are also directly influenced because, e.g. lower permeability retards the CO_2 flow.
- Porosity is also a direct parameter of the geological model and it seems obvious that the variation of the available pore space influences the arrival times. The pressure is indirectly influenced by the compressibility of CO_2 in the pore space.
- The measurements for the relative permeability relationship allow for a large range of interpretations (see Section 6.1.2.2). Since the relative permeability is directly multiplied by the permeability, which is a sensitive parameter one could infer that relative permeability is also sensitive to the pressure curve and the arrival times.
- The capillary pressure measurements are also uncertain and are not scaled to the permeability and porosity field. However, the implementation of the Leverett-J function to scale the capillary pressure only slightly influenced the pressure at the injection (not shown in this work), thus the capillary pressure is assumed to have a smaller influence on the measurements.
- The skin factor at the injection well simulates the drilling mud around the borehole which effectively decreases the permeability. The pressure measured directly at the injection well could be influence by this effect. For the arrival times the influence is assumed to be low.
- The variation of anisotropy presented in Kempka and Kühn (2013) and Section 6.1.3.2 showed that the plume propagation is highly influence by the anisotropy in the x- and y-directions, thus the arrival time is sensitive to the anisotropy ratio.

How many of these parameters should be chosen for calibration of the model? On one hand, the more degrees of freedom are chosen the better will be the calibration of the model by adapting the parameters. On the other hand, increasing the number of parameters results in increased parameter correlation and the uniqueness of the calibration will be questionable. Finsterle (1999a) (p.38) stated that an overparameterisation results in higher parameter uncertainty and the effectiveness of the calibrated model is reduced.

6.1.6 History Matching Based on Inverse Modeling

Based on the discussion of the known data, the results of previous investigations, and the sensitivity of the parameters, the procedure and model assumptions for history matching are chosen. For all simulations a 2p2c model neglecting nonisothermal effects (implemented in DuMu^x), which are assumed to be low, for a 5 km x 5 km domain discretized by the hexahedron mesh is applied for numerical simulations. The hexahedron mesh is chosen because it resolves the channel structure more exactly than the tetrahedron mesh. Since cell-center finite volume method results in better convergence than the box method, it is applied for

the simulations (Model 4 in Table 6.2). The computational costs for simulating the complex, heterogeneous model are very high, thus a systematic procedure with adequate simulation time is required. Therefore, the applied approach for history matching consists of three steps:

- In the first step, an inverse modeling approach that is implemented in iTOUGH2 (Finsterle (1999b)) instead of trial and error runs is applied to match the pressure at the injection well for the first 50 days, since for this data the highest sensitivity is expected. In the same step the arrival time at Ktzi 200 is matched as well. The different steps of the inverse modeling method as a tool for automatic model calibration are described in detail in Finsterle (1999b) and are briefly presented in Appendix A. Three parameters are chosen for matching the pressure and the arrival time. Only three degrees of freedoms are allowed since the aim is to match pressure and arrival times with less degrees of freedom than in the previous approach where 6 degrees of freedom were necessary (see Section 6.1.3.2) trying to reduce the arbitrariness of the results.
- After matching of the pressure curve for first 50 days and the arrival time at Ktzi 200, the calibrated model is extrapolated to the whole simulation time of 1650 days, trying to match the pressure at the injection well over the whole period and the pressure at Ktzi 202 for the measured time frame.
- In a last step, the second arrival time at Ktzi 202 is matched by including a geological feature as the low permeable "barrier" based on the investigations presented in Section 6.1.3.1.

History Matching Procedure For the first step of matching the pressure at the injection well for the first 50 days and the first arrival time the following measurements are the basis: Since no measurement is available for the pressure for the first 17 days, 11 times steps between 17 and 50 days are used to fit the pressure. For the arrival time, which is observed after 21.7 days a step function is applied for the matching which is 0 at the beginning and jumps to 1 when the CO_2 has arrived.

Different combinations of estimated parameters and different weights to the measurements are chosen. For Case A, a multiplier for the overall heterogeneous porosity field (M_{phi}), for the permeability far-field (M_K), and the permeability directly at the well (M_{Kwell}) are chosen for modification. The well region, where M_{Kwell} is applied, contains only the cells 5 m around the injection well and should represent the skin effect. The results of Case A are not credible because the porosity is decreased too much (M_{phi}=0.2519) to match the data. This reduction would lead to a maximum porosity of about 0.066. In addition, the permeability at the well is increased which was not the idea of the skin factor at the well where the permeability is normally reduced. The pressure fit for the first 50 days is seen in Figure 6.14a. The first peak is adequately fitted but the pressure does not drop back sufficiently after 38 days. The CO_2 arrives at Ktzi 200 after 9.6 days. Thus, the CO_2 reaches the well much earlier than expected. The total sensitivities for the three parameters (51.7 for M_{phi}, 0.0095 for M_K and 0.0026 for M_{Kwell}) show that the system only reacts strongly to the porosity. The very low

porosity dominates the system behavior. In addition, the standard deviation for the arrival time (0.1) is too high for a sufficient match.

Since the effect of a separate multiplier for the well region seems to be very small, it seems that the skin factor at the well is not relevant for the the pressure at the injection well. The far-field region seems to be much more sensitive. Thus, different matching parameters are chosen for the next cases. Additionally, the standard deviation for the arrival time is reduced (0.02) and the lower limit for the porosity is increased to avoid porosities that are too small. Five additional cases are set up (B-F). In Cases B-E, an overall permeability (M_K) and porosity multiplier (M_{phi}) are chosen. In addition, the parameter n of the relative permeability relationship (see Equation 6.1 and 6.2) is varied. For Case B, both parameters n_w and n_{CO2} are fitted by using one value n_{both}. Only n_{CO2} is fitted in Cases C-E. In Case D, the lower bond M_{phi} is decreased compared to Case C (0.6 instead of 0.7). The weighting for the arrival time is reduced in Case E (0.05) compared Case D to achieve a more exact pressure fit. In Case F, a different set of multipliers is chosen: the porosity field is still matched by the multiplier M_{phi} whereas the permeability field multiplier M_K depends directly on M_{phi} by the Kozeny-Carman (Scheidegger (1960)) relation with a porosity of 0.2 as a basis: $M_K = (M_{phi} \cdot 0.2)^3 \cdot (1 - 0.2)^2 / (0.2^3 \cdot (1 - M_{phi} \cdot 0.2)^2)$. The lower limit for M_{phi} is set to 0.2. Additionally, the relative permeability for CO_2 (n_{CO2}) and water (n_w) are separately varied. The standard deviation for the arrival time is set to 0.05 as in Case E.

Case	Parameter 1	Parameter 2	Parameter 3	Arrival at Ktzi 200	Arrival at Ktzi 202
A	M_K = 0.1049	M_ϕ = 0.2519	M_{Kwell} = 7.5211	9.6 days	-
B	M_K = 0.1045	M_ϕ = 0.7569	n_{both} = 1.6376	25.73 days	-
C	M_K= 0.1067	M_ϕ = 0.7048	n_{CO_2} = 1.5376	24.98 days	317.47 days
D	M_K= 0.1226	M_ϕ = 0.6	n_{CO_2} = 1.1497	21.71 days	216.60 days
E	M_K= 0.1445	M_ϕ = 0.6	n_{CO_2} = 1.845	25.8 days	292.74 days
F	M_ϕ = 0.5555 M_K = 0.1388	n_w = 9.46	n_{CO_2} = 1.3403	21.81 days	210.16 days

Table 6.7: Best fit and corresponding arrival times.

Table 6.7 shows the best fit parameters for each Case and the corresponding arrival times. In Figure 6.14a and b the pressure curves for all cases are compared to the measurements for the first 50 days. The pressure is sufficiently matched in all cases, even though the peaks are slightly underestimated. In Case B, the CO_2 arrives later than observed and the fitting of the permeability relationship with only one value for water and CO_2 in Case B is physically not evident because the two fluids have completely different properties. However, it is a first attempt to investigate the sensitivity of the measurements on the relative permeabilities. For n_{both} the total sensitivity is 113, whereas the sensitivity for M_K is 235.3 and for M_{phi} is 130.8. Thus, n_{both} is less sensitive than the two other parameters but still sensitive enough for further investigations. A fit for the first 50 days is also possible with this assumption. Case C fits the pressure very well but the arrival is too late. Whereas Case D and F fit the arrival time almost exactly. As described before, Case E is a slight modification of Case D (higher standard deviation for the arrival time) with the purpose to achieve a better pressure match. However, the pressure match is only slightly improved whereas the arrival time is

more poorly estimated. Case F produces similar results as Case D. The new estimation parameter n_w which changes the relative permeability curve of water (see Figure 6.15) has only a small influence of the system behavior during the first 50 days. This is confirmed by the total sensitivity coefficients which are 218.4 for M_{phi} (including M_K), 34.3 for n_{CO_2} and 10.8 for n_w. Thus, the variation of the porosity combined with permeability variation dominates the system behavior.

To limit the computational costs the maximum number of iterations is set to 3. The matches could be improved by applying more iteration steps. However, in the scope of this work the presented matches are sufficient. It is now more important to focus on the extrapolation to longer time scales and on the match of the second arrival time.

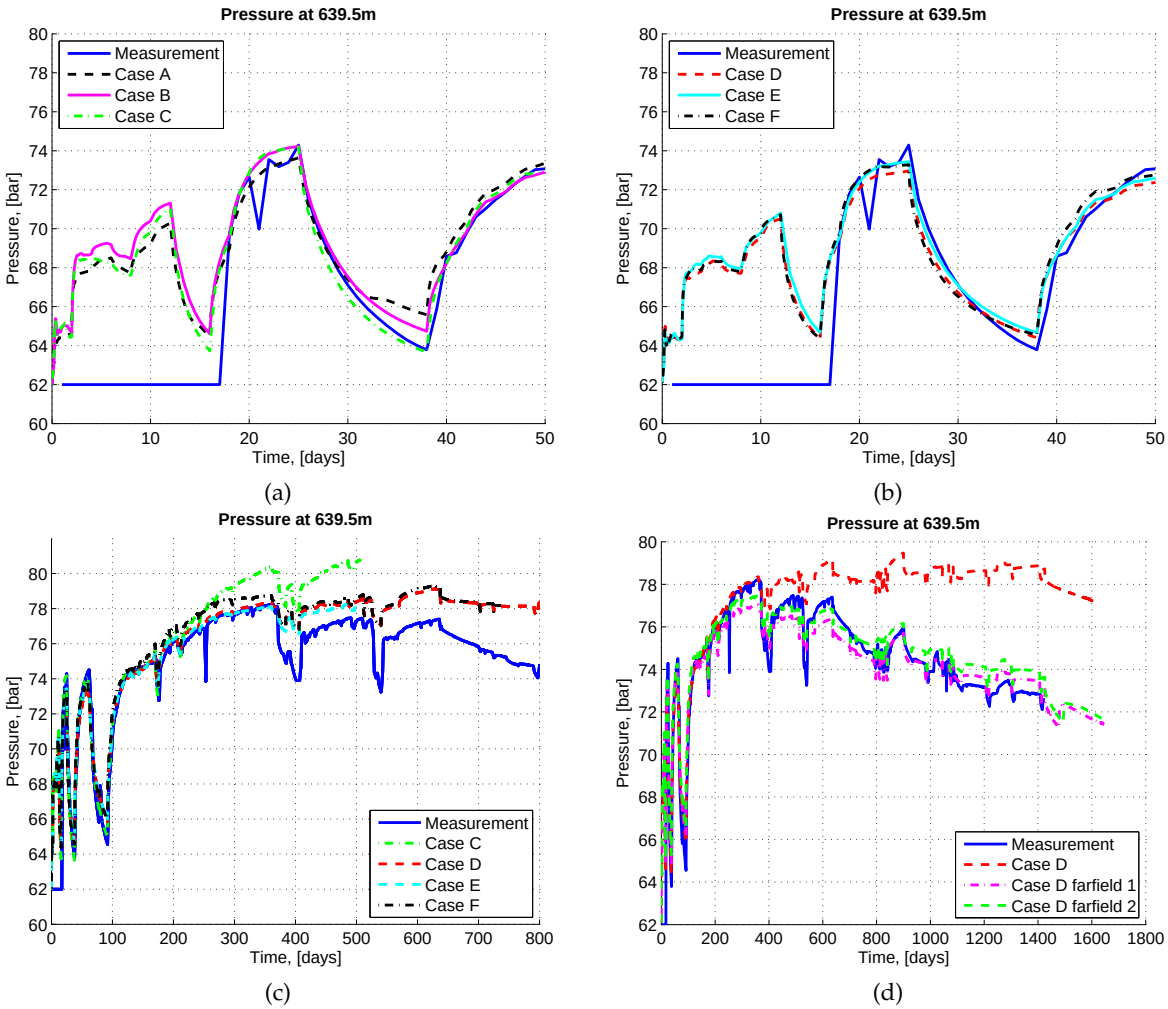

Figure 6.14: Pressure evolution over time for the different matches at Ktzi 201.

Case C-F are chosen for further extrapolation to longer time scales. Their pressure curves are presented in Figure 6.14c for a simulation time of 600 days. All Cases (C-F) do not fit the pressure over the whole simulation time. The pressure curve of Case C starts diverging from the measured data after about 180 days. Cases D and E match the pressure well for about 380 days whereas Case F diverges earlier (about 150 days), but follows the same

trend as Case D. In Case C, the permeability (M_K=0.1067) and the relative permeability (n_{CO_2}=1.5376, see Figure 6.15 for the effect on krn) are both lower in comparison with Case D or E which could be a reason for the earlier increase of the pressure. The relative permeability of water seems to increase its influence on the system behavior at about 150 days and the pressure is increased because of the smaller relative permeability of water in Case F. Overall, the pressure curve is too high in all simulations at longer time scales.

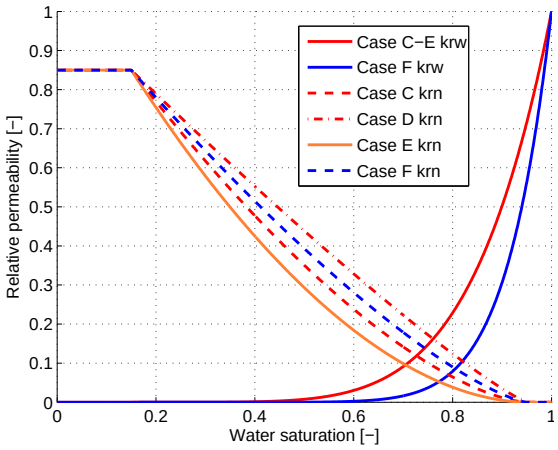

Figure 6.15: Relative permeability curves for the different cases.

One can conclude from the results that a fit of the pressure curve over the whole simulation time with global multipliers for the whole domain is not possible without introducing more degrees of freedom. The investigation by Kempka and Kühn (2013) and the study in Section 6.1.3.2 show that a better match is possible by distinguishing between a near-well and far-field multiplier for permeability. This distinction is adopted for Case D because it fits the pressure at least for 380 days and the most exact arrival time at Ktzi 200 is achieved. Within the far-field region the original permeability and porosity values of the geological model are used. Thus, the multipliers of Case D for the porosity and the permeability are only applied in the near-well region. The relative permeability is kept the same in the whole domain (n_{CO_2}=1.1497).

For Case D-farfield1, a near-well region of 1000 m x 900 m is defined around the injection well (which is located at x=3242.7 m and y=2803.7 m) between the coordinates x=2700-3700 m and y=2400-3300 m. This is the region where the CO_2 distributes approximately in the first 400 days. As presented in Figure 6.14d, the pressure curve is closer to the measurements at longer time scales and the trend of pressure decrease after 400 days can be observed for Case D-farfield1. Since the pressure is underestimated between 200 and 800 days a second trial-and-error run is performed (D-farfield2) where the near-well region is enlarged by 100 m in every direction (x=2600-3800 m and y=2300-3400 m). The pressure curve is closer to the measurements for about 800 days for Case D-farfield2 compared to Case D-farfield1. At time scales larger than 800 days, Case D-farfield1 fits the pressure curve better than Case D-farfield2. The pressure measurements at Ktzi 202 which are only available between about 600 and 1200 days after injection starts, are better matched by Case D-farfield1 (see Figure 6.16).

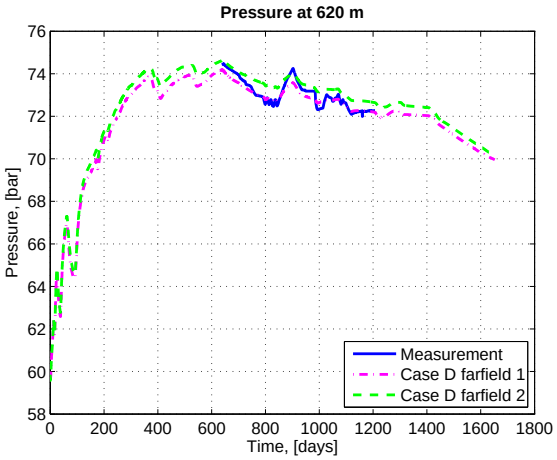

Figure 6.16: Pressure evolution over time at Ktzi 202 at 620 m depth.

The pressure is not exactly fitted in both cases, but satisfactorily enough. The maximum deviation is in the order of 1 bar. A more exact match would be possible by systematically adapting the far-field or by including multipliers in the far-field by many trial-and-error runs.

The last step in this history matching procedure is the matching of the arrival time at Ktzi 202. In Case D, the CO_2 arrives at the well after 216.6 days which is much earlier than observed. The distinction between near-well and far-field results in an even earlier arrival (208.52 days in Case D-farfield1). Thus, for the two Cases that fit the pressure well, (Case D-farfield1 and Case D-farfield2) a barrier between Ktzi 201 and Ktzi 202 is included based on the investigation in Section 6.1.3.1 (Case D-farfield1-b1 and D-farfield2-b2). The barrier is 150 m long and 20 wide and is located at x=3200-3350 m and y=2840-2860 m. The depth of the barrier is 5 m in Case D-farfield1-b1 and 6 m in Case D-farfield2-b2 from the top of the domain. The arrival times for the different cases are presented in Table 6.8. The barrier enlarges the arrival time and the observed arrival of 271 days is almost reached. Figure 6.17 shows a Section through Ktzi 201 and Ktzi 202 for Case D and D-farfield2-b2 after 255 days of the injection period. The CO_2 has already arrived at Ktzi 202 in Case D whereas it is shortly before arrival in Case D-f2-barrier. It is retained at the barrier and flows underneath the barrier as soon as enough CO_2 is accumulated. The pressure and the first arrival time are only slightly affected. Thus, the fit of the arrival time at Ktzi 202 is possible by including a distinct geological feature.

Testcase	Arrival at Ktzi 200	Arrival at Ktzi 202
D-farfield1	21.17 days	208.52 days
D-farfield1-b1	21.51 days	254.28 days
D farfield2-b2	21.45 days	264.47 days

Table 6.8: Arrival times for the far-field and barrier variations.

The CO_2 plume evolution after 1652 days is presented in Figure 6.18 for Case D and Case D-farfield1. The CO_2 mainly distributes in the northern direction. The trend in the north-

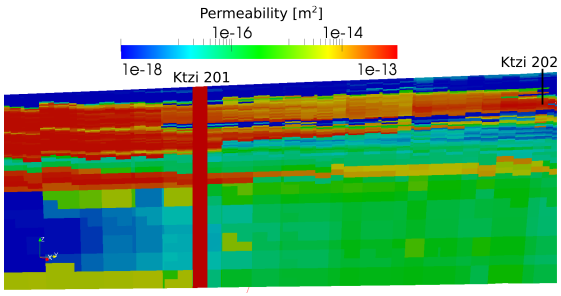

(a) Case D - permeability field

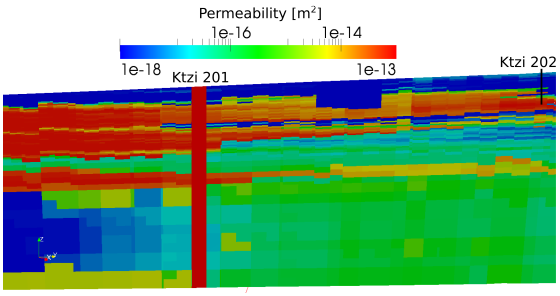

(b) Case D-farfield2-b2 - permeability field including a barrier

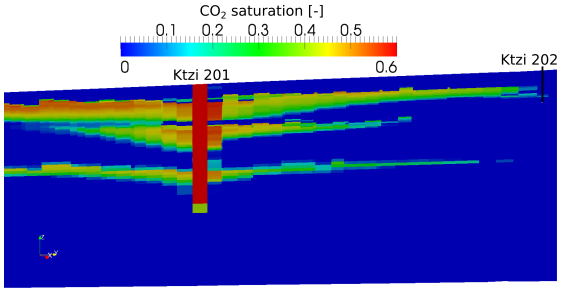

(c) Case D - CO_2 saturation

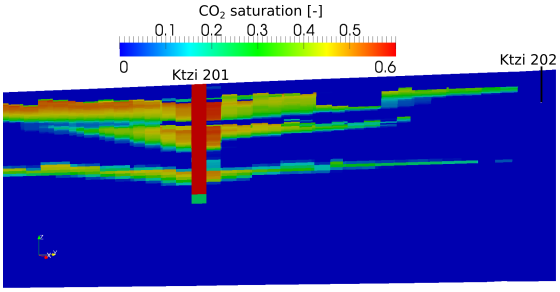

(d) Case D-farfield2-b2 CO_2 saturation

Figure 6.17: Section through Ktzi 201 and Ktzi 202: Permeability field and CO_2 plume expansion after 255 days.

western direction presented by the seismic measurements cannot be completelty reproduced by the model. The distinction between near-well and far-field in Case D-farfield1 shows a more distinctive expansion of the CO_2 plume.

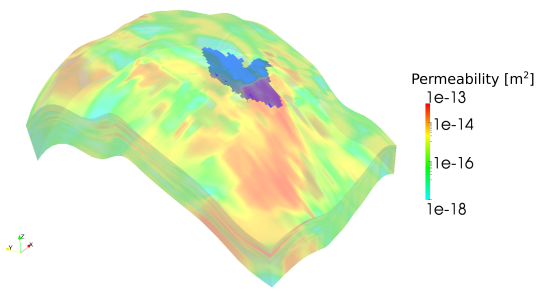

(a) Case D

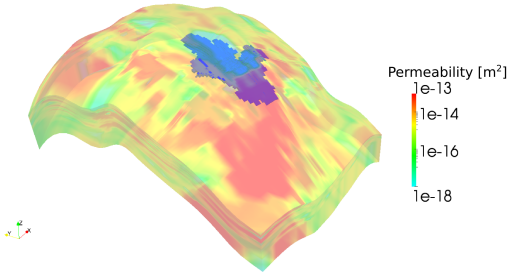

(b) Case D-farfield1

Figure 6.18: Plume evolution after 1652 days for Case D and Case D-f1 (10 times exaggerated).

Discussion of the Results To match the measurement data is challenging, thus a closer look at the inverse modeling results is required. Case D (the best fit from the inverse modeling approach) is first chosen for discussion. The pressure for the first 50 days and the arrival time is sufficiently matched. However, the extrapolation to longer time scales result in a pressure output that is to high.

Parameter	Initial Guess	Best fit	σ'_p (conditional)	σ_p (marginal)	$\Gamma = \frac{\sigma'_p}{\sigma_p}$
M_K	0.7943	0.1226	0.0348	0.0430	0.811
M_ϕ	1	0.6 (lower bond)	0.0558	0.0958	0.583
n_{CO_2}	1.25	1.1497	0.0891	0.17342	0.514

Table 6.9: Inverse modeling results: Initial guess, best estimate, conditional and marginal standard deviation, and the measure of independence (ratio conditional and marginal standard deviation) of the parameters for Case D.

Table 6.9 shows the best fit parameters, the conditional and marginal standard deviation, and a measure for the overall parameter correlation for Case D. The marginal standard deviation is in an acceptable order of magnitude. However, the ratio of conditional and marginal standard deviation, which is a measure of independence is only between 0.5 to 0.6 for the porosity and the relative permeability. This means that the uncertainty could still be reduced by lowering the correlation between the parameters by the choice of other input parameters or other measurement data. The correlation coefficient between the porosity multiplier M_ϕ and the factor for the relative permeability relationship n_{CO_2} that is shown in the upper triangle of Table 6.10 also shows this trend (-0.792). The direct correlation shown in Table 6.11 has a similar negative value and can be physically interpreted as follows: A decrease of M_ϕ can be almost completely compensated by an increase of n_{CO_2}. This correlation is based on the arrival time: A lower porosity results in earlier arrival time because the same amount of CO_2 has less pore space to distribute into before arriving at Ktzi 200. The earlier arrival can be compensated by a reduction of the relative permeability (increase of n_{CO_2}) which results in slower CO_2 plume propagation. The pressure changes would result in a positive correlation because an increase of porosity decreases the pressure since more pore space is available where the compressible gas CO_2 can distribute. The compressibility of CO_2 is two orders of magnitude higher than the compressibility of the rock (see Person et al. (2010)). Therefore, a higher porosity means that more pore space containing CO_2 is available and the overall compressibility increases and the pressure peak at the injection will be lower. The pressure reduction could be compensated by a lower relative permeability which is equivalent to a larger n_{CO_2}. For these two parameters M_ϕ and n_{CO_2}, the arrival time dominates the correlation in this particular case.

Parameter	M_K	M_ϕ	n_{CO_2}
M_K	0.18420E-02	-0.265	0.528
M_ϕ	-0.10870E-02	0.91554E-02	-0.792
n_{CO_2}	0.39286E-02	-0.13141E-01	0.30073E-01

Table 6.10: Covariance matrix for Case D: The diagonal contains the variances, the lower triangle the covariances and the upper triangle the correlation coefficient.

The permeability multiplier M_K and the relative permeability factor n_{CO_2} are positively correlated for both the indirect correlation (Table 6.10) and the direct correlation (Table 6.11). This can be directly interpreted from the definition of the total permeability which is defined as: K^n_{tot}=M_K K k_{rn}. A decrease of M_K reduces the overall permeability for the CO_2 phase

and the pressure and the arrival time are increased. The decrease of the overall permeability can be compensated by an increase of k_{rn} which is ensured by a decrease of n_{CO_2}. However, the correlation between these two parameters is lower than the correlation between porosity and relative permeability of CO_2 .

Parameter	M_K	M_ϕ	n_{CO_2}
M_K	1.000	0.296	0.540
M_ϕ	0.296	1.000	-0.796
n_{CO_2}	0.540	-0.796	1.000

Table 6.11: Matrix of direct correlations for Case D.

The direct correlation between the porosity (M_ϕ) and permeability (M_K) is slightly positive, whereas the correlation coefficient is negative. The direct correlation is easier to interpret physically than the correlation coefficient because indirect effects of other parameters influence the correlation coefficient (see Finsterle (1999a)). The slightly positive correlation is again based on the dominating arrival time. A decrease of permeability would result in a later arrival which can be compensated with a lower porosity. Considering the pressure data the correlation would be negative. A decrease of the permeability results in an increase of the required injection pressure. As explained before, this increase can be slightly compensated by an increase of the porosity because more pore space is available where the compressible gas CO_2 can distribute. Overall, the correlation between M_ϕ and M_K is the lowest, which is desirable.

The total sensitivities for the three parameters are 11.1 for M_K, 35.0 for M_ϕ and 41.2 for n_{CO2}. Here, the relative permeability is the most sensitive parameter for the total matching in this particular case. It is the most sensitive parameter for the pressure whereas the porosity is the most sensitive parameter for the arrival time. However, the sensitivity strongly depends on the initial weighting of the measurements. In other cases, porosity is more sensitive than relative permeability. Overall, one can summarize that the sensitivity of relative permeability is in the same order of magnitude as the sensitivity of permeability and porosity.

In Case F, the correlation between porosity and permeability is fixed using the Kozeny-Carman relationship. Thus, the positive correlation of the two parameters is physically motivated and seems to be required for an exact arrival time. The correlations of Case F are briefly discussed as well. The adoption of the relative permeability of water as a degree of freedom does not bring new changes in the system behavior, although the relative permeability is significantly reduced (see Figure 6.15). Tables 6.12, 6.13, and 6.14 show the inverse modeling results, the covariance matrix, and the direct correlation matrix for Case F, respectively.

The measure of independence Γ for all three parameters is smaller than for the parameters used in Case D, thus the chosen estimation parameters strongly depend on each other. The direct correlation between all parameters is high (see Table 6.13). Since permeability and porosity are varied in combination by changing M_ϕ, the correlation between the other parameters and permeability and porosity is now concentrated in M_ϕ. The indirect influence on the correlation coefficient reduces the correlation between M_ϕ and n_{CO_2}. The relative

permeabilities are directly correlated: an increase of relative permeability of CO_2 can be compensated by an decrease of the relative permeability of water (for the curves see Figure 6.15). The variance for n_w is high, which corresponds to a high estimation uncertainty. Pressure and arrival time do not react sensitively with a change of the relative permeability of water. The total sensitivity of n_w is only 10.8 whereas the sensitivity of n_{CO_2} is 34.4 and of M_ϕ 218.4. The combined variation of porosity and permeability dominates the system behavior.

Parameter	Initial Guess	Best fit	σ'_p (conditional)	σ_p (marginal)	$\Gamma = \frac{\sigma'_p}{\sigma_p}$
M_ϕ	0.86	0.5555	0.72494E-02	0.0132061	0.549
n_{CO_2}	1.35	1.3403	0.71574E-01	0.17246	0.415
n_w		8.0	0.13494E+01	3.4884	0.387

Table 6.12: Inverse modeling results: Initial guess, best estimate, conditional and marginal standard deviation, and the measure of independence (ratio conditional and marginal standard deviation) of the parameters for Case F.

Parameter	M_ϕ	n_{CO_2}	n_w
M_ϕ	0.17441E-03	0.206	0.410
n_{CO_2}	0.46820E-03	0.29742E-01	-0.724
n_w	0.18883E-01	-0.43566E+00	0.12169E+02

Table 6.13: Covariance matrix for Case F: The diagonal contains the variances, the lower triangle the covariances and the upper triangle the correlation coefficient.

Parameter	M_ϕ	n_{CO_2}	n_w
M_ϕ	1.000	0.799	0.828
n_{CO_2}	0.799	1.000	-0.906
n_w	0.828	-0.906	1.000

Table 6.14: Matrix of direct correlations for Case F.

6.1.7 Conclusions

The main observations and conclusions can be summarized as follows:

- Overall, a fit for the pressure for the first 50 days and the first arrival time can be achieved by inverse modeling. The correlations between the parameters can be analyzed and they show that there is still an uncertainty in the estimation. For the initial injection period, different sets of three parameters each lead to equally good fits.
- An extrapolation to longer time scales is possible only up to a certain time. The pressure measurement shows a decrease after about 380 days which could not be represented by the simulations. Therefore the pressure for the whole simulation time of

1650 days can not be fitted satisfactorily by applying the inverse modeling approach for the first 50 days only.

- A most evident choice would be to match the pressure curve for the whole simulation time by the inverse approach, which is not feasible in the scope of this work due to very high computational costs. However, the maximal residuals (in this study in the order of 1 bar) are expected to be higher than desired.
- The deviation of the pressure curve at longer time scales suggests that the permeability and porosity are higher in the far-field than in the near-well region. Thus, a fit of the pressure for the whole simulation time is possible by introducing a new degree of freedom (see discussion in Section 6.1.5): a distinction between a near-well field and far-field with no or a lower reduction of the permeability and porosity. A satisfactory fit with a maximum deviation of about 1 bar from the measurements is presented.
- Within the given uncertainty of the geological model the matching of the second arrival time is easily possible. A fit can be performed by including a small geological feature, in this case a low permeable barrier, without influencing the pressure.
- The plume shape shows a predominant expansion in the northern direction. The expansion in the northwestern direction as shown by seismic measurements could not be represented by the model. It thus seems obvious that the geological model needs to be adjusted or, alternatively, the anisotropy in x and y direction has to be applied for fitting the plume behavior.
- The correlation between the parameters is high between some parameters. With regard to the measurements, the pressure curve and the arrival time, the correlations between the parameters are different in some cases. The total correlation depends on the data that has the highest influence on the system, which can be influenced by the weighting of the measurement.
- The investigation shows that the calibrated model is able to predict the evolution of the pressure for a limited extrapolation time, whereas the prediction of the evolution of the CO_2 in space seems to not be reliable.

Further Remarks The investigations help to improve the understanding -and to some degree predict- how the system reacts. For example, permeability and porosity are highly sensitive values for the pressure and the arrival time. Relative permeability of CO_2 is also a very sensitive parameter (in one of the inverse cases it is even the most sensitive one). In the previous approach (see Section 6.1.3.2, Kempka and Kühn (2013)) the relative permeability was assumed to be known. Here, the question arises how reliable is the measurement of relative permeability? Since a large range for the relationship is proposed depending on the measurement data, it seems that a lot of uncertainties exist. The displacement of water is not a sensitive process in the initial injection period, but seems to increase its influence at later time scales. In the framework of uncertainty classification, the uncertainties considered in the history matching approach such as the permeability or porosity field, and the

relative permeabilities, could be ranked to statistical uncertainty because the parameters can be described by probability density functions.

For more reasonable predictions the geological model should be further updated and the uncertainties reduced. Here, the information about the system behavior gained by the simulations could be incorporated. Data from measurements in the far-field would be required to gain new significant information. For the pilot site Ketzin a lot of measurements are available, which will probably not be the case for an industrial operated storage project. However, the changing system behavior at longer time scales can not exclusive clarified with the available information.

6.2 Study on Pressure Propagation for a Realistic Storage Formation [1]

The study has been initiated by Germany's Federal Ministry of Economics and Technology and the Federal Ministry of Education and Research in 2009. The aim of this simulation based study was to investigate the pressure impact of CO_2 injection into a possible realistic storage site in the North German Basin on a neighboring structure, which may be also suitable for CO_2 storage. It is important to gain information how close two possible storage site can be operated without influencing each other. The focus is on the influence of model boundary conditions and petrophysical parameters. In the following section the results, which are discussed in detail in Schäfer et al. (2011), are briefly summarized. Additionally, the various uncertainties which are investigated in the study, are integrated into the uncertainty framework.

6.2.1 Model Set-up

The data of a saline aquifer from the North German Basin is used to simulate the injection of 1 Mt CO_2 per year over a period of 10 years into an anticlinal dome structure and the post-injection time of 30 years. The main aim is the prediction of the pressure in a structure at a distance of 31 km. Figure 6.19a shows the model domain with the injection structure A and the structure for pressure observation B. The selected model domain is about 40 x 60 km wide and about 540 m thick; the reservoir layer has a thickness of 20 m. The injection of CO_2 takes place in a depth of 1500 m into the sandstone layer shown in Figure 6.19b. An overhead claystone layer as caprock and a second claystone layer as bedrock are considered in the model domain. For simulation of the CO_2 injection and post-injection period a 2p2cni model (see Section 2.4.2) implemented in the simulator MUFTE-UG (Bielinski (2006)) is applied.

[1] This study is published in Schäfer, F., Walter, L., Class, H., and Müller, C. The regional pressure impact of CO_2 storage: a showcase study from the North German Basin. Environmental Earth Sciences, 65 (7):2037– 2049, 2011.

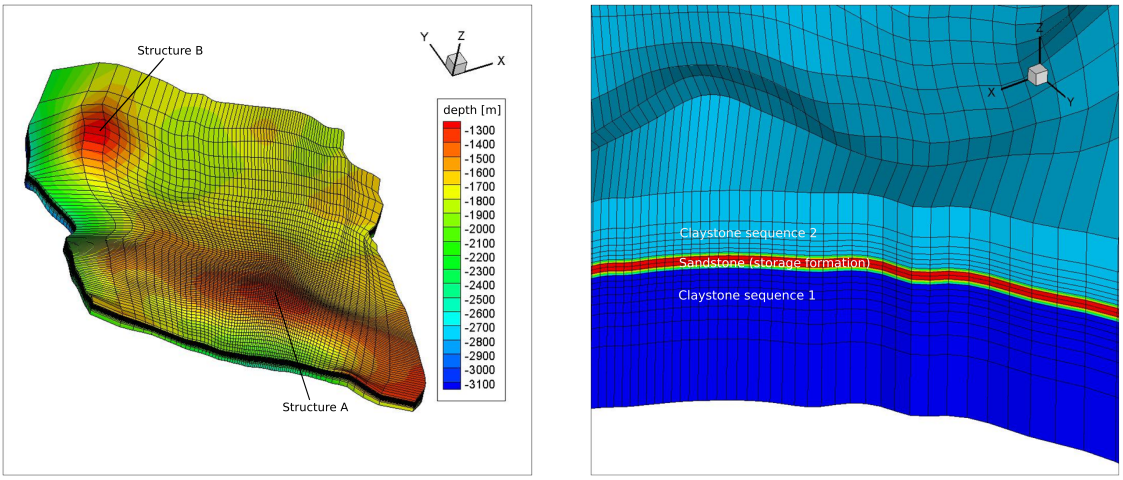

(a) Model domain (4 times vertically exaggerated)

(b) Geological layers (16 times vertically exaggerated)

Figure 6.19: Model domain with the injection structure A and the observation structure B and geological layering.

Six different scenarios are set up varying in boundary conditions, injection temperature, and reservoir permeability. The base case (Scenario 1) has a sealing fault at the western boundary. The lateral boundary condition at the western boundary is therefore a Neumann no flow condition and the lateral boundary in the east is an open constant head boundary. Scenario 2 represents a fully closed domain, where all lateral boundaries are no-flow conditions, which represents a compartmentalized portion of the storage formation. The opposite is addressed in Scenario 3, where all boundaries are hydraulically open. In Scenario 4 rock compressibility (see Equation 2.20) is neglected, resulting in a constant porosity over time. The injection temperature is increased to 63°C instead of 35°C in Scenario 5. The same (no-flow) boundary conditions as in Scenario 2 are applied in Scenario 6, and the permeability is increased to 550 mD instead of 110 mD. For more details about the model set-up, the parameters used, and the scenarios one is referred to Schäfer et al. (2011).

6.2.2 Classification Attempt for Associated Uncertainties

The results are discussed in detail in Schäfer et al. (2010) and Schäfer et al. (2011) and are briefly summarized in the following. Figure 6.20 shows the pressure history curve over the simulation time of 40 years at 5 and 31 km distance from the injection site. The boundary conditions strongly influence the pressure response, especially in the structure 31 km from the injection site (see Scenario 1-3). The lowest pressure is observed for Scenario 3 (open boundaries) at both locations. The brine can be displaced out of the domain through the open boundaries. The closed boundaries (Scenario 2) strongly increase the pressure response in Structure B, whereas almost no influence is observed in 5 km distance from injection. The western boundary is closer to the injection site than the eastern boundary, thus the difference in the pressure peak at 5 km distance between Scenario 1 (closed western boundary) and Scenario 3 (open boundaries) is larger than between Scenario 1 and 2

(closed boundaries). The eastern boundary is further away and has less influence on the pressure at 5 km distance. At Structure B, the maximum pressure peak is observed earlier for Scenario 3 with open boundaries compared to Scenario 1, whereas the maximum pressure is not reached in the given simulation time for Scenario 2. Neglecting compressibility (Scenario 4) greatly increases the pressure at both locations. Rock compressibility moderates the pressure peak. Thus, the negligence of rock compressibility results in higher pressure peaks and faster pressure propagation. The influence of rock compressibility is very strong in the presented example, because a large amount of CO_2 is injected into a thin injection formation, which results in a high pressure peak at injection. The overall pressure is strongly increased over a large area where the porosity changes (see Figure 1.2 in Chapter 1). The injection temperature has almost no influence on the pressure response (Scenario 5). The increase of permeability in Scenario 6 compared to Scenario 2 decreases the pressure peak at 5 km distance from injection (see Figure 6.20a). At 31 km from injection the maximum pressure peak in Scenario 6 occurs earlier than in Scenario 2, where the maximum pressure is not reached during the simulation time.

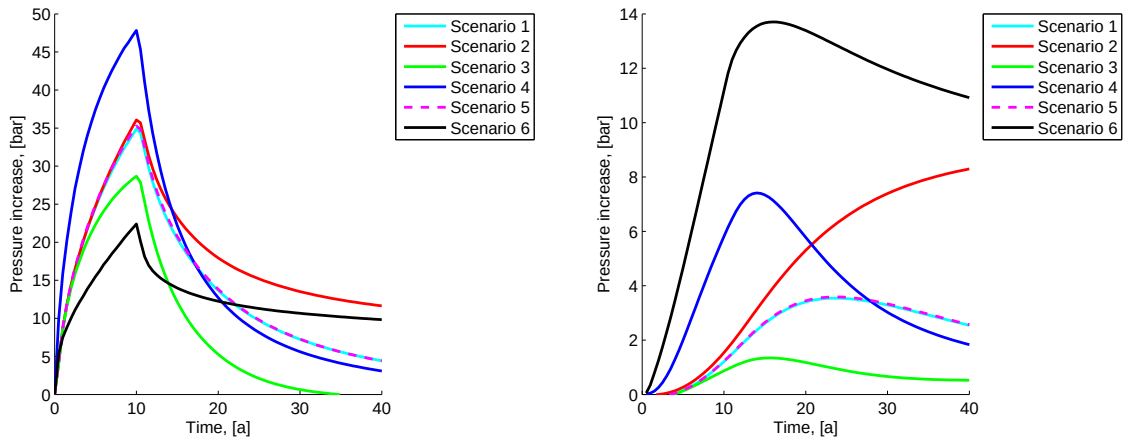

Figure 6.20: Pressure increase in 5 km and 31 km distance from injection

A quantification of the uncertainties is not done in the recent study of Schäfer et al. (2011), but the investigated uncertainties can be discussed considering the different levels of uncertainties introduced in Chapter 4. The investigation of the different boundary conditions can be classified as scenario uncertainty because the different boundaries stand for different geological features like sealing faults or compartmentalized portions of the storage formation. However, boundary conditions can often be ranked as recognized ignorance as well, because it is an assumption made in the model set-up. To take compressibility into account is a choice in the model concept and neglecting the compressibility is an uncertainty of the recognized ignorance level. The variation of the injection temperature and the permeability could be done statistically if an adequate distribution for the parameters was available. A statement regarding which level of uncertainty is the most relevant is difficult in this case because the parameters were not investigated systematically.

7 Final Remarks

7.1 CCS and Public Acceptance

In this section, the acceptance of CCS in Germany and how the developed risk assessment concept and uncertainty investigations presented in this thesis can help in the communication process are discussed.

As explained in the introduction, the public in Germany has many concerns about CCS and in particular about CO_2 storage. Schulz et al. (2010) summarized the situation in Germany and analyzed the reasons of low acceptance concerning CCS. One main fact they pointed out is that the knowledge about the CCS technology is sparse, and providing more information about CCS helps to increase the overall acceptance of the technology. This was observed by several studies in different countries. In general, Schulz et al. (2010) summarized that the perception of risk depends highly on intuitive or subjective perception factors such as the possibility of the individual to control them, the voluntariness of taking the risks, the trust in the politician and operators handling the risks, fairness of the division of benefits and losses (see also Renn et al. (2007) p.78ff). They added that in the case of CCS the values that people have are also important. Many people prefer to support renewable energy instead of CCS to reduce the CO_2 emissions. Schulz et al. (2010) emphasized that the question of trust is very important; the people do not trust the industry or regulators to have the risks under control. Additionally, the perception is influenced by the fact that there is a certain degree of dissent on the CCS technology among the experts (Wassermann et al. (2011)), which reduces the trust in the experts. In a Delphi approach, Wassermann et al. (2011) identified the consensus and dissent on various aspects regarding CCS among experts in Germany. One of the main topics of dissent that has been identified is the potential of CCS to mitigate the CO_2 emissions. The opponents fear that the technology hinders the transition to renewable energy supply (undermining better option argument), whereas, the proponents believe that CCS is a good opportunity to mitigate the CO_2 emissions. Another important key factor Schulz et al. (2010) pointed out is the fairness in the context with CCS technology. The benefit of CCS is a global effect and locally the people only see the losses. The acceptance strongly decreases when people are directly affected by the technology, e.g, living close to a possible storage site and when they do not see a direct benefit. In Germany, the cost-benefit problem is strengthened by the geological situation that the largest potential for CO_2 storage sites are found in the northern and eastern part of Germany, whereas many large energy production plants and high energy consumption areas are situated in the higher populated western and southern parts of Germany (Wassermann et al. (2011)).

Looking at the situation of the two German federal states Scheswig-Holstein and Brandenburg, Schulz et al. (2010) highlighted that the local situation is important to consider as well.

In Schleswig-Holstein the people fear that CCS will be in competition to the wind energy that is a source of income for many farmers. In addition, water suppliers are afraid of ecological risks for the drinking water due to brine displacement and infiltration. The situation in Brandenburg is different; here the small scale pilot project Ketzin was seen positively, because CCS was seen as a chance to preserve their own brown coal energy supply. However, the enforced actions to get a permission for explorations for a suitable storage site arose the criticism of the public in Brandenburg.

For a better understanding of the perception of risks associated with CO_2 storage, it is tried to classify them by the different classifications and types of risks that are presented in the Risk Governance Model (Renn (2008b)) summarized in Section 3.1. In the phase of risk appraisal four elements that influence risk perception were presented. One of these elements is the "semantic associations linked to the risk source " (Renn (2008b) p. 20). As described in Schulz et al. (2010), CO_2 storage is pulled together with atomic waste disposal during the discussion in Germany. In the context of the atomic waste debate, the trust in the politicians and operators were unsettled. Thus, the trust in the politician and operators handling CCS and especially the storage of CO_2 is low as well. In addition, CO_2 was compared to a more hazardous substance: the atomic waste, thus, people see it much more dangerous compared to expert's assessment. Another of the four elements for risk perception is the trust and credibility of the actors. The association of CO_2 storage with atomic waste disposal shows that the people do not trust the actors in the field of CCS as well.

If one tries to classify the CO_2 storage technology into the five semantic risk images described in Section 3.1.3, it is difficult to find an appropriate class. Looking at the situation in Germany, it seems that many people see CCS as a "risk as pending danger". On one hand this class suits it because it is a technical risk source that is not voluntarily taken by the people. On the other hand, the risks of this class are of catastrophic potential. The potential of the risk that could occur from the events such as CO_2 leakage, brine displacement or seismic activities are considered low by most experts. Under extremely unlikely conditions, if the rising CO_2 pools in a sink, the risk of suffocation is given. However, the amount of leaking CO_2 is very small and it will be mixed rapidly at the surface. The salt infiltration into drinking water aquifers could result in a loss of drinking water resources or high remediation costs or, in worst case situation, in impacts on wildlife habitats or pollution of surface waters. It is clear that these risk have to be considered and well investigated for each selected site and that there is still a number of open questions regarding risks. The catastrophic potential seen by experts is low if the storage site is properly selected. However, many people perceive the risks like a pending danger. As Schulz et al. (2010) discussed in detail, the people often know less about the topic and this probably results in such a perception. Thus, CCS risks can be classified as a pending danger because many people perceive them like this.

It is also interesting to rank CCS according to the traffic light model. Six risk classes named after Greek mythology were presented in Renn et al. (2007) (see Section 3.1.3). Here, CO_2 storage risks could be related to the class "Medusa" (see Figure 7.1). It is characterized by low extent of damage and low probability, but not exactly predictable because a lack of data and many uncertainties in the available data. However, CO_2 storage has a high potential for

mobilization. According to the traffic light model the risk would be acceptable, but the high mobilization potential requires actions to achieve a better acceptance for the technology.

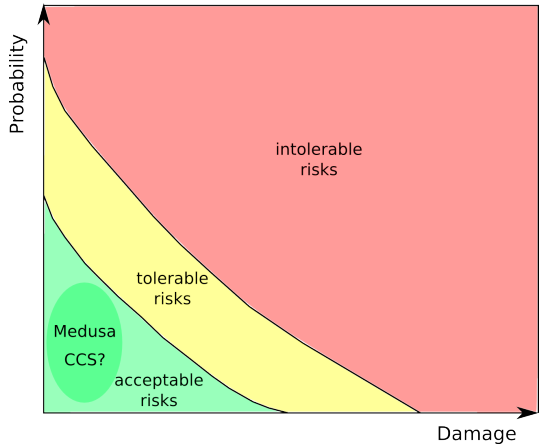

Figure 7.1: Traffic light model according to Renn (2008b)p.163 and possible ranking for CCS.

The ranking according to the three challenges complexity, uncertainty and ambiguity is helpful to find the best procedure for the communication and participation process as well as the risk management process. The four types of risk are discussed in Section 3.1.3: linear, complex, uncertain, and ambiguous risks. The risk assessment for CO_2 storage can be classified as a highly complex (e.g. complexity of the flow and transport processes), uncertain (e.g. lack of knowledge for the geological data), and ambiguous (e.g. different interpretation of outputs by actors and stakeholders) risk. This means especially for the communication and participation process that the involved people, all stakeholders, and the general public, has to be addressed during the process.

As shown in Renn (2008b), p.280, for this type of risk a participatory type of discourse should be chosen, where all actors such as agency staff, external experts, and all stakeholders (industry, directly affected groups, and the general public) are involved. Schulz et al. (2010) presented recommendations for the communication and the dialog with the public that is affected by a CO_2 storage site exploration: First, the regional differences and characteristics should be considered to establish a successful communication. A very important point is to increase the knowledge on risk related to CO_2 storage by the natural scientists and engineers. Sufficient knowledge is an important basis for the communication process. In addition, they claim more empirical analysis on the perception of CO_2 storage in the public in required. Finally, the acceptance can only be improved by an open and fair dialog. This was also shown during the Delphi workshop carried out by Wassermann et al. (2011). A main consensus was related to the communication process regarding CO_2 storage. The experts agreed that the German Federal Government should take an active part in the communication process and that a dialogue platform between stakeholders should be introduced.

The risk assessment concept presented in this work belongs to the phase of risk appraisal in the overall governance approach where damage and probability are estimated. One important point, that is related to the concept presented in this work, is the fact that the overall

communication and participation process should be based on a good basis of knowledge. Thus, methods are required to increase the knowledge on risk of CO_2 storage. The developed concept presents a systematic framework to investigate various uncertainties and to derive damage and risk values, which can be used as a basis for concern assessment, risk evaluation, risk management, and risk communication. It is important to present the results in a way that non experts are able to interpret them as well. The procedure of first identifying and ranking the uncertainties into different levels of knowledge can help to understand the overall situation. At the beginning of the assessment the uncertainties that are considered and weighted to be the most important ones and the uncertainties that are not considered are clearly presented and discussed. In the interpretation of the results the uncertainties that were not considered are included in the discussion as well.

How the results are presented is also important. The presented risk assessment concept provides different values on how the results can be presented: a mean damage value, a probability that a certain threshold will not be exceeded, or a value of the probability weighted expectation of the damage, can be derived by the analysis. The choice of the value that is presented should be chosen depending on the problem and the people that want to be informed. In addition, all remaining uncertainties should be revealed and discussed since the presentation of, for example, only an expected value does not provide information about assumptions made and it is difficult for the people to trust the estimation. The conceptual and numerical model is complicated for non-experts to understand. Additionally, the model reduction technique which is applied is also very complex. Thus, participation of stakeholders during the risk assessment procedure would help to improve the understanding of the methods used and to interpret the final results. An up-to-date study by Scheer (2013) intensively investigates the role of simulations in the political decision making processes. In particular CCS is chosen for investigation of function and communication of simulations.

The participatory aspect was not included into the development of the risk assessment concept presented in this work. Stakeholders were consulted and asked which risk is seen to be the most important one that should be investigated. Water suppliers clearly state that the salt infiltration is a relevant problem. The risk which could come along with salt water intrusion into freshwater aquifers was seen as more relevant than the risks associated with CO_2 leakage. Thus, the concept is applied to the salt infiltration problem. However, the stakeholders were not involved in the development process of the concept. Here, a large potential is available to improve the procedure. In an ongoing project called CO_2BRIM[1], CCS is investigated in an integrated natural and social science approach. Participatory numerical modeling is applied to investigate the risks and concerns regarding CCS. Up until know, first workshops have been organized and methods for the identification of potential storage sites have been discussed.

[1] CO_2BRIM Projekt: Mehrstufige und regionale Charkterisierung potentieller CO_2-Speicherformationene unter besonderer Berücksichtigung von Soleaufstiegsrisiken - ein integrierter natur- und sozialwissenschaftlicher Ansatz (http://www.co2brim.hydrosys.uni-stuttgart.de/)

7.2 Summary

Carbon capture and storage is considered as one option to reduce the CO_2 emissions to the atmosphere and to mitigate global warming by the IPCC (Metz et al. (2005)). In this thesis, the focus is on storage of CO_2 in suitable storage sites in the subsurface. The assessment of the risks that could occur during the storage process is an important task. Numerical simulations are an appropriate tool for investigation of processes in the subsurface where experimental research is limited. The main objective of the study is the development of a systematic risk assessment concept under consideration of different kinds of uncertainties. The concept can be applied to different risk sources. Brine displacement and infiltration into freshwater aquifers is seen as a relevant topic for water suppliers and is chosen for investigation in the thesis. An additional aim is to identify uncertainties for realistic storage sites and to improve the understanding of the system behavior by systematical investigations.

The risk assessment concept and the various uncertainty studies are based on numerical simulations in the subsurface. In Chapter 2 the basics for numerical simulation of CO_2 storage and associated brine displacement are shortly presented. The relevant processes and the conceptual models that are applied are described.

Chapter 3 presents a brief introduction to the theory of risk assessment. Different concepts of risk and the risk governance model are shortly introduced to get an overview as to how the risk assessment concept that is developed in Chapter 4 can be integrated into the theory. In addition, the statistical tools that are used in the concept, mainly the model reduction technique, is summarized.

In Chapter 4 a risk assessment concept to systematically investigate risk related events in the subsurface and to quantify damage and risk is presented. In the overall risk governance model, the risk assessment concept presented in this thesis belongs to the phase of risk appraisal. The risk assessment concept is based on the differentiation of uncertainties into levels of knowledge: statistical uncertainty, scenario uncertainty, and recognized ignorance. The concept is a systematic investigation of the three different levels of uncertainty. In the end, risk is determined. The definition of damage and risk is an important step and has to be individually chosen for each investigation. To determine probabilities Monte Carlo simulations are performed. The high computational costs due to the complex physics in the conceptual and numerical model and the large spatial and temporal scales that are required for CO_2 storage investigations are handled by applying a model reduction technique for the Monte Carlo runs. Additionally, model coupling in space is used as an optional tool which is efficient to reduce computational costs. If the model output does not represent an adequate measure for damage and risk additional analytical approximations can be applied to easily translate the output of the numerical model into values that can be compared to criteria.

In the main part of the thesis (Chapter 5) the concept is applied to investigate brine displacement and infiltration. Three approaches to assess the risk of salt infiltration are presented which are partly based on each other. In the first part, the overall risk assessment concept except the investigation of recognized ignorance, is followed. First scenario uncertainty is considered and the damage, which is defined as the brine discharge into the water aquifer of six different scenarios, is determined. The scenarios consider geological features such as

a crack in the caprock, a fault zone from the reservoir up to the aquifer, or a zone of low permeability in the domain. Choosing one of the scenarios, the parameter range of three uncertain parameters (permeability of the reservoir, permeability along the fault zone, and anisotropy) which belong to the level of statistical uncertainty is analyzed using the model reduction technique aPC combined with PCM. Probabilities for the damage to occur are derived and risk can be finally determined for the chosen scenario. Water suppliers are interested in concentrations in the freshwater aquifer which can be compared to water quality criteria. The damage (brine discharge) is therefore translated into concentrations via simple analytical approximations.
The brine discharge derived in the first approach is a conservative estimate because the salinity is constant over all layers from the storage reservoir up to the water aquifer. Thus, recognized ignorance is reduced in the second approach by accounting for a variable salt concentration over depth. To reduce computational costs spatial model coupling is applied. In the upper region where no CO_2 exists, a one-phase, two-component model that accounts for a water and salt component is applied and coupled to the two-phase model used in the lower part (storage reservoir). For selected scenarios of the first approach and an additional one accounting for low permeabilities in the intermediate aquifers, the damage defined as the salt discharge into the freshwater aquifer is determined. The damage values which directly account for salt discharge are more realistic than in the first approach. In principle, salt concentrations can be directly derived but to account for the mixing in the freshwater aquifer, additional 2D simulations including groundwater flow are applied. The third approach is directly based on the previous investigations and uses the results of the second approach to derive salt concentrations at water production wells. Only the water aquifer as a 2D domain is modeled and the salt discharge into the aquifer is based on the value of one of the Scenarios of the previous approach. Statistical uncertainty is investigated for the permeability, the water production rate, and the well distance using the model reduction technique. Important information about the influence of the three parameters on the salt concentration is derived. The damage and risk (salt concentration) determined at the water production well can be directly compared to the water quality criteria.

In Chapter 6 uncertainties of two realistic storage reservoirs are investigated and classified into the different levels of uncertainties presented in the risk assessment concept. Important knowledge about the influence of the considered uncertainties on the model response is derived which helps to define an appropriate model for risk assessment. The influence of the boundary conditions, the injection temperature, rock compressibility, or permeability on the pressure response in a neighboring structure are investigated for a possible storage formation in the North German Basin. For the pilot site Ketzin, a systematic history matching approach is presented including detailed preliminary investigations on various uncertainties. Uncertainties in the available modeling data and the model assumptions are considered. Inverse modeling including 3 degrees of freedom is applied for history matching of measurement data for pressure for the first 50 days and first arrival time. A satisfactory matching of the pressure is achieved but an extrapolation to a longer time span is limited (400 days). The pressure over the simulation time of 1800 days can be matched by introducing an additional degree of freedom, the distinction of near-well and far-field. The second arrival time can be easily matched by including a distinct geological feature. Overall, important information is

collected for future risk assessment tasks.

Finally, risk perception of CCS in Germany is discussed and an attempt is made to classify CCS into selected risk types and classifications presented in the risk governance approach in Section 7.1. In addition, the input that can be provided by the developed risk assessment approach is discussed.

7.3 Conclusions

The following conclusions for risk assessment in general can be drawn:

- The risk assessment concept presented in this work provides a feasible strategy to systematically investigate uncertainties and to derive risk estimates. The method helps to gain more knowledge about CO_2 storage risks and uncertainties.
- For comprehensive risk assessment it is important to consider uncertainty on different levels (statistical uncertainty, scenario uncertainty, and recognized ignorance). The discussion and systematic differentiation of the uncertainties in the risk assessment concept presented in this work help to improve the comprehensibility. The choice of the uncertainties considered in risk assessment should be based on expert knowledge and the interest of stakeholders and the public (see Section 7.1). Additionally, the assumptions made for the modeling procedure should be carefully chosen.
- Several model assumptions result in conservative estimations of damage and risk, which can be seen as a type of worst case approximations. If many uncertainties exist, worst case approximations are a reasonable way to determine what could occur under unfavorable conditions. However, overly conservative assumptions may lead to unacceptably high risks and thus may unnecessarily prevent the implementation of a (CO_2 storage) project .
- The three approaches for investigating brine displacement which follow the developed risk assessment concept show various possibilities as to how the results can be presented: for example mean damage or risk values, probability density function or cumulative distribution function for the damage, or an probability weighted expectation of damage. As already discussed in Section 7.1 the selection of presented results is important, e.g. for making decisions and should be chosen depending on the situation.
- The model reduction technique aPC combined with PCM is an efficient tool, to handle the huge computational costs caused by the complexity of the conceptual model, the requirement of large model domains, and long time scales in combination with thousands of Monte Carlo runs. However, a weakness of the polynomial approach is the extrapolation beyond the range of the snapshot runs where the polynomials can result in overshooting or underestimations. This has to be considered precisely for risk assessment. Overall, it is a good trade-off between desired accuracy and computational effort. In addition, model coupling in space is also a very efficient approach to reduce computational costs.

Several conclusions from the three applications of the presented risk assessment concept for the event of brine displacement which could result in the salinisation of freshwater aquifers can be drawn.

- The first approach for determining damage and risk in terms of brine discharge depending on different geological features and uncertain parameters provides important information for the overall system behavior. Whether salt infiltrates into a freshwater aquifer depends strongly on the geology. An overview of how, and which geological features (e.g. a fault zone) intensify the risk of brine infiltration into freshwater aquifers is thus provided. In addition, the parameters such as the permeability of the reservoir or the fault zone influence the salt infiltration rate decisively.
- The reduction of recognized ignorance by accounting for a variable salt mass fraction in the second approach significantly reduces the predicted damage (salt discharge into the freshwater aquifer). Additionally, the flow is mainly observed along the fault zone, and almost no salt infiltrates into the aquifer in regions with intact aquitard layers.
- The ranking of the scenarios is the same in both approaches, the conservative approach with constant salinity and the approach accounting for variable density. Thus the significance of the various geological features is well determined by the conservative, constant salinity approach.
- In the current investigation, recognized ignorance, here the assumption made in the conceptual model to account for the salt content outweighs more than statistical and scenario uncertainty.
- Whether or not salt is produced by a water production well depends on the distance of the well and its pumping rate. In addition, the mixing in the aquifer is a key process that influences the production of salt. The mixing strongly depends on the dispersive processes, which are caused by heterogeneities in the geology, and in the numerical models on the grid resolution. Thus it is important to properly account for dispersion and to resolve the grid adequately if quantitative risk values for the salt concentration are derived.
- Overall, the problem of salt infiltration into a freshwater aquifer seems to be locally confined, which only occurs if certain geological features, such as a crack in the caprock or a fault zone are present.

The uncertainty studies and the history matching for the pilot site Ketzin and for the realistic storage formation in the North German Basin provide important information for risk assessment. Some of the most significant findings are summarized here:

- The uncertainty studies show that the pressure and CO_2 plume expansion is strongly influenced by (i) the model assumptions (recognized ignorance) on the conceptual model or the grid type and its resolution, (ii) reservoir properties permeability, and porosity combined with the compressibility of CO_2. Whereas rock compressibility,

the domain size, and the applied boundary conditions mainly influence the pressure evolution. The two latter ones can be interpreted either as scenario uncertainty or recognized ignorance and confirm the requirement of large model domains to predict pressure response adequately.

- The history matching procedure for the Ketzin site shows that a calibration of the model is possible and that the calibrated model is able to predict the pressure for a certain time. Reasonable predictions for long time scales (several hundred years) especially for the CO_2 plume expansion are not reliable. The geological model needs to be continuously updated. The study also shows that a good model calibration is necessary and important to gain reasonable results in risk assessment.

- Predictions with the calibrated Ketzin model are possible but limited in terms of predicting the CO_2 plume expansion for longer time scales. At this point one could argue whether predictions based on numerical simulations are reasonable if too many uncertainties exist and the model does not completely represent the measurement data. Kinzelbach (1992) summarized six typical questions in the field of economics of groundwater quality which can be investigated by transport models: (i) interpretation of measurements, (ii) predictions of the behavior of the contaminant plume in the future, (iii) planning of remediation measures, (iv) planning of measure for water production, (v) planning of control systems, and (vi) balancing of the disposition of the contaminant in the environment. All these applications can be transferred to numerical simulations of CO_2 storage. Although the prediction of the CO_2 plume expansion, which corresponds to application (ii) is limited, the models are useful because reasonable approximations can be provided. The spatial expansion of the heterogeneities (the channel characteristic for the Ketzin site) has a strong influence on the CO_2 plume evolution whereas its influence on the pressure is minor. The prediction of the pressure signal which is possible with the calibrated Ketzin model is relevant for several of the applications described above (e.g. (iii), (iv), or (v)). Thus the model can contribute important information to several of the applications even though the heterogeneous structure is not exactly known. However, if the uncertainties are high it is very important to consider different scenarios, e.g. different variations of the geological model for predicting the CO_2 plume evolution.

During the investigations of brine displacement and infiltration into freshwater aquifers and the history matching of the Ketzin site data several modeling and numerical challenges have been encountered.

- The choice of the conceptual model is very important. Neglecting compositional effects results in overestimation of, e.g. the CO_2 plume and the corresponding pressure signal or the salt concentrations. The assumption of considering only two dimensions for investigating the salt evolution in a water aquifer is also a conservative estimation because the mixing in the third dimension is neglected. Thus, the resulting estimates for risk assessment are mostly conservative which is often applicable to get worst case scenario approximations. However for history matching and the prediction of the

pressure and the CO_2 plume expansion for real sites, this assumption would be not practicable and more complex models are required to adequately represent the measurements.

- The strongly heterogeneous permeability and porosity field of the Ketzin site requires an adequate interpolation technique to transfer the data of the geological model to the applied grid. In addition the simulations with a hexahedron mesh lead to strong convergence problems which has been reduced by applying the cell-centered finite volume method instead of the box-method.

- Another challenge is the choice of the domain size. Simplified or small domains can strongly influence the results. The radially symmetric domain used in the brine displacement study due to limitations on computational capacity yields an unrealistic circular fault zone, but is practicable for identification of relevant geological features. In addition, the radially symmetric domain cannot account for groundwater flow which overestimates the salt discharge into the water aquifers. If small domain sizes are chosen the boundary condition can strongly affect the pressure evolution.

- The grid size is limited due to computational capacity. For the brine displacement problem, the limitation in the grid size yields a very broad representation of the fault zone, which is not a realistic assumption but adequate for identification of the influence of such geological features. In addition, large grid cells overestimate the dissolution, e.g. of the CO_2 in the brine phase because the whole cell has to be filled by dissolved CO_2 before a CO_2 phase appears.

- For the investigation of salt infiltration into a freshwater aquifer for determination of salt concentration at water production wells as well as for the history matching in the heterogeneous channel structure at the Ketzin site, grid effects on the results were encountered. The triangular grid used for the prediction of the salt concentrations at a water production well results in increased mixing (numerical dispersion). Thus, to represent dispersion properly is another challenge which strongly depends on the grid type and its resolution and description of the dispersive process. For the Ketzin site, the heterogeneous channel structure could not be resolved properly by a tetrahedron mesh because the vertical representation of the channels could not be provided over the whole domain. It could be better represented by a hexahedron mesh. Thus, the grid type is very important to consider depending on the problem to solve.

In this thesis, on the one hand simplified conceptual models for understanding principle processes have been applied- here for the event of brine displacement. Important information about the relevant processes and geological features that can yield damage and risk have been identified. A physical range that is possible to occur has been provided. On the other hand, realistic and complex models have been applied, which are computationally very costly, to match measurements and to predict pressure evolution at the injection well and the CO_2 plume expansion at a real site. Valuable information about how the pressure signal and the plume evolution react in the heterogeneous field, and the influence of various parameters could be gained. The calibrated Ketzin model can provide a realistic estimation

of the pressure evolution, even if the time scale for prediction is limited. The complex models are required to adequately represent the reality and give reasonable predictions.
However, the history matching procedure for the Ketzin site showed that it is already very difficult to predict pressure and plume expansion close to the injection site even though a lot of data is available. The reliability of the description of the heterogeneities in Ketzin are still an open question. Brine displacement can happen at a much larger scale, far away from the injection site, where much less data is available. Knowledge of discrete heterogeneities or reliable statistics of heterogeneous parameter distributions are typically not available. Therefore the use of a geological model including detailed permeability and porosity distributions may not always be feasible for this application. Estimations with simplified conceptual models are thus needed to provide a physical range of what may be possible, in addition to preferably realistic models.

7.4 Outlook

A lot of different aspects could be further investigated for the research field of risk assessment for CO_2 storage. Some ideas are summarized in the following:

- For the event of brine displacement the concept could be applied to more realistic geologies. The fault zone that is applied in this work has a huge lateral extension. Further, realistic migration scenarios along salt domes could be investigated as it is planned in the CO_2BRIM project.
- For the salt concentration at water production wells, more realistic set-ups could be considered as well. 3D simulations including several production wells in the areas of salt pollution could be performed. To provide more comprehensive results, the salt concentrations in the lateral extension could be visualized in a map as it was done for contaminants by Troldborg et al. (2008). Here, the influence of different contaminated sites on supply wells was investigated. With the provided particle trace maps it could be shown which contaminated sites have an impact on the water supply. In the context of salt infiltration into freshwater aquifers the map could indicate which regions will be contaminated and which water production well could be affected by the salt. The interpretation of such a map would be more intuitive for non-experts.
- The presented concept could be applied to other risk related events such as CO_2 leakage through the caprock. The rise of the CO_2 has to be adequately described. In addition, geomechanical effects due to a pressure increase triggered by the CO_2 injection should be considered. Therefore, fully coupled models are required to adequately describe the feedback between the flow and the geomechanical processes (Darcis (2012), Häberle and Ehlers (2011)). If CO_2 leaks, geochemical processes in shallower aquifers could be investigated as well to predict the influence of CO_2 and mobilized heavy metals on the groundwater.

- The applied model reduction technique and the model coupling approach are efficient tools to reduce computational costs. In addition, sequential coupling in time could be applied to further reduce the computation time (see Darcis (2012)).
- For the Ketzin site, the risk assessment concept could be applied to an updated geological model (based on the information provided by the history matching approaches) to investigate risk scenarios for e.g. CO_2 leakage through the fault zone in the northern direction from the injection site.
- As discussed in Section 7.1, stakeholders and the general public should be involved in the risk assessment process, which is planned in the CO_2BRIM project.
- To resolve the numerical challenges which have been faced in this work, the efficiency of the parallel runs should be further increased to account for more grid cells for resolving heterogeneous fields or the mixing of salt and CO_2 properly. Additionally, adaptive grid refinement is an efficient tool to refine the mesh where it is required without increasing the grid size unnecessarily. The implementation of adaptive grid refinement for the implicit models in DuMu^x would help to resolve several of the encountered challenges. For the decoupled models which already uses adaptive grid refinement, the dispersion process is needed to simulate the saltwater problem.

Bibliography

Aisopou, A., Binning, P. J., Chambon, J., and Bjerg, P. L. Pesticide breakthrough at drinking water wells generated from diffuse and point source application. Technical report, DTU Environment, 2012.

Apps, J., Zheng, L., Zhang, Y., Xu, T., and Birkholzer, J. Evaluation of potential changes in groundwater quality in response to CO_2 leakage from deep geologic storage. *Transport in Porous Media*, 82:215–246, 2010.

Askey, R. and Wilson, J. *Some basic hypergeometric polynomials that generalize Jacobi polynomials*, volume 54. Memoirs of the American Mathematical Society, AMS, Providence, 1985.

Baber, K., Mosthaf, K., Flemisch, B., Helmig, R., Müthing, S., and Wohlmuth, B. Numerical scheme for coupling two-phase compositional porous-media flow and one-phase compositional free flow. *IMA Journal of Applied Mathematics*, 77:887–909, 2012.

Batzle, M. and Wang, Z. Seismic properties of pore fluids. *Geophysics*, 57:1396–1408, 1992.

Bechmann, G. *Risiko und Gesellschaft: Grundlagen und Ergebnisse interdisziplinärer Risikoforschung*. Westdt. Verlag, 1997.

Bedford, T. and Cooke, R. *Probabilistic Risk Analysis - Foundation and Methods*. Cambridge University Press, U.K, 2001.

Benson, S., Hepple, M. R., Apps, J., Tsang, C., and Lippmann, M. Lessons learned from natural and industrial analogues for storage of carbon dioxide in deep geological formations. *Lawrence Berkeley National Laboratory, Berkeley, CA. LBNL-51170.*, 2002.

Bergman, P. and Winter, E. Disposal of carbon dioxide in aquifers in the US. *Energy Conversion and Management*, 36 (6-9):523–526, 1995.

Bielinski, A. *Numerical simulation of CO_2 sequestration in geological formations*. PhD thesis, Institut für Wasserbau, Universität Stuttgart, 2006.

Binning, P. J. and Celia, M. A. Pseudokinetics arising from the upscaling of geochemical equilibrium. *Water Resour. Res.*, 44(7):W07410, July 2008.

Birkholzer, J., Apps, J., Zheng, L., Y., U., Xu, T., and Tsang, C.-F. Research project on CO_2 geological storage and groundwater resources: water quality effects caused by CO_2 intrusion into shallow groundwater. Technical Report L-L1251, Lawrence Berkeley National Laboratory, 2008.

Birkholzer, J., Zhou, Q., and Tsang, C. Large-scale impact of CO_2 storage in deep saline aquifers: A sensitivity study on pressure response in stratified systems. *International Journal of Greenhouse Gas Control*, 3:181–194, 2009.

Bonnesen, E., Larsen, F., Sonnenborg, T., Klitten, K., and Stemmerik, L. Deep saltwater in chalk of morth-west europe: origin, interface charactersitics and development over geological time. *Hydrogeology Journal*, 17:1643–1663, 2009.

Bowden, A. and Rigg, A. Assessing reservoir performance risk in CO_2 storage projects. *Paper 547, presented at 7th international Conference on Greenhouse Gas Control Technologies, Vancouver, Canada*, 5–9 September, 2004.

Bradbury, J. A. The policy implications of differing concepts of risk. *Science Technology Human Values*, 14 (4):380–399, 1989.

Brooks, A. and Corey, A. Hydraulic properties of porous media. *Hydrology Papers*, 3, 1964.

Celia, M. A., Nordbotten, J. M., Court, B., Dobossy, M., and Bachu, S. Field-scale application of a semi-analytical model for estimation of CO_2 and brine leakage along old wells. *International Journal of Greenhouse Gas Control*, 5:257–269, 2011.

Class, H., Helmig, R., and Bastian, P. Numerical simulation of non-isothermal multiphase multicomponent processes in porous media.: 1.An efficient solution technique. *Advances in Water Resources*, 25(5):533–550, 2002.

Class, H., Ebigbo, A., Helmig, R., Dahle, H., Nordbotten, J., Celia, M., Audigane, P., Darcis, M., Ennis-King, J., Yaqing, F., Flemisch, B., Gasda, S., Jin, M., Krug, S., Lagregere, D., Naderi, A., Pawar, R., Sbai, A., Thomas, S., Trenty, L., and Wei, L. A benchmark-study on problems related to CO_2 storage in geologic formations - summary and discussion of the results. *Computational Geosciences*, 13:409–434, 2009.

Darcis, M., Class, H., Flemisch, B., and Helmig, R. Sequential model coupling for feasibility studies of CO_2 storage in deep saline aquifers. *Oil & Gas Science and Technology – Rev. IFP Energies nouvelles*, 66(1):93–103, 2011.

Darcis, M. *Coupling Models of Different Complexity for the Simulation of CO_2 Storage in Deep Saline Aquifers*. PhD thesis, Institut für Wasser- und Umweltsystemmodeierung, Universität Stuttgart, 2012.

Diersch, H.-J. G. and Kolditz, O. Variable-density flow and transport in porous media: approaches and challenges. *Advances in Water Resources*, 25:899–944, 2002.

Dlugokencky, E. and Tans, P. Trends in atmospheric carbon dioxide, noaa/esrl. Online 23 April 2013. URL `www.esrl.noaa.gov/gmd/ccgg/trends/`.

Duan, Z. and Sun, R. An improved model calculating CO_2 solubility in pure water and aqueous NaCl solutions from 273 to 533 K and from 0 to 2000 bar. *Chemical Geology*, 193: 257–271, 2003.

Ebigbo, A., Helmig, R., Cunningham, A., Class, H., and Gerlach, R. Modelling biofilm growth in the presence of carbon dioxide and water flow in the subsurface. *Advances in Water Resources*, 33, 7:762–781, 2010.

Elder, J. Transient convection in a porous medium. *Journal of Fluid Mechanics*, 27 (3):609–623, 1967.

Faragher, J. Probabilistic methods for the quantification of uncertainty and error in computational fluid dynamics simulations. Technical report, Australian Government Department of Defence Defence Science and Technology Organisation, 2004.

Fenghour, A., Wakeham, W., and Vesovic, V. The viscosity of carbon dioxide. *Journal of Physical and Chemical Reference Data*, 27(1):31–44, 1998.

Finsterle, S. iTOUGH2 Sample Problems. Technical report, Lawrence Berkely National Laboratory, University of California, 1999a.

Finsterle, S. iTOUGH2 User's Guide. Technical report, Lawrence Berkeley National Laboratory, 1999b.

Flemisch, B., Darcis, M., Erbertseder, K., Faigle, B., Lauser, A., Mosthaf, K., Müthing, S., Nuske, P., Tatomir, A., Wolff, M., and Helmig, R. DuMu^x: DUNE for multi-phase, component, scale, physics, ... flow and transport in porous media. *Advances in Water Resources*, 34 (9):1102–1112, 2011.

Förster, A., Norden, B., Zinck-Jorgensen, K., Frykman, P., Kulenkampff, J., Spangenberg, E., Erzinger, J., Zimmer, M., Kopp, J., Borm, G., Juhlin, C., Cosma, C.-G., and Hurter, S. Baseline characterization of the CO2SINK geological storage site at Ketzin, Germany. *Environmantal Geosciences*, 13:145–161, 2006.

Fritz, J., Flemisch, B., and Helmig, R. Decoupled and multiphysics models for non-isothermal compositional two-phase flow in porous media. *International Journal of Numerical Analysis & Modeling*, 9,1:17–28, 2012.

Garabedian, S., LeBlanc, D., Gelhar, L., and Celia, M. Large-scale natural gradient tracer test in sand and gravel, Cape Cod, Massachusetts 2. Analysis fo spatial moments for a nonreactive tracer. *Water Resources Research*, 27 (5):911–924, 1991.

Garcia, J. Density of aqueous solutions of CO_2. Technical Report 49023, Earth Sciences Division, Lawrence Berkely National Laboratory, 2001.

Häberle, K. and Ehlers, W. Carbon dioxide storage in the subsurface: an approach including solid deformations and phase transition. *Proceedings in Applied Mathematics and Mechanics*, 11:473–474, 2011.

Helmig, R., Flemisch, B., Wolff, M., Ebigbo, A., and Class, H. Model coupling for multiphase flow in porous media. *Advances in Water Resources*, 51:52 – 66, 2013.

Helmig, R. *Multiphase flow and transport processes in the subsurface.* Springer, Berlin, Germany, 1997.

Helton, J. C. Treatment of uncertainty in performance assessments for complex systems. *Risk Analysis*, 14(4):483–511, 1994.

Henry, H. Effects of dispersion on salt encroachment in coastal aquifers. *US Geol Surv Water Suppl Pap*, 1613-C:71–84, 1964.

Hoffman, F. O. and Hammonds, J. S. Propagation of uncertainty in risk assessments: The need to distinguish between uncertainty due to lack of knowledge and uncertainty due to variability. *Risk Analysis*, 14(5):707–712, 1994.

Holtz, M. Residual gas saturation to aquifer influx: A calculation method for 3-D computer reservoir model construction. *SPE Paper*, 75502, 2002.

Huyakorn, P., S., Andresen, P., Mercer, J., W., and White, H. Saltwater intrusion in aquifers: Development and testing of a three-dimensional finte element model. *Water Resources Research*, 23 (2):293–312, 1987.

IAPWS. IAPWS (The International Association for the Properties of Water and Steam). Release on the IAPWS industrial formulation 1997 for the thermodynamic properties of water and steam., 1997. URL `http://www.iapws.org/`.

Johannsen, K., Kinzelbach, W., Oswald, S., and Wittum, G. The saltpool benchmark problem - numerical simulation of saltwater upconing in a porous medium. *Advances in Water Resources*, 25(3):335–348, 2002.

Johnson, P. C. and Ettinger, R. A. Heuristic model for predicting the intrusion rate of contaminant vapors into buildings. *Environmental Science and Technology*, 25:1445–1452, 1991.

Juhlin, C., Giese, R., Zinck-Jorgensen, K., Cosma, C., Kazemeini, H., Juhojuntti, N., Lüth, S., Norden, B., and Förster, A. 3D baseline seismics at Ketzin, Germany: the CO2SINK project. *Geophysics*, 72:121–132, 2007.

Kaplan, S. and Garrick, B. On the quantitative definition of risk. *Risk Analysis*, 1 (1):11–27, 1981.

Keating, E., Newell, D., Viswanathan, H., Carey, J., Zyvoloski, G., and Pawar, R. CO_2/brine transport into shallow aquifers along fault zones. *Environmental Science and Technology*, 47: 290–297, 2013.

Kempka, T. and Kühn, M. Numerical simulations of CO_2 arrival times and reservoir pressure coincide with observations from the Ketzin pilot site, Germany. *Environmental Earth Sciences*, Special Issue:1–11, doi:10.1007/s12665–013–2614–6, 2013.

Kempka, T., Kühn, M., Class, H., Frykman, P., Kopp, A., Nielsen, C., and Probst, P. Modelling of CO_2 arrival time at Ketzin - Part I. *International Journal of Greenhouse Gas Control*, 4:1007–1015, 2010.

Kharaka, Y. K., Thordsen, J. J., Kakouros, E., Ambats, G., Herkelrath, W. N., Beers, S. R., Birkholzer, J. T., Apps, J. A., Spycher, N. F., Zheng, L., Trautz, R. C., Rauch, H. W., and Gullickson, K. S. Changes in the chemistry of shallow groundwater related to the 2008

injection of CO_2 at the ZERT field site, Bozeman, Montana. *Environmantal Earth Sciences*, 60(2):273–284, 2010.

Kinzelbach, W. *Numerische Methoden zur Modellierung des Transport von Schadstoffen im Grundwasser*. PhD thesis, Schriftenreihe Walsser Abwasser Band 2, Oldenbourg Verlag, München Wien, 1992.

Knopf, S., May, F., Müller, C., and Gerling, J. P. Neuberechnung möglicher Kapazitäten zur CO_2-Speicherung in tiefen Aquifer-Strukturen. *ENERGIEWIRTSCHAFTLICHE TAGESFRAGEN 60*, 4:76–80, 2010.

Kolditz, O., Ratke, R., Diersch, H.-J. G., and Zielke, W. Coupled groundwater flow and transport: 1. Verification of variable density flow and transport models. *Advances in Water Resources*, 21(1):27–46, 1998.

Kopp, A. *Evaluation of CO_2 injection processes in geological formations for site screening*. PhD thesis, Institut für Wasserbau, Universität Stuttgart, 2009.

Kopp, A., Binning, P., Johannsen, K., Helmig, R., and Class, H. A contribution to risk analysis for leakage through abandoned wells in geological CO_2 storage. *Advances in Water Resources*, 33(8):867–879, 2010.

Kumar, A., Ozah, R., Noh, M., Pope, G., Bryant, S., Sepehrnoori, K., and Lake, L. Reservoir simulation of CO_2 storage in deep saline aquifers. *SPE Journal*, 10 (3):336–348, 2005.

Lange, T., Sauter, M., Heitfeld, M., Klünker, J., Brosig, K., Jahnke, W., Helmig, R., Kissinger, A., Ebigbo, A., and Class, H. Hydraulic fracturing in unconventional reservoirs - Determining the risks in the geological system Part 1. *Environmental Earth Sciences, in press*, doi:10.1007/s12665-013-2803-3, 2013.

Lauser, A., Hager, C., Helmig, R., and Wohlmuth, B. A new approach for phase transitions in miscible multi-phase flow in porous media. *Advances in Water Resources*, 34(8):957–966, 2011.

Le Treut, H., Somerville, R., Cubasch, U., Ding, Y., Mauritzen, C., Mokssit, A., Peterson, T., and Prather, M. Historical overview of climate change. In Solomon, S., Qin, D., Manning, M., Chen, Z., Marquis, M., Averyt, K., Tignor, M., and Miller, H., editors, *Climate Change 2007: The Physical Science Basis. Contribution of Working Group I to the Fourth Assessment Report of the Intergovernmental Panel on Climate Change*. Cambridge University Press, 2007.

Lemieux, J.-M. Review: The potential impact of underground geological storage of carbon dioxide in deep saline aquifers on shallow groundwater resources. *Hydrogeology Journal*, 19:757–778, 2011.

Lewicki, J., Birkholzer, J., and Tsang, C.-F. Natural and industrial analogues for leakage of CO_2 from storage reservoirs: identification of features, events, and processes and lessons learned. *Environmental Geology*, 52:457–467, 2007.

Lu, C., Sun, Y., Buscheck, T., Hao, Y., White, J., and Chiaramonte, L. Uncertainty quantification of CO_2 leakage through a fault with multiphase and nonisothermal effects. *Greenhouse Gases: Science and Technology*, 2:445–459, 2012.

Martens, S., Kempka, T., Liebscher, A., Lüth, S., Möller, F., Myrttinen, A., Norden, B., Schmidt-Hattenberger, C., Zimmer, M., and Kühn, M. Europe's longest-operating onshore CO_2 storage site at Ketzin, Germany: a progress report after three years of injection. *Environmental Earth Sciences*, doi 10.1007/s12665-012-1672-5, 2012.

Maul, P. R., Metcalfe, R., Pearce, J., Savage, D., and West, J. M. Performance assessments for the geological storage of carbon dioxide: Learning from the radioactive waste disposal experience. *International Journal of Greenhouse Gas Control*, 1(4):444–455, 2007.

Metz, B., Davidson, O., de Coninck, H., Loos, M., and Meyer, L. *IPCC Special Report on Carbon Dioxide Capture and Storage. Technical Report, Intergovernamental Panel on Climate Change (IPCC)*. Cambridge University Press, U.K, 2005.

Michaelides, E. Thermodynamic properties of geothermal fluids. *Geothermal Resources Council Transactions*, 5:361–364, 1981.

Mosthaf, K., Baber, K., Flemisch, B., Helmig, R., Leijnse, A., Rybak, I., and Wohlmuth, B. A coupling concept for two-phase compositional porous-medium and single-phase compositional free flow. *Water Resources Research*, 47:W10522, 2011.

Nicot, J.-P. Evaluation of large-scale CO_2 storage on fresh-water sections of aquifers: An example from the Texas Gulf Coast Basin. *International Journal of Greenhouse Gas Control*, 2 (4):582–593, October 2008.

Norden, B. and Frykman, P. Geological modelling of the Triassic Stuttgart Formation at Ketzin, Germany. *International Journal of Greenhouse Gas Control, in press*, http://dx.doi.org/10.1016/j.ijggc.2013.04.019, 2013.

Norden, B., Förster, A., Vu-Hoang, D., Marcelis, F., Springer, N., and Le Nir, I. Lithological and petrophysical core-log interpretation in CO_2SINK, the European CO_2 onshore research storage and verification project. *SPE Reservoir Evaluation & Engineering*, 13 (2): 179–192, 2010.

Oladyshkin, S. and Nowak, W. Data-driven uncertainty quantification using the arbitrary polynomial chaos expansion. *Reliability Engineering & System Safety*, 106:179–190, 2012.

Oladyshkin, S., de Barros, F., and Nowak, W. Global sensitivity analysis: A flexible and efficent framework with an example from stochastic hydrology. *Advances in Water Resources*, 37:10–22, 2012.

Oladyshkin, S., Class, H., Helmig, R., and Nowak, W. An integrative approach to robust design and probabilistic risk assessment for CO_2 storage in geological formations. *Computational Geosciences, Springer.*, 15(3):565–577, 2011a.

Oladyshkin, S., Class, H., Helmig, R., and Nowak, W. A concept for data-driven probabilistic risk assesssment and application to carbon dioxide storage in geological formations. *Advances in Water Resources, Elsevier.*, 34:1508–1518, 2011b.

Oldenburg, C., Jordan, P., Nicot, J.-P., Mazzoldi, A., Gupta, A., and Bryant, S. Leakage risk assessment of the in salah CO_2 storage project: Applying the certification framework in a dynamic context. *Energy Procedia*, 4:4154–4161, 2011.

Oldenburg, C. Screening and ranking framework for geologic CO_2 storage site selection on the basis of health, safety, and environmental risk. *Environmental Geology*, 54:1687–1694, 2008.

Oldenburg, C. M. and Pruess, K. Dispersive transport dynamics in a strongly coupled groundwater-brine flow system. *Water Resources Research*, 31(2):289–302, 1995.

Oldenburg, C. M., Bryant, S. L., and Nicot, J.-P. Certification framework based on effective trapping for geologic carbon sequestration. *International Journal of Greenhouse Gas Control*, 3(4):444–457, 2009.

Oswald, S. and Kinzelbach, W. Three-dimensional physical benchmark experiments to test variable-density flow models. *Journal of Hydrology*, 290:22–42, 2004.

Parry, M., Canziani, O., Palutikof, J., and Co-authors. Technical summary. In Parry, M., Canziani, O., Palutikof, J., van der Linden, P., and Hanson, C., editors, *Climate Change 2007: Impacts, Adaptation and Vulnerability. Contribution of Working Group II to the Fourth Assessment Report of the Intergovernmental Panel on Climate Change*. Cambridge University Press, 2007.

Person, M., Banerjee, A., Rupp, J., Medina, C., Lichtner, P., Gable, C., Pawar, R., M.A., C., McIntosh, J., and Bense, V. Assessment of basin-scale hydrologic impact of CO_2 sequestration, illinois basin. *International Journal of Greenhouse Gas Control*, 4:840–854, 2010.

Pruess, K. Leakage of CO_2 from geologic storage: Role of secondary accumulation at shallow depth. *International Journal of Greenhouse Gas Control*, 2:37–46, 2008.

Renn, O. Concepts of risk: An interdiscipkinary review. *GAIA*, 17/1:50–66, 2008a.

Renn, O., Schweizer, P.-J., Dreyer, M., and Kinke, A. *Risiko: Über den gesellschaftlichen Umgang mit Unsicherheiten*. oekom Verlag, München, 2007.

Renn, O. *Risk Governance: Coping with Uncertainty in a Complex World*. earthscan, 2008b.

Riquelme, R., Lira, I., Perez-Lopez, C., Rayas, J. A., and Rodriguez-Vera, R. Interferometric measurement of a diffusion coef[U+FB01]cient: comparison of two methods and uncertainty analysis. *Journal of Physics D: Applied Physics*, 2007.

Rohrmann, B. and Renn, O. *Risk perception research: An introduction, in O. Renn and B.Rohrmann: Cross-Cultural Risk Perception: a Servey of Empirical Studies*. Kluver, 2000.

Rowe, W. D. Understanding uncertainty. *Risk Analysis*, 14(5):743–750, 1994.

Rutqvist, J., Birkholzer, J., and Tsang, C.-F. Coupled reservoir-geomechanical analysis of the potential for tensile and shear failure associated with CO_2 injection in multilayered reservoir-caprock systems. *International Journal of Rock Mechanics & Mining Sciences*, 45: 132–143, 2008.

Rychlik, I. and Ryden, J. *Probability and risk analysis - An introdoction for Engineers*. Springer Berlin / Heidelberg, 2006.

Rygaard, M., Arvin, E., Bath, A., and Binning, P. Designing water supplies: Optimizing drinking water composition for maximum economic benefit. *Water Research*, 45(12):3712–3722, 2011.

Schäfer, F., Walter, L., Class, H., and Müller. Projekt CO_2-Drucksimulation: Regionale Druckentwicklung bei der Injection von CO_2 in salinare Aquifere. Technical report, Bundesanstalt für Geowissenschaften und Rohstoffe (BGR), 2010.

Schäfer, F., Walter, L., Class, H., and Müller, C. The regional pressure impact of CO_2 storage: a showcase study from the North German Basin. *Environmental Earth Sciences*, 65 (7):2037–2049, 2011.

Scheer, D. *Simulationen in politischen Entscheidungsprozessen Funktion und Kommunikation von Computersimulationen am Beispiel der Carbon Capture & Storage-Technologie*. PhD thesis, Institut für Sozialwissenschaften, Universität Stuttgart, 2013. in preparation.

Scheidegger, A. *The physics of flow through porous media*. Macmillian Co., New York, U.S.A., 1960.

Schmorak, S. and Mercado, A. Upconing of fresh water-sea water interface below pumping wells, field study. *Water Resources Research*, 5 (6):1290–1311, 1969.

Schulz, M., Scheer, D., and Wassermann, S. Neue Technik, alte Pfade? zur Akzeptanz der CO_2-Speicherung in Deutschland. *GAIA*, 17/1:287–296, 2010.

Segol, G. *Classic groundwater simulations proving and improving numerical models.* Prentice Hall, 1994.

Siirila, E. R., Navarre-Sitchler, A. K., Maxwell, R. M., and McCray, J. E. A quantitative methodology to assess the risks to human health from CO_2 leakage into groundwater. *Advances in Water Resources*, 36:146–164, 2012.

Slovic, P. Perception of risk. *Science*, 236:280–285, 1987.

Soanes, C. and Stevenson, A. *Oxford Dictionary of English*. Oxford University Press, 2010.

Soize, C. and Ghanem, R. Physical systems with random uncertainties: chaos representations with arbitrary probability measure. *SIAM Journal of Scientific Computing*, 26(2): 395–410, 2004.

Somerton, W., El-Shaarani, A., and Mobarak, S. High temperature behavior of rocks associated with geothermal type reservoirs. *Society of Petroleum Engineers*, SPE-4897, 1974.

Span, R. and Wagner, W. A new equation of state for carbon dioxide covering the fluid region from the triple-point temperature to 1100 K at pressures up to 800 MPa. *Journal of Physical and Chemical Reference Data*, 25(6):1509–1596, 1996.

Spycher, N. and Pruess, K. CO_2-H_2O mixtures in the geological sequestration of CO_2. II. Partitioning in chloride brines at 12–100°C and up to 600 bar. *Geochimica et Cosmochimica Acta*, 69(13):3309–3320, 2005.

Todd, D. K. *Groundwater Hydrology*. John Wiley and Sons, New York, 1980.

Trenberth, K., Jones, P., Ambenje, P., Bojariu, R., Easterling, D., Tank, A. K., Parker, D., Rahimzadeh, F., Renwick, J., Rusticucci, M., Soden, B., and Zhai, P. Observations: Surface and atmospheric climate change. In Solomon, S., Qin, D., Manning, M., Chen, Z., Marquis, M., Averyt, K., Tignor, M., and Miller, H., editors, *Climate Change 2007: The Physical Science Basis. Contribution of Working Group I to the Fourth Assessment Report of the Intergovernmental Panel on Climate Change*. Cambridge University Press, 2007.

Troldborg, M., Lemming, G., Binning, P. J., Tuxen, N., and Bjerg, P. L. Risk assessment and prioritisation of contaminated sites on the catchment scale. *Journal of Contaminant Hydrology*, 101:14–28, 2008.

Villadsen, J. and Michelsen, M. *Solution of differential equation models by polynomial approximation*. Prentice-Hall, 1978.

Voss, C., Simmons, C., and Robinson, N. Three-dimensional benchmark for variable-density flow and transport simulation: matching semi-analytic stability modes for steady unstable convection in an inclined porous box. *Hydrogeology Journal*, 18 (1):5–23, 2010.

Voss, C. I. and Souza, W. R. Variable density flow and solute transport simulation of regional aquifers containing a narrow freshwater-saltwater transition zone. *Water Resources Research*, 23(10):1851–1866, 1987.

Walker, W., Harremoes, P., Rotmans, J., van der Sluijs, J., van Asselt, M., Janssen, P., and Krayer von Krauss, M. Defining uncertainty: A conceptual basis for uncertainty management in model-based decision support. *Integrated Assessment*, 4:5–17, 2003.

Walter, L., Oladyshkin, S., Class, H., Darcis, M., and Helmig, R. A study on pressure evolution in a channel system during CO_2 injection. *Energy Procedia*, 4:3722 – 3729, 2011. 10th International Conference on Greenhouse Gas Control Technologies.

Walter, L., Binning, P. J., Oladyshkin, S., Flemisch, B., and Class, H. Brine migration resulting from CO_2 injection into saline aquifers – an approach to risk estimation including various levels of uncertainty. *International Journal of Greenhouse Gas Control*, 9:495–506, 2012.

Wan, X. and Karniadakis, G., E. Multi-element generalized polynomial chaos for arbitrary polynomial measures. *SIAM Journal of Scientific Computing*, 28(3):901–928, 2006.

Wang, S. and Jaffe, P. R. Dissolution of a mineral phase in potable aquifers due to CO_2 releases from deep formations; effect of dissolution kinetics. *Energy Conversion and Management*, 45(18–19):2833–2848, 2004.

Wassermann, S., Schulz, M., and Scheer, D. Linking public acceptance with expert knowledge on CO_2 storage: outcomes of a Delphi approach. *Energy Procedia*, 4:6353–6359, 2011.

Wiener, N. The homogeneous chaos. *American Journal of Mathematics*, 60:897–936, 1938.

Wiese, B., J., B., Enachescu, C., Würdemann, H., and Zimmermann, G. Hydraulic characterisation of the Stuttgart formation at the pilot test site for CO_2 storage, Ketzin, Germany. *International Journal of Greenhouse Gas Control*, 4:960–971, 2010.

Wildenborg, A., Leijnse, A., Kreft, E., Nepveu, M., Obdam, A., Orlic, B., Wipfler, E., van der Grift, B., van Kesteren, W., Gaus, I., Czernichowski-Lauriol, I., Torfs, P., and Wójcik, R. Risk assessment methodology for CO_2 storage—the scenario approach. *In: Benson, S.M. (ed.) The CO_2 Capture and Storage Project for Carbon Dioxide Storage in Deep Geological Formations for Climate Change Mitigation.*, CH. 33:1293–1316, 2005. Elsevier, Amsterdam.

Wojtkiewicz, S. F., Eldred, M. S., Field, R. V., Urbina, A., and Red-Horse, J. Uncertainty quantification in large computational engineering models. *American Institute of Aeronautics and Astronautics*, 14, 2001.

Würdemann, H., Möller, F., Kühn, M., Heidug, W., Christensen, N., Borm, G., Schilling, F., and the CO2SINK Group. CO2SINK – from site characterisation and risk assessment to monitoring and verification: One year of operational experience with the field laboratory for CO_2 storage at Ketzin. *International Journal of Greenhouse Gas Control*, 4(6):938–951, 2010.

Xiu, D. and Karniadakis, G., E. Modeling uncertainty in flow simulations via generalized polynomial chaos. *Journal of Computational Physics*, 187:137–167, 2003.

Yamamoto, H., Zhang, K., Karasaki, K., Marui, A., Uehara, H., and Nishikawa, N. Numerical investigation concerning the impact of CO_2 geologic storage on regional groundwater flow. *International Journal of Greenhouse Gas Control*, 3(5):586–599, 2009.

Zheng, L., Apps, J. A., Zhang, Y., Xu, T., and Birkholzer, J. T. On mobilization of lead and arsenic in groundwater in response to CO_2 leakage from deep geological storage. *Chemical Geology*, 268(3–4):281–297, 2009.

A Brief Introduction to the Theory of Inverse Modeling

The inverse modeling approach implemented in iTOUGH2 (Finsterle (1999b)) is applied for the first step of matching the pressure at the injection well and the arrival time at Ktzi 200. In the following, the inverse modeling procedure is briefly summarized. For details, one is referred to Finsterle (1999b). Inverse modeling is a method to estimate model parameters from discrete measurements in space and time. The model is automatically calibrated against the observation. First the conceptual forward model has to be developed. Here, DuMu^x is applied and coupled with iTOUGH2 via an input file procedure. In the second step, all input parameters that should be estimated are defined. Vector $\mathbf{p}$ contains all these input parameters. For each estimated parameter, an initial guess is given in vector $\mathbf{p_0}$. The measurement data that is compared to the model output is chosen at discrete points in space and time. All the measurement data is written in vector $\mathbf{z}^*$ and the model output is held in the vector $\mathbf{z}(\mathbf{p})$. The difference between the measurement and the model output is defined as the residual vector $\mathbf{r}$ with the entries:

$$r_i = z_i^* + z_i,\ i = 1, ..., m \tag{A.1}$$

at each calibration point i. The measured data is often of a different type and magnitude, e.g., pressure and saturation. Thus each residual has to be weighted by an individual standard deviation. The next step is the forward simulation that is performed with DuMu^x in the presented approach using the current input vector $\mathbf{p}$. The model response is compared with the measured data ($\mathbf{z}^*$) by formulating the objective function S, which is an integral measure of misfit. The properties of the residuals influence the choice of the objective function. If the measurement errors are normally distributed the maximum likelihood approach leads to least square estimators. The objective function can be defined as:

$$S_f = \mathbf{r^T C_{zz}^{-1} r} \tag{A.2}$$

where $\mathbf{C_{zz}}$ is the covariance matrix of the measurements. To find the best agreement between the observation and the results of the numerical model the objective function has to be minimized. Here, a minimization algorithm that is based on the calculation of the second derivatives is used. The objective function is reduced by iteratively adapting the parameters depending on the sensitivity of the calculated response on the parameters. The Levenberg-Marquardt method is an adequate minimization algorithm for nonlinear problems. If the convergence criteria are reached and no further reduction of the objective function can be achieved or the fixed maximum number of iteration steps are reached, the iteration is stopped. The last parameter set is defined as the best fit ($\hat{\mathbf{p}}$) for matching the measurement.

In the end, a detailed analysis of the residuals, the best fit ($\hat{\mathbf{p}}$) and the sensitivity of the estimated parameters is possible. Some of the most important measures are shortly summarized. The sensitivity coefficients (Jacobien matrix) $J_{ij} = \partial z_i / \partial p_j$ are a measure of the impact of a small parameter change on the system. Higher absolute values mean a lower estimation uncertainty of the parameter. For the derivation of the sensitivity coefficient one is referred to Finsterle (1999b)p.40/41. For comparison the sensitivity coefficients are scaled with the standard deviation of the observation i and the parameter j:

$$J_{ij} = \frac{\partial z_i}{\partial p_j} \frac{\sigma_{pj}}{\sigma_{zi}} \tag{A.3}$$

The total sensitivity is the sum of the sensitivity coefficients. A measure of the goodness of the fit is the estimated error variance, which is defined as:

$$s_0^2 = \frac{\mathbf{r^T C_{zz}}^{-1} \mathbf{r}}{m - n} \tag{A.4}$$

where m-n is the degree of freedom. From the covariance matrix $\mathbf{C_{pp}}$ of the estimated parameters different kinds of information can be gained: the uncertainty of the estimates, which can be high if the measurement is not sensitive enough and the correlation between the parameters. The covariance matrix of the estimated parameters can be approximated as:

$$\mathbf{C_{pp}} = s_0^2 (\mathbf{J^T C_{zz}^{-1} J})^{-\mathbf{1}} \tag{A.5}$$

where $\mathbf{J}$ is the Jacobi matrix. The diagonal of the covariance matrix contains the variances σ_p^2 of the estimated parameters and the off-diagonal elements are the covariances c_{ij}. From these values a correlation coefficient can be derived:

$$r_{ij} = \frac{c_{ij}}{\sqrt{\sigma_{pi}^2 \sigma_{pj}^2}},\ r_{ij} = -1, ..., 1\,. \tag{A.6}$$

The correlation coefficient is defined between -1 and 1. A correlation coefficient of 0 means that the parameters i and j are not correlated. A strong correlation exits if the values are close to -1 or 1. Two parameters are highly correlated if a change of one parameter can be balance by a change of the other parameter. Thus, the uncertainty of one parameter influences the uncertainty of the other. Positive correlation means that a similar status of the system can be reached by increasing both parameters. Two parameters are negative correlated if a similar system response can be reached by simultaneously increasing one and decreasing the other parameter. In addition, iTOUGH2 presents a matrix of direct correlation. The physical interpretation of the direct correlation is easier. It shows how one parameter can directly compensated the change of the other parameter. Whereas the correlation coefficient r_{ij} is difficult to interpret physically if more than two parameters are considered because the other parameters indirectly influence the correlation. For the construction of the direct correlation matrix one is referred Finsterle (1999b).

The diagonal elements of $\mathbf{C_{pp}}$ (σ_p^2) is a measure of uncertainty. The marginal standard deviation σ_p is the square root of the diagonal elements and is a measure of the uncertainty of a parameter without regard to the value of the other parameters. Whereas the conditional

standard deviation σ'_p gives the uncertainty of a parameters assuming that all the other parameters are exactly known. Thus, the ratio of the conditional and marginal standard deviations is an overall measure of the independence of parameter i:

$$\Gamma_i = \frac{\sigma'_{pi}}{\sigma_{pi}}, \Gamma = 0, ..., 1\,. \tag{A.7}$$

High values of Γ_i indicate that the parameter i is independent from the other parameters. If a low ratio is given, the uncertainty σ_{pi} could be lowered by reduction of the correlation to the other varied parameters. In the matrix presented in the analysis below, the elements of the lower triangular matrix represent the covariances and the elements of the upper triangular matrix are the correlation coefficient r_{ij}.

Institut für Wasser- und Umweltsystemmodellierung
Universität Stuttgart

Pfaffenwaldring 61
70569 Stuttgart (Vaihingen)
Telefon (0711) 685 - 64717/64749/64752/64679
Telefax (0711) 685 - 67020 o. 64746 o. 64681
E-Mail: iws@iws.uni-stuttgart.de
http://www.iws.uni-stuttgart.de

Verzeichnis der Mitteilungshefte

5 Plate, Erich: *Beitrag zur Bestimmung der Windgeschwindigkeitsverteilung in der durch eine Wand gestörten bodennahen Luftschicht*,
und
Röhnisch, Arthur; Marotz, Günter: *Neue Baustoffe und Bauausführungen für den Schutz der Böschungen und der Sohle von Kanälen, Flüssen und Häfen; Gestehungskosten und jeweilige Vorteile*, sowie Unny, T.E.: *Schwingungsuntersuchungen am Kegelstrahlschieber*, 1967

6 Seiler, Erich: *Die Ermittlung des Anlagenwertes der bundeseigenen Binnenschiffahrtsstraßen und Talsperren und des Anteils der Binnenschiffahrt an diesem Wert*, 1967

7 *Sonderheft anläßlich des 65. Geburtstages von Prof. Arthur Röhnisch mit Beiträgen von* Benk, Dieter; Breitling, J.; Gurr, Siegfried; Haberhauer, Robert; Honekamp, Hermann; Kuz, Klaus Dieter; Marotz, Günter; Mayer-Vorfelder, Hans-Jörg; Miller, Rudolf; Plate, Erich J.; Radomski, Helge; Schwarz, Helmut; Vollmer, Ernst; Wildenhahn, Eberhard; 1967

8 Jumikis, Alfred: *Beitrag zur experimentellen Untersuchung des Wassernachschubs in einem gefrierenden Boden und die Beurteilung der Ergebnisse*, 1968

9 Marotz, Günter: *Technische Grundlagen einer Wasserspeicherung im natürlichen Untergrund*, 1968

10 Radomski, Helge: *Untersuchungen über den Einfluß der Querschnittsform wellenförmiger Spundwände auf die statischen und rammtechnischen Eigenschaften*, 1968

11 Schwarz, Helmut: *Die Grenztragfähigkeit des Baugrundes bei Einwirkung vertikal gezogener Ankerplatten als zweidimensionales Bruchproblem*, 1969

12 Erbel, Klaus: *Ein Beitrag zur Untersuchung der Metamorphose von Mittelgebirgsschneedecken unter besonderer Berücksichtigung eines Verfahrens zur Bestimmung der thermischen Schneequalität*, 1969

13 Westhaus, Karl-Heinz: *Der Strukturwandel in der Binnenschiffahrt und sein Einfluß auf den Ausbau der Binnenschiffskanäle*, 1969

14 Mayer-Vorfelder, Hans-Jörg: *Ein Beitrag zur Berechnung des Erdwiderstandes unter Ansatz der logarithmischen Spirale als Gleitflächenfunktion*, 1970

15 Schulz, Manfred: *Berechnung des räumlichen Erddruckes auf die Wandung kreiszylindrischer Körper*, 1970

16 Mobasseri, Manoutschehr: *Die Rippenstützmauer. Konstruktion und Grenzen ihrer Standsicherheit*, 1970

17 Benk, Dieter: *Ein Beitrag zum Betrieb und zur Bemessung von Hochwasserrückhaltebecken*, 1970

18 Gàl, Attila: *Bestimmung der mitschwingenden Wassermasse bei überströmten Fischbauchklappen mit kreiszylindrischem Staublech*, 1971, vergriffen

19 Kuz, Klaus Dieter: *Ein Beitrag zur Frage des Einsetzens von Kavitationserscheinungen in einer Düsenströmung bei Berücksichtigung der im Wasser gelösten Gase*, 1971, vergriffen

20 Schaak, Hartmut: *Verteilleitungen von Wasserkraftanlagen*, 1971

21 *Sonderheft zur Eröffnung der neuen Versuchsanstalt des Instituts für Wasserbau der Universität Stuttgart mit Beiträgen von* Brombach, Hansjörg; Dirksen, Wolfram; Gàl, Attila; Gerlach, Reinhard; Giesecke, Jürgen; Holthoff, Franz-Josef; Kuz, Klaus Dieter; Marotz, Günter; Minor, Hans-Erwin; Petrikat, Kurt; Röhnisch, Arthur; Rueff, Helge; Schwarz, Helmut; Vollmer, Ernst; Wildenhahn, Eberhard; 1972

22 Wang, Chung-su: *Ein Beitrag zur Berechnung der Schwingungen an Kegelstrahlschiebern*, 1972

23 Mayer-Vorfelder, Hans-Jörg: *Erdwiderstandsbeiwerte nach dem Ohde-Variationsverfahren*, 1972

24 Minor, Hans-Erwin: *Beitrag zur Bestimmung der Schwingungsanfachungsfunktionen überströmter Stauklappen*, 1972, vergriffen

25 Brombach, Hansjörg: *Untersuchung strömungsmechanischer Elemente (Fluidik) und die Möglichkeit der Anwendung von Wirbelkammerelementen im Wasserbau*, 1972, vergriffen

26 Wildenhahn, Eberhard: *Beitrag zur Berechnung von Horizontalfilterbrunnen*, 1972

27 Steinlein, Helmut: *Die Eliminierung der Schwebstoffe aus Flußwasser zum Zweck der unterirdischen Wasserspeicherung, gezeigt am Beispiel der Iller*, 1972

28 Holthoff, Franz Josef: *Die Überwindung großer Hubhöhen in der Binnenschiffahrt durch Schwimmerhebewerke*, 1973

29 Röder, Karl: *Einwirkungen aus Baugrundbewegungen auf trog- und kastenförmige Konstruktionen des Wasser- und Tunnelbaues*, 1973

30 Kretschmer, Heinz: *Die Bemessung von Bogenstaumauern in Abhängigkeit von der Talform*, 1973

31 Honekamp, Hermann: *Beitrag zur Berechnung der Montage von Unterwasserpipelines*, 1973

32 Giesecke, Jürgen: *Die Wirbelkammertriode als neuartiges Steuerorgan im Wasserbau*, und Brombach, Hansjörg: *Entwicklung, Bauformen, Wirkungsweise und Steuereigenschaften von Wirbelkammerverstärkern*, 1974

33 Rueff, Helge: *Untersuchung der schwingungserregenden Kräfte an zwei hintereinander angeordneten Tiefschützen unter besonderer Berücksichtigung von Kavitation*, 1974

34 Röhnisch, Arthur: *Einpreßversuche mit Zementmörtel für Spannbeton - Vergleich der Ergebnisse von Modellversuchen mit Ausführungen in Hüllwellrohren*, 1975

35 *Sonderheft anläßlich des 65. Geburtstages von Prof. Dr.-Ing. Kurt Petrikat mit Beiträgen von*: Brombach, Hansjörg; Erbel, Klaus; Flinspach, Dieter; Fischer jr., Richard; Gàl, Attila; Gerlach, Reinhard; Giesecke, Jürgen; Haberhauer, Robert; Hafner Edzard; Hausenblas, Bernhard; Horlacher, Hans-Burkhard; Hutarew, Andreas; Knoll, Manfred; Krummet, Ralph; Marotz, Günter; Merkle, Theodor; Miller, Christoph; Minor, Hans-Erwin; Neumayer, Hans; Rao, Syamala; Rath, Paul; Rueff, Helge; Ruppert, Jürgen; Schwarz, Wolfgang; Topal-Gökceli, Mehmet; Vollmer, Ernst; Wang, Chung-su; Weber, Hans-Georg; 1975

36 Berger, Jochum: *Beitrag zur Berechnung des Spannungszustandes in rotationssymmetrisch belasteten Kugelschalen veränderlicher Wandstärke unter Gas- und Flüssigkeitsdruck durch Integration schwach singulärer Differentialgleichungen*, 1975

37 Dirksen, Wolfram: *Berechnung instationärer Abflußvorgänge in gestauten Gerinnen mittels Differenzenverfahren und die Anwendung auf Hochwasserrückhaltebecken*, 1976

38 Horlacher, Hans-Burkhard: *Berechnung instationärer Temperatur- und Wärmespannungsfelder in langen mehrschichtigen Hohlzylindern*, 1976

39 Hafner, Edzard: *Untersuchung der hydrodynamischen Kräfte auf Baukörper im Tiefwasserbereich des Meeres*, 1977, ISBN 3-921694-39-6

40 Ruppert, Jürgen: *Über den Axialwirbelkammerverstärker für den Einsatz im Wasserbau*, 1977, ISBN 3-921694-40-X

41 Hutarew, Andreas: *Beitrag zur Beeinflußbarkeit des Sauerstoffgehalts in Fließgewässern an Abstürzen und Wehren*, 1977, ISBN 3-921694-41-8, vergriffen

42 Miller, Christoph: *Ein Beitrag zur Bestimmung der schwingungserregenden Kräfte an unterströmten Wehren*, 1977, ISBN 3-921694-42-6

43 Schwarz, Wolfgang: *Druckstoßberechnung unter Berücksichtigung der Radial- und Längsverschiebungen der Rohrwandung*, 1978, ISBN 3-921694-43-4

44 Kinzelbach, Wolfgang: *Numerische Untersuchungen über den optimalen Einsatz variabler Kühlsysteme einer Kraftwerkskette am Beispiel Oberrhein*, 1978, ISBN 3-921694-44-2

45 Barczewski, Baldur: *Neue Meßmethoden für Wasser-Luftgemische und deren Anwendung auf zweiphasige Auftriebsstrahlen*, 1979, ISBN 3-921694-45-0

46 Neumayer, Hans: *Untersuchung der Strömungsvorgänge in radialen Wirbelkammerverstärkern*, 1979, ISBN 3-921694-46-9

47 Elalfy, Youssef-Elhassan: *Untersuchung der Strömungsvorgänge in Wirbelkammerdioden und -drosseln*, 1979, ISBN 3-921694-47-7

48 Brombach, Hansjörg: *Automatisierung der Bewirtschaftung von Wasserspeichern*, 1981, ISBN 3-921694-48-5

49 Geldner, Peter: *Deterministische und stochastische Methoden zur Bestimmung der Selbstdichtung von Gewässern*, 1981, ISBN 3-921694-49-3, vergriffen

50 Mehlhorn, Hans: *Temperaturveränderungen im Grundwasser durch Brauchwassereinleitungen*, 1982, ISBN 3-921694-50-7, vergriffen

51 Hafner, Edzard: *Rohrleitungen und Behälter im Meer*, 1983, ISBN 3-921694-51-5

52 Rinnert, Bernd: *Hydrodynamische Dispersion in porösen Medien: Einfluß von Dichteunterschieden auf die Vertikalvermischung in horizontaler Strömung*, 1983, ISBN 3-921694-52-3, vergriffen

53 Lindner, Wulf: *Steuerung von Grundwasserentnahmen unter Einhaltung ökologischer Kriterien*, 1983, ISBN 3-921694-53-1, vergriffen

54 Herr, Michael; Herzer, Jörg; Kinzelbach, Wolfgang; Kobus, Helmut; Rinnert, Bernd: *Methoden zur rechnerischen Erfassung und hydraulischen Sanierung von Grundwasserkontaminationen*, 1983, ISBN 3-921694-54-X

55 Schmitt, Paul: *Wege zur Automatisierung der Niederschlagsermittlung*, 1984, ISBN 3-921694-55-8, vergriffen

56 Müller, Peter: *Transport und selektive Sedimentation von Schwebstoffen bei gestautem Abfluß*, 1985, ISBN 3-921694-56-6

57 El-Qawasmeh, Fuad: *Möglichkeiten und Grenzen der Tropfbewässerung unter besonderer Berücksichtigung der Verstopfungsanfälligkeit der Tropfelemente*, 1985, ISBN 3-921694-57-4, vergriffen

58 Kirchenbaur, Klaus: *Mikroprozessorgesteuerte Erfassung instationärer Druckfelder am Beispiel seegangsbelasteter Baukörper*, 1985, ISBN 3-921694-58-2

59 Kobus, Helmut (Hrsg.): *Modellierung des großräumigen Wärme- und Schadstofftransports im Grundwasser*, Tätigkeitsbericht 1984/85 (DFG-Forschergruppe an den Universitäten Hohenheim, Karlsruhe und Stuttgart), 1985, ISBN 3-921694-59-0, vergriffen

60 Spitz, Karlheinz: *Dispersion in porösen Medien: Einfluß von Inhomogenitäten und Dichteunterschieden*, 1985, ISBN 3-921694-60-4, vergriffen

61 Kobus, Helmut: *An Introduction to Air-Water Flows in Hydraulics*, 1985, ISBN 3-921694-61-2

62 Kaleris, Vassilios: *Erfassung des Austausches von Oberflächen- und Grundwasser in horizontalebenen Grundwassermodellen*, 1986, ISBN 3-921694-62-0

63 Herr, Michael: *Grundlagen der hydraulischen Sanierung verunreinigter Porengrundwasserleiter*, 1987, ISBN 3-921694-63-9

64 Marx, Walter: *Berechnung von Temperatur und Spannung in Massenbeton infolge Hydratation*, 1987, ISBN 3-921694-64-7

65 Koschitzky, Hans-Peter: *Dimensionierungskonzept für Sohlbelüfter in Schußrinnen zur Vermeidung von Kavitationsschäden*, 1987, ISBN 3-921694-65-5

66 Kobus, Helmut (Hrsg.): *Modellierung des großräumigen Wärme- und Schadstofftransports im Grundwasser*, Tätigkeitsbericht 1986/87 (DFG-Forschergruppe an den Universitäten Hohenheim, Karlsruhe und Stuttgart) 1987, ISBN 3-921694-66-3

67 Söll, Thomas: *Berechnungsverfahren zur Abschätzung anthropogener Temperaturanomalien im Grundwasser*, 1988, ISBN 3-921694-67-1

68 Dittrich, Andreas; Westrich, Bernd: *Bodenseeufererosion, Bestandsaufnahme und Bewertung*, 1988, ISBN 3-921694-68-X, vergriffen

69 Huwe, Bernd; van der Ploeg, Rienk R.: *Modelle zur Simulation des Stickstoffhaushaltes von Standorten mit unterschiedlicher landwirtschaftlicher Nutzung*, 1988, ISBN 3-921694-69-8, vergriffen

70 Stephan, Karl: *Integration elliptischer Funktionen*, 1988, ISBN 3-921694-70-1

71 Kobus, Helmut; Zilliox, Lothaire (Hrsg.): *Nitratbelastung des Grundwassers, Auswirkungen der Landwirtschaft auf die Grundwasser- und Rohwasserbeschaffenheit und Maßnahmen zum Schutz des Grundwassers*. Vorträge des deutsch-französischen Kolloquiums am 6. Oktober 1988, Universitäten Stuttgart und Louis Pasteur Strasbourg (Vorträge in deutsch oder französisch, Kurzfassungen zweisprachig), 1988, ISBN 3-921694-71-X

72 Soyeaux, Renald: *Unterströmung von Stauanlagen auf klüftigem Untergrund unter Berücksichtigung laminarer und turbulenter Fließzustände*,1991, ISBN 3-921694-72-8

73 Kohane, Roberto: *Berechnungsmethoden für Hochwasserabfluß in Fließgewässern mit überströmten Vorländern*, 1991, ISBN 3-921694-73-6

74 Hassinger, Reinhard: *Beitrag zur Hydraulik und Bemessung von Blocksteinrampen in flexibler Bauweise*, 1991, ISBN 3-921694-74-4, vergriffen

75 Schäfer, Gerhard: *Einfluß von Schichtenstrukturen und lokalen Einlagerungen auf die Längsdispersion in Porengrundwasserleitern*, 1991, ISBN 3-921694-75-2

76 Giesecke, Jürgen: *Vorträge, Wasserwirtschaft in stark besiedelten Regionen; Umweltforschung mit Schwerpunkt Wasserwirtschaft*, 1991, ISBN 3-921694-76-0

77 Huwe, Bernd: *Deterministische und stochastische Ansätze zur Modellierung des Stickstoffhaushalts landwirtschaftlich genutzter Flächen auf unterschiedlichem Skalenniveau*, 1992, ISBN 3-921694-77-9, vergriffen

78 Rommel, Michael: *Verwendung von Kluftdaten zur realitätsnahen Generierung von Kluftnetzen mit anschließender laminar-turbulenter Strömungsberechnung*, 1993, ISBN 3-92 1694-78-7

79 Marschall, Paul: *Die Ermittlung lokaler Stofffrachten im Grundwasser mit Hilfe von Einbohrloch-Meßverfahren*, 1993, ISBN 3-921694-79-5, vergriffen

80 Ptak, Thomas: *Stofftransport in heterogenen Porenaquiferen: Felduntersuchungen und stochastische Modellierung*, 1993, ISBN 3-921694-80-9, vergriffen

81 Haakh, Frieder: *Transientes Strömungsverhalten in Wirbelkammern,* 1993, ISBN 3-921694-81-7

82 Kobus, Helmut; Cirpka, Olaf; Barczewski, Baldur; Koschitzky, Hans-Peter: *Versucheinrichtung zur Grundwasser und Altlastensanierung VEGAS, Konzeption und Programmrahmen*, 1993, ISBN 3-921694-82-5

83 Zang, Weidong: *Optimaler Echtzeit-Betrieb eines Speichers mit aktueller Abflußregenerierung*, 1994, ISBN 3-921694-83-3, vergriffen

84 Franke, Hans-Jörg: *Stochastische Modellierung eines flächenhaften Stoffeintrages und Transports in Grundwasser am Beispiel der Pflanzenschutzmittelproblematik*, 1995, ISBN 3-921694-84-1

85 Lang, Ulrich: *Simulation regionaler Strömungs- und Transportvorgänge in Karstaquiferen mit Hilfe des Doppelkontinuum-Ansatzes: Methodenentwicklung und Parameteridentifikation*, 1995, ISBN 3-921694-85-X, vergriffen

86 Helmig, Rainer: *Einführung in die Numerischen Methoden der Hydromechanik*, 1996, ISBN 3-921694-86-8, vergriffen

87 Cirpka, Olaf: *CONTRACT: A Numerical Tool for Contaminant Transport and Chemical Transformations - Theory and Program Documentation* -, 1996, ISBN 3-921694-87-6

88 Haberlandt, Uwe: *Stochastische Synthese und Regionalisierung des Niederschlages für Schmutzfrachtberechnungen*, 1996, ISBN 3-921694-88-4

89 Croisé, Jean: *Extraktion von flüchtigen Chemikalien aus natürlichen Lockergesteinen mittels erzwungener Luftströmung*, 1996, ISBN 3-921694-89-2, vergriffen

90 Jorde, Klaus: *Ökologisch begründete, dynamische Mindestwasserregelungen bei Ausleitungskraftwerken*, 1997, ISBN 3-921694-90-6, vergriffen

91 Helmig, Rainer: *Gekoppelte Strömungs- und Transportprozesse im Untergrund - Ein Beitrag zur Hydrosystemmodellierung*-, 1998, ISBN 3-921694-91-4, vergriffen

92 Emmert, Martin: *Numerische Modellierung nichtisothermer Gas-Wasser Systeme in porösen Medien,* 1997, ISBN 3-921694-92-2

93 Kern, Ulrich: *Transport von Schweb- und Schadstoffen in staugeregelten Fließgewässern am Beispiel des Neckars*, 1997, ISBN 3-921694-93-0, vergriffen

94 Förster, Georg: *Druckstoßdämpfung durch große Luftblasen in Hochpunkten von Rohrleitungen 1997*, ISBN 3-921694-94-9

95 Cirpka, Olaf: *Numerische Methoden zur Simulation des reaktiven Mehrkomponententransports im Grundwasser*, 1997, ISBN 3-921694-95-7, vergriffen

96 Färber, Arne: *Wärmetransport in der ungesättigten Bodenzone: Entwicklung einer thermischen In-situ-Sanierungstechnologie*, 1997, ISBN 3-921694-96-5

97 Betz, Christoph: *Wasserdampfdestillation von Schadstoffen im porösen Medium: Entwicklung einer thermischen In-situ-Sanierungstechnologie*, 1998, ISBN 3-921694-97-3

98 Xu, Yichun: *Numerical Modeling of Suspended Sediment Transport in Rivers*, 1998, ISBN 3-921694-98-1, vergriffen

99 Wüst, Wolfgang: *Geochemische Untersuchungen zur Sanierung CKW-kontaminierter Aquifere mit Fe(0)-Reaktionswänden,* 2000, ISBN 3-933761-02-2

100 Sheta, Hussam: *Simulation von Mehrphasenvorgängen in porösen Medien unter Einbeziehung von Hysterese-Effekten*, 2000, ISBN 3-933761-03-4

101 Ayros, Edwin: *Regionalisierung extremer Abflüsse auf der Grundlage statistischer Verfahren*, 2000, ISBN 3-933761-04-2, vergriffen

102 Huber, Ralf: *Compositional Multiphase Flow and Transport in Heterogeneous Porous Media*, 2000, ISBN 3-933761-05-0

103 Braun, Christopherus: *Ein Upscaling-Verfahren für Mehrphasenströmungen in porösen Medien*, 2000, ISBN 3-933761-06-9

104 Hofmann, Bernd: *Entwicklung eines rechnergestützten Managementsystems zur Beurteilung von Grundwasserschadensfällen*, 2000, ISBN 3-933761-07-7

105 Class, Holger: *Theorie und numerische Modellierung nichtisothermer Mehrphasenprozesse in NAPL-kontaminierten porösen Medien,* 2001, ISBN 3-933761-08-5

106 Schmidt, Reinhard: *Wasserdampf- und Heißluftinjektion zur thermischen Sanierung kontaminierter Standorte*, 2001, ISBN 3-933761-09-3

107 Josef, Reinhold:, *Schadstoffextraktion mit hydraulischen Sanierungsverfahren unter Anwendung von grenzflächenaktiven Stoffen*, 2001, ISBN 3-933761-10-7

108 Schneider, Matthias: *Habitat- und Abflussmodellierung für Fließgewässer mit unscharfen Berechnungsansätzen*, 2001, ISBN 3-933761-11-5

109 Rathgeb, Andreas: *Hydrodynamische Bemessungsgrundlagen für Lockerdeckwerke an überströmbaren Erddämmen*, 2001, ISBN 3-933761-12-3

110 Lang, Stefan: *Parallele numerische Simulation instätionärer Probleme mit adaptiven Methoden auf unstrukturierten Gittern*, 2001, ISBN 3-933761-13-1

111 Appt, Jochen; Stumpp Simone: *Die Bodensee-Messkampagne 2001, IWS/CWR Lake Constance Measurement Program 2001*, 2002, ISBN 3-933761-14-X

112 Heimerl, Stephan: *Systematische Beurteilung von Wasserkraftprojekten,* 2002, ISBN 3-933761-15-8, vergriffen

113 Iqbal, Amin: *On the Management and Salinity Control of Drip Irrigation,* 2002, ISBN 3-933761-16-6

114 Silberhorn-Hemminger, Annette: *Modellierung von Kluftaquifersystemen: Geostatistische Analyse und deterministisch-stochastische Kluftgenerierung,* 2002, ISBN 3-933761-17-4

115 Winkler, Angela: *Prozesse des Wärme- und Stofftransports bei der In-situ-Sanierung mit festen Wärmequellen,* 2003, ISBN 3-933761-18-2

116 Marx, Walter: *Wasserkraft, Bewässerung, Umwelt - Planungs- und Bewertungsschwerpunkte der Wasserbewirtschaftung,* 2003, ISBN 3-933761-19-0

117 Hinkelmann, Reinhard: *Efficient Numerical Methods and Information-Processing Techniques in Environment Water,* 2003, ISBN 3-933761-20-4

118 Samaniego-Eguiguren, Luis Eduardo: *Hydrological Consequences of Land Use / Land Cover and Climatic Changes in Mesoscale Catchments*, 2003, ISBN 3-933761-21-2

119 Neunhäuserer, Lina: *Diskretisierungsansätze zur Modellierung von Strömungs- und Transportprozessen in geklüftet-porösen Medien*, 2003, ISBN 3-933761-22-0

120 Paul, Maren: *Simulation of Two-Phase Flow in Heterogeneous Poros Media with Adaptive Methods*, 2003, ISBN 3-933761-23-9

121 Ehret, Uwe: *Rainfall and Flood Nowcasting in Small Catchments using Weather Radar*, 2003, ISBN 3-933761-24-7

122 Haag, Ingo: *Der Sauerstoffhaushalt staugeregelter Flüsse am Beispiel des Neckars - Analysen, Experimente, Simulationen -,* 2003, ISBN 3-933761-25-5

123 Appt, Jochen: *Analysis of Basin-Scale Internal Waves in Upper Lake Constance,* 2003, ISBN 3-933761-26-3

124 Hrsg.: Schrenk, Volker; Batereau, Katrin; Barczewski, Baldur; Weber, Karolin und Koschitzky, Hans-Peter: *Symposium Ressource Fläche und VEGAS - Statuskolloquium 2003, 30. September und 1. Oktober 2003,* 2003, ISBN 3-933761-27-1

125 Omar Khalil Ouda: *Optimisation of Agricultural Water Use: A Decision Support System for the Gaza Strip,* 2003, ISBN 3-933761-28-0

126 Batereau, Katrin: *Sensorbasierte Bodenluftmessung zur Vor-Ort-Erkundung von Schadensherden im Untergrund*, 2004, ISBN 3-933761-29-8

127 Witt, Oliver: *Erosionsstabilität von Gewässersedimenten mit Auswirkung auf den Stofftransport bei Hochwasser am Beispiel ausgewählter Stauhaltungen des Oberrheins*, 2004, ISBN 3-933761-30-1

128 Jakobs, Hartmut: *Simulation nicht-isothermer Gas-Wasser-Prozesse in komplexen Kluft-Matrix-Systemen*, 2004, ISBN 3-933761-31-X

129 Li, Chen-Chien: *Deterministisch-stochastisches Berechnungskonzept zur Beurteilung der Auswirkungen erosiver Hochwasserereignisse in Flussstauhaltungen,* 2004, ISBN 3-933761-32-8

130 Reichenberger, Volker; Helmig, Rainer; Jakobs, Hartmut; Bastian, Peter; Niessner, Jennifer: *Complex Gas-Water Processes in Discrete Fracture-Matrix Systems: Upscaling, Mass-Conservative Discretization and Efficient Multilevel Solution,* 2004, ISBN 3-933761-33-6

131 Hrsg.: Barczewski, Baldur; Koschitzky, Hans-Peter; Weber, Karolin; Wege, Ralf: *VEGAS - Statuskolloquium 2004,* Tagungsband zur Veranstaltung am 05. Oktober 2004 an der Universität Stuttgart, Campus Stuttgart-Vaihingen, 2004, ISBN 3-933761-34-4

132 Asie, Kemal Jabir: *Finite Volume Models for Multiphase Multicomponent Flow through Porous Media*. 2005, ISBN 3-933761-35-2

133 Jacoub, George: *Development of a 2-D Numerical Module for Particulate Contaminant Transport in Flood Retention Reservoirs and Impounded Rivers,* 2004, ISBN 3-933761-36-0

134 Nowak, Wolfgang: *Geostatistical Methods for the Identification of Flow and Transport Parameters in the Subsurface,* 2005, ISBN 3-933761-37-9

135 Süß, Mia: *Analysis of the influence of structures and boundaries on flow and transport processes in fractured porous media*, 2005, ISBN 3-933761-38-7

136 Jose, Surabhin Chackiath: *Experimental Investigations on Longitudinal Dispersive Mixing in Heterogeneous Aquifers,* 2005, ISBN: 3-933761-39-5

137 Filiz, Fulya: *Linking Large-Scale Meteorological Conditions to Floods in Mesoscale Catchments,* 2005, ISBN 3-933761-40-9

138 Qin, Minghao: *Wirklichkeitsnahe und recheneffiziente Ermittlung von Temperatur und Spannungen bei großen RCC-Staumauern*, 2005, ISBN 3-933761-41-7

139 Kobayashi, Kenichiro: *Optimization Methods for Multiphase Systems in the Subsurface - Application to Methane Migration in Coal Mining Areas*, 2005, ISBN 3-933761-42-5

140 Rahman, Md. Arifur: *Experimental Investigations on Transverse Dispersive Mixing in Heterogeneous Porous Media,* 2005, ISBN 3-933761-43-3

141 Schrenk, Volker: *Ökobilanzen zur Bewertung von Altlastensanierungsmaßnahmen,* 2005, ISBN 3-933761-44-1

142 Hundecha, Hirpa Yeshewatesfa: *Regionalization of Parameters of a Conceptual Rainfall-Runoff Model*, 2005, ISBN: 3-933761-45-X

143 Wege, Ralf: *Untersuchungs- und Überwachungsmethoden für die Beurteilung natürlicher Selbstreinigungsprozesse im Grundwasser,* 2005, ISBN 3-933761-46-8

144 Breiting, Thomas: *Techniken und Methoden der Hydroinformatik - Modellierung von komplexen Hydrosystemen im Untergrund*, 2006, 3-933761-47-6

145 Hrsg.: Braun, Jürgen; Koschitzky, Hans-Peter; Müller, Martin: *Ressource Untergrund: 10 Jahre VEGAS: Forschung und Technologieentwicklung zum Schutz von Grundwasser und Boden,* Tagungsband zur Veranstaltung am 28. und 29. September 2005 an der Universität Stuttgart, Campus Stuttgart-Vaihingen, 2005, ISBN 3-933761-48-4

146 Rojanschi, Vlad: *Abflusskonzentration in mesoskaligen Einzugsgebieten unter Berücksichtigung des Sickerraumes,* 2006, ISBN 3-933761-49-2

147 Winkler, Nina Simone: *Optimierung der Steuerung von Hochwasserrückhaltebecken-systemen,* 2006, ISBN 3-933761-50-6

148 Wolf, Jens: *Räumlich differenzierte Modellierung der Grundwasserströmung alluvialer Aquifere für mesoskalige Einzugsgebiete*, 2006, ISBN: 3-933761-51-4

149 Kohler, Beate: *Externe Effekte der Laufwasserkraftnutzung*, 2006, ISBN 3-933761-52-2

150 Hrsg.: Braun, Jürgen; Koschitzky, Hans-Peter; Stuhrmann, Matthias: *VEGAS-Statuskolloquium 2006,* Tagungsband zur Veranstaltung am 28. September 2006 an der Universität Stuttgart, Campus Stuttgart-Vaihingen, 2006, ISBN 3-933761-53-0

151 Niessner, Jennifer: *Multi-Scale Modeling of Multi-Phase - Multi-Component Processes in Heterogeneous Porous Media*, 2006, ISBN 3-933761-54-9

152 Fischer, Markus: *Beanspruchung eingeerdeter Rohrleitungen infolge Austrocknung bindiger Böden,* 2006, ISBN 3-933761-55-7

153 Schneck, Alexander: *Optimierung der Grundwasserbewirtschaftung unter Berücksichtigung der Belange der Wasserversorgung, der Landwirtschaft und des Naturschutzes*, 2006, ISBN 3-933761-56-5

154 Das, Tapash: *The Impact of Spatial Variability of Precipitation on the Predictive Uncertainty of Hydrological Models,* 2006, ISBN 3-933761-57-3

155 Bielinski, Andreas: *Numerical Simulation of CO_2 sequestration in geological formations*, 2007, ISBN 3-933761-58-1

156 Mödinger, Jens: *Entwicklung eines Bewertungs- und Entscheidungsunterstützungssystems für eine nachhaltige regionale Grundwasserbewirtschaftung*, 2006, ISBN 3-933761-60-3

157 Manthey, Sabine: *Two-phase flow processes with dynamic effects in porous media - parameter estimation and simulation,* 2007, ISBN 3-933761-61-1

158 Pozos Estrada, Oscar: *Investigation on the Effects of Entrained Air in Pipelines,* 2007, ISBN 3-933761-62-X

159 Ochs, Steffen Oliver: *Steam injection into saturated porous media – process analysis including experimental and numerical investigations*, 2007, ISBN 3-933761-63-8

160 Marx, Andreas: *Einsatz gekoppelter Modelle und Wetterradar zur Abschätzung von Niederschlagsintensitäten und zur Abflussvorhersage, 2007,* ISBN 3-933761-64-6

161 Hartmann, Gabriele Maria: *Investigation of Evapotranspiration Concepts in Hydrological Modelling for Climate Change Impact Assessment*, 2007, ISBN 3-933761-65-4

162 Kebede Gurmessa, Tesfaye: *Numerical Investigation on Flow and Transport Characteristics to Improve Long-Term Simulation of Reservoir Sedimentation*, 2007, ISBN 3-933761-66-2

163 Trifković, Aleksandar: *Multi-objective and Risk-based Modelling Methodology for Planning, Design and Operation of Water Supply Systems*, 2007, ISBN 3-933761-67-0

164 Götzinger, Jens: *Distributed Conceptual Hydrological Modelling - Simulation of Climate, Land Use Change Impact and Uncertainty Analysis*, 2007, ISBN 3-933761-68-9

165 Hrsg.: Braun, Jürgen; Koschitzky, Hans-Peter; Stuhrmann, Matthias: *VEGAS – Kolloquium 2007,* Tagungsband zur Veranstaltung am 26. September 2007 an der Universität Stuttgart, Campus Stuttgart-Vaihingen, 2007, ISBN 3-933761-69-7

166 Freeman, Beau: *Modernization Criteria Assessment for Water Resources Planning; Klamath Irrigation Project, U.S.*, 2008, ISBN 3-933761-70-0

167 Dreher, Thomas: *Selektive Sedimentation von Feinstschwebstoffen in Wechselwirkung mit wandnahen turbulenten Strömungsbedingungen*, 2008, ISBN 3-933761-71-9

168 Yang, Wei: *Discrete-Continuous Downscaling Model for Generating Daily Precipitation Time Series*, 2008, ISBN 3-933761-72-7

169 Kopecki, Ianina: *Calculational Approach to FST-Hemispheres for Multiparametrical Benthos Habitat Modelling,* 2008*,* ISBN 3-933761-73-5

170 Brommundt, Jürgen: *Stochastische Generierung räumlich zusammenhängender Niederschlagszeitreihen*, 2008, ISBN 3-933761-74-3

171 Papafotiou, *Alexandros: Numerical Investigations of the Role of Hysteresis in Heterogeneous Two-Phase Flow Systems*, 2008, ISBN 3-933761-75-1

172 He, Yi: *Application of a Non-Parametric Classification Scheme to Catchment Hydrology*, 2008, ISBN 978-3-933761-76-7

173 Wagner, Sven: *Water Balance in a Poorly Gauged Basin in West Africa Using Atmospheric Modelling and Remote Sensing Information*, 2008, ISBN 978-3-933761-77-4

174 Hrsg.: Braun, Jürgen; Koschitzky, Hans-Peter; Stuhrmann, Matthias; Schrenk, Volker: *VEGAS-Kolloquium 2008 Ressource Fläche III*, Tagungsband zur Veranstaltung am 01. Oktober 2008 an der Universität Stuttgart, Campus Stuttgart-Vaihingen, 2008, ISBN 978-3-933761-78-1

175 Patil, Sachin: *Regionalization of an Event Based Nash Cascade Model for Flood Predictions in Ungauged Basins*, 2008, ISBN 978-3-933761-79-8

176 Assteerawatt, Anongnart: *Flow and Transport Modelling of Fractured Aquifers based on a Geostatistical Approach,* 2008, ISBN 978-3-933761-80-4

177 Karnahl, Joachim Alexander: *2D numerische Modellierung von multifraktionalem Schwebstoff- und Schadstofftransport in Flüssen*, 2008, ISBN 978-3-933761-81-1

178 Hiester, Uwe: *Technologieentwicklung zur In-situ-Sanierung der ungesättigten Bodenzone mit festen Wärmequellen,* 2009, ISBN 978-3-933761-82-8

179 Laux, Patrick: *Statistical Modeling of Precipitation for Agricultural Planning in the Volta Basin of West Africa,* 2009, ISBN 978-3-933761-83-5

180 Ehsan, Saqib: *Evaluation of Life Safety Risks Related to Severe Flooding,* 2009, ISBN 978-3-933761-84-2

181 Prohaska, Sandra: *Development and Application of a 1D Multi-Strip Fine Sediment Transport Model for Regulated Rivers,* 2009, ISBN 978-3-933761-85-9

182 Kopp, Andreas: *Evaluation of CO_2 Injection Processes in Geological Formations for Site Screening,* 2009, ISBN 978-3-933761-86-6

183 Ebigbo, Anozie: *Modelling of biofilm growth and its influence on CO_2 and water (two-phase) flow in porous media,* 2009, ISBN 978-3-933761-87-3

184 Freiboth, Sandra: *A phenomenological model for the numerical simulation of multiphase multicomponent processes considering structural alterations of porous media*, 2009, ISBN 978-3-933761-88-0

185 Zöllner, Frank: *Implementierung und Anwendung netzfreier Methoden im Konstruktiven Wasserbau und in der Hydromechanik*, 2009, ISBN 978-3-933761-89-7

186 Vasin, Milos: *Influence of the soil structure and property contrast on flow and transport in the unsaturated zone*, 2010, ISBN 978-3-933761-90-3

187 Li, Jing: *Application of Copulas as a New Geostatistical Tool*, 2010, ISBN 978-3-933761-91-0

188 AghaKouchak, Amir: *Simulation of Remotely Sensed Rainfall Fields Using Copulas*, 2010, ISBN 978-3-933761-92-7

189 Thapa, Pawan Kumar: *Physically-based spatially distributed rainfall runoff modelling for soil erosion estimation*, 2010, ISBN 978-3-933761-93-4

190 Wurms, Sven: *Numerische Modellierung der Sedimentationsprozesse in Retentionsanlagen zur Steuerung von Stoffströmen bei extremen Hochwasserabflussereignissen*, 2011, ISBN 978-3-933761-94-1

191 Merkel, Uwe: *Unsicherheitsanalyse hydraulischer Einwirkungen auf Hochwasserschutzdeiche und Steigerung der Leistungsfähigkeit durch adaptive Strömungsmodellierung*, 2011, ISBN 978-3-933761-95-8

192 Fritz, Jochen: *A Decoupled Model for Compositional Non-Isothermal Multiphase Flow in Porous Media and Multiphysics Approaches for Two-Phase Flow*, 2010, ISBN 978-3-933761-96-5

193 Weber, Karolin (Hrsg.): *12. Treffen junger WissenschaftlerInnen an Wasserbauinstituten*, 2010, ISBN 978-3-933761-97-2

194 Bliefernicht, Jan-Geert: *Probability Forecasts of Daily Areal Precipitation for Small River Basins,* 2011, ISBN 978-3-933761-98-9

195 Hrsg.: Koschitzky, Hans-Peter; Braun, Jürgen: *VEGAS-Kolloquium 2010 In-situ-Sanierung - Stand und Entwicklung Nano und ISCO -,* Tagungsband zur Veranstaltung am 07. Oktober 2010 an der Universität Stuttgart, Campus Stuttgart-Vaihingen*,* 2010*,* ISBN 978-3-933761-99-6

196 Gafurov, Abror: *Water Balance Modeling Using Remote Sensing Information - Focus on Central Asia,* 2010, ISBN 978-3-942036-00-9

197 Mackenberg, Sylvia: *Die Quellstärke in der Sickerwasserprognose: Möglichkeiten und Grenzen von Labor- und Freilanduntersuchungen,* 2010, ISBN 978-3-942036-01-6

198 Singh, Shailesh Kumar: *Robust Parameter Estimation in Gauged and Ungauged Basins,* 2010, ISBN 978-3-942036-02-3

199 Doğan, Mehmet Onur: *Coupling of porous media flow with pipe flow,* 2011, ISBN 978-3-942036-03-0

200 Liu, Min: *Study of Topographic Effects on Hydrological Patterns and the Implication on Hydrological Modeling and Data Interpolation,* 2011, ISBN 978-3-942036-04-7

201 Geleta, Habtamu Itefa: *Watershed Sediment Yield Modeling for Data Scarce Areas,* 2011, ISBN 978-3-942036-05-4

202 Franke, Jörg: *Einfluss der Überwachung auf die Versagenswahrscheinlichkeit von Staustufen,* 2011, ISBN 978-3-942036-06-1

203 Bakimchandra, Oinam: *Integrated Fuzzy-GIS approach for assessing regional soil erosion risks,* 2011, ISBN 978-3-942036-07-8

204 Alam, Muhammad Mahboob: *Statistical Downscaling of Extremes of Precipitation in Mesoscale Catchments from Different RCMs and Their Effects on Local Hydrology,* 2011, ISBN 978-3-942036-08-5

205 Hrsg.: Koschitzky, Hans-Peter; Braun, Jürgen: *VEGAS-Kolloquium 2011 Flache Geothermie - Perspektiven und Risiken,* Tagungsband zur Veranstaltung am 06. Oktober 2011 an der Universität Stuttgart, Campus Stuttgart-Vaihingen, 2011, ISBN 978-3-933761-09-2

206 Haslauer, Claus: *Analysis of Real-World Spatial Dependence of Subsurface Hydraulic Properties Using Copulas with a Focus on Solute Transport Behaviour,* 2011, ISBN 978-3-942036-10-8

207 Dung, Nguyen Viet: *Multi-objective automatic calibration of hydrodynamic models – development of the concept and an application in the Mekong Delta,* 2011, ISBN 978-3-942036-11-5

208 Hung, Nguyen Nghia: *Sediment dynamics in the floodplain of the Mekong Delta, Vietnam,* 2011, ISBN 978-3-942036-12-2

209 Kuhlmann, Anna: *Influence of soil structure and root water uptake on flow in the unsaturated zone,* 2012, ISBN 978-3-942036-13-9

210 Tuhtan, Jeffrey Andrew: *Including the Second Law Inequality in Aquatic Ecodynamics: A Modeling Approach for Alpine Rivers Impacted by Hydropeaking,* 2012, ISBN 978-3-942036-14-6

211 Tolossa, Habtamu: *Sediment Transport Computation Using a Data-Driven Adaptive Neuro-Fuzzy Modelling Approach,* 2012, ISBN 978-3-942036-15-3

212 Tatomir, Alexandru-Bodgan: *From Discrete to Continuum Concepts of Flow in Fractured Porous Media,* 2012, ISBN 978-3-942036-16-0

213 Erbertseder, Karin: *A Multi-Scale Model for Describing Cancer-Therapeutic Transport in the Human Lung,* 2012, ISBN 978-3-942036-17-7

214 Noack, Markus: *Modelling Approach for Interstitial Sediment Dynamics and Reproduction of Gravel Spawning Fish,* 2012, ISBN 978-3-942036-18-4

215 De Boer, Cjestmir Volkert: *Transport of Nano Sized Zero Valent Iron Colloids during Injection into the Subsurface*, 2012, ISBN 978-3-942036-19-1

216 Pfaff, Thomas: *Processing and Analysis of Weather Radar Data for Use in Hydrology*, 2013, ISBN 978-3-942036-20-7

217 Lebrenz, Hans-Henning: *Addressing the Input Uncertainty for Hydrological Modeling by a New Geostatistical Method*, 2013, ISBN 978-3-942036-21-4

218 Darcis, Melanie Yvonne: *Coupling Models of Different Complexity for the Simulation of CO_2 Storage in Deep Saline Aquifers*, 2013, ISBN 978-3-942036-22-1

219 Beck, Ferdinand: *Generation of Spatially Correlated Synthetic Rainfall Time Series in High Temporal Resolution - A Data Driven Approach*, 2013, ISBN 978-3-942036-23-8

220 Guthke, Philipp: *Non-multi-Gaussian spatial structures: Process-driven natural genesis, manifestation, modeling approaches, and influences on dependent processes*, 2013, ISBN 978-3-942036-24-5

221 Walter, Lena: *Uncertainty studies and risk assessment for CO_2 storage in geological formations*, 2013, ISBN 978-3-942036-25-2

Die Mitteilungshefte ab der Nr. 134 (Jg. 2005) stehen als pdf-Datei über die Homepage des Instituts: www.iws.uni-stuttgart.de zur Verfügung.